Optimising Carbon Type Differentiation Techniques to Reduce Dust Emissions in Blast Furnace Ironmaking

By

John Lewis

A thesis presented to Swansea University for the fulfilment of the requirements for the degree of Engineering Doctorate (EngD) in Materials Engineering

Faculty of Science and Engineering, Swansea University, 2023

Author Declaration

DECLARATION

This work has not previously been accepted in substance for any degree and is not being currently submitted in candidature for any degree.

Signed 

Date: 16/02/2023

STATEMENT 1

This thesis is the result of my own investigations, except where otherwise stated. Other sources are acknowledged by footnotes giving explicit references. A bibliography is appended.

Signed 

Date: 16/02/2023

STATEMENT 2

I hereby give my consent for my work, if relevant and accepted, to be available for photocopying and for inter-library loans after the expiry of a bar on access approved by the University.

Signed 

Date: 16/02/2023

STATEMENT 3

The University's ethical procedures have been followed and, where appropriate, that ethical approval has been granted.

Signed 

Date: 16/02/2023

Abstract

The manufacturing process of iron, using the blast furnace (BF) generates dust as a by-product, which is recycled, however, the generation of the dust in excess is undesirable. A comprehensive review of the dust has determined that each of the raw materials for blast furnace ironmaking contributes to its formation, including several forms of carbon thus addressing the hypothesis 'The raw materials that feed the blast furnace are expelled into the gas stream and all influence the blast furnace dust.' The current technique for quantifying coal originating carbon type mostly in the form of coal char, referred to as the nominal term Low Order Carbon (LOC) within BF dust consists of thermogravimetric analysis (TGA) however, this technique does not allow for samples of dust to be analysed in a timely manner, in line with the ever-changing conditions of the blast furnace. In this work, the TGA method has been trialled for use with BF dust, with improvements offered to the heating profile, allowing for faster analysis. Moreover, alternative techniques have been trialled, in combination with various characterisation methods such as X-ray diffraction, Scanning Electron Microscopy, total carbon and Optical Emission Spectroscopy. The 'Winkler Method' which was originally designed to quantify charcoal in soil sediment has been successfully adapted and optimised to suit LOC quantification in BF dust, showing a good correlation with the original benchmark technique. This answered the hypothesis, 'Thermal techniques can be used to differentiate carbon sources in dust generated in blast furnaces that use granulated coal injection.' The techniques for LOC quantification were applied to dust samples spanning a 9 month period. to determine the process parameters that influence the LOC presence within the dust. It was found that the resolution of sampling is key to identify relationships between process parameters and LOC within the dust. A novel technique to continuously monitor the dust output of the furnace found that the dust output and the LOC within the dust are related, where the increasing dust output leads to increasing concentrations of LOC within the carbon profile of the dust itself. Process parameters including blast pressure, blast volume, and production rate were considered to increase the dust output from the furnace based on the work of the dust probe, thus answering the hypothesis 'Coal combustion in the raceway can be impacted by process parameters and the evidence can be found in the fingerprint of blast furnace dust.' A node mapping exercise was used to model an ideal set of process conditions for low dust operations. The foundations to make macro advances in carbon and dust output reduction in blast furnace ironmaking are laid out in this thesis.

Acknowledgements

The academic guidance provided by Dr Hollie Cockings has been totally faultless, her enthusiasm for the subject has kept me motivated throughout this thesis and her direction has been second to none.

My gratitude to the staff of the Materials and Manufacturing Academy (M2A), for the wealth of opportunities and support throughout. The support has been truly phenomenal and the attitude to research matched.

Dr Mark Greenslade, thank you for your industrial guidance, ensuring the thesis stays relevant to industry. And to the rest of the Tata Steel blast furnace team for the continued guidance and thesis influence.

Dr Laura Baker, thank you for the initial inspiration to do this thesis and continued support throughout, providing publishing opportunities and opportunities to present my work to all levels in industry. Your continued advocation and fierce determination in industry is inspirational.

A special thank you to Dr Daniel Stewart for continued support throughout, including answering questions without a care for the time zone and in-depth analysis and discussion.

Gratitude to the list of experts, who have helped shape my thesis, including Peter Warren, Dr Julian Steer, Stefan Born, and Dr Adam Hunt.

I'd like to thank my wife and daughter, Becky and Evelyn. Who continued to believe in me even when I didn't. Thanks for providing the foundation for me to complete my studies and making allowances for me to take every opportunity that was presented to me.

Thanks to my best friend and colleague who took the leap with me to study the Doctorate. Matthew Thomas, thanks for all the work you have done to continuously review my work and give me ideas to keep the thesis momentum. Thanks for sharing this journey with me.

I'd also like to acknowledge the financial support that was provided by the Materials and Manufacturing Academy (M2A) which has been made possible through funding from the European Social Fund via the Welsh Government, Tata Steel UK and Swansea University EPSRC impact.

Table of Contents

List of Figures

List of Tables

List of Appendices

List of Abbreviations

DTF – Drop Tube Furnace

MAD – Microwave Assisted Dissolution

XRD – X-ray Diffraction

XRF – X-ray Fluorescence

VM – Volatile Matter

TGA – Thermogravimetric Analyser

PCI – Pulverised Coal Injection

GCI – Granulated Coal Injection

FTIR – Fourier Transform Infrared

IM – Inherent Moisture

CRR – Coke Replacement Ratio

BOF – Basic Oxygen Furnace

BOS – Basic Oxygen Steelmaking

EAF – Electric Arc Furnace

BF4 – Blast Furnace 4

BF5 – Blast Furnace 5

MOGADOR - Model for Gas Reduction and Ore Reduction

SEM – Scanning Electron Microscope

EBSD - Electron Back Scatter Detection

EDS – Energy Dispersive Spectroscopy

EHT – Electron High Tension

LOC – Low Order Carbon

HOC – High Order Carbon

CET – CanmetEnergy Technique

BET – Brunauer Emmett Teller Surface Area

CRM – Certified Reference Material

PI – Process Information

Introduction

1.1 Background

1.1.1 Steelmaking

Steel has been at the forefront of research since Henry Bessemer discovered the first technique for mass-production, around the 1850's. The process has evolved from blowing air through molten pig iron to remove impurities, to our current methods of manufacturing which include Basic Oxygen Steelmaking (BOS) and Electric Arc Furnace (EAF)[1]. These are based on the fundamental principles of Bessemer, with improved processing and secondary steelmaking to further refine the steel into desired grades depending on the requirements of the downstream sector. Within an integrated steel manufacturer, iron is produced in Blast Furnaces which is subsequently converted into steel using the BOS process.

1.1.2 Blast Furnace Ironmaking

The blast furnace is the provider of molten iron for the steel plant. The focus here is providing a good quality product for the steel plant to convert using the oxygen furnace process. Hot air is blasted into the bottom of the furnace with fuel in the form of oxygen and coal. Reductants, Ores, and fluxes are added to the top, and liquid iron and slag are tapped from the bottom. There must be tight control on operational parameters and the quality of the raw material inputs must remain in focus to produce a good product for the steel plant. Extensive research has been conducted in the field of ironmaking, however, there is still work to be carried out to ensure an understanding of the process of furnace fuelling and how it can be optimised to ensure the environmental impact of ironmaking is reduced. Ironmaking has progressed substantially since the initial invention and industrialisation, whereby the off gas is now recycled to be used elsewhere as a natural gas substitute on site and the dust generated is filtered and reused in the sintering process. At present this dust is generated in surplus and the minimisation of the dust will have a net environmental benefit. The current climate demands that research is focussed on minimising environmental impact and thus it is key for the steel industry, along with other foundation industries, to adapt.

1.1.3 Blast Furnace Fuelling and Environmental Considerations

Currently, the fuelling process of a blast furnace is focused on the conditions required for producing a good quality iron for use in downstream processes. Sufficient heat is required to melt the descending burden of fluxes, reductants and ores. The degree of heat here is governed by the heating of air in the stoves before blasting, the degree of oxygen enrichment, the quality, and the volume of fuel within the furnace. Coke is the dominant fuel used in the process, it can generate heat and retain structural integrity within the conditions of the furnace. The large coke structures provide a degree of permeability for air to move through the furnace, whilst allowing the burden to descend the furnace in a controlled manner. Being a prime fuel source, it is expensive, hence the desired tendency for increasing the use of injection coal. Coal is often used to offset the volume of coke used as a fuel; however, this has many considerations. Coal doesn't provide the same structural integrity as coke; it generally combusts in the furnace readily[2]. Also, the heat generated is less than that of coke, hence the requirement to control oxygen enrichment. Coal has a cooling effect on the air in the raceway thus oxygen is added to drive productivity in this case, to counter the effect of raceway cooling, and to improve the degree of gasification and reducing conditions of the furnace[3].

Despite coal combusting readily in the blast furnace, when increasing the levels of coal usage, the combustion within the furnace must be sufficient to prevent it from leaving the furnace as unburnt material. This is fundamentally a waste of coal; coals should be selected to optimise coal conversion to maximise heat generated through combustion and the degree of gasification of the coal. Coal which ascends the furnace and leaves in the gas waste stream ultimately adds to the volume of dust and with excess dust, the supply will exceed the ability of the sinter plant to recycle it, as well as contribute to an increase in carbon emissions.

1.2 Thesis Aims and Objectives

The aim of this thesis is to first understand what blast furnace dust is, what material constituents it is made up of and what are the key differences between the dust collected in the different abatements of the blast furnace gas cleaning system. The second aim is to evaluate if coal gasification within the blast furnace is incomplete under normal conditions and determine the potential coal properties and process

variables that influence the degree of gasification within the blast furnace. To understand how coal reacts within the furnace, it is key to identify the sources of carbon in the dust. Fingerprinting the origins of the dust can paint a picture of the degree of coal gasification within the process and the raw materials being used. The process for carrying out the carbon identification within blast furnace dust is time consuming, hence there is a drive to reduce the time limitations of the analysis technique, so the maximum amount of data can be collected routinely. Once this information can be obtained, changes in operating conditions and raw material inputs can be tracked against data from the dust itself[4]. This will determine the key conditions that influence the degree of gasification of coal within the furnace. From this information, there is the possibility to improve the coal selection process, the coal processing itself, oxygen enrichment conditions, productivity rates, coke rates, and coal rates. This will ultimately drive down the cost of manufacture, reduce waste in the process and improve the understanding of the process. Data-driven decisions can be made based on information provided by the fingerprint analysis of the dust. If it can be shown which parameters have the largest impact on the presence of coal and subsequent forms it presents within the dust, these can be optimised to improve the degree of coal gasification within the furnace. The scientific hypotheses tested in this thesis are as follows:

1. ‘The raw materials that feed the blast furnace are expelled into the gas stream and all influence the blast furnace dust’
2. ‘Thermal techniques can be used to differentiate carbon sources in dust generated in blast furnaces that use granulated coal injection’.
3. ‘Coal combustion in the raceway can be impacted by process parameters and the evidence can be found in the fingerprint of blast furnace dust’

1.3 Industrial Net-Zero Alignment

A new report from UK Steel calls for a positive policy environment to achieve the government's target of a 95% reduction in steelmaking emissions by 2050 and the Climate Change Committee's recommendation of near-zero emissions from ore-based steelmaking by 2035. The report highlights the opportunity to reindustrialise and create green jobs while ensuring a market for net-zero steel is created[5]. The challenges to achieving net-zero UK steel manufacturing include high electricity prices, lack of a

market for net-zero steel, and industries choosing to import high-emission steel. The UK has a first-mover advantage in achieving net-zero steel and transforming existing steel jobs into green jobs, securing the local economies' future. Various decarbonisation technologies can be utilised, including electrified steelmaking, carbon capture and storage, and hydrogen-based steelmaking[5].

Tata Steel in the UK has a goal of producing net-zero steel by 2050 at the latest and reducing CO_2 emissions by 30% by 2030. Tata Steel UK is finalising a decarbonisation roadmap focussed on using locally available steel scrap, and the UK government is providing consultation[6]. Hence the plans for the UK are yet to be unveiled but as a group, some of the global strategies from TATA Steel have been outlined, TATA Steel are taking significant measures to establish a formal circular economy for steel in India[7]. The company has commissioned a 0.5MT PA scrap processing unit in FY2020-21, which is the first shredding unit in India, and has plans to set up several more units across different regions. Tata Steel is determined to increase the utilisation of scrap charge in the steel-making process, improve existing processes, and adopt the best available technologies to maximise waste heat recovery, utilise by-product gases, and dehumidify hot blast in blast furnaces[7]. The company is also striving to reduce emissions in Indian operations by enhancing the quality of raw materials such as iron ore and coking coal. Moreover, Tata Steel is committed to boosting the share of renewable energy generation, with 150 MW worth of renewable energy projects being phased in across its Indian sites and plans to commission 11.8 MW of solar power plants at its Thailand facilities by FY2022-23[7]. The company has raised the internal carbon pricing to promote appraisal of carbon abatement projects in India. TATA Steel is dedicated to achieving carbon-neutral steel production in Europe by 2050 and plans to transition to hydrogen-based steelmaking by gradually replacing blast furnaces with a combination of DRI technology and electric arc furrnaces (EAF) by 2026[7]. The company plans to commission several EAF units to convert collected and processed scrap into steel, while also shifting from metallurgical coal to cleaner fuel like natural gas. Furthermore, Tata Steel is upscaling pilots of Carbon Capture & Utilisation (CCU) and Hydrogen-based steelmaking in India, with a successful 5-tonnes per day pilot plant commissioned at Jamshedpur to capture CO_2 from Blast Furnace gas[7]. The company is also piloting new technologies in partnership with academia and the government to achieve deep decarbonisation, with a focus on CCU, hydrogen-based steelmaking, use of biomass, and alternate

ironmaking routes. These efforts align with TATA Steel's commitment to net-zero emissions and its collaborations with universities and other organisations to achieve a sustainable future[7].

Reducing the blast furnace dust output in the UK can align with net zero strategies by reducing the carbon footprint of the steel production process. Blast furnaces are a significant source of carbon emissions in the steel industry, and dust output is a by-product of their operation. By reducing the amount of dust generated, the overall carbon emissions from the steel production process can be reduced, contributing to net-zero goals. Additionally, the dust can contain valuable metal particles that can be recycled, the dust can be a source of iron, further reducing the need for virgin raw materials to supply the blast furnace, thus contributing to a circular economy[8].

1.4 List of Published Works

1) Chapter 4.2 – Carbon Type Differentiation

Lewis, J., Cockings, H.L., Stewart, D. J. C., Russell, J., Thomas, M.H., Greenslade, M. Investigating carbon type differentiation techniques for blast furnace dust. Journal of Ironmaking and Steelmaking 2137911 (2022). DOI: 10.1080/03019233.2022.2137911. [First Name Author].

2) Chapter 4.4 – Integrating Technology onto the Plant

Lewis, J., Cockings, H.L., Harvey, J.M., Dłotko, P., Greenslade, M. Monitoring the Impact of Process Parameters on Blast Furnace Dust Parameters. *Proceedings of the 6th International Conference on Clean Technologies in the Steel Industry (EOSC and CTSI 2022).* (2022). **In Press**, (2022) [First Name Author]**.**

3) Chapter 3.3 – Experimental and Methods

Stewart, D. J. C., Lewis, J., Thomson, D., Barron, A. R. Waste COVID-19 Facemasks as an Auxiliary Iron Reductant in the Rotary Hearth Furnace. *Proceedings of the 8th International Conference on Engineering and Technology (BICET 2021).* DOI: 10.1038/s41598-022-06691-w. [Second Name Author]**.**

2 Literature Review

2.1 Introduction

Numerous studies have investigated the combustion behaviour of coal and the formation of char in the blast furnace. The characterisation of coal properties, such as proximate and ultimate analyses, and the assessment of its reactivity and combustion kinetics are crucial in understanding the behaviour of coal in the blast furnace. Moreover, the formation and behaviour of char in the blast furnace are influenced by several factors, such as coal properties, the injection rate, and the blast furnace operating conditions.

This literature review aims to provide a comprehensive overview of the current state of knowledge regarding the combustion of coal and the formation of char in the blast furnace. The review will focus on recent studies that have investigated coal properties, combustion behaviour, and char formation in the blast furnace. Additionally, the review will discuss the challenges associated with the combustion of coal and the formation of char in the blast furnace and highlight the research gaps and future directions in this field.

The COVID-19 pandemic however has had a significant impact on various fields of research, including blast furnace research. Many research institutions and universities had to close their laboratories and offices to prevent the spread of the virus, resulting in a halt to ongoing experiments and research projects. The restrictions on travel and face-to-face meetings also disrupted collaborations between researchers and the sharing of knowledge and resources. Additionally, the pandemic caused disruptions in the global supply chain, leading to shortages of certain equipment, materials, and reagents needed for research. Hence the limitations and restrictions of an up-to-date literature review[9,10].

2.2 Steelmaking

Steel, an alloy of iron with less than 2% carbon is mass-produced worldwide. For around 3000 years, steel has been used for the manufacture of a wide variety of products such as knives and bowls, through to modern-day cars, white goods, and steel structures. There are over 3500 known grades of steel, which makes it a versatile material that can be applied to a huge variety of sectors. There are two types of mass

steel production, 72% of steel is generated using the basic oxygen furnace (BOF) route and 28% is produced using the EAF route. The BOF route relies on a blast furnace which utilises a multitude of raw materials, including iron ore, coal, coke, limestone, and steel scrap. Iron ore, coal, and coke produce the liquid iron for conversion in the BOF[1].

Figure 1 shows a graph of steel production in the world with a breakdown of China versus the rest of the world (ROW), the recent total steel production is 1905 million tonnes produced in the world in 2022. The growth of steel manufacturing from 1950 has been tracked in Figure 2. The largest steel producer in the world at present is by far China as per Figure 3. The EU produced around 9.3% of the total input into the world market. This puts into perspective the demand for steel in the world today, it demonstrates a global requirement for steel and clearly demonstrates the requirement for blast furnace ironmaking to maintain capacity for demand[1].

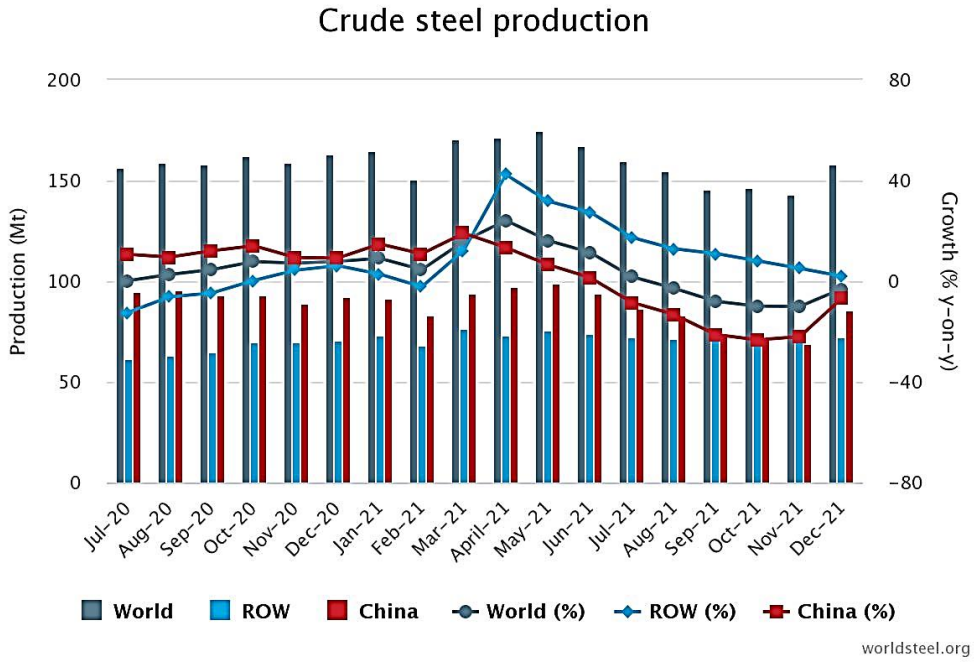

Figure 1 Annual global steel production[1]

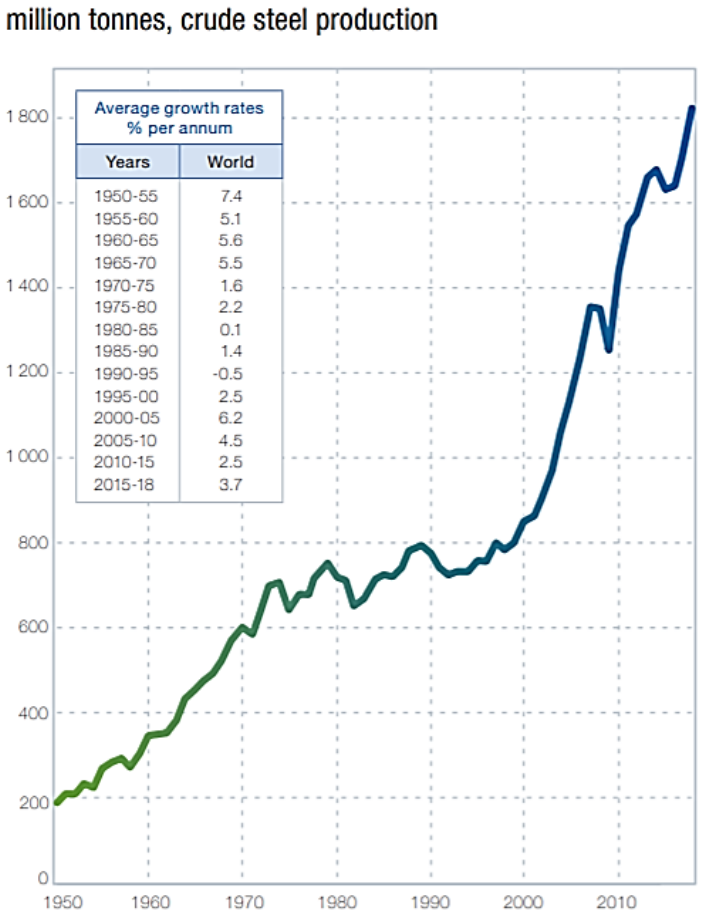

Figure 2 Global steel production growth[1]

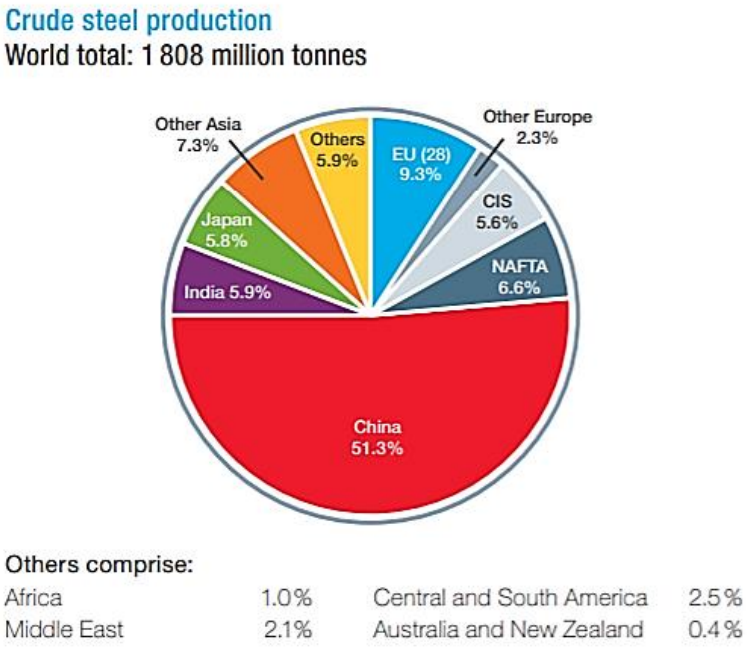

Figure 3 Global steel production by country[1]

2.3 Blast Furnace Ironmaking

A blast furnace is a large mechanical, steel-framed structure, lined with refractory brick designed to reduce iron ore into liquid iron. The blast furnace is fuelled using metallurgical coke, coal, and oxygen-enriched air. Burden materials within the furnace include sinter, iron ore pellets, and iron ore lump[11]. Iron ore can be either fed into the furnace as pellets or lump. Lump ore generally contains more iron oxides per wt% than pellets, which are made by agglomerating dusts of iron ore with lower iron content and poorer quality ores. Iron ore lump is charged in the furnace as mined and screened; the properties of the lump material allow for this. The wt% of iron in iron ore lump can range from approximately 50% to 70%, depending on the geographical location of mining[12]. Sinter is a material born from waste produced across the site. Materials such as ore, coke, coal, lime (CaO), and revert materials are thermally fused via gas-fired burners to produce a solid agglomerate with a relatively high iron content. The revert materials in this case are by-products from other manufacturing processes onsite, with high iron or carbon content. These can typically include scale from the cold mill or hot mill, blast furnace flue dust, and basic oxygen steelmaking (BOS) slurry. A study conducted by Umadevi *et al.* on the use of mill scale in sinter making found that the total Fe and FeO contents of sinter increased with the increase in mill scale addition. Sinter productivity decreased with the increase in mill scale addition due to a decrease in sinter bed permeability, while sinter strength and size initially increased and reached a maximum at 40-50 kg/t of sinter and then declined. Sinter reduction degradation index and reducibility decreased with the increase in mill scale addition due to the increase in FeO content. However, the desired sinter properties, except productivity, can be obtained with the use of 40-50 kg mill scale per tonne of sinter[13]. Fluxes are also used within the furnace, for the benefit of impurity removal for slag production, including limestone and magstone[14].

2.4 Reducing Conditions in the Blast Furnace

To reduce iron ore to iron, many reactions are required throughout the furnace, these are generated by the hot air blast, coke, and coal injection. In the stack, the upper level of the furnace as per Figure 4, the reactions are as per Equations 2.1, 2.2, and 2.3. Hematite (Fe_2O_3) iron ore is reduced to magnetite (Fe_3O_4), wustite (FeO) and metallic

iron respectively (Fe). During this process the iron ore charged at the top of the furnace will soften and liquify, this trickles through the coke layers, as it descends to the hearth of the furnace. At the hearth of the furnace, the material is cast through the taphole[15].

$$3Fe_2O_3 + CO = CO_2 + 2Fe_3O_4 \quad \textbf{2.1}$$

$$Fe_3O_4 + CO = CO_2 + 3FeO \quad \textbf{2.2}$$

$$FeO + CO = CO_2 + Fe \; or \; FeO + C = CO + Fe \quad \textbf{2.3}$$

In the stack of the furnace, the temperature can range between 800°C and 1150°C, this suits the indirect reduction of wustite to metallic iron. The high gas-to-solid contact time found within this area allows for more reduction in this zone. Also, if the reducibility of the ore is high, the reduction reactions are fast. This should be considered when controlling coke rates and furnace rates[16].

In the hearth of the furnace, there is a vast range in temperature between 900°C and 2000°C. This area of the furnace is further subdivided into the cohesive zone, the deadman zone, and the combustion zone. Any unreduced iron from the middle section of the furnace descends into the cohesive zone as fayalite and calcium ferrites, which mix with slag[17]. Within the cohesive zone, there is an increase in temperature; this ranges between 1050°C and 1150°C, liquid iron is formed at this stage with very little porosity. Within the active coke zone, coke reacts with oxygen in the hot blast, forming carbon monoxide to aid in the reduction of iron oxides to metallic iron. The series of reactions within this section is known as the Boudouard reaction. This reaction is endothermic which allows reductant rates per tonne of hot metal to be increased, thus providing the heat for the endothermic reaction. The Boudouard reaction is as per Equations 2.4 and 2.5[15,18].

$$FeO + CO \leftrightarrow Fe + CO_2 \quad (> 1150°C) \quad \textbf{2.4}$$

$$CO_2 + C \leftrightarrow 2CO \quad \textbf{2.5}$$

In the deadman zone, coke is not exposed to oxygen and therefore oxidation does not take place, hence the residence time within the furnace can be up to several weeks[19].

In the raceway, oxygen is blasted via tuyeres, to ascend the furnace. This is the hottest part of the furnace where oxygen from the hot blast is combined with fuel materials such as coke and coal to produce a raceway flame[19].

Furnace charging has a direct impact on furnace stability. The material is fed from the top via a Paul Wurth chute system which is a rotating arm that allows precise control of material distribution within the furnace. With trajectory control, the chute lays material in distinct separate rings of iron ore and coke and once a ring has been laid, the chute angle changes, laying a layer of material on top. Burden layers depend entirely on the angle of repose of the material, enhancing the permeability of the coke layers, which allows for better gas-to-solid contact and controls the retention time of material within the furnace. This allows less resistance for gas to permeate through the process, resulting in better efficiency and reduction conditions of the furnace[19,20].

Thermal control is important within the blast furnace and can be measured via the hot metal silicon (Si) content. Materials containing silica (SiO_2) at around 70-75 wt% enter the furnace through the ferrous burden of iron ore and sinter, the majority of which enters the primary slag. The silicon that is measured in the hot metal is from the coke or coal ash, due to the formation of silicon monoxide gas (SiO.) Many operating factors can impact the silicon content of hot metal which demonstrates the level of thermal control. A high cohesive zone within the furnace allows for more silicon monoxide and carbon interaction, producing a high silicon hot metal. If pressure at the top of the furnace is high, this produces high silicon in hot metal. If low-velocity air is blasted into the furnace, again the time increases for interactions between silicon monoxide and carbon, increasing the hot metal silicon. The amount of direct and indirect reduction will also impact the hot metal silicon[19,21].

The productivity of a furnace is dependent on the rate of coke gasification, directly in front of the tuyeres. This rate is directly impacted by the coke charge rate, coal charge rate, oxygen enrichment, and the thermal condition of the furnace. Furnace productivity can be calculated as per Equation 2.6[19].

$$Production\ Rate\ =\ E\ \times\ \frac{Total\ Oxygen\ Flow}{Coke\ rate\ +\ (A\ \times\ Coal\ Rate)\ +\ (Si)} \quad \textbf{2.6}$$

$E = Production\ rate\ and\ actual\ charge\ rate\ correction\ factor$

$A\ =\ Replacement\ ratio\ of\ coal$

$$=\ 2C\% + 2.5H\% - 2H_2O\% - 86 + 0.9Ash\%$$

$(Si)\ =\ Hot\ metal\ silicon\ content$

As shown in equation 2.6, using less fuel such as coal and coke increases productivity. An increased coal-to-coke ratio also increases productivity. Oxygen enrichment and hot metal silicon reduction will also increase productivity. This equation is good to use under stable furnace conditions. Coal injection has a cooling effect on the raceway flame, allowing for further oxygen enrichment, thus increasing productivity. Often when issues or instability in the blast furnace arise, there are more factors to consider when controlling productivity and this equation cannot be relied upon[19]. Respective zones discussed in this section can be identified in Figure 4.

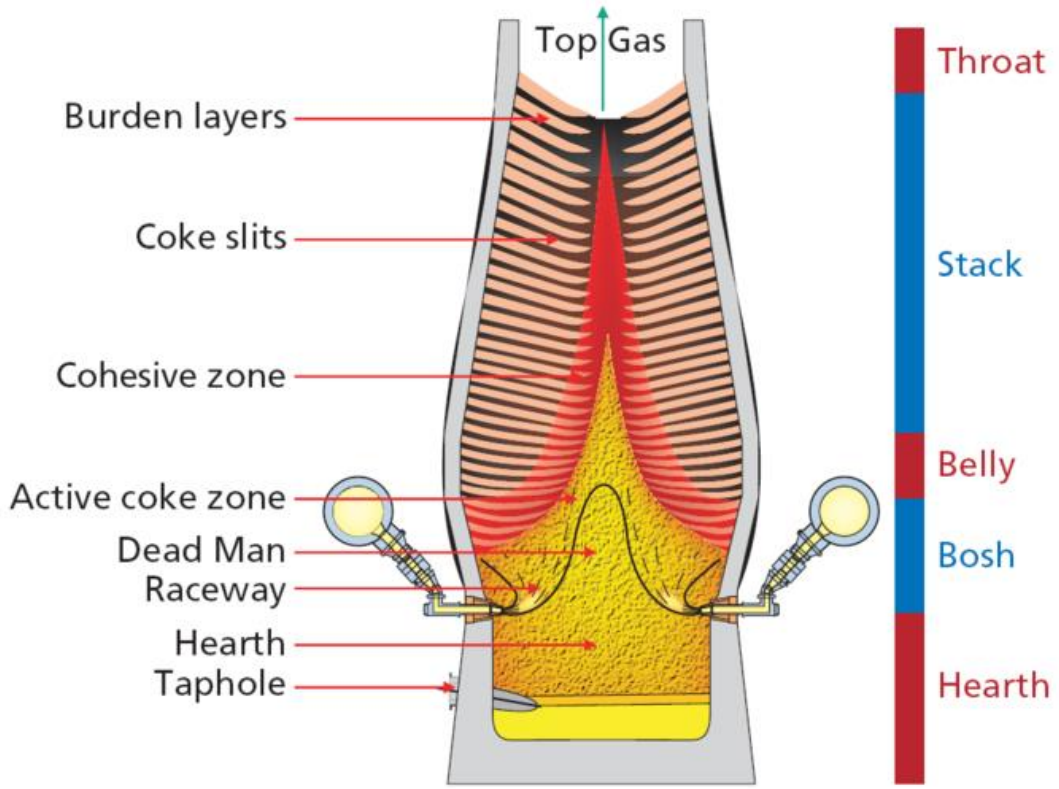

Figure 4 Blast furnace cross-section with zones and items annotated[19]

2.5 Metallurgical Coke

Coke is a strong carbonaceous material that is resistant to melting under high thermal conditions. Coke making is considered by many, an art form that has taken the industry years to master. It is silver/black in colour as per Figure 5. Due to the production process and transportation, the size of coke can vary. Coke up to 25mm is considered nut coke, this is fragments of coke broken away from the larger lumps of coke. Coke larger than this size fraction is known as lump coke, this is prime coke for ironmaking. Normally, a blend of nut and lump coke is added to the furnace to reduce waste from the coke-making process. Material less than 5mm is referred to as breeze, this is typically transported directly to the sinter plant to be used as fuel in the sintering process. However, issues arise when moisture is high in the coke, generally above 7%, breeze material sticks to the lumps and nuts. As the material is top charged into the furnace, the blast air, at this point running at 1m/s, blows breeze off the coke and into the top gas stream[22].

To be suitable for blast furnace ironmaking, coke must have a degree of permeability, to allow gas to permeate and travel through the furnace. It must be able to withstand temperatures of more than 2000^{o}C and must be able to maintain structural integrity. Below the melting zone, coke must remain the only solid material present, this provides support for the total blast furnace content weight above. The permeability of the material allows both slag and iron to trickle through ready for tapping in the hearth of the furnace[23]. Coke generates heat energy during combustion, this is sufficient to allow for the melting of the predominately ferrous burden. As per the Boudouard reactions, the generation of reducing gases for iron making, relies on the oxygen from the blast, reacting with carbon in the coke. Iron produced in the blast furnace contains carbon which is further processed at the BOS plant. Coke provides carbon for the carburisation of the hot metal[19].

Figure 5 Metallurgical coke for blast furnace ironmaking[19]

To produce metallurgical coke, a blend of coal is carbonised within an oven. The oven is sealed to prevent air ingress and therefore prevent combustion. Coal is a natural product, mainly carbon-based, and it is full of impurities. Coking is a purification process, where volatile matter is driven off by heat, in the absence of oxygen. The product is a crystalline carbon structure with <1% volatile matter remaining. The coking cycle is a batch process that takes approximately 18 hours from start to finish[12]. Potentially valuable by-products are formed in the coke-making process. By-products such as gas and tar are extracted from the process and cleaned, the gas is subsequently used to power other areas of the steel plant. The quality of this gas is important and therefore a fine balance between coke and by-product quality is helped by extensive research into raw materials and coke-making processes.

2.5.1 Coke Quality Requirements for Blast Furnace Ironmaking

To produce coke suitable for ironmaking, coal chemistry is vital. Coals are selected based on rank and type of coal, bituminous coals are used to produce coke of superior strength and reasonable reactivity, whilst maintaining viable cost-based manufacture. Other considerations are oven removal, the degree of swelling is important, and the pressure generated during coking. Following the process, Table 1 outlines the typical coke chemistry required for a consistent and good-quality coke product[12,24].

Table 1 Typical analysis of metallurgical coke[19]

Typical Coke Analysis	Analyte	%
Coke Analysis	**Fixed Carbon**	87-92
	Nitrogen	1.2-1.5
	Ash	8-11
	Sulphur	0.6-0.8
	Volatile Matter	0.2-0.5
Ash Analysis	**Silica**	52.0
	Alumina	31.0
	Iron	7.0
	Lime	2.5
	Potassium	1.8
	Magnesia	1.2
	Sodium	0.7
	Phosphorous	0.3
	Manganese	0.1
	Zinc	<0.02

From a physical quality perspective, coke must be lump sized with a narrow particle size distribution band. It should be resistant to breakage during transportation and have abrasion resistance. Coke should also have a high resistance to chemical attack, whilst maintaining good structural integrity post-attack[15].

2.5.2 Mechanisms for Coke Degradation in the Blast Furnace

During transportation, stabilisation occurs where particles that have sharp edges abrade against hard surfaces and other lumps of coke. These edges are removed, and coke breeze is formed. The remaining coke is strong, but the generated fines at this point creates an environmental problem. Once the coke has passed the stock house screens, any breeze remaining on the surface of the large coke lumps will be blown into the top gas of the furnace[25].

Also, within the furnace, coke will undergo breakage and degradation. This has a direct impact on flue dust levels within the top gas. There are several mechanisms of breakdown as the coke descends the furnace. Within the charging zone, directly at the

top of the furnace, coke will abrade and break down mechanically, due to the fall from the chute and the impact made as it lands. At the throat and stack layers, both coke and ore are separate entities and here, drying occurs of the particles causing fines to move into the top gas[26]. Recirculating elements such as zinc, sulphur, and alkali metals are deposited on the burden during the descent. As the temperature increases within the stack to over 900^{o}C, oxidation of coke occurs. This phenomenon occurs as the temperature continues to rise over 1000^{o}C within this zone. Despite the effects of gasification, the majority of coke degrades via mechanical abrasion. In the cohesive zone, where particles begin to soften and deformation begins, particles begin to agglomerate together. The reduced permeability due to agglomeration leads to the blast gases moving through the coke layers. The effect of coke gasification increases within this area of the furnace, the temperature is between 1000^{o}C and 1300^{o}C, therefore reaction rates are much higher than in previous conditions. During this stage, the contact between the materials within the furnace is much greater, therefore there is further mechanical abrasion on the coke particles, causing further breakdown[27].

In the active coke zone, there is a bed of permeable coke, which allows for the molten iron and slag to drip down through to the hearth of the furnace. Any remaining iron oxides are reduced via the hot coke in this area of the furnace. Also, the carbon content of the iron is increased at this stage due to the carburisation of the coke. The coke in this part of the furnace is broken down via consumption within the iron. In the raceway, where hot oxygen-enriched air is blasted through the coke in the zone, particles move at a high velocity. Also, gasification occurs in coal, which is injected via the tuyeres. The temperature in this zone is over 2000^{o}C due to the exothermic oxidation of coke. The high-velocity movement of particles ensures the coke degrades, but the high temperatures and gasification of coal generates soot, which rises to the top of the furnace and ultimately journeys to the top gas flue dust. At this point, the consumption of coke is the highest[28]. Finally, the coke descends to the hearth, where it is now referred to as the deadman structure. This structure allows molten iron and slag to accumulate before tapping. The temperature is lower in this zone as it lies underneath the reaction zones. Coke in this area can survive up to 60 days. Very little degradation occurs here, the reactivity of the remaining coke is much less within this area. Degradation does occur however, through consumption from the liquid iron, generating a carburising reaction with the liquid iron being tapped[29].

To reduce and control the amount of degradation and breakdown, the quality of the coke is measured before it is fed into the furnace. Measurements of cold strength and reactivity are taken at the laboratory. The cold strength is a relatively simple tumble test where coke is analysed for size distribution, and a known size distribution of coke is tumbled in a Micum drum. This is resized, and the measure of coke remaining over 40mm is given as an M40 value, this should be over 78% for the coke to be suitable for iron making. Any coke under 10mm is also quoted as an M10 value, this should be less than 7% of coke. This is a measure of abradability, whereas hot strength is a measure of reactivity[30]. This test is referred to as the coke strength after reaction (CSR) and coke reduction index (CRI). This test introduces 5 l/min CO_2 to a 500g coke sample in an Inconel vessel, after 1.5 hours the sample is cooled under N_2 and tumbled in a tumbling rig. The degree of breakdown before tumbling and after is measured, giving a result of CRI and CSR respectively. CRI should be <29%, which is a measure of reducibility. The value for CSR should be >58%, this considers material broken down before tumbling, and is deduced from the material which remains above 9.52mm after tumbling. Providing these quality indicators are met, and the chemistry of the coke is in line with expected values, there should be no issues with early breakdown within the furnace, and because this testing is routine, any coke that reaches the furnace has met the criteria. This information would provide more control with flue dust in the top gas generation[19].

2.6 Coal Injection in the Blast Furnace

To produce iron viably, the cost of production should be reduced. Coke is a very expensive commodity, the level of coke production at integrated steel plants often demands that coke is imported from 3rd party suppliers to maintain full operation. This has an inevitable cost for the business. Coal is used as a fuel to replace prime metallurgical coke, this has significant cost benefits to the process. 20kg of coke replaced per tonne of hot metal produced can reduce the cost of iron manufacture by £1000 per day based on extremely low coke prices[31]. Coke will never be fully replaced within a blast furnace as it is required to act as a support for the descending burden in the form of a deadman. However, reducing the consumption of coke has both a cost impact and environmental impact due to the coke manufacturing process[32]. Coal is injected through the tuyeres. In a total fuel consumption of 500kg/tHM, approximately 200kg/tHM is coal injected at the tuyeres. The injection of

coal has an impact on the coke in the raceway zone. The conditions are more severe due to the high-velocity plume of coal, which leads to coke degradation through mechanical means and chemical attack from alkali metals within the coal. Despite this, coal has an impact on reduction conditions within the furnace[33]. Coal injection will increase hydrogen within the furnace in the temperature range of 800^{o}C to 1100^{o}C. Hydrogen is effective when reducing iron oxides, hence reduction increases. Also, the remaining unburnt soot from the plume is more reactive than coke, therefore this will be used up preferentially to coke for direct reduction. Finally, the alkali metal attack on the coke is reduced, this is beneficial for the coke that falls to the bottom of the furnace since the chemical direct reduction on this coke is less, therefore the structural integrity of the coke is better at the bottom of the furnace[15].

2.7 Stages of Coal Combustion in the Blast Furnace

Coal injected into the furnace undergoes combustion, this process is complex and is both a chemical and physical transformation. As the temperature of the surrounding condition increases, the evolution of the combustion of the particle of coal follows, as shown in Figure 6[34].

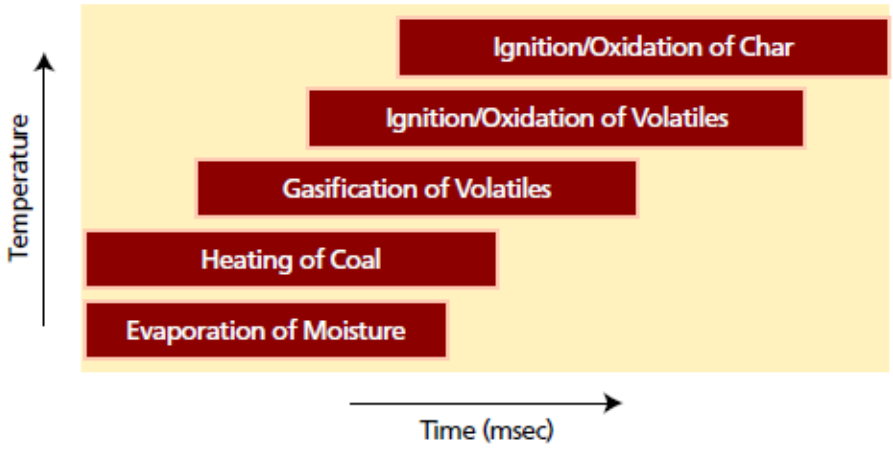

Figure 6 The evolution of the combustion of a coal particle[34]

2.7.1 Evaporation of Moisture

Evaporation of moisture or drying begins as the particle first enters the blast furnace through the tuyere. This process is limited by heat transfer and is influenced by the temperature of the surrounding conditions, particle size, moisture content, and the porosity of the coal. The blast temperature at the point the particle enters the furnace is between 1100^{o}C and 1250^{o}C, this means that the coal can experience a heating rate

of up to 10^5 K/s. This causes the inherent moisture in the coal to be lost almost instantly. Coals will absorb moisture during storage and processing, and finely granulated coals will absorb more moisture with increased surface area. The heat within the furnace is transferred to the coal via convection and radiation. This causes the transfer of moisture from within the particle, to the outer surface of the particle before rapid evaporation of moisture occurs. This stage has no impact on the further pyrolysis time, once the coal is dry, the further processes of evolution continue as expected. The coal will start to lose moisture from 105ºC. The heating rate at this stage can impact the nature of the products of pyrolysis and the char produced. Moisture is held predominately within channels of pores within the coal structure. The moisture of the coal will depend on any previous processing if it has been heated it may have lost some moisture already. Also, the humidity of the area it is stored or mined can determine the moisture content[35].

Complete drying of coal does not occur under 300ºC, therefore moisture is predominately lost above this temperature. It appears that this stage is almost instant due to the high temperatures experienced within this area. The transfer of heat to coal particles is expressed using Equation 2.7. Due to the short residence time of coal within the raceway, input coal particle size and moisture content must be controlled. This is to ensure efficient drying of the particle before it exits the raceway, which leads to increased burnout. The process of drying can be accelerated by increasing the hot blast temperature and increasing oxygen to increase the effects of the endothermic reactions[12].

$$Q = \frac{KcAp\ [(T1/T2)]}{Rp} \qquad \textbf{2.7}$$

$Where$

$Q\ =\ Heat\ Flow$

$Kc\ =\ Thermal\ Conductivity\ of\ the\ Coal$

$Ap\ =\ Surface\ Area\ of\ the\ Coal$

$T1\ =\ Temperature\ of\ the\ Coal\ surface$

$T2\ =\ Temperature\ of\ the\ centre\ of\ the\ Coal$

$Rp\ =\ Radius\ of\ the\ particle\ bound\ to\ the\ pore\ surface$

2.7.2 Heating of Coal

Following drying, the coal will reach a pyrolysis temperature; the cycle of heating to this temperature is referred to as the heating of coal. Here, the particle shrinks, and the degree of shrinkage is determined by the original moisture and coal type. As the moisture within the coal converts from liquid to steam, the overall volume increases. If pores are not sufficiently large enough to allow for an increase in volume, pressure is created. This causes cracking and breakdown of the coal particle. Also, during the heating of coal, any pores break down. The rate of heating affects the overall process of devolatilisation with an increase in heating rate releasing more volatiles from the coal. Devolatilisation is another name for this thermal decomposition process, where large organic compounds within the coal, gasify and are released. The rate of heating depends on the properties of the coal such as pore structure and particle size, as well as the temperature within the combustion zone. Smaller particles are subjected to heating rates, and with the high temperatures found at the raceway, coal can reach ignition temperature within 10 milliseconds[34].

2.7.3 Gasification of Volatiles

Gasification of volatiles follows the drying process, non-condensable light gases, tar, and char is given off the coal, and the tar gets converted to soot particles. Carboxyl, hydroxyl, and aliphatic bonds are the first groups to be gasified, due to the weak bonds to the carbon structure, these are broken at low temperatures. The bonds between the carbon atoms within the coal are broken down at higher temperatures. During devolatilisation, combustible gases are given off in the form of methane, hydrogen, and carbon monoxide, when these combust, copious amounts of energy is produced to further release volatiles. The rate at which devolatilisation occurs is governed by the thermal rate of reaction, this can be influenced by particle size, heating rates, and coal type[36].

2.7.4 Ignition/Oxidation of Volatiles

The next stage is the ignition/oxidation of volatiles. This occurs when the temperature is sufficient to ignite the gasified volatile matter. This process is very rapid and can occur within milliseconds. During devolatilisation, there are zones found within the coal particle. There is a char zone, this is the material that remains after pyrolysis is complete. Also, there is an active zone, here the material is undergoing pyrolysis. And

finally, an unreacted internal zone, here the heat isn't sufficient for pyrolysis, hence the material remains unreacted until the conditions allow for pyrolysis. Ignition of volatile matter occurs between 450°C and 500°C depending on coal type and particle size. The difference between pulverised coal injection (PCI) and granulated coal injection (GCI) would show in the ignition temperature. Pulverised coal injection is finer than the product of granulated coal injection. Free radicals are released during this process which reacts with oxygen within the furnace to produce, CO_2 and H_2O as per Equations 2.8, 2.9, and 2.10[37].

$$Volatile\,(HC) \leftrightarrow CO_2 + H_2O \quad \textbf{2.8}$$

$$Volatile\,(HC) \leftrightarrow CO + H_2O \quad \textbf{2.9}$$

$$CO + {}^{1}/_{2}\,O_2 \leftrightarrow CO_2 \quad \textbf{2.10}$$

During the initial stages of pyrolysis, the weak bonds, mainly the C-H bonds are the first to break down. There is an increase in aromatic hydrogen concentration, due to the fragmentation. Depending on the size of the fragment, smaller fragments will vaporise as tar. Following this, at higher temperatures, cross-linking reactions occur to aid in the production of methane (CH_4). If methane is not produced, the larger fragments are likely to react with each other to produce large aromatic compounds, these are difficult to vaporise and require higher temperatures to do so. During devolatilisation, there is a softening and solidification of the coal itself. This is due to gases being released, which changes the particle structure. The residue that remains is described as a char. This char should have ignited in the raceway, if it has not, there is a high chance that the char will exit the furnace in the top gas. In terms of oxidation, the gas phase oxidation occurs away from the coal particle, due to the release of volatile matter. During pyrolysis, as the reaction slows, the release of the volatile matter becomes less, this brings the flame front closer to the coal particle. Once pyrolysis is almost complete, the gas phase flame front is in contact with the coal particle. This allows for oxygen to be in contact with the char surface and pores allowing oxidation to commence. Oxidation occurs in the latter stages of pyrolysis when the conditions are consistent. For this to occur, the volatile matter should be released and ignited uniformly, if not oxygen is unable to reach the char surface in a timely manner. This can mean that the char and volatile are pyrolyzed in parallel. This

is slower than the homogenous gas phase reaction and will allow for char to leave the raceway without igniting or oxidising completely[38].

2.7.5 Ignition/Oxidation of Char

The final stage is the ignition/oxidation of the chars produced. This is a relatively slow process, and completion of this stage is dependent on the residence time of the coal within the furnace. The reaction begins with the carbon on the surface of the coal particle oxidising to carbon monoxide (CO) or carbon dioxide (CO_2). At lower temperatures, the reaction favours the oxidation of carbon to CO_2. It is important to note at higher temperatures, that carbon oxidises to CO at the surface, to allow for further oxidation to CO_2 away from the char. The process rate is controlled by the rate of oxygen diffusion to the particle and the rate of reaction. At low temperatures, the oxidation of char is controlled by the chemical reaction rate. At higher temperatures, the rate of oxidation is controlled by the oxygen diffusion to the char surface. At moderate temperatures, a combination of the two controls the rate of oxidation. The rate of reaction and oxidation can be mapped out and predicted by global reaction or intrinsic reactivity models. Global reaction models are based mainly on the activation energy of the reaction; therefore, this creates a limitation on the accuracy of the prediction due to the complex nature of the material in question. Intrinsic reactivity models use the absolute reaction rate when analysing the reaction on the char surface. The intrinsic reactivity models do not consider the effects of pores within the material itself and can't produce accurate predictions of oxidation[39].

During the combustion of char, fragmentation is likely, reducing the initial particle mass and increasing the surface area of the char. This increases the rate of reaction providing a false prediction of coal combustion. The reaction of the solid residue char after the combustion of volatile matter is known as the post-flame zone. The oxidation of char is the largest contributor to the heat released during combustion. The rate at which the reaction occurs is dependent on the diffusivity of the oxidiser within the furnace which can include oxygen, hydroxides, and carbon dioxides. Due to the porosity of coal char, it has a very large surface area for the reactions to occur. The temperature required to overcome the activation energy is high, and heat transfer to the particle is required. The rate of heat transfer is expressed as a heat transfer coefficient[12]. The rate of reaction is given in Equation 2.11.

$$RC = \frac{Ap\ mox}{(1/Kf + 1/Kc)} \quad \textbf{2.11}$$

$Kc = Chemical\ Reaction\ Constant$

$Kf = Mass\ Transfer\ Constant$

$Ap = External\ surface\ area\ of\ the\ particle.$

$mox = Mass\ of\ the\ char$

$The\ reaction\ constant\ Kc\ can\ be\ expressed\ by\ using\ an$

$effectiveness\ factor\ and\ intrinsic\ chemical\ reaction\ rate\ constant$

$$Kc = \frac{ήiKsAsdp(\rho)}{6}$$

$$ήi = \frac{1\ (1/Tan(3\Phi) - 1/3\ \Phi e)}{\Phi e}$$

$$\Phi e = \frac{dp}{6}\sqrt{\frac{KsAs\rho}{De}}$$

$ήi = Effectiveness\ factor$

$\Phi e = Thiele\ Modulus$

$As = Surface\ Area\ of\ the\ particle$

$dp = Particle\ Diameter$

$\rho = Density\ of\ char$

$De = Effective\ Diffusity$

$Ks = Radiation\ Coefficient\ of\ the\ Surface$

When the Thiele modulus is less than 0.1, the reaction occurs within the particle itself. When this number reaches over 5, the reaction takes place only near the surface. This process is described as diffusion-limited combustion, due to the location of the reaction being relative to Thiele's modulus. In events of low temperature and small particle size, the reaction kinetics of oxidation is important to control the char oxidative kinetics. For small particles both diffusional and kinetic resistances are important. In terms of a blast furnace, in the raceway, both char and coke are trying to diffuse with oxygen. Both are competing for diffusion. The reaction mechanisms for both coal and

coke are the same, however the reactivity changes, due to the difference in chemical and physical structure[40].

To effectively predict the reaction rate, knowledge of oxidiser concentration and reaction rate as a function of the char surface area is required. Different coals will burnout differently under the same conditions due to differences in the structure of the char residue produced. The resistance to diffusion due to the large surface area within the porous structure can be different due to variations within the pore structure from coal to coal. The porous structure creates a large surface area within the coal particle; however, the pore channels are small, which creates a natural resistance to diffusion. Effective diffusivity within the porous char particles is further reduced by the volume fraction of voids in the particle. Another factor is the fragmentation of char, this can reduce initial particle mass by up to 30%, and this influences char reactivity and ash formation[41]. The fragmentation increases the total external particle surface area, which increases the rate of reaction. With fragmentation and changes in particle structure during combustion, the reaction rate will fluctuate. Initially, when pores grow and surface area increases, the reaction rate increases. When pores collapse due to fragmentation, the surface area decreases, and the reaction rate decreases. The importance of particle size can be seen in the overall coal burnout. Burnout is better for the smaller particle size of pulverised coal injection, as opposed to worse burnout in granulated coal injection processes. The difference is due to the difference in surface area to mass ratio. Despite being described as a separate reaction, the oxidation of char is coincidental with the devolatilisation and combustion of volatile phases of the reaction[41].

2.8 Optimising Coal Burnout in the Raceway

Coal burnout potential has been a heavily researched field and it is thought the understanding of coal burnout and coal properties relates to the usefulness of the material as a blast furnace injectant.

2.8.1 Coal Properties for Injection

Coals and other materials such as biomass or polymers are typically blended for use as an injectant into the furnace, at the GCI plant[43]. The properties of an injectant are important to ensure that the desired effect on the furnace is realised. The injectant is required to combust in the raceway, providing the heat and carbon required for the

Boudouard reactions for iron reduction, whilst fully gasifying, reducing the impact on the dust generated by the process[44].

Coals selected for injection are normally anthracitic high-rank coal or bituminous medium-ranked coals as per Figure 7[45]. The high fixed carbon within these types of coal provides the carbon for reaction with oxygen to form CO_2 and CO for the reduction of iron ore to iron[33]. Injection coal properties are usually controlled through the blending of various coal types to achieve the desired criteria such as cost, slag formation, volatile matter and ash constituents which has been discussed further using the work of Shan Wen Du *et al.* in section 2.8.3 of the literature review. The ability for coal to fully gasify within the raceway is critical to coal originating carbon reaching the dust. When conditions for complete gasification are not favourable, there will be a net gain in dust produced by the process, which is an undesired effect[46]. Although coal type and properties are not a lone influence on coal combustibility in the raceway, the correct blend quality certainly contributes to this.

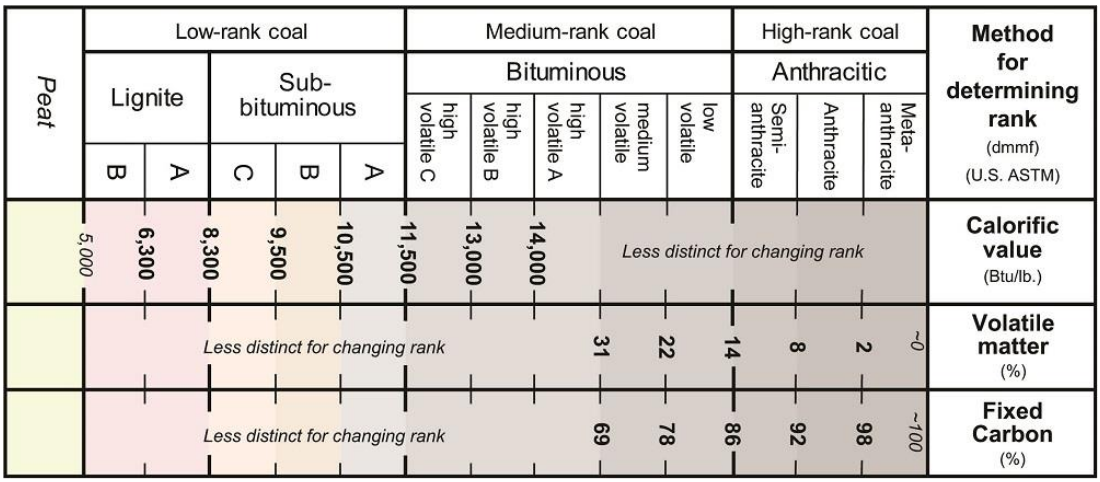

Figure 7 Coal rank system[45]

2.8.2 Coal in the Blast Furnace Raceway

The raceway is a section of the furnace around 0.5m and 1.5m long at the bottom of the furnace, where the hot air and coal enter, this is confirmed in the raceway measurements carried out in the *Charfoco* report[49]. Here the conditions are most favourable for coal combustion, with temperatures in excess of 2200^{o}C and the atmosphere enriched with oxygen[47]. It is unlikely that char or coal leaving this section of the furnace will combust further on the journey to the top of the furnace, because the temperatures and gas conditions become less favourable with depleting oxygen conditions and lower temperatures when ascending the furnace. With

increased moisture of the coal or, larger particle size and lower coal reactivity it is less likely that the five key stages of combustion outlined in section 2.7 will be complete, causing the coal to form a char instead of a gas[48]. A work package within the *Charfoco* report aimed to optimise measurement methods for monitoring the raceway, including depth, gas composition, and temperature. Mathematical modeling was used to position instruments and different techniques were piloted. Furnace trials at Port Talbot showed that raceway temperatures increased with decreased coal injection rates and alkali metal concentrations varied with injection rates. Raceway measurement during two campaigns revealed two detectable size levels, and larger tuyere diameters produced longer, higher-level raceways. Laser and radar sensors were planned for continuous implementation to evaluate operational conditions and their impact on flue dust. Lowering injection rates resulted in increased temperature, thus suggesting a theory that coal injection has a cooling effect on the flame front[49].

2.8.3 Experimental Coal Burnout Studies

The drop tube furnace (DTF) has been used extensively as a research tool for coal burnout as it recreates the high temperatures and short residence times of the raceway. Work by Tiwari *et al.*, Shan Wen Du *et al.*, Thong *et al.* and Steer *et al.* has all been conducted using variations of a DTF as similar to the one used by Shan Wen Du *et al.* that is depicted in Figure 8[50].

.

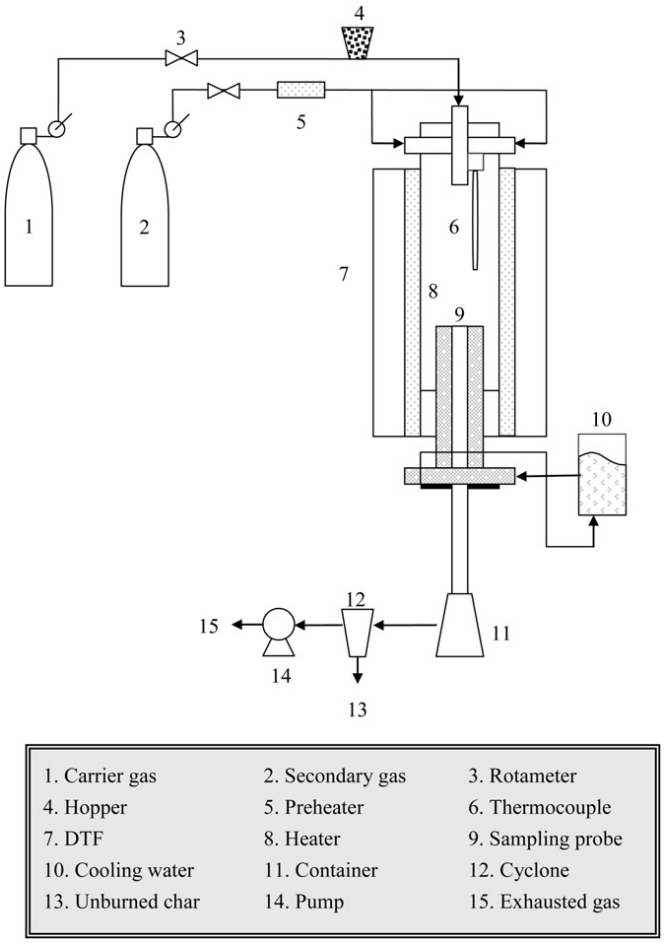

Figure 8 Drop tube furnace set up[50]

Tiwari *et al.* used the drop tube furnace to compare experimental data for coal burnout potential with actual burnout in the DTF, the coal for the experiment was initially dried at 110^{o}C in an air atmosphere, in a drying oven. The material was fed through a vibratory feeder at a rate of 1.5kg/hr. The combustor was set at 1000^{o}C. The oxygen levels varied depending on the test, these levels were 21%, 25%, and 31%[51]. Tiwari *et al.* derived a prediction model which was aimed at calculating burnout potential of a coal based on its physical properties, the CBP model is represented mathematically as per Equation 2.12[51].

$$CBP\ of\ Coal = \frac{r - s - t - u}{v + w - x} \quad \textbf{2.12}$$

$where$

$r = 500\ \times\ (\%C + (2.1\ \times\ Ash) + (2\ \times\ IM) + VM)$

$s = 5\ \times\ (\%C + VM)\ \times\ (IM + (1.1\ \times\ Ash))$

$t = 5\ \times\ \left(IM^2 + (1.1\ \times\ Ash^2) + (2.1\ \times\ Ash\ \times\ IM)\right)$

$u = 5\ \times\ 10^4$

$v = 500\ \times\ \%H$

$w = (IM\ \times\ Ash)\ \times\ O$

$x = 100\ \times\ H$

$IM\ =\ Inherent\ moisture$

$VM\ =\ Volatile\ matter$

$\%C\ =\ Elemental\ carbon\ \%$

$\%H\ =\ Elemental\ hydrogen\ \%$

$O\ =\ Elemental\ oxygen\ \%$

$Hence$

$$CBP\ of\ Coal\ Blend = \sum (CBP\ of\ Coal\ \times\ W_{tp})$$

$Where$

$W_{tp}\ =\ Proportion\ of\ individual\ coal$

For each coal type and blend, Tiwari *et al.* reports a positive correlation between CBP and calculated burnout at the various oxygen concentrations. The graphs as per Figure 9, show that as the calculated CBP of the coal blend increases, the degree of burnout also increases[51].

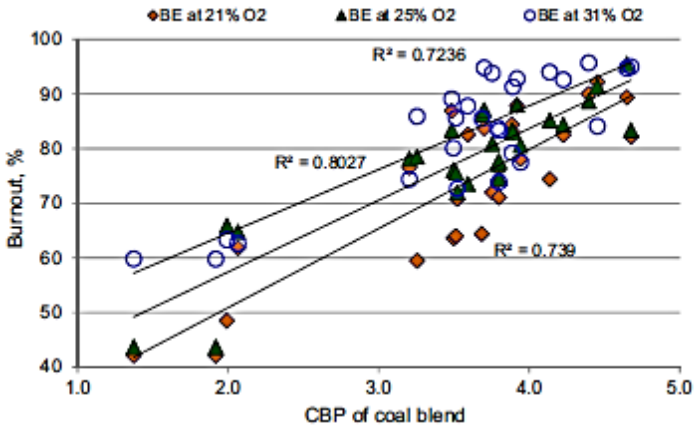

Figure 9 Effect of CBP on burnout[51]

The paper surmises that the CBP of an individual coal and coal blend can be used to estimate the degree of burnout. It also shows that burnout efficiency increases with increased oxygen concentration. The paper is a forward step in estimating burnout efficiency based on the measured properties of the coal[51].

A paper outlining a technique to predict coal conversion behaviour in the blast furnace was written by Thong *et al.* [52]. Thong *et al.* derived a five stage model for predicting coal burnout based on the physical and chemical properties of the coal. This paper considers more properties than the work of Tiwari *et al.* The first parameter was the chemical parameter, this was based on the volatile matter and fixed carbon values. Parameter 1 (P_1) was derived using Equation 2.13. Thong explains that volatile matter leaks from coal and ignites at lower temperatures than carbon, leaving the residue with an increased surface area. This accelerates the conversion process. Fixed carbon supplies carbon for oxidation, to produce the gas for the reduction process in the blast furnace.

$$P_1 = \frac{C_{fix}}{VM} \qquad \textbf{2.13}$$

$$C_{fix} = Fixed\ carbon\ content$$

$$VM = Volatile\ matter\ content$$

The second parameter is the petrographic parameter (P_2). This focuses on the detection and quantification of macerals within the sample. Macerals within coal can often differentiate between otherwise chemically similar coals. Thong's technique incorporates the main three maceral groups, liptinite, vitrinite, and inertinite. Liptinite

lends itself to high conversion due to the increase in hydrogen, this is accounted for in Equation 2.14[52].

$$P_2 = \frac{L + V/R^2}{I^{1.25}} \quad \textbf{2.14}$$

$L = Liptinite\ content$

$R = Vitrinite\ reflection\ degree$

$V = Vitrinite\ content$

$I = Inertinite\ content$

The third parameter is the physical parameter (P_3). Thong *et al.* describe one of the most influencing physical characteristics as being microstructure. The influence on conversion is driven by specific surface area. As described previously, the BET process was used to analyse the specific surface area. Image analysis of a 100x magnified image of the pulverised raw coals was carried out to determine the porosity in terms of density. Equation 2.15 combines the two equations, into a single equation[52].

$$P_3 = \frac{P}{A_s} \quad \textbf{2.15}$$

$P = Porosity\ based\ microscopy\ of\ coal's\ cross\ section$

$A_s = Specific\ surface\ area$

Parameter four (P_4) is the kinetic parameter. Thong suggests that coal conversion occurs in the raceway during the 30-50ms residence time. Activation energy is deemed important as this is the barrier required to be overcome before the reaction occurs, in such a tight time frame. High activation energy coals would require longer residence times, hence lower conversion. The activation energy was determined using a Tammann furnace setup, similar to a TGA the mass loss is calculated while under different isothermal conditions, the exact details of which were not disclosed. Parameter four is simply quoted as activation energy as per Equation 2.16[52].

$$P_4 = E_a \quad \textbf{2.16}$$

$E_a = Activation\ energy\ (kJ/mole)$

The final parameter (P_5) is an external parameter. For the combustion of coal and conversion, oxygen is required. Thong *et al.* outline that their previous research has confirmed the influence of the O/C atomic ratio on the conversion degree. If this ratio is <1, he confirms that only pyrolysis and gasification occur. Complete combustion occurs in coals with a ratio of >2. Parameter five accounts for this ratio using the amount of atomic carbon and oxygen particles in Equation 2.17[52].

$$P_5 = \frac{O}{C} \quad \textbf{2.17}$$

$$O = Amount\ of\ atomic\ oxygen\ particles$$

$$C = Amount\ of\ atomic\ carbon\ particles$$

η_{BIR} is a value of conversion in terms of percentage as measured from the BIR. η_{theor} is a theoretical value based on the five parameters outlined previously.

$$\eta_{theor} = a \times (P_1)^2 - b \times (P_1)^2 + c \times (P_2)^2 + \frac{d}{(P_3)^e} + f \times P_4 + g \times P_5 + h \quad \textbf{2.18}$$

$$\eta_{theor} = Calculated\ conversion\ degree$$

$$a - h = Constant\ coefficient$$

[52]The difference between the calculated conversion degree and the experimental can be seen in Figure 10. There is a good correlation that can be observed. This paper outlines that it is possible to predict the outcome of coal in a raceway based on analysis. One concern surrounding this topic is the relatively small dataset analysed. With a vast variety of PCI and GCI coals available for purchase and the great ranges in properties, this is a relatively small dataset[52].

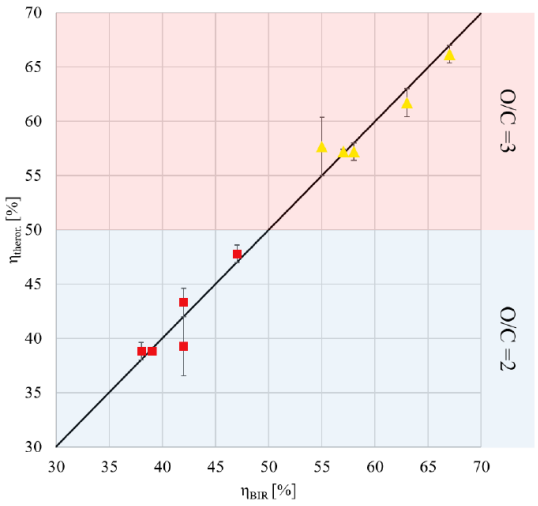

Figure 10 Comparison of conversion degrees[52]

Shan-Wen Du *et al.*, also investigated the pulverised coal burnout in the blast furnace, simulated by a DTF[50]. Binary blends were tested under DTF conditions, to simulate the conditions when injecting fuel coal into the blast furnace. It was outlined that blends of coal are used to reduce the cost of PCI operations [50].

The fuel ratio which was the equivalent of volatile matter to fixed carbon ratio, was used to compare against the burnout of the coal. The initial findings as per Figure 11 show good repeatability of the experiment and a direct correlation between burnout and fuel ratio when analysing material from 100-200 mesh with the exception of coals A and C. Fuel ratio is outlined in Figure 11. The difference was suggested by Shan-Wen Du *et al.*, to be attributed to the maceral and mineral content within the coal. Coal A as opposed to B has high vitrinite and lower inertinite concentrations. Vitrinite is more reactive than inertinite or liptinite hence the low concentration of vitrinite can be attributed to low burnout[50].

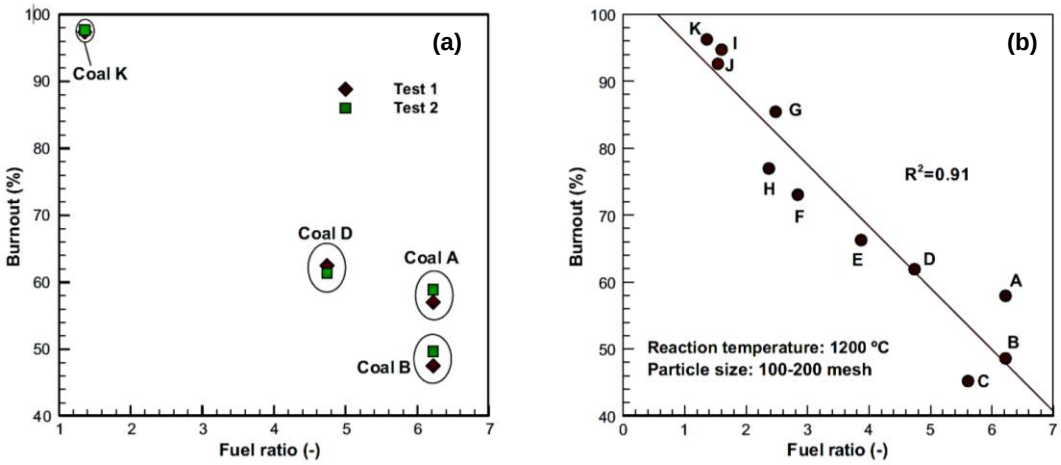

Figure 11 Fuel ratio of coals and burnout a) Coal A, B, D, K b) All coal within the study [50]

According to Figure 12, the experimental work also shows that with an increase in reaction temperature, there was an increase in subsequent burnout. The effect of temperature is more profound in coals with a higher fuel ratio, than those with a low fuel ratio such as Coal I. It is stated that an increase in blast temperature would promote less unburnt char, ascending the furnace and exiting in the flue dust[50].

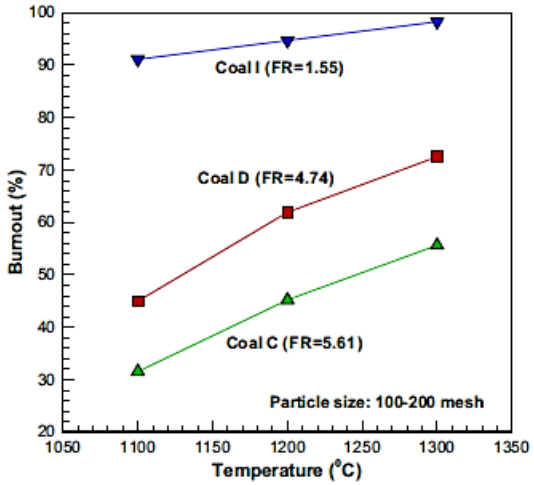

Figure 12 Effects of temperature on burnout[50]

Also investigated was the effect of particle size. As coal particle size decreases, the degree of burnout increases. This effect can be attributed to the increase in reaction surface. The effect is witnessed in the difference between granulated coal injection and pulverised coal injection. There is an improvement seen with pulverised coal injection due to the increase in reaction surface. The improvements witnessed are often offset by the cost of pulverisation, as opposed to granulation. The effects are depicted in Figure 13[50].

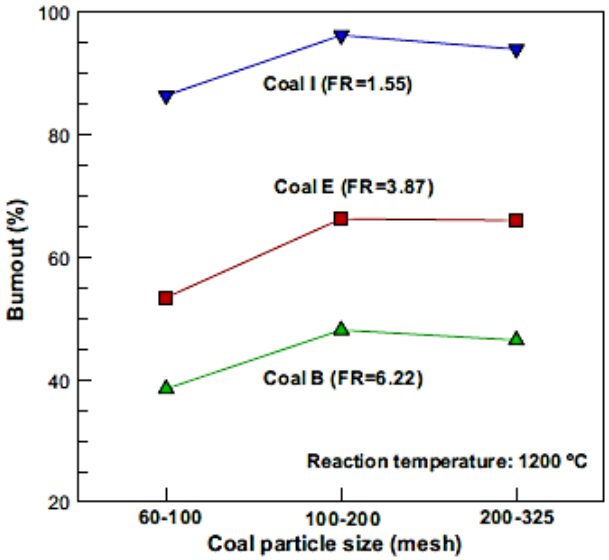

Figure 13 Effect of particle size on burnout[50]

The final series of experiments was the effect of blending coals with higher and lower fuel ratios. The reaction temperature was maintained at 1200^{o}C, and the particle size was tightly controlled at 100-200 mesh, to negate the effects of these individual parameters. As per Figure 14, the burnout behaviour of blended coals can be predicted linearly, based on the burnout behaviour of the individual coals within the blends[50]

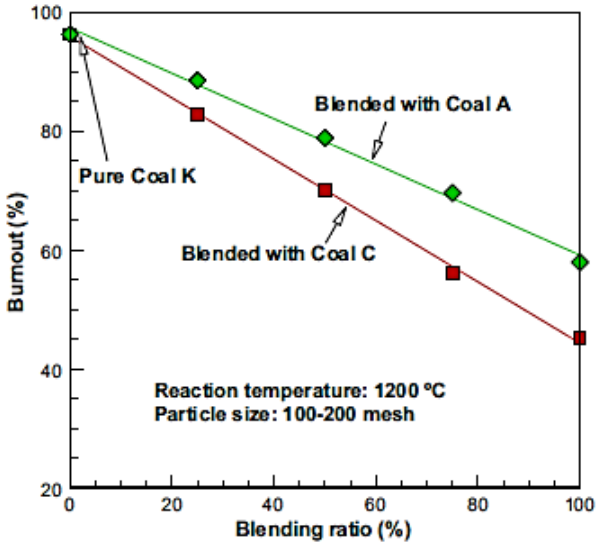

Figure 14 Effect of blending ratio on burnout[50]

Steer et al. used the DTF to evaluate the effect of particle grinding on coal burnout. The burnout analyses carried out in this series of experiments, concluded that with increasing volatile and residence time, burnout increases. A note to mention, as

per Figure 15, some of the larger particle sizes had higher burnouts than the smaller ones. It was indicated that additional grinding could be detrimental to the burnout of the smaller-size fractions. It was also observed that at low residence times, the additional grinding required to produce the smaller size fractions, had a negligible impact on burnout on the low volatile coals. The differences seen can have an important implication for the processing of coal. The results indicate that some coal types do not need to be processed as much as others, this could result in a cost-saving[54].

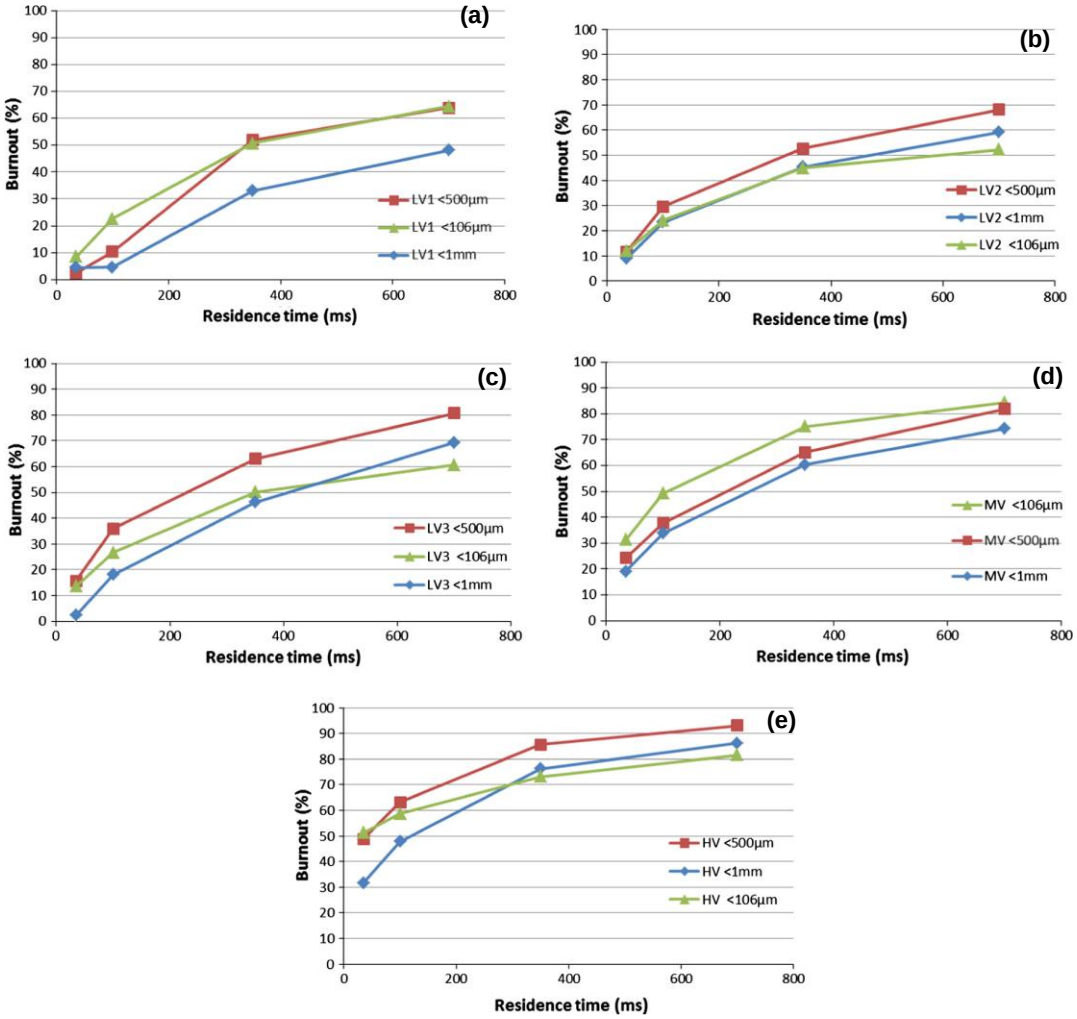

Figure 15 The effects of residence times on burnout with various coals at <106µm, <500µm and <1mm a) LV1 series b) LV2 series c) LV3 series d) MV series e) HV series [54]

An observation made during the analysis was that the chars produced, all seemed to have different physical sizes and shapes, depending on the size and coal type used to produce the char. Larger coal PSD's tended to fragment, whereas smaller coal PSD's tended to swell when char was produced, as shown in Figure 16. It can be seen that for the larger coal PSD, high volatile (HV) and LV1 and LV2 coals

fragmented the most LV in this case refers to low volatile content coals. The mid volatile (MV) coals changed little at 35 ms but for the <106-micron classification, MV and HV samples had the larger swelling. The degree of swelling, according to Steer *et al.* is important; the increased porosity and open network of a swollen char allows for increased gas diffusion. A fragmented char would have increased surface area, with a fractured internal surface that could have different surface chemistry. Despite the effect of fragmentation and swelling being rather profound, there was no correlation between these effects and overall burnout. It does however explain why burnout of larger particle classifications does not differ as significantly from the smaller particle classification as expected[54].

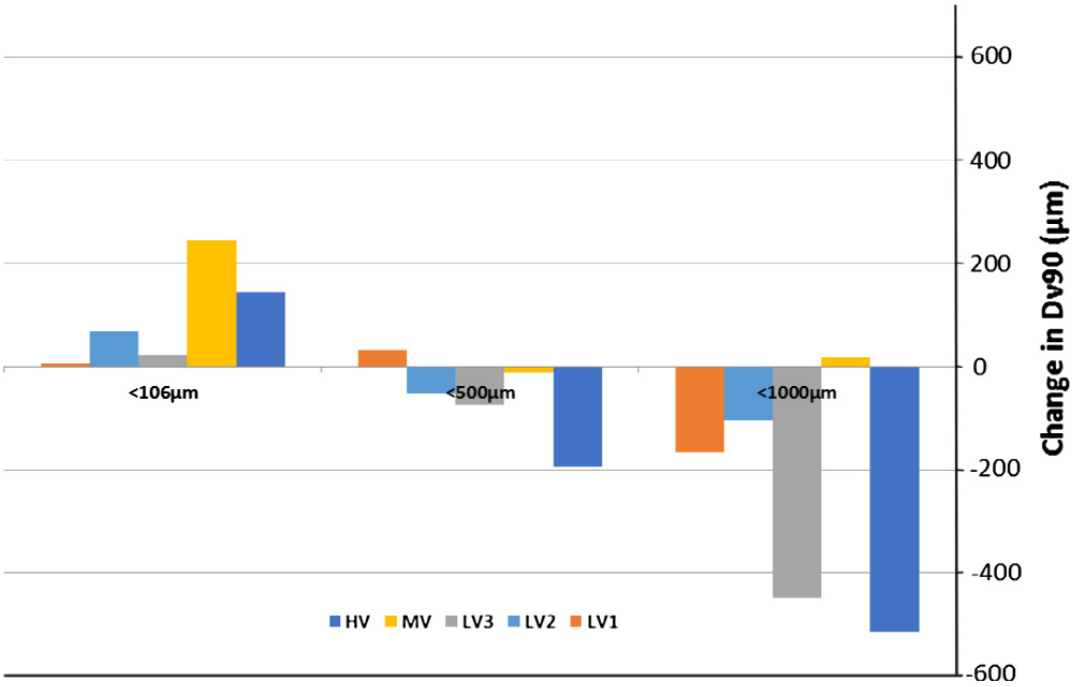

Figure 16 The difference in DV90 of particles[54]

Steer *et al.*, investigated the theory that minerals within coal can impact the combustion and gasification of the coal. Powder X-Ray Diffraction (XRD) analysis was carried out on the char obtained from the DTF to quantify the presence of such mineral phases. The increased levels of mullite and cristobalite in LV2, LV3 and HV coals of larger size and longer residence times can be attributed to better burnout. These minerals have been shown to improve the rate of combustion. Also, the changes in illite present with the changing particle size and residence times, suggest that it converts to another phase or forms a non-crystalline, amorphous phase more readily in <500-micron particle-size coals. Potassium within the illite has been shown to

improve combustion in coal, this could illustrate the improvements in these coals for burnout[55].

Further techniques were used to understand the effects of grinding on the surface chemistry of the coal using the XPS technique. The spectra for the chars obtained after a residence time within the DTF of 700 ms had greater peak asymmetry and peak shoulders in the higher binding energy region. This was associated with more carbon-oxygen bonding. The spectra indicate that grinding, changes the surface chemistry, either by reducing the number of reactive functional groups, or the physical effects with different particle sizes[54].

Finally, Steer *et al.* also investigated the surface chemistry using the Carbon Auger Electron Spectroscopy technique. This technique involves the use of an electron beam to excite the electronic states of near-surface atoms. When the atoms decay from the excited state, auger electrons are emitted. The results in Table 2 showed the dominant bonding within the chars was SP3. When grinding the coals to a smaller particle size, there was a reduction in SP2, this gave a much-improved burnout profile for LV1 coal compared to grinding the other coals. Also, the chars from LV1 have higher SP2 bond character, this increase suggests thermal structural ordering of the carbons related to the SP2 bonding. Which has been linked to reductions in char reactivity. The smaller particle size classes of each coal had lower SP2 character compared to the larger classes, and higher char burnout at low residence time. This trend was also reflected with HV, LV2 and LV1 coals. On the contrary, the results indicated no direct correlation between the SP2 for each of the coals and burnout. This suggests that other variables such as swelling, fragmentation, and surface oxygen bonding are likely to play the dominant role in the reactivity of the coals[54].

Table 2 XPS carbon auger[54]

XPS Carbon Auger (C_{KLL}) *D* parameter and sp^2 bonding character of coal samples.

	D (eV)	% sp^2 (absolute)
Graphite[a]	22.5	–
Diamond[a]	14.3	–
LV1 106 μm	14.2	0.0
LV1 500 μm	15.1	8.2
LV1 1000 μm	16.5	20.8
LV2 106 μm	14.2	0.0
LV2 500 μm	14.6	3.5
LV2 1000 μm	15.2	9.0
HV 106 μm	14.4	1.3
HV 500 μm	14.2	0.0
HV 1000 μm	14.4	1.3

[a] Lascovich et al. [55].

Charfoco was a collaborative report written for the European Commission research fund for coal and steel included inputs from Tata Steel, Aachen University, ArcelorMittal and the ASBL centre of metallurgical research. The report summarises a series of testing packages carried out at these establishments to understand some of the reasons for varying coal levels in the flue dust. The report applies knowledge of the coal evolution cycle to real-life scenarios and explains the effects of varying conditions on the combustion and consumption of coal in the raceway[49].

The first of the work packages investigated coal conversion, char production, characterisation and the interaction with coke and iron ore reduction conditions. The conversion was investigated using two different sample types, the first was PCI (Particle size 90-125 μm) and the second GCI (50% < 250 μm, 100% <1000 μm). However, four coals were used overall for this trial fitting within the two sample types. The results showed that the conversion degree of PC coals was higher than GC coals under the same conditions simulating the first part of the raceway. This was expected due to the increased surface area for reaction. The chemistry of the coals influenced coal conversion, particularly the volatile matter content, low volatile appeared favourable for conversion. Also investigated were micro-structure, ash content and specific surface area although these had less of an impact on conversion. It appeared that char experiencing low conversion could be characterised by numerous dense particles in the microstructure which did not undergo reaction. The reactivity of coal seemed dependent on volatile matter and the reactivity of char was dependent on the

surface area[49]. As part of the report, Oxygen enrichment was investigated at CanmetEnergy, it was observed that increased oxygen content showed no significant effect on the conversion degree. The overall conclusion for the conversion trials was that complete conversion could not be reached under high injection rate conditions [49].

Wing *et al.* explored a study of PCI coals in a new injection rig at CanmetEnergy as per Figure 17. The coals were injected into the bench-scale coal injection facility where the Air is preheated and maintained at 1350^{o}C through the reactor. The carrier gas used to maintain an inert atmosphere is N_2. The coal following combustion exits the reactor and is cooled by water at the quench stations. The final residue is filtered and dried before analysis [55].

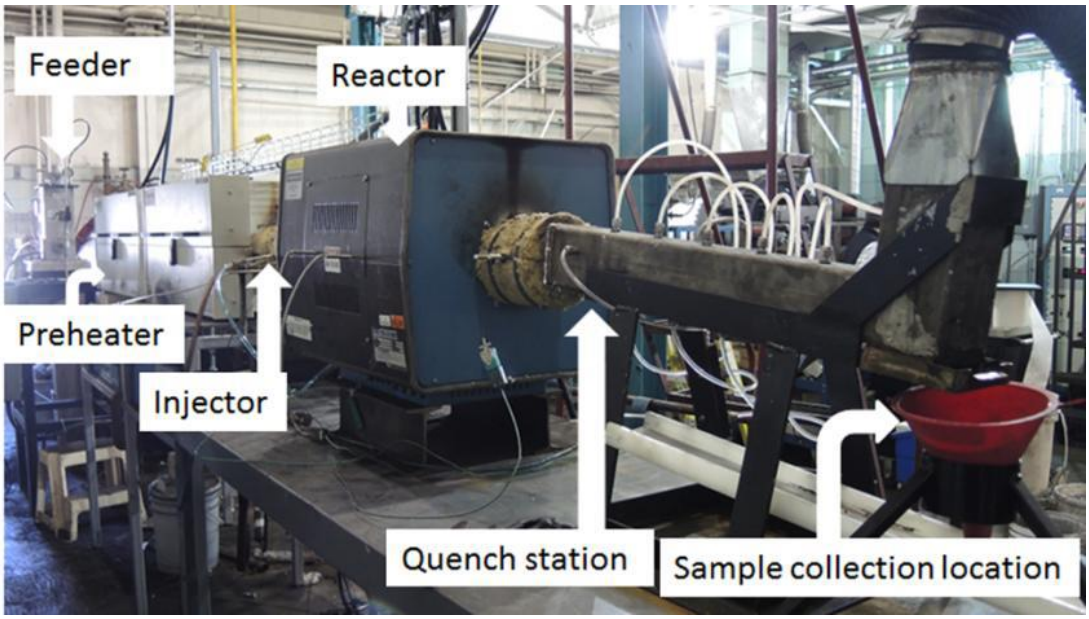

Figure 17 New injection rig and facility in Ottawa[55]

The combustibility of the coals was measured and calculated, and the results for 21% O_2 atmosphere show a heavy reliance of parent coal volatile matter on the degree of burnout. As expected, high volatile coals displayed a high degree of burnout. When changing the oxygen atmosphere percentage, there is a similar trend as per Figure 18[55].

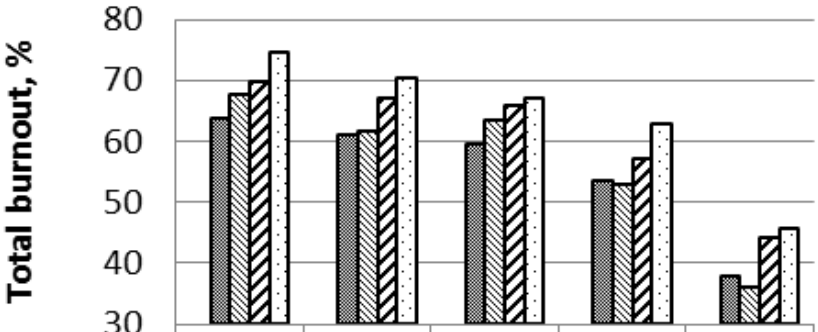

	A	B	C	D	C
VM	36.86	33.78	30.10	24.69	16.44
21%O2	63.59	60.92	59.48	53.44	37.71
23%O2	67.59	61.66	63.47	52.9	35.88
25%O2	69.9	66.96	65.78	57.2	44.15
28%O2	74.47	70.38	67.12	62.84	45.74

Figure 18 Burnout at varying oxygen atmospheres[55]

Wing *et al.* discuss that the increase of volatile matter allows for a greater amount of rapid gas evolution, within the coal particle. Cenospheres form within the particle which will not only combust readily but provide extra surface area. Cenospheres are characterised as low-density, irregular porous structures that are created as a by-product of the coal combustion process and are predominantly comprised of non-metallic materials and minerals, and most importantly, char[56]. When coal volatile decreases, exinite and liptinite levels within coal decrease, and the remaining vitrinite will convert into a coke-like structure rather than forming cenospheres. These coke structures are less combustible than cenospheres, based on the surface area[55].

Dry ash-free carbon forms (DAF) were analysed. It was found that the amount of char within the carbonaceous material decreases with the increase in oxygen. The variation of coke in the sample is much smaller for many of the coals. Wing *et al.*, suggest that the information displayed in Figure 19 and Figure 20, means that with an increase in oxygen level, more char is consumed in the raceway. Also, low-volatile coals produce larger amounts of coke during combustion due to differences in petrographic components such as exinite/liptinite and vitrinite[55].

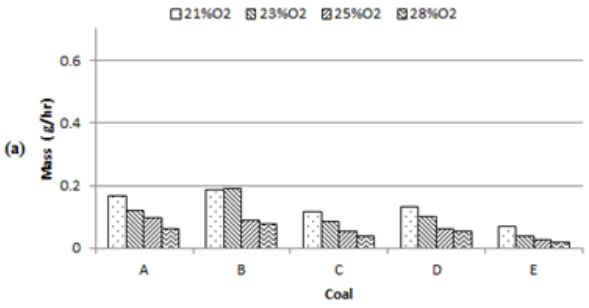

Figure 19 DAF values at varying oxygen levels for the different coal types[55]

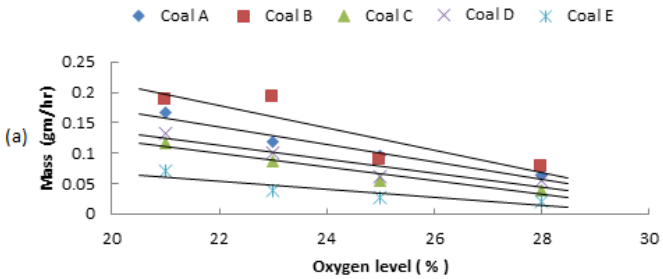

Figure 20 DAF values at varying oxygen levels for the different coal types[55]

The BET analysis as per Figure 21 shows that low volatile coals show lower surface area in comparison to other coals at all O_2 levels. Coal A had the only variation in surface area with varying oxygen enrichment conditions. There is no conclusive relationship. However, when Barrett-Joyner-Halenda's (BJH) analysis was carried out for cumulative micropore area, it was discovered that low volatile coals had decreased micropore area. Similar to BET analysis, BJH used the data from an N_2 adsorption test, accounting for the volume of adsorbate relating to pressure, a mesopore distribution can be calculated. BJH is more comprehensive than BET as it accounts for both macro and micro pores within a solid structure. This may show that low-volatile material is less reactive than high-volatile coals. However, Wing *et al.* suggest that before this conclusion can be drawn, further work must be carried out to test the hypothesis[55].

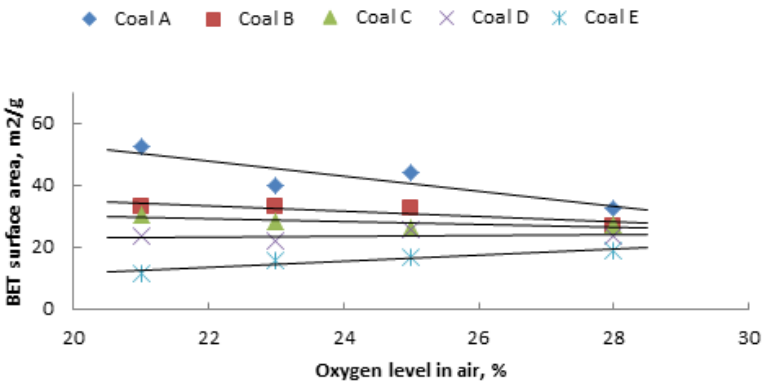

Figure 21 BET surface area analysis at varying oxygen levels[55]

2.9 Coal Char Formation, Reactivity and Transportation in the Blast Furnace

Despite optimisation of coal injection, the work using DTF experimental rigs outlined in section 2.8.3 shows that char generation is inevitable. This solid char is likely to be carried over and transported to the dust and hence work by Pohlmann *et al.*, Sima-Ella and the *Charfoco Report* has been aimed at understanding what happens to the char in the blast furnace after it has been produced.

2.9.1 Coal Char Formation

Pohlmann *et al.* investigated the reactivity to CO_2 of chars prepared in O_2/N_2 and O_2/CO_2 mixtures for PCI in a blast furnace relating to char petrographic characteristics[57]. The chars produced were produced using a DTF with the varying gas mixtures. An important consideration during the preparation of the materials in this work showed that grinding coal using a swing/ring mill generates heat, if this technique is used in future work it may contribute to a loss of moisture[57].

According to Pohlmann *et al.*, the injection of coal in a low oxygen atmosphere, <2.5% O_2 in an N_2 atmosphere, produces devolatilisation without significant combustion. At 10% O_2, burnout can be of the order of 60-90%, based on the mechanisms of conventional combustion and oxy-combustion atmospheres. The introduction of CO_2 was an attempt to recreate conditions higher up in the furnace. Burnout was calculated using Equation 2.19, this is based on the assumption that ash in the material did not transform any further than during the standard ISO ash test[53,57].

$$Burnout\ (\%) = \left[1 - \left(\frac{Ash_{Coal}}{100 - Ash_{Coal}}\right)\left(\frac{100 - Ash_{Char-comb}}{Ash_{Char-comb}}\right)\right] \times 100 \qquad \textbf{2.19}$$

The resultant chars were analysed using an optical microscope and examined using incident polarized light using a lambda retarder plate. The Brunauer-Emmett-Teller (BET) test was carried out coincidentally with Dubinin-Radushkevich testing to calculate the surface area. These two methods complimented each other, the CO_2 doesn't fill large pores well from the Dubinin-Radushkevich test and the N_2 from the BET has a slow diffusion rate. The resultant chars were tested also for reactivity to CO_2, at high temperatures. The analysis was carried out thermogravimetrically, where an 8mg sample of char was heated to 1000°C under an N_2 flow of 60ml min^{-1} at a heating rate of 30°C min^{-1}. The reactant gas was changed to CO_2 and the flow rate and temperature were maintained until there was no further weight loss. These weights were considered using Equation 2.20, where m_o is the initial sample weight and m is the instantaneous sample weight[57].

$$x = \left(\frac{m_o - m}{m_o}\right) X\ 100 \qquad \textbf{2.20}$$

The formula for apparent reactivity at $R_{50\%}$ on an ash-free basis was calculated using Equation 2.21[57].

$$R_{50\%} = \frac{1}{m_o}\left(\frac{dm}{dt}\right)_{50\%} \qquad \textbf{2.21}$$

An estimate of the intrinsic reactivity of the carbonaceous material within the char, once the effect of surface area has been subtracted, is given by the apparent reactivity, divided by the surface area. According to Pohlmann *et al.*, the morphology of the chars generated using the O_2/CO_2 and O_2/N_2 conditions, were identical. The particles with high concentrations of vitrinite generated cenospheres with incipient anisotropic optical texture. This was found in the high volatile bituminous coal. Also, small anisotropic domains in the mid-volatile bituminous coal and well-developed

anisotropic domains in the low-volatile bituminous coals were observed. These can be seen in Figure 22, where a and b refer to the high-volatile bituminous coals, c and d are the mid-volatile bituminous coals, and e and f are the low-volatile bituminous coals[57].

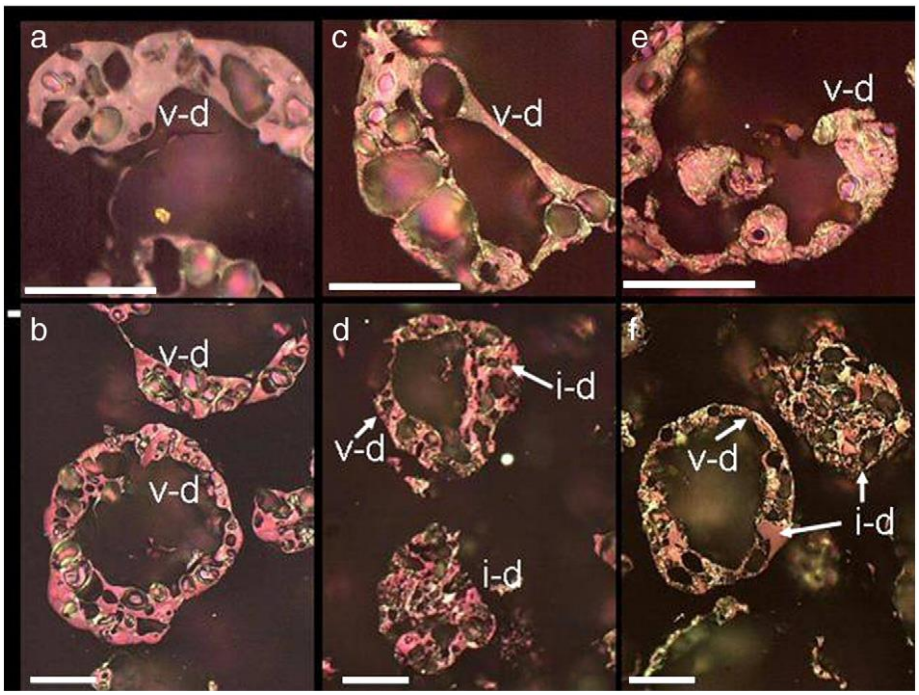

Figure 22 Optical microscopy of the char material a) High volatile bituminous coal high magnification b) High volatile bituminous coal low magnification c) Mid volatile bituminous coal high magnification d) Mid volatile bituminous coal low magnification e) Low volatile bituminous coal high magnification f) Low volatile bituminous coal magnification [57]

The CO_2 reactivity measurements showed that an increase in burnout in the material results in an increase in apparent reactivity with CO_2. This was attributed to the increase in the surface area within the pores of the char. The drop in intrinsic reactivity of extensively burned chars was attributed to the consumption of reactive material remaining in the char due to the thermal history of the char. The apparent reactivity to air measured at low temperatures allowed for more time for diffusion throughout the porosity within the char. This allowed for more diffusion to occur. The combustion pattern would mean that chars devolatilised in a moderate oxygen environment would combust first, according to this research. This was attributed to the increased surface area measured by N_2 of the char as opposed to the two-step produced chars. Pohlmann *et al.* indicated that these coal chars would react similarly in the blast furnace stack[57].

2.9.2 Coal Char Reactivity

Work by Sima-Ella looked at simple kinetic analysis to determine the intrinsic reactivity of coal chars. A TGA was used to gather kinetic data, allowing the author to estimate values of Arrhenius activation energy and pre-exponential factors[58]. Sima-Ella believes that the kinetic information of coal chars can allow for an improvement in process performance predictions and stresses the importance of the accuracy of the predictions. It was explained that reactivity is characterised by the rate constant *k* which can be factored into the activation energy *E* and a pre-exponential factor *A* via the Arrhenius equation in Equation 2.22. *T* is the absolute temperature and R=8.314 × 10^{-3}kj K^{-1} mol^{-1} is the gas constant. It was suggested that activation energy is the dominant factor in the reactivity equation. This impacts the temperature sensitivity of the reaction rate. The pre-exponential factor is relative to the material structure. Based on this information, it was stated that char reactivity can be sufficiently characterised by activation energy alone[58].

$$k(T) = A \exp\left(-\frac{E}{RT}\right) \qquad \textbf{2.22}$$

The material that was analysed was BPL (Calgon), a steam-activated carbon, derived from bituminous coal. Analysis of the material can be seen as per Table 3. The activated carbon was subjected to an N_2 atmosphere with a flow rate of 16.7 ml min^{-1} and heated at 10°C min^{-1} to 400°C to initiate oxidation, held at temperature for 15 minutes. After this process, dry air (20% O_2) was introduced to the sample. Non-isothermal runs of different rates from 20-600°C were carried out. Rates included 5, 10, 15, 20, 30 and 50°C min^{-1}. Isothermal runs were carried out at 475, 500, 525, 550 and 575°C. Isothermal runs are where the temperature is held for a predetermined time[58].

Table 3 Properties of BPL - activated carbon[58]

	Properties of BPL-activated carbon
Moisture wt%	2
Ash Content wt%	8
Fixed Carbon wt%	90
BET Surface area m^2/g	1, 004
Particle Size mm (max)	4

As per Table 4, the reactivity increases with increasing temperature, which is as expected[58].

Table 4 Reactivity values for isothermal oxidation[58]

	Reactivity values for isothermal oxidation of BPL in air
Temperature (ºC)	Reactivity, k ($s^{-1} \times 10^{-5}$)
475	3.834
500	6.416
525	15.578
550	25.259
575	34.224

Of the data in Figure 23, linear regression analysis was carried out, and obtained were values of E= 123.3 +- 10.9kj mol^{-1} and ln(A/s) = 9.72 +- 1.65. The non-isothermal analysis estimated values of E and A using Doyle and Coats-Redfern approximations for a given heating rate. These were selected for the relative simplicity of the values in the thermal analysis field. Doyle's approximation of the function of x is derived from observing a linear relationship between ln$p(x)$ and x. Values of A and E can be estimated from values of the intercept of a plot of ln[ln(1-a)] against 1/T. Where a is equal to the fractional weight conversion, or ultimately the oxidation. Coats-Redfern says that A and E can be estimated from the intercept and slope of a plot of ln[- ln(1-a)/T^2] and 1/T[58].

The information from the non-isothermal TGA tests and concluded that a heating rate of 25ºC min^{-1} for Doyle's approximation. 17ºC min^{-1} was the optimum heating rate for the Coats-Redfern approximations. The values of E and A were calculated using the approximations and yielded values of E= 129.4 ± 0.9kj mol^{-1} and ln(A/s^{-1}) = 10.34 +- 0.05. Which tied in well with the isothermal tests carried out on the TGA. Overall, the paper outlined a good approach to kinetic analysis. It was summarised by recommending a non-isothermal test, using the Coats-Redfern method for predicting values of E and A. Based on the relative simplicity and error confidence level, this is the preferred method, there is also an improvement in time. Non-isothermal tests are faster than isothermal tests[58].

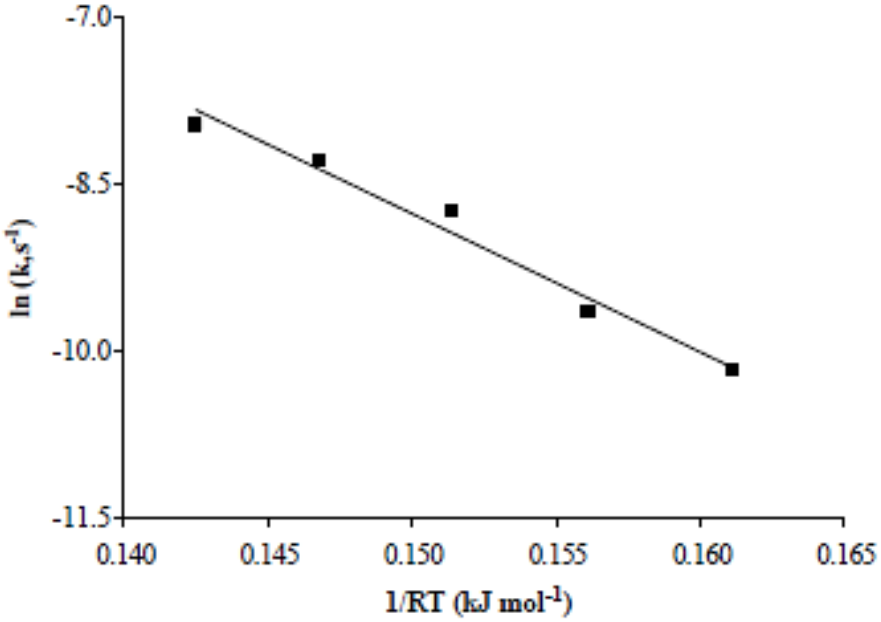

Figure 23 Reactivity parameters A and E, isothermal method[58]

2.9.3 Effects of Char in the Blast Furnace

Within the *Charfoco* report the effect of coal char on its ascent to the top of the blast furnace was examined. A work package was completed to determine what impact the coal char had on the descending burden[49]. The report investigates the influence of char on coke, pellets, sinter reaction and softening behaviour in the raceway. A direct observation made was that the activation energy of coke significantly impacted the presence of char. A blast furnace simulation test named as Hoogovens Simulation (HOSIM) was carried out to simulate the stack zone of the furnace. This was carried out to investigate pellet swelling behaviour in the presence of char. The cohesive zone of the furnace was simulated with isothermal reduction followed by softening under high temperatures. It was observed that char influenced the reduction behaviour by limiting gas flow into the porous sinter structure. The reduction time increased as the reaction was slowed. The effect appeared higher at higher temperatures in the stack zone simulations. In the cohesive zone simulations, the reduction was enhanced in the presence of char. Here temperatures are higher which would increase char consumption. It was observed that sinter had a higher reduction degree, and this could be explained by char preferentially remaining within the macro-pores of the structure[49].

The swelling behaviour of pellets was evaluated at 900ºC and 1050ºC, observations were made that char-coated pellets were less prone to swelling in the furnace. This could be explained by the char acting as a passivating layer on the surface to prevent swelling, or the Boudouard reaction on the surface would generate the CO_2 from ore reduction which led to observations of higher metallic Fe content measured in the pellets. Softening behaviour was tested in the absence of reducing gas. Reduction time decreased during softening in an inert atmosphere under load with the presence of char. Again, this shorter reduction time was attributed to the Boudouard reaction, the presence of char between pellet boundaries allows for higher gas permeability and prevents any intergrowth of pellets. Higher bed shrinkage was observed in pellets coated with char, this was due to the ability of char to maintain narrow channels along pellet boundaries, thus mitigating the loss of initial inter-pellet voids experienced at higher temperatures. At lower reduction temperatures, where char gasification was not viable, the char forms a physical barrier to gas flow, limiting gas diffusion. At higher temperatures, a Boudouard reaction between the char and CO_2 from iron ore reduction enhanced the reduction degree significantly[49].

The final work package of the *Charfoco* report consisted of applying the different measurements techniques into a model, titled the Model for Gas Reduction and Ore Reduction (MOGADOR). The higher reactivity of coal char, compared to coke was accounted for and the impact of char on the softening and melting characteristics of the burden materials. This model was used to simulate two complementary approaches, the first was the stick-on burden. This approach considers both coke and char together and modified coke reactivity. The model changed the constant of equilibrium in the Boudouard reaction from coke to coke *and* char. The simulations showed that with coke and char, equilibrium in the cohesive zone was positioned higher in the furnace, char being more reactive than coke, meant that it would gasify earlier in the process. The second approach is the transport by gas, this considered char particles separately, replacing the theoretical calculation of Boudouard kinetics with data from the first work package to simulate the consumption of char by the Boudouard reaction. In the modified coke reactivity case, the reactions took place within a larger area which impacted the shape of the cohesive zone. The calculations and simulations showed under normal injection rates of 240 kg/tHM of PCI, around 50% of coal left the raceway as char[49].

Overall, this report is useful to the work as it explains what happens to the coal and char as these materials travel through varying furnace conditions. It explains why char and coal can be seen in the blast furnace dust.

2.10 Analysis of Blast Furnace Dust

To investigate the effects of coal properties on top gas carbon, it is important to understand the constituents of the top gas. Previous studies have investigated the phenomena using various techniques, isolation of different reactivities using thermogravimetric analysis, and microscopy.

2.10.1 Origin of Blast Furnace Dust

Flue dust is defined as the solid residue found within the blast furnace top gas; it is a revert material that is reused in the sintering process. Flue dust is ultimately a by-product of the ironmaking process, with little value for resale, hence it is used as a revert in the sinter plant to produce a ferrous-rich agglomerate. The material is a combination of the various raw materials that enter the furnace, at different stages of combustion. The typical chemistry includes a mixture of carbon, ferrous oxides, ZnO, SiO_2, MgO, Al_2O_3, and other minor element oxides. It is important to ensure the material does not enter landfill or is emitted to the atmosphere and is recycled or reused due to high carbon content. It can be dangerous to landfill as it contains toxic elements such as zinc, cadmium, chromium, and arsenic, which have been concentrated from the raw materials during the blast furnace process. There are undesirable alkaline metals present which prevent direct recycling of the material in many cases, the presence of zinc and alkaline metals would cause issues with the furnace's refractory life if it was recycled in the furnace[42].

The top-loaded materials such as ore, flux, and coke generate dust during drying, this dust is usually part of the flue dust. The unburnt char from coal injection is the other primary constituent. The complexity of flue dust can vary significantly based on the operating conditions of the furnace. This makes analysis particularly difficult, parameters such as O_2 rate and productivity are hypothesised to influence the constituents of the flue dust itself[59].

Work by Xiao *et al.* informs how blast furnace dust is generated. Everyday, a substantial quantity of blast furnace dust is produced as waste or by-product in the iron

and steel industries. The reducing gas produced by coke moves from the bottom to the top of the furnace, transferring energy to the burden and causing a decrease in temperature[60]. The blast furnace gas is eventually discharged from the top of the furnace and into the downcomer, where collisions and physicochemical reactions among burdens and frictional wear between burdens and furnace walls generate a lot of particles, including iron ore dust, metal iron dust, unburned coal, and coke dust. When the buoyancy of BF gas to particles is greater than its gravity, it rises into the dust removal system along with the top gas. The chemical reactions involved in the formation of blast furnace dust are highly intricate. These include indirect reduction reactions via CO and H_2 at low-temperature regions within the furnace and direct reduction reactions through carbon at high-temperature zones. Coke carbon is burned in the raceway to generate CO_2, which is reduced to CO due to the excessive carbon in the furnace. The reaction between coke and water vapor is another significant source of CO and H_2. The CO and H_2 move upwards and react with iron ore in a counter-current reaction, reducing hematite to magnetite and FeO, ultimately resulting in the formation of metallic iron[60]. A lattice change takes place during the transformation of hematite to magnetite, which distorts the crystal lattice and causes significant internal stress, leading to iron ore pulverisation. Figure 24 demonstrates the distortion of lattices and a gradual loss of oxygen atoms during the reduction of iron oxide. After several reduction reactions, the H_2 and CO content gradually decreases while the H_2O and CO_2 content increases, forming mixed blast furnace gas. A small amount of fine dust in raw materials and reduced products transforms into a gas phase with high-temperature conditions. This process results in the high iron content of blast furnace dust and the primary occurrence of iron oxides. These chemical reactions illustrate that the carbonaceous substances within the dust primarily come from coke fines, followed by unburned pulverised coals[60].

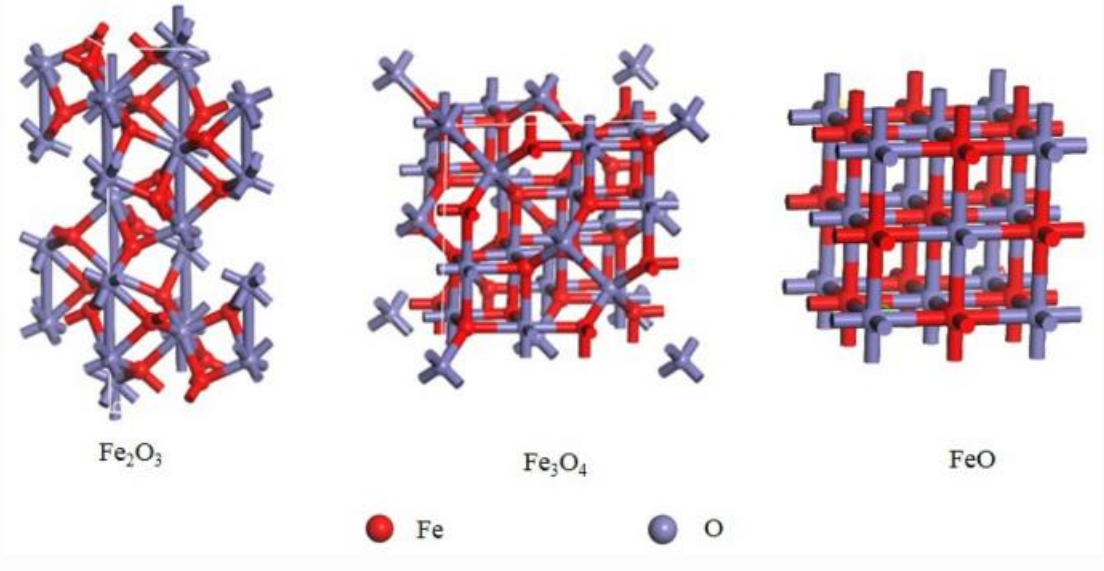

Figure 24 Schematic diagram of lattices of major iron oxides [60]

It was found that except for iron and carbon, non-ferrous metals like zinc and lead also made up a large degree of the dust. This is primarily due to their oxides being reduced by CO and H_2 as per equation 2.23. After reduction, the resulting products are cooled and re-oxidized in the downcomer, which leads to the formation of different minerals in the dust[60].

$$MxOy + CO\ (H_2) \rightarrow M +\ CO_2\ (H_2O) MxOy + CO\ (H_2) \rightarrow M + CO_2\ (H_2O)$$

2.23

$$M + O \rightarrow MxOy M +\ O \rightarrow\ MxOy$$

$$Where\ M = Interchangeable\ zinc\ or\ lead$$

2.10.2 Low Order and High Order Carbon

The primary challenge when analysing blast furnace dust through quantitative analysis is effectively separating the different types of carbonaceous materials. One way to achieve this is through microscopic examination, which can help identify the different particles based on their morphologies. However, this method is time-consuming and relies heavily on the expertise of the operator. Additionally, it's not suitable for very small particles due to the potential damage to morphological characteristics[61].

Blast furnace dust contains three main categories of carbonaceous materials: char, coke, and soot. Char and soot both come from coal that undergoes rapid pyrolysis. Coal particles that are introduced into a hot blast during the pulverisation process undergo fast heating and release gases as they swell. In the PCI process, the outer surface of the coal particle reaches solidification temperature before the centre reaches softening temperature, and the internal pressure starts to develop, eventually leading to the eruption of the outer crust of the coal particle. The remaining solid after eruption forms cenospheres, which continue to combust as they enter the raceway. Uncombusted cenospheres are carried to the upper shaft of the furnace, where their structure has already been severely damaged. These fragments of cenospheres collectively referred to as char which for the purpose of this thesis will be described as low order carbon. Soot is produced from the explosive release of gas and ejection of tar droplets into the hot blast, which undergo secondary pyrolysis and solidification. Soot is much less reactive than char due to its highly crystalline structure, making it difficult to gasify once it escapes from the hot raceway. Identifying the microscopic characteristics of these particles can be challenging, as char and soot can have similar morphologies to coal/coke fusinite, coke in blast furnace dust is referred to as high order carbon[62].

Low order carbon (LOC) and high order carbon (HOC) are terms that are specific to this thesis as they are not scientific terms, but best describe the differences between char and coke in the dust by categorising them based on their respective differences in reactivity and resulting temperature of combustion and explained in Section 2.10.3. It is not strictly correct to refer to the materials as char and coke due to the degree of overlap in the combustion temperatures of each., hence the terms LOC and HOC are more appropriate.

A common approach to speciation is thermogravimetric analysis (TGA), which involves gradually increasing the temperature to initiate combustion of different carbonaceous materials. The initial combustion temperature varies depending on the reactivity of the carbon types. By measuring the quantity of sample mass change during sequential combustion, the amount of different materials present can be determined. Unfortunately, the overlapping combustion temperature ranges among the different carbonaceous materials introduce significant uncertainty in quantitative analysis[55].

2.10.3 Quantifying Coal Originating Carbon in Blast Furnace Dust

The resultant chars from the burnout work by Wing *et al.* discussed in section 2.8.3 were analysed in terms of carbon characterisation, CanmetEnergy uses a TGA technique named the CanmetEnergy Technique (CET). The process uses differences in minimum starting temperatures of combustion for various carbonaceous forms due to the thermal history of the carbon, 475°C for lower order carbon and 600°C for higher order carbon respectively. With the increasing order of crystallinity, the reactivity of carbonaceous material decreases. This is useful to predict the behaviour of chars in the raceway. To exploit the various minimum starting temperatures, a heating profile was used as per Figure 25[55].

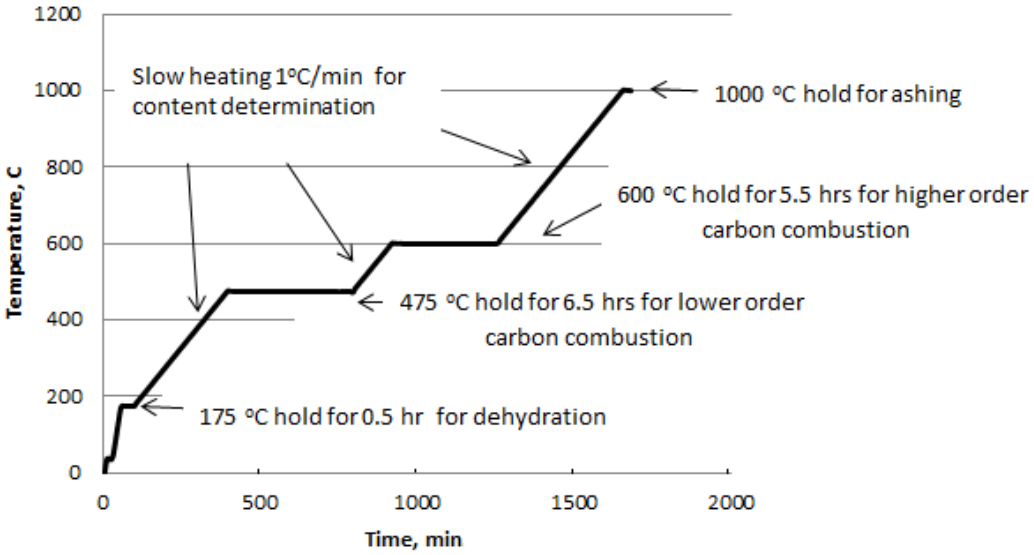

Figure 25 Heating profile for TGA experiments[55]

The characterisation process using the TGA was demonstrated to work, Wing *et al.* displayed a combustion profile which identifies two distinct forms of carbon, as per Figure 26. The first peak, the lower carbon form, is identified as amorphous char with a lower combustion temperature. The other form is identified as coke, this is more crystalline and hence has a higher combustion temperature[55].

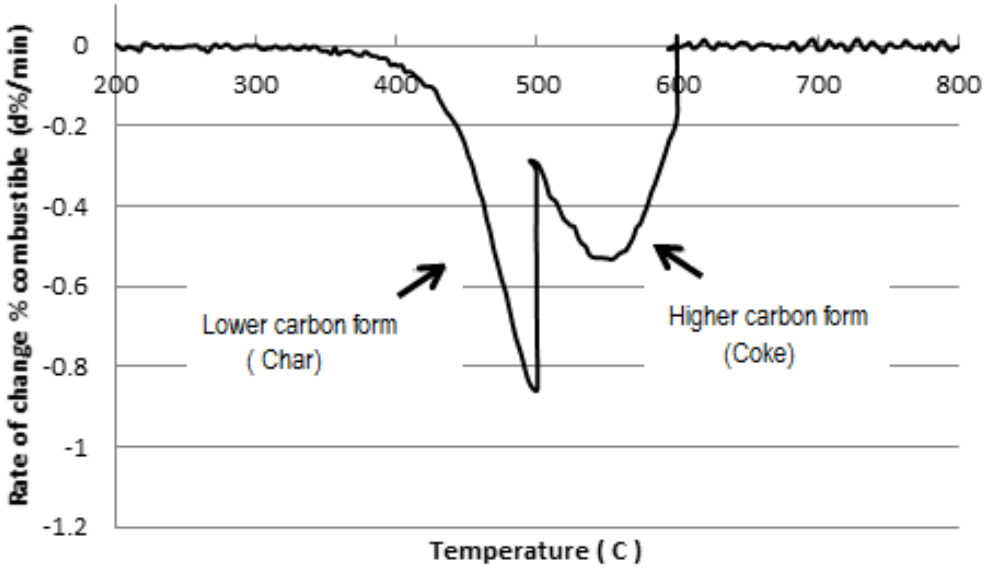

Figure 26 TGA carbon form separation[55]

Wing *et al.* published a separate research paper using this technique, looking into carbon type differentiation for diagnosing pulverised coal injection conversion. This paper is particularly interesting, as the research has been applied to an industrial setting for the diagnosis of PCI combustion issues in a blast furnace. The difficulty of obtaining a representative sample due to the nature of gas cleaning is discussed. This is carried out in two stages, dry and wet scrubbing. Both processes yield different fractions of flue dust. The heavy, more coarse particles drop out during dry cleaning. The lighter, finer particles are captured by wet scrubbing. It is important to analyse both of these portions. Rapid pyrolysis of coal is discussed in terms of the pressure differential seen between the surface of the particle and within the particle. The differences in temperature across the cross-section of the particle mean that the particle pressure internally is greater than the surface, hence the particle bursts and forms cenospheres within the flue dust. As can be witnessed in Figure 27, in the SEM images of char and soot. Soot is formed when tar droplets are excreted from the coal particles during cenosphere formation and swelling of the coal. These travel to the top of the furnace and out into the dust[59].

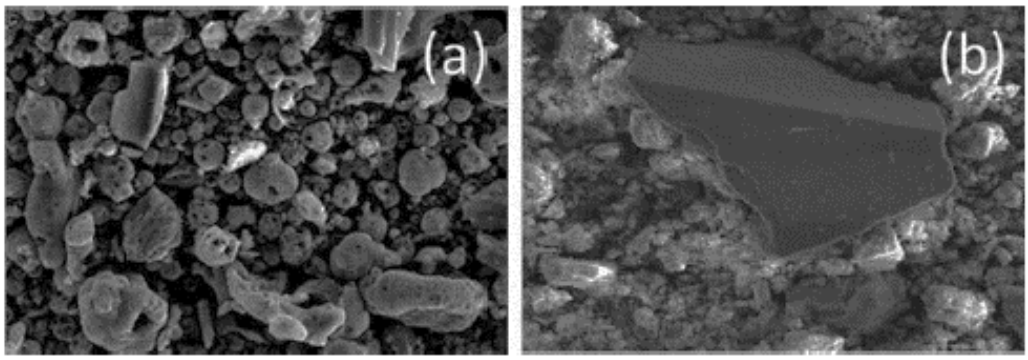

Figure 27 Morphology of char and soot, (a) cenosphere structure of char, (b) soot particle in industrial dust sample[59]

The technique discussed by Wing *et al.*, for the differentiation of carbon is to sieve the flue dust before TGA analysis is carried out. The material was sieved using a 150-micron sieve, thus removing the larger coke particles from the sample as per Figure 28. This portion was weighed to calculate the ash coke portion, removing a large potential source of contamination for the TGA tests. It has been found that there is an overlap in combustion temperature between LOC and HOC within flue dust. Removing this size fraction by sieving helps to counteract this effect[59].

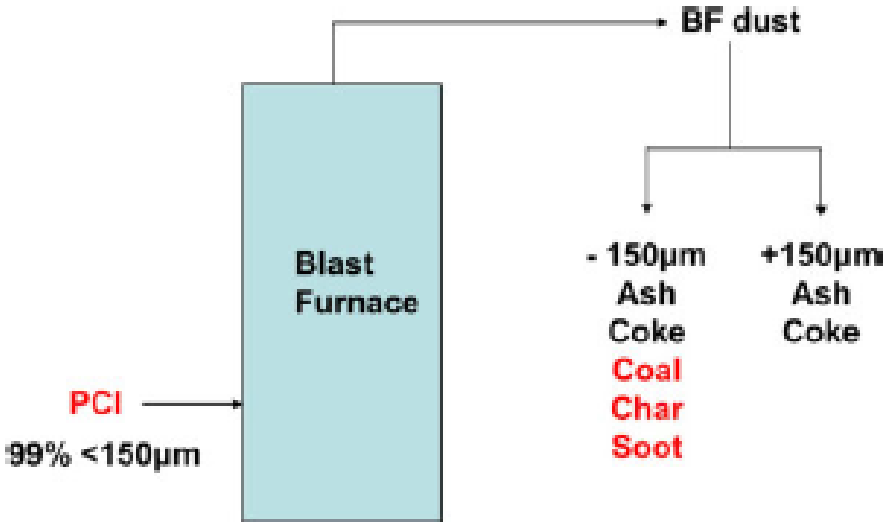

Figure 28 Fractionation of flue dust[59]

A TGA test was initially carried out using the heating profile in Figure 29, the heating profile included a hold at 125^{o}C for sample dehydration. The char was expected to be driven off during the ramp to 600^{o}C and hold. The soot was expected to be driven off with the subsequent ramp and held to 1000^{o}C. The results of this

showed a differentiation, as measured by weight % loss between char and soot within the particle as per Figure 30[59].

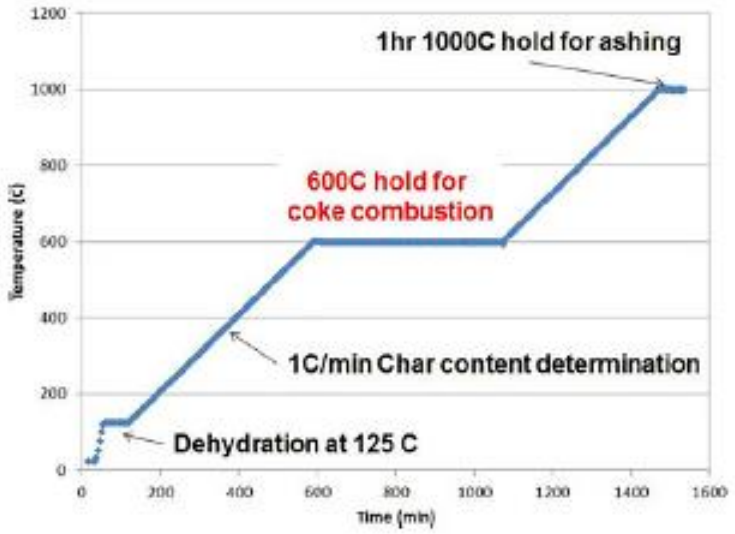

Figure 29 TGA heating profile of carbon type differentiation[59]

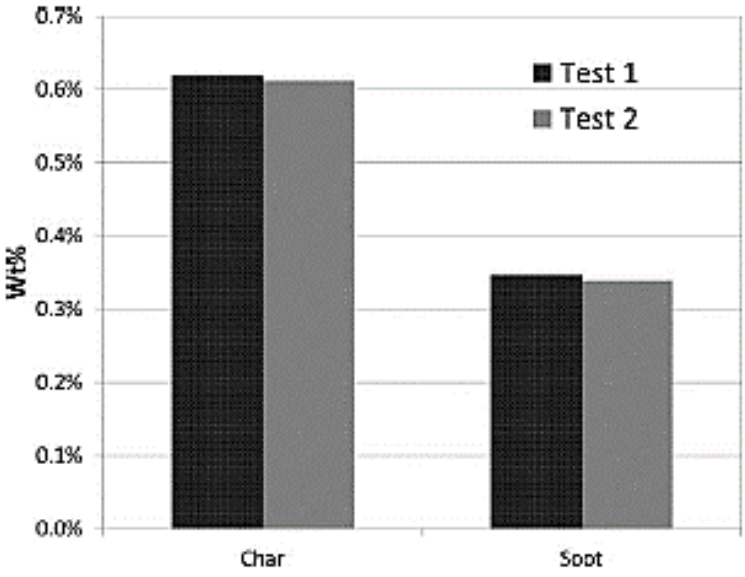

Figure 30 TGA results of carbon type differentiation[59]

The technique was implemented into ArcelorMittal Dofasco, for diagnosis of PCI conversion. Wing *et al.* decided to focus on the material from the wet scrub operation, as this yielded the majority of coal char particles over a dry scrub process. It should be noted that the injection rate was low at the time of the trial ~140 kg/tHM, hence it should be expected to see good coal combustion. During testing it was found

that there was still an overlap between char and coke combustion in the TGA data, hence Wing *et al.* introduced a further hold at 475°C as per Figure 31[59].

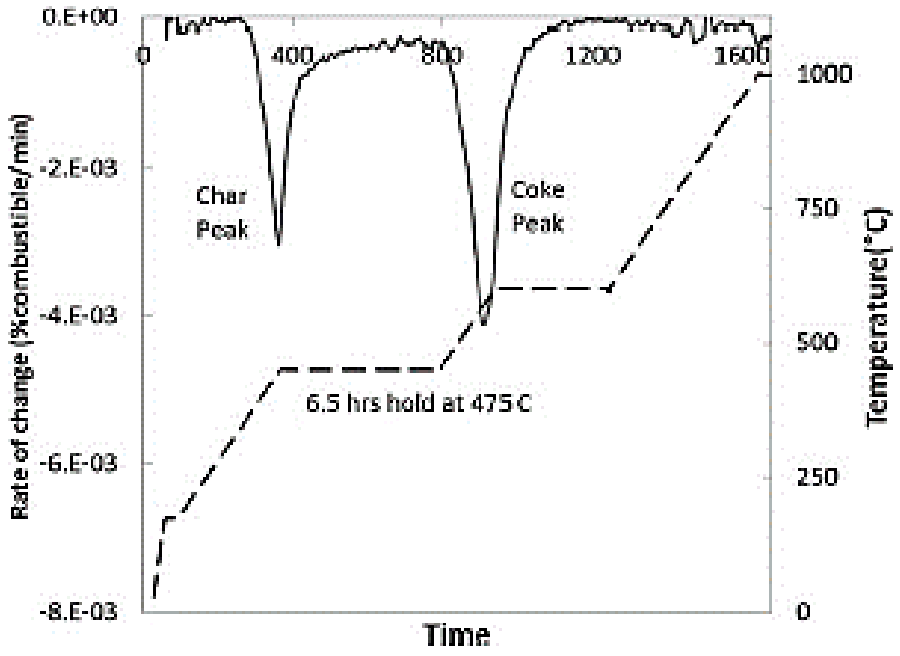

Figure 31 Modification of heating profile for sludge analysis in the industrial sample[59]

It was found during the research that three distinct forms of carbon within a flue dust sample could be accurately measured. Further work was required to establish key factors influencing the degree of gasification of coal in the raceway. Although Wing *et al.* did anticipate during this research that oxygen enrichment of the furnace was a key factor. Also noted was that a 50°C reduction in blast temperature led to an increase of 74% in unburnt PCI residues leaving the furnace. Of these residues, a 45% increase in char content was noted. This paper demonstrates a strong technique for the materials within flue dust based on the individual combustion properties of the carbon materials[59].

Schwalbe from ThyssenKrupp steel manufacturer carried out some investigation work into carbonaceous forms in BF dust at high coal injection rates. During the introduction, flue dust testing was compared to a blood test. Information can be gathered about a furnace and diagnosis can be carried out at different zones of the furnace, similar to a blood test with a human. Schwalbe explains that flue dust is made up of both carbon and non-carbon-bearing materials such as gangue and fluxes. From the carbon-bearing materials, it is stated that gasification in the absence of oxygen would transform coal into coke, soot or graphite as per Figure 32[63].

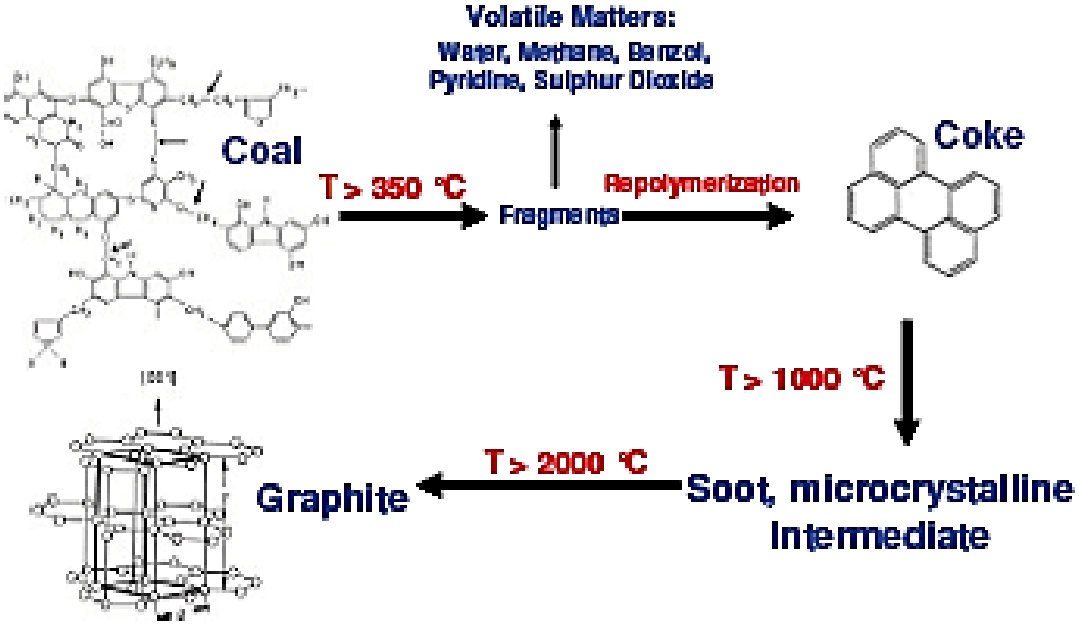

Figure 32 Carbon by tempering process[63]

Schwalbe used a furnace capable of being heated to 1600^{o}C at a specific ramp rate, with an O_2/Ar gas mix atmosphere. This furnace was connected to a quadrupolar mass spectrometer. A thermobalance was used to measure the mass loss of the sample during the heating cycle. A typical spectrum was given in Figure 33. The area under the graph was analysed to give the respective percentages of carbon from coal or coke. Schwalbe also states that there's a third constituent, graphite. This cannot be measured before 1600^{o}C, therefore XRD was applied to analyse the graphite portion[63].

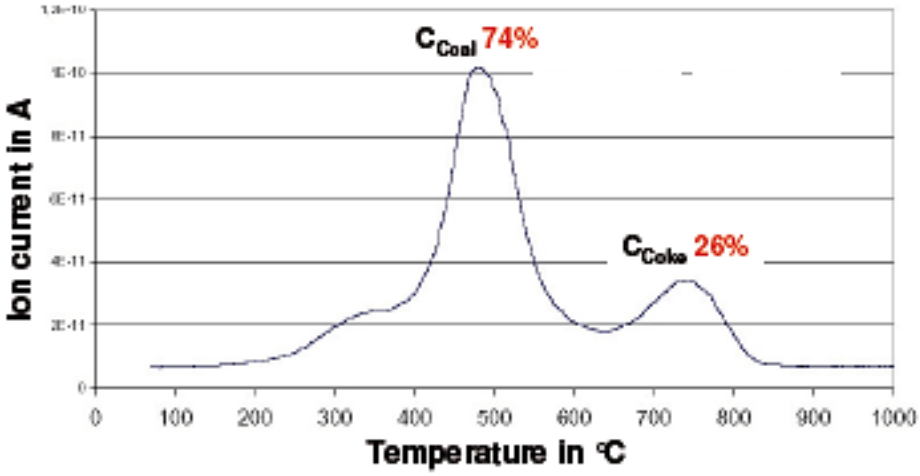

Figure 33 Degasifying-curve of typical top gas dust[63]

It was noticed initially that the XRD information from the raw dust samples was polluted. In particular, the graphite peak 002-reflex was contaminated by the 101-reflex of alpha quartz as per Figure 34. To counter this, a process of microwave-assisted dissolution (MAD) was developed. The dust was washed with mineral acids and peroxide before retesting using the XRD. The comparison as per Figure 35 was striking. He concluded that the XRD was no longer necessary, a simple weight difference before MAD will be suitable for determining graphite content, as proven by XRD that no remaining material remains after MAD[63].

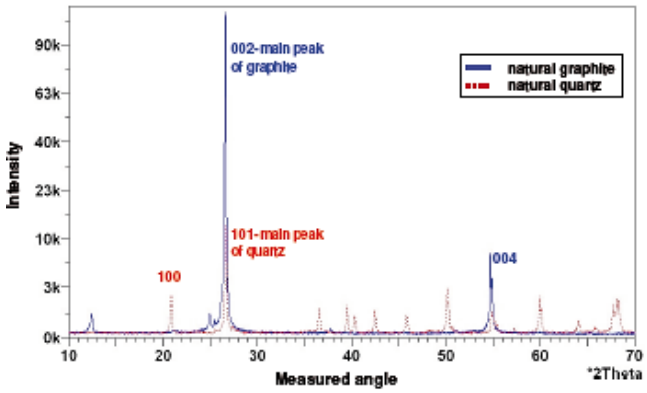

Figure 34 XRD with alpha quartz pollution[63]

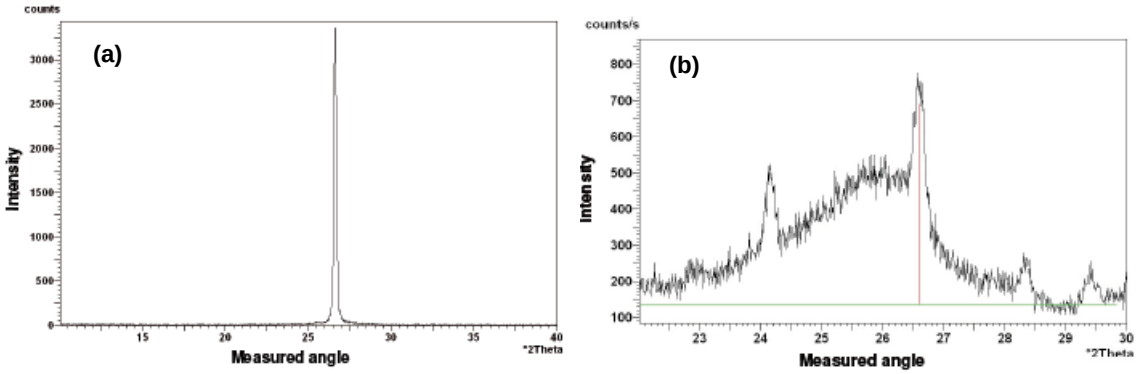

Figure 35 XRD spectra of the sample a) treated with MAD and b) before MAD[63]

A paper studying structure characteristics and combustibility of carbonaceous materials from blast furnace flue dust was written by Di Zhao. Experimental procedures were carried out on flue dust from an unidentified steel plant including, particle size analysis, scanning electron microscopy (SEM), X-ray diffraction, polarisation microscopy and TGA[64]. Di Zhao took samples of dust from two particular abatements of the gas cleaning system, bag dust from hop pockets and gravitational dust. Also used were coal and lump coke from the same steel plant. These samples were prepared by drying at 105^{o}C and crushed to <0.074mm particle size. To study pyrolysis, the coke particles were heated to 1300^{o}C in a muffle furnace and held in an N_2 atmosphere for 25 minutes. Also discussed was floatation as an option for separating carbon from the other components. However, in this work, an acid wash to remove inorganic matter from the sample was undertaken. The dust samples were washed with hydrochloric acid for 24 hours at 50^{o}C, filtered and mixed with hydrofluoric acid for 36 hours. Finally, the material was rinsed with excess deionised water. The whole process was repeated until the ash constituent remained less than

5%. A comparison using proximate and ultimate analysis from before and after washing can be seen in Table 5[64].

Table 5 Proximate and ultimate analysis before and after chemical washing[64]

Proximate analysis and ultimate analysis of all samples (%).

Samples	Proximate analysis, %			Ultimate analysis, %				
	FC_d[a]	A_d	V_d	C_d	H_d	O_d[a]	N_d	S_d
BD	10.9	81.64	7.46	11.67	0.69	5.43	0.18	0.39
GD	64	31.96	4.03	66.01	0.67	1.22	0.13	0.28
CK	85.5	12.83	1.67	83.82	0.59	0.65	0.34	0.74
CA	68.3	9.54	22.15	82.6	3.49	3.02	0.88	0.46
BD-aw	88.59	4.01	7.4	89.99	0.09	5.32	0.15	0.44
GD-aw	89.78	5.1	5.12	93.21	0.07	1.18	0.14	0.3
CK-aw	96.35	2.03	1.62	96.32	0.14	0.59	0.27	0.65
CC-aw	83.62	1.37	15.01	95.67	0.19	1.74	0.61	0.42

FC, fixed carbon; V, volatile matter; A, ash; d, dry basis.
[a] Calculated by difference; aw, acid-washing treatment.

The information in Table 5, shows that the material has been demineralised effectively. The ash content, which contains the basic oxides has been reduced significantly. The fixed carbon value in the first column shows that the material remaining after washing is predominately carbon. Table 6 shows the relative particle size distribution of the material. As displayed it shows similarities between coal (CA) and bag dust (BD), the paper states that this similarity would suggest that BD is predominately made up of coal[64].

Table 6 Particle size distribution[64]

Table 2
Results from the analysis of particle size distribution.

Samples	<38 μm	38–63 μm	63–90 μm	90–180 μm	180–250 μm	250–425 μm	>425 μm	Average particle size
GD	0	2.12	7.76	45.07	27.3	17.75	0	170.43
BD	86.47	11.13	2.4	0	0	0	0	14.64
CA	83.74	12.69	3.57	0	0	0	0	13.74

Di Zhao discusses that carbon origins cannot be accurately defined from SEM images. However, observations were made using petrographic analysis. Di Zhao observed that particles from both BD after washing and GD after washing were predominately coke particles. This suggests that the degree of coal gasification in the blast furnace was very high. XRD was used to analyse the spatial packing of the graphite flake layer, the information can be found in Figure 36. The presences of (0 0 2) and (1 0 0) bands corresponding to the lattice structure of graphite, were present in all samples. The (0 0 2) band at 20^o is present due to the turbostratic structure between

graphite and the amorphous structures. Also observed was the shift of this peak to a higher 2-theta value in the GD and BD and CK, indicating a more ordered microcrystalline structure, indicating that more coke was present[64].

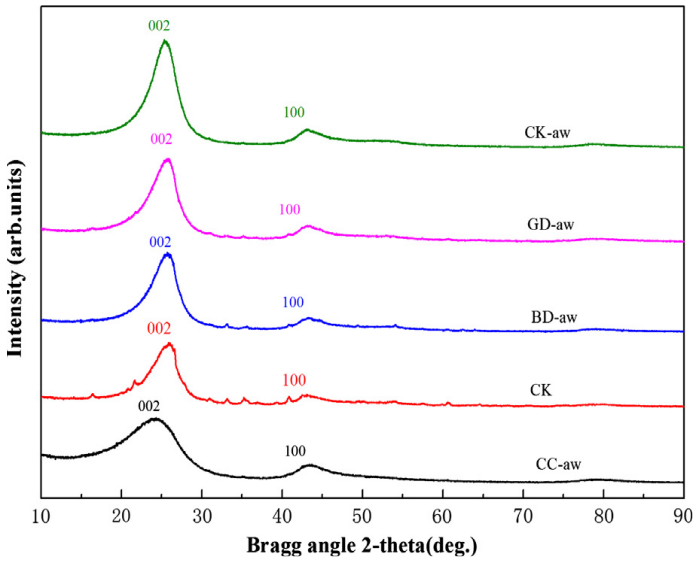

Figure 36 XRD analysis of BF dust[64]

The TGA analysis can be seen in Figure 37. The peak weight loss rate occurs between 600-700^{o}C, which Di Zhao indicated is a confirmatory result of the petrographic analysis, that both GD and BD are predominately fine coke material[64].

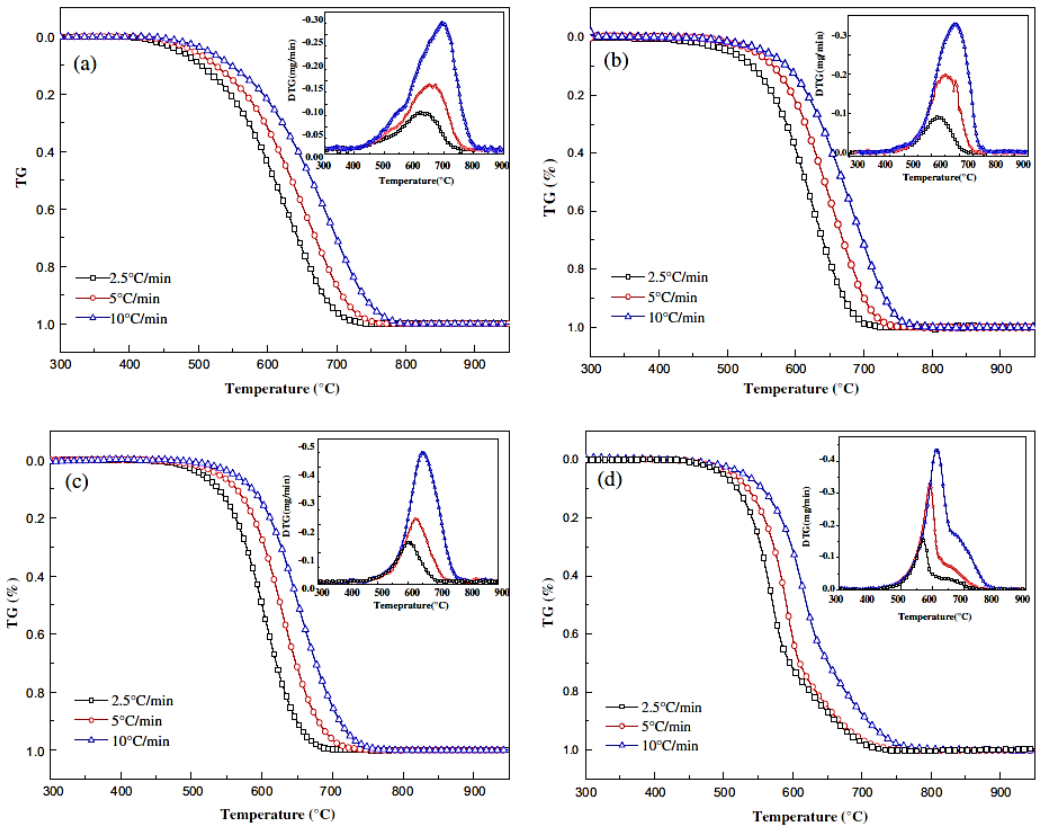

Fig. 4. Conversion and conversion rate of four samples at three different heating rates: (a) GD-aw, (b) BD-aw, (c) CK-aw, (d) CC-aw.

Figure 37 TGA profiles of BF dust(a) GD-aw, (b) BD-aw, (c) CK-aw, (d) CC-aw [64]

The paper concludes that particle analysis can be used to classify the two types of dust samples. The petrographic analysis confirms that the carbonaceous materials in BD-aw and GD-aw are from coke fines, in the order of 95% of the material. The XRD differentiated between the graphite degree of the samples, the L_c values allowed the materials to be ranked as CK>GD>BD>CC. Di Zhao indicates that coke fines from BD and GD originate from the softening zones in the blast furnace. The carbon structure appears to consist of mainly an aromatic structure with a smaller part amorphous structure. Finally, the combustion reactivity of BD was higher than GD, which can be attributed to a less ordered crystalline structure[64]. This paper is good in terms of identifying the presence of different ordered carbon but doesn't allow for quantification of each carbon type with any degree of accuracy[64].

2.11 The Influence of Process Parameters on Coal Combustion

Process data is often used to inform decision making in industry. A paper by Steer *et al.* compares the properties of coal injectants measured in the laboratory with blast

furnace process information to determine relationships that could be applied to help maximise coal injection rates. The study aimed to investigate whether laboratory test results for injection coals could be used to predict the blast furnace performance during production. Statistical data analysis techniques were used to compare laboratory test results with production measurements over a two-month trial period[65].

Pearson's coefficients are useful for measuring linear relationships, but in cases where variables show non-linear relationships, Spearman's correlation coefficients are more appropriate. The data in Table 7 is divided into moderate and high correlations, with the highest correlations associated with blast furnace process variables. There are moderate correlations between laboratory analysis of coal and chars with blast furnace variables, including the char gasification reactivity with the coal rate and coke rate. The article highlights the importance of process variables in controlling the blast furnace process, which masks the effects of fluctuations in coal properties[65].

Table 7 Pearson's correlation of variables and measurements[65]

Dependent Variable	Independent Variable	Number of Data Points	Correlation Coefficient	Dependent Variable	Independent Variable	Number of Data Points	Correlation Coefficient
Gasification	Volatile matter	10856	−0.668 **	Production rate	Oxygen flow	17773	0.819
Sulphur	<125 µm particles	4708	0.669 **	Production rate	Blast pressure	17773	0.800
Burnout	Sulphur	7787	0.669 **	Production rate	Top pressure	17773	0.833
Burnout	<125 µm particles	4179	0.673 **	Production rate	Total volume	17773	0.903
Burnout	Gasification	11642	−0.643 **	Production rate	Blast volume	17773	0.844
Gasification	Coke rate	11915	−0.685 **	Coke rate	Coal rate	17773	0.842
Gasification	Coal rate	11915	0.600 **	Coke rate	Carbon dioxide	17773	−0.842
Oxygen enrichment	Oxygen flow	17773	0.730	Coal rate	Hydrogen	17773	−0.818
Oxygen enrichment	Nitrogen	17773	−0.636 **	Coal rate	Nitrogen	17773	−0.805
Oxygen flow	Blast pressure	17773	0.713	Blast pressure	Top pressure	17773	0.893
Oxygen flow	Top pressure	17773	0.641	Blast pressure	Total volume	17773	0.883
Oxygen flow	Total gas volume	17773	0.701	Blast pressure	Blast volume	17773	0.853
Oxygen flow	Nitrogen	17773	0.668 **	Top pressure	Total volume	17773	0.865
Coal rate	Carbon dioxide	17773	0.693 **	Top pressure	Blast volume	17773	0.862
Carbon dioxide	Nitrogen	17773	−0.690 **	Total gas volume	Blast volume	17773	0.966
Hydrogen	Nitrogen	17773	−0.750 **	-	-	-	-

Note: ** means significant at the 0.01 level (99%).

Figure 38 shows the results of coal burnout, with a trend opposite to that of gasification results, indicating that lower DTF burnouts are associated with higher coal rates in the blast furnace, except for Coal D. Figure 39 displayed a similar ascending pattern for the gasification reactivity against coal rate as shown in Spearman's correlation in Table 7, indicating that lower DTF char reactivity is associated with higher blast furnace coal injection rates. However, Coal D's volatile matter content and DTF burnout reactivity showed wider variability compared to the other blends, possibly due to supply variation or contamination with other coals on the stockyard. In contrast, coal A had a narrow gasification range[65].

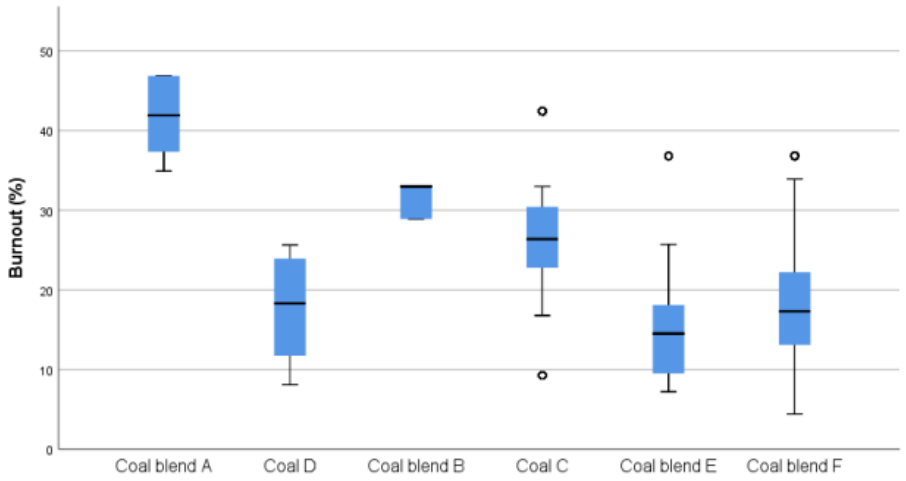

Figure 38 Range of coal burnout for each of the coals/coal blends used during observed blast furnace production [65]

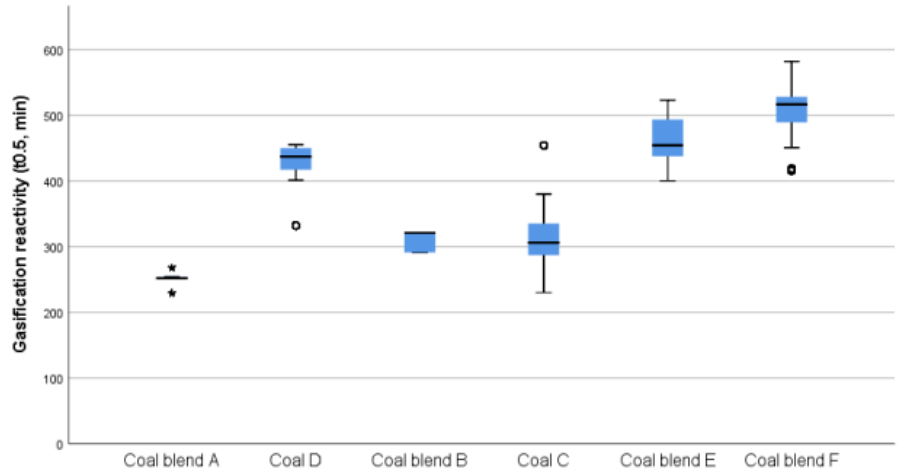

Figure 39 Box plots of the range of char gasification reactivity for each of the coals/coal blends used[65]

The data analysis presented in Figure 40 shows that the model fitting for the blast furnace coal injection rate has a 95% accuracy in explaining the relationship, as confirmed by the scatter plot comparing predicted versus actual coal rates. The most significant predictor of the coal rate identified by the model is the type of coal used, which is consistent with the experience of blast furnace operators. However, the measured coal properties, such as volatile matter content or DTF burnout, do not seem to have a significant relationship with the coal injection rate, as the multiple regression analysis showed only a small relationship with char gasification. Nonetheless, in combination with the box plots, the findings suggest that there may be a potential link

between higher coal injection rates, lower burnouts, and lower char gasification rates[65].

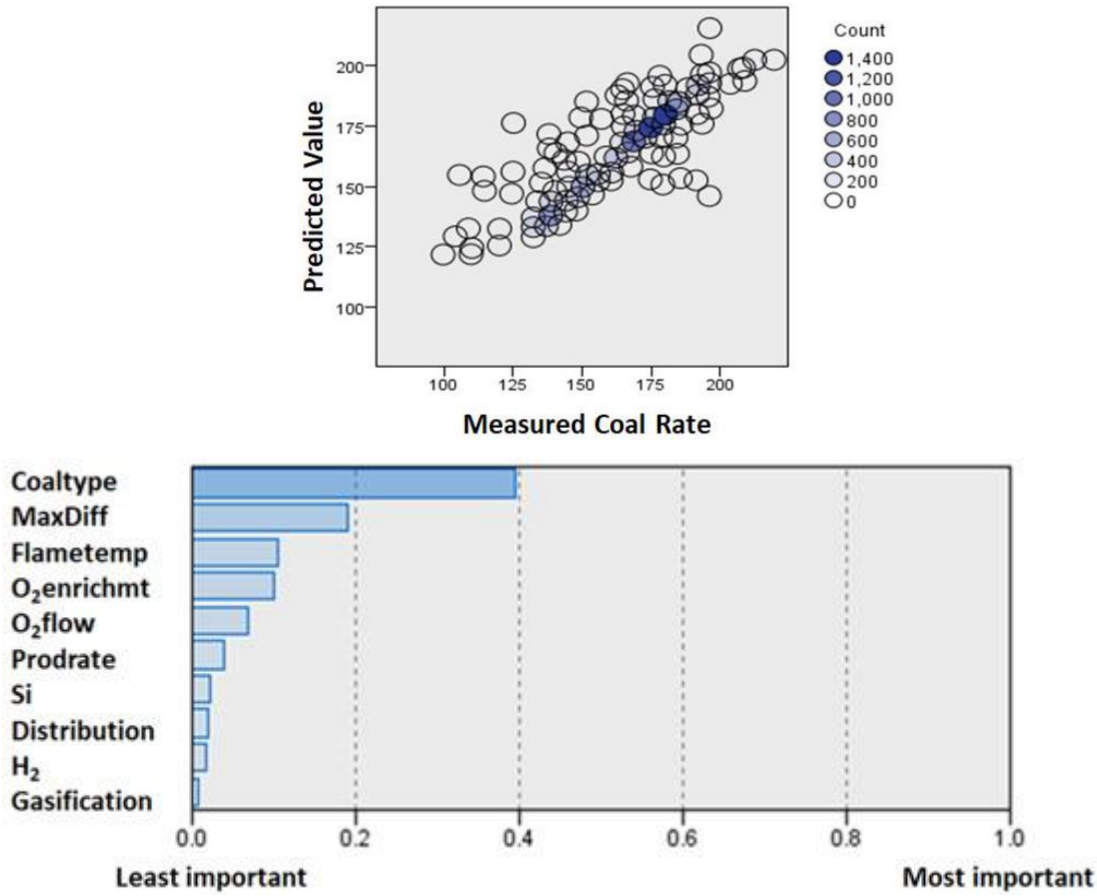

Figure 40 Relationship between the measured and predicted injection coal rate in the multiple linear regression model[65]

The study found strong correlations between production variables, making it challenging to differentiate more subtle relationships with laboratory measured coal properties. However, combining the findings of the Spearman's correlation, box plots, and multiple regression models indicated that the coal injection rates were higher for chars with lower gasification reactivity. The study also highlighted the importance of the type of coal used in the blast furnace compared to the coal rate. However, a consistent relationship was not observable across all the injection coals, suggesting the possibility of other non-tested variables, insufficient sampling frequency, or testing inconsistencies. The study was limited by the composite coal samples taken over a 12-hour shift period and the practicalities of coal blending, which results in variability that would not be accounted for[65].

The work by Schwalbe outlined in section 2.10.3 also discussed correlating the data for the differentiated carbon types with operational data. The key parameters considered were coke consumption, coal injection rate and the atomic ratio of oxygen to carbon O/C. For the first parameter carbon from coke and carbon from coal are graphed against the coke rate and coal rate respectively. There was no dependency for coke carbon versus rate, however, a correlation between coal carbon and injection rate was observed with a high degree of certainty of 65% as per Figure 41[63].

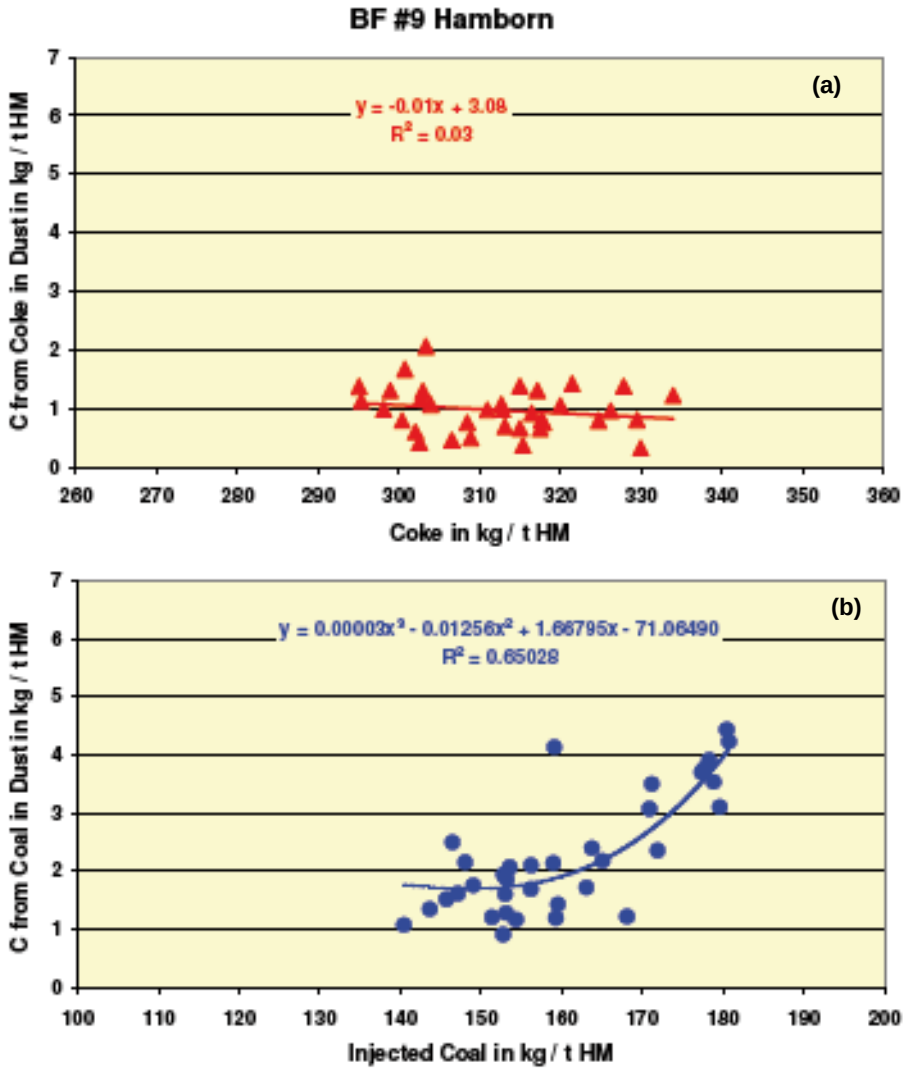

Figure 41 Carbon contents versus rate of origin a) carbon from Coke in dust b) carbon in Coal in dust [63]

The O/C component was finally compared. There seems to be a decrease in both top gas dust and coal carbon as per Figure 42 with an increasing O/C ratio. The

observation is that with an increasing O/C ratio it appears that more coal conversion and gasification can be observed in Figure 42[63].

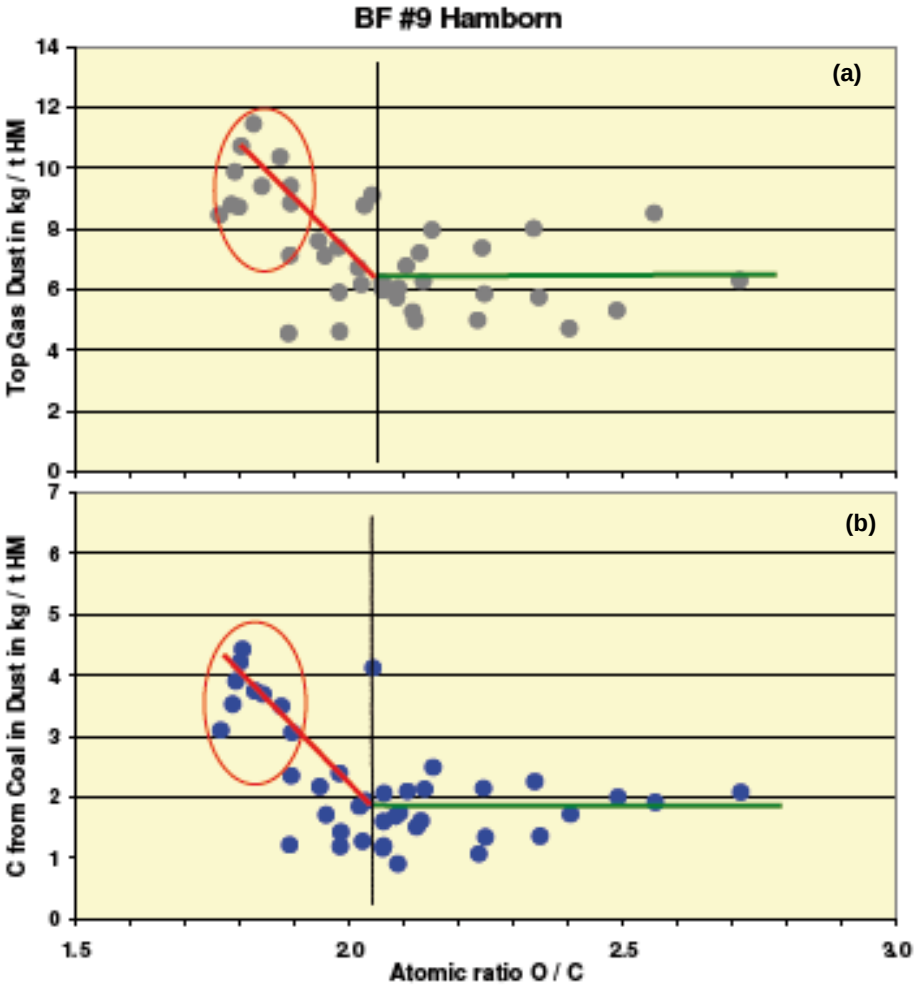

Figure 42 Scatter graphs of process parameters a) Top gas dust versus atomic ratio O/C b) carbon from Coal in dust versus atomic ratio O/C[63]

Overall, this paper can be useful in terms of comparison against furnaces at Port Talbot. Also useful to this study is the method of MAD for the XRD sample. The lack of information about sampling leads to many questions about sample representativeness[63].

A paper by Gao *et al.* that proposed injecting Iron Bearing Dust (IBD) into blast furnaces along with pulverised coal showed that the addition of Fe_2O_3 and CaO improved the combustion of the coal, as indicated by the decrease in ignition and burnout temperature as per Figure 43[66]. The combustibility index, ignition index, and burnout index of the coal also improved with the addition of the additives. The use of Fe_2O_3 and CaO additives in the coal reduced the activation energy during

combustion, suggesting that these additives are potential catalysts for coal combustion. The study also suggested that the use of IBD as a substitute for catalytic combustion could promote the combustion of fuel and reduce the accumulation of unburned coal in the blast furnace process[66].

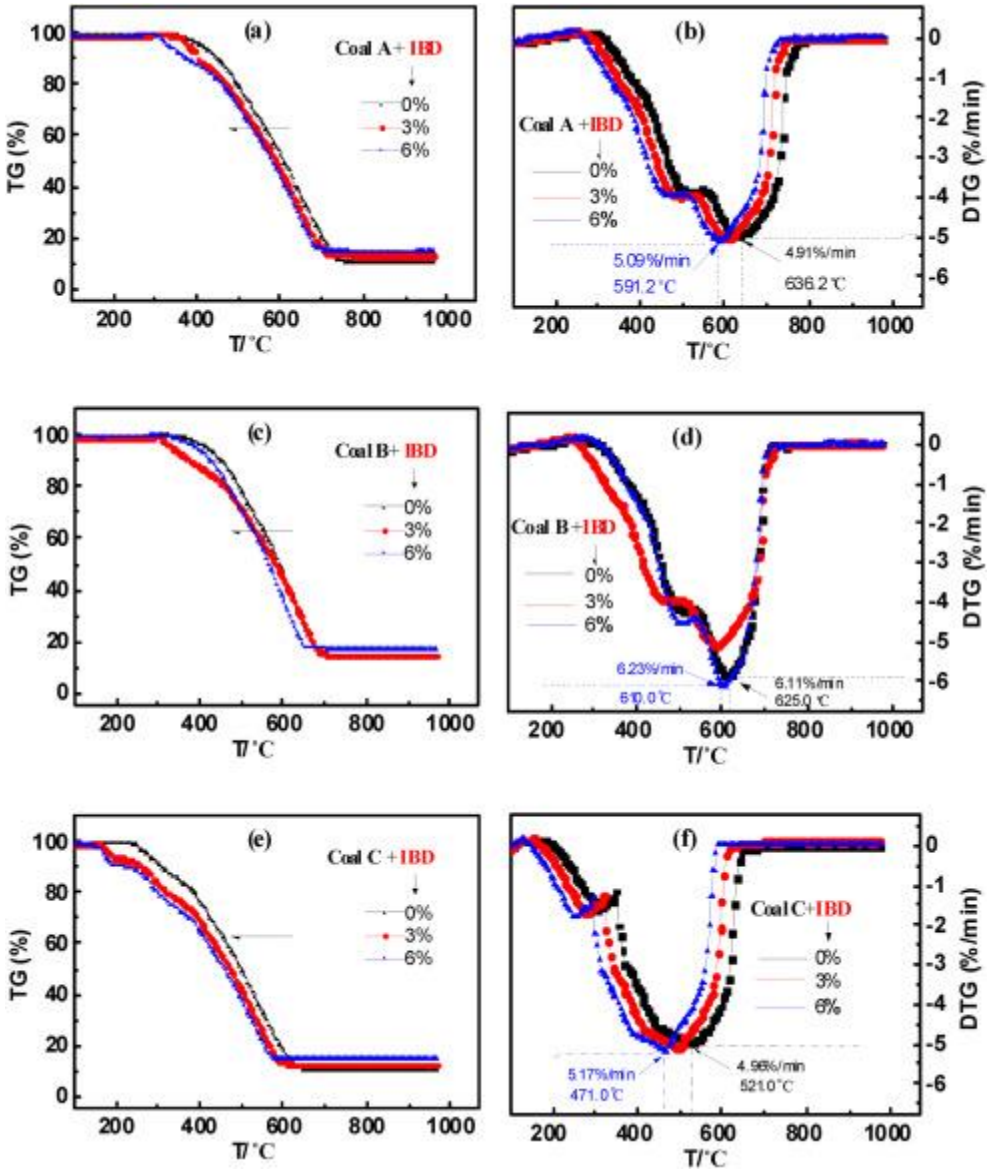

Figure 43 TG–DTG curves of the combustion processes. (a) Coal A blending with IBD (b) Coal A blending with IBD (c) Coal B blending with IBD (d) Coal B blending with IBD (e) Coal C blending with IBD (f) Coal C blending with IBD[66]

Also discussed was that higher coal injection rates can have a negative effect on blast furnace performance, including lower coal burnout and gasification rates, as well as changes in the char properties during combustion. It is stated that type of coal used in injection also plays a critical role in determining the reactivity and combustion rates, with different coals showing varying levels of performance. The use of coal blends can

help strike a balance between injection rates and reactivity, thereby enhancing blast furnace performance. Furthermore, modelling techniques can be used to predict the impact of coal injection rates on blast furnace performance, with accuracy levels of up to 95%[66].

3 Materials and Experimental Methods

3.1 Experimental Objectives

The literature review of this thesis explored the current work on coal combustion and formation of the blast furnace dust. This led to the following experimental objectives which were aimed at answering the research questions presented by the gaps in the literature, which were born from the current studies and will be addressed in subsequent chapters of this thesis.

For the experiments in chapter 4.1, characterisation of blast furnace dust has been researched, to gain an understanding of how the dust is formed, a characterisation of the physical and chemical properties of the dust will be completed, coincidentally with a characterisation of the raw materials that feed the blast furnace. In previous studies, the work done by XRD to highlight phases in the material have been insignificant, this work will include a fully identified spectra highlighting the common phases found within blast furnace dust. Using this information, it can be clear as to which raw materials from the process have a presence within the dust. This work will help inform the hypothesis presented in the aims section of this thesis, 'The raw materials that feed the blast furnace are expelled into the gas stream and all influence the blast furnace dust.' To inform the work of later chapters, the comparison between the analytes present in the dust and slurry from each abatement has been made to determine which material is most representative of the bulk of the material for subsequent carbon type analysis. The relationships between carbon and the other analytes within the material has been investigated to determine the presence of any dependencies. The scope of this series of experiments is aimed at understanding the constituents of blast furnace dust and to inform subsequent carbon type differentiation chapter of the most suitable and representative sample to be used.

Carbon source fingerprinting or type differentiation has been researched previously for the purposes of diagnosing coal char presence in the blast furnace dust. This work has only previously been applied to dusts from furnaces using the pulverised coal injection system. The experiments in chapter 4.2 aim to confirm that the techniques recognised in literature are still applicable to blast furnaces that use granulated coal injection systems and seek an alternative technique that will allow for extended sample throughput without affecting the accuracy of the result. This will

answer the hypothesis ‘Thermal techniques can be used to differentiate carbon sources in dust generated in blast furnaces that use granulated coal injection.’ The process for analysing each sample for the current carbon type differentiation technique is excessive, currently it takes around 30 hours to complete a single sample, creating a lack of data for the dust from a continuously changing blast furnace process. This means that to complete a more data rich study on the effects that process parameters can have on the coal char presence within the dust, a suitable alternative should be investigated.

The current literature comparing blast furnace operating parameters and conditions against the presence of coal char in the dust is limited. This is because the blast furnace is a highly complex chemical reactor, and it is thought that many processes will influence the dust generated coincidentally. The aim of the experiments within chapter 4.3, is to inform subsequent chapters of which parameters have a larger influence on the LOC presence within the dust, to provide focus for more in-depth analysis. The work uses data from each stage of the blast furnace process to compare to the degree of LOC present within the dust. As stated previously LOC is indicative of the amount of char present within the dust. The coal burnout characteristics of the coal used in the blast furnace throughout the project will also be analysed to determine which of the blends should theoretically burnout better and the data from the LOC quantification will determine if coal type has a significant influence on the dust generation. The process operating conditions from the blast furnace have been analysed to determine if any of these have an influence on the LOC within the dust. This work will help inform the hypothesis ‘Coal combustion in the raceway can be impacted by process parameters and the evidence can be found in the fingerprint of blast furnace dust.’

The aims of the experiments within chapter 4.4 were firstly to diagnose the set of conditions that lead to an outbreak of dust in the blast furnace. A novel application for a dust in water monitor was investigated. Within this chapter the aim was to determine if the dust mass flow was related to the LOC within the dust, before using the live information to provide a live comparison for the dust exiting the furnace against the normal operating parameters. With sufficient data, a model of conditions for each condition of dust output level can be identified using node mapping for grouping the variables most influential on the dust output.

3.2 Material Sampling

To quantify and characterise the flue dust for sources of carbonaceous material, a representative sample is required, all samples were taken from the blast furnaces of TATA Steel UK. As per the diagram shown in Figure 44, the material in the downcomer enters a dust catcher. The method of catching dust varies between each furnace at Port Talbot. BF4 has a cyclone and BF5 has a dust catcher. Both offer challenges in terms of sampling material required for analysis and it is important to understand both to ensure representative samples are obtained. The importance of representative sampling was outlined in the work of Wing *et al.* discussed in section 2.8.3.

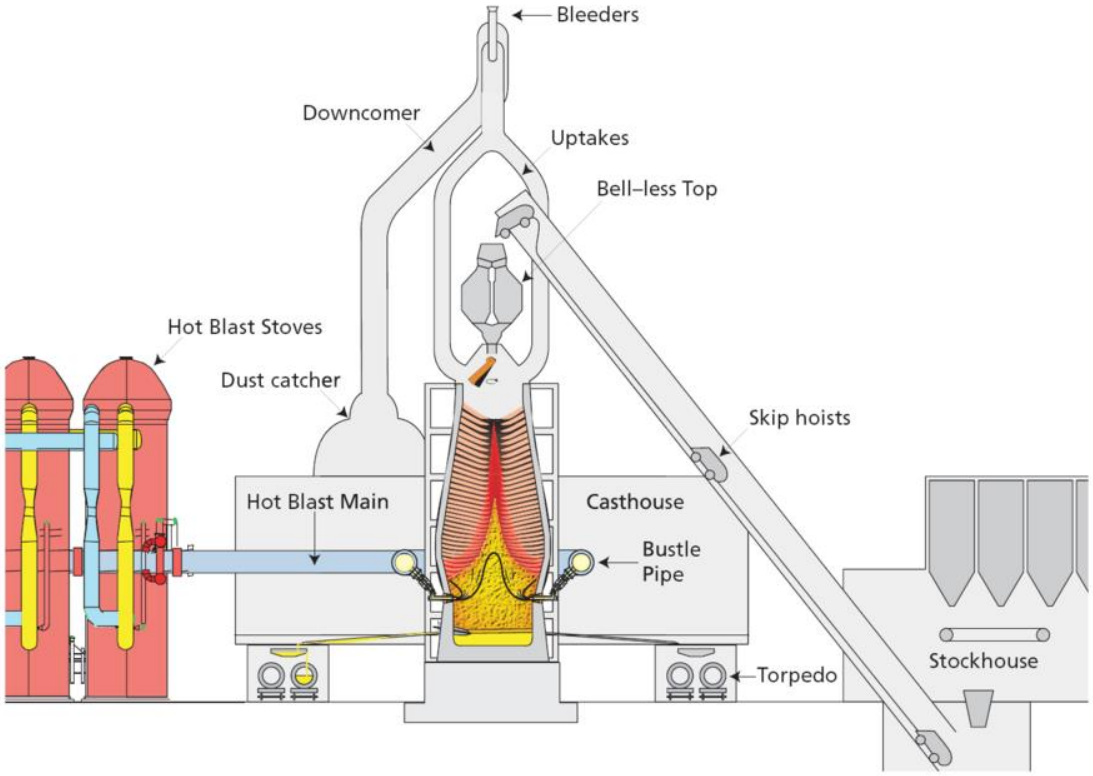

Figure 44 Blast furnace schematic[19]

The dust catcher, also known as the gravity separator, consists of large chambers, designed to reduce the velocity of the air stream drastically to encourage particles present, to drop vertically. The direction of the stream also changes from horizontal to vertical with the use of a target plate. As the air slows and moves down, gravity causes the large particles to drop out of the stream. There is an efficiency issue here though since smaller particles will continue in the stream and exit the dust catcher

and further processing via wet scrubbing is required to remove the finer particles from the air stream. A diagram showing the dust catcher process is seen in Figure 45[67].

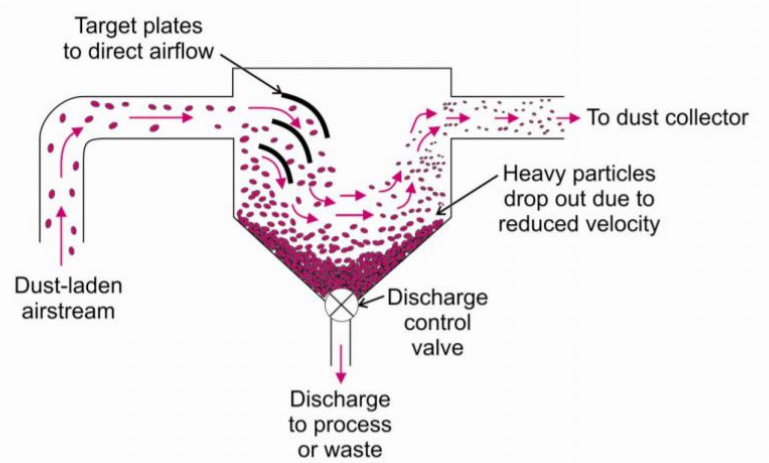

Figure 45 Dust catcher / gravity fed system[67]

The cyclone, as present in BF4, relies on centrifugal force to remove the finer particles, where inlet air is forced to spin and form a vortex. The change in direction causes inertia on the particles, which causes the particles to continue in the original direction, which is opposite to the air stream direction. As per Figure 46, two vortices are formed, a larger one at the top to separate the larger particles. A smaller vortex is formed at the bottom to collect the finer particles. Cyclones can handle high temperatures; the abatements also reduce the load on primary collectors. It can be difficult to predict the performance of a cyclone and cyclones require very consistent inlet conditions to work effectively. Often cyclones are used to remove larger particles before the stream continues to a second abatement such as a bag filter[67].

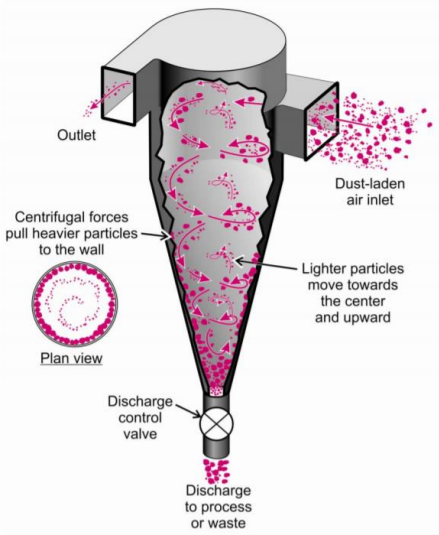

Figure 46 Cyclone system fitted at BF4[67]

Based on this information, it is important to consider the source of the sample and the bias in terms of particle size. A computational assessment of improved abatement options was carried out and a paper was written by Winfield *et al.* outlining the separation efficiency of the current abatements in situ[68]. The designs of each abatement were modelled and post processing of data from the dust particle size distribution generated the curves as per Figure 47, it can be assumed that the material collected post-abatement at BF4 will consist of a large range of particle sizes. This would indicate that almost all of the material could be captured before it goes to wet scrubbing. Also, as per Figure 47, the efficiency of the dust catcher is displayed. The data shows that there is good efficiency in collecting the larger size fractions, however, a distinct lack of efficiency in separating the finer particles can be observed. The separation efficiencies of BF4 and BF5 abatements are calculated to be 99.4% and ~68% respectively. Also, discussed in the paper by Winfield, is that the efficiency of the abatement on BF5 can vary depending on the degree of fullness and flow rate of the gas stream[68].

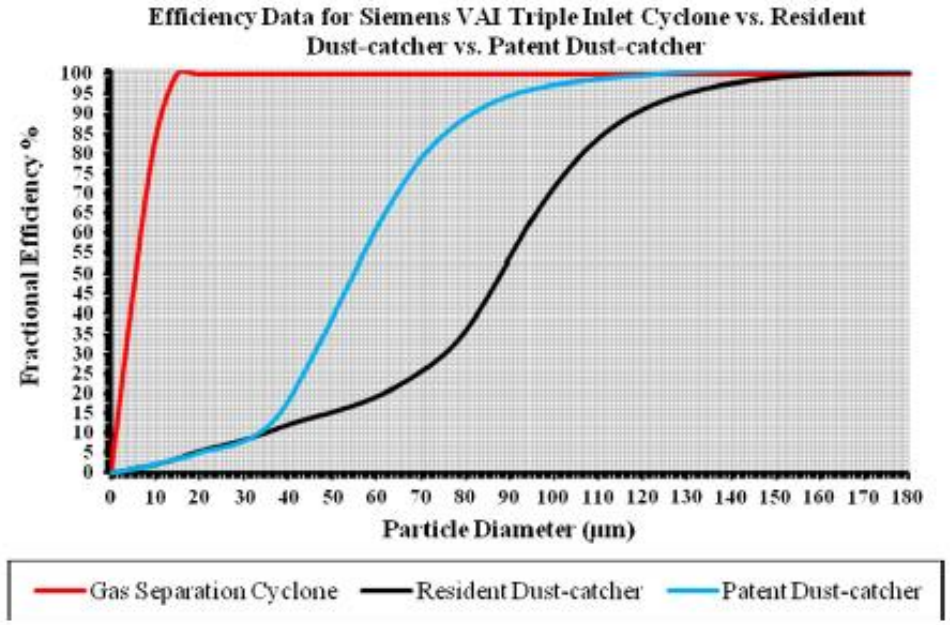

Figure 47 Particle separation efficiency of flue dust abatements[68]

3.2.1 Flue Dust

The efficiency of the BF4 cyclone technology indicated in this study gives confidence that the material obtained from BF4 is representative of the material in the downcomer. However, there are challenges when obtaining a sample from the abatement. The design of the cyclone considers the primary purpose, which is to separate dust from the gas stream. Due to increased dust stripping efficiency, ~32% more dust is collected per tonne of hot metal than BF5. This means that the dust is collected more frequently from BF4 to ensure that the mass of dust in the cyclone is maintained at a minimum level.

Every few hours, a lorry parks under the valve to be filled with flue dust for transport to the stockyards. The valve is opened until the lorry is full and is closed again. The sample is required to be taken from the overspill generated during this process. This makes the stockpile sampling difficult, due to the mass of material available. Despite the limitations when obtaining the material, the sample itself is representative of the material available for sampling. To obtain this sample, the best practice that could be implemented was to take any overspill totally.

BF5 by design is different, as there is less dust generated, and ultimately less has to be moved to the stockyards. The material is dropped underneath the abatement, and this is scooped up a loaded onto the lorry for transport. This material was less representative of the dust in the downcomer than BF4, but a more representative

sample could be taken from a small stockpile. The gas stream following this abatement moves through a wet scrubber as per Figure 48 for further cleaning of the finer particles from the gas stream.

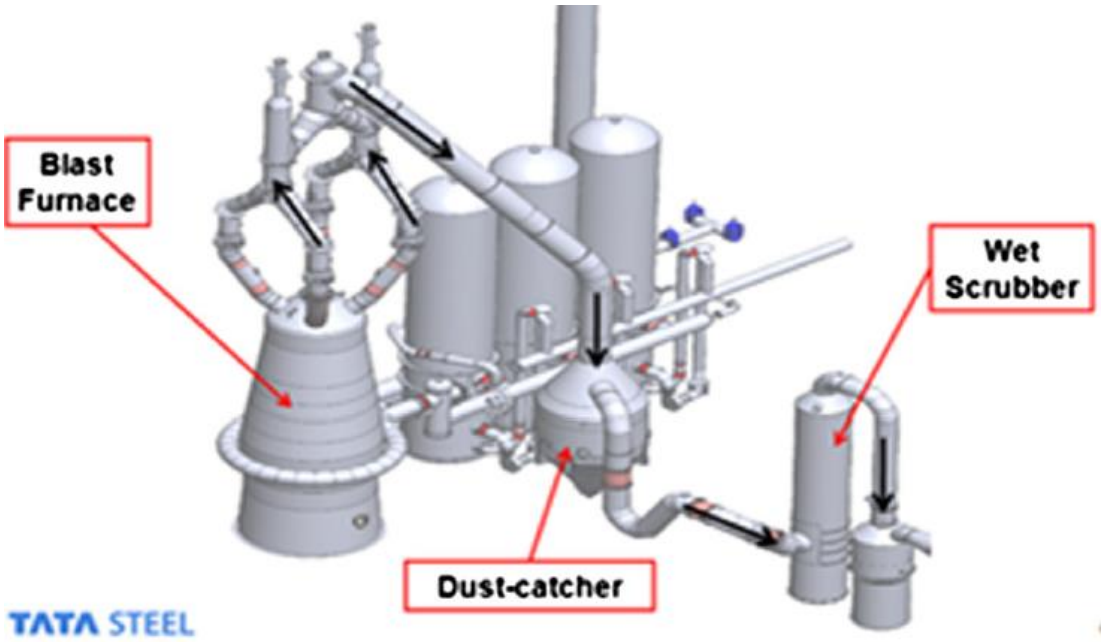

Figure 48 BF5 abatement schematic

3.2.2 Flume Sample

It is clear from the studies carried out in the research by Winfield *et al*., that some of the material from the furnaces was not available in these stockpiles. Hence, there was a requirement to capture the remaining material that passes through the dust catcher in the gas stream. Following dry abatement, on both furnaces, the gas is passed through a wet scrubbing abatement. The water used for washing, which contains the dust from the gas stream is transferred to a pond designed for separation called a weir. This is the large circular pond as seen in Figure 49. In the weir, there is a large paddle to agitate the water, this pushes the material that sinks to the bottom of the pond into the middle of the weir. The excess water flows over the side of the weir and should be clear of BF dust. This concentrated water at the bottom of the weir forms a sludge, which is pumped directly to the stockyards and is labelled as betsi. It can be assumed that betsi due to the nature of the abatements before it, is biased towards the finer less dense particles. It is thought that these particles contain more ferrous based particles as opposed to the more carbon based particles that would be captured in the dry abatement. To obtain the most representative sample and to avoid obtaining the legacy pond sample, the sample was taken from the flume running into the pond. The material

in the pond already may have been resident for hours or even days, therefore is unrepresentative of the material collected from the dust catcher or cyclone.

To collect the material, a plastic vessel was submerged in the middle of the stream. The stream has a depth of 50cm, the opening of the vessel was 50mm and the sample container held 500ml of water. Once submerged for 5 seconds, the vessel was removed from the stream and a lid was placed on for transportation. The same vessel was used for both BF4 and BF5 and was washed between samples to improve the repeatability of the sampling technique. The residence time of the vessel and the submerged depth were controlled to improve repeatability.

The sample was agitated by shaking for 10 seconds, before being filtered using a vacuum filtration system. The filter being used was a Glass Fibre Circle (GFC) filter with a pore size of 0.7µm, sufficient to capture the fine particles from the water sample. The material remaining on the filter was dried in an oven at 105^{o}C, in an air atmosphere until a constant mass was obtained. This was kept in a desiccator for analysis. The material that remained embedded on the filter was retained until an appropriate analysis technique was optimised.

Figure 49 BF5 at Port Talbot with weir

3.2.3 Bulk Density

The bulk density of the material was a critical measure for determining the steps required to obtain the manual sample. This measure was also used to quantify the

presence of more dense particulates in the work to compare dust from different abatements. A further use for bulk density values were that they could be used as a direct comparison to the outputs from alternative carbon type differentiation techniques, to determine its suitability as a replacement for the techniques outlined in section 2.10.3. Bulk density forms part of the equation to calculate the total mass of the sample to be taken to ensure it is representative. The bulk density analysis was carried out in accordance with ISO 11272:2017[69]. Here, a steel open-topped vessel of known dimensions and mass was filled to the top with the chosen material, in this case, the material was flue dust. The material was levelled off at the top to ensure it was flat and weighed. The mass of the vessel was subtracted from the total combined mass and this value was divided by the volume of the vessel to give a bulk density. This is the loose bulk density which differs from tap density, which is when the vessel is tapped against a solid surface during filling to fill any voids in the material. This gives an increased bulk density figure, which is why it is important to note which density is used. Either can be used depending on the application. In this application the material is stacked underneath the abatement in a loose form, hence loose density is required. The calculated bulk density of the flue dust material was 890 kg/m^3. The calculation was as follows in equation 3.1.

$$BD = \frac{(Mt - Mv)}{Vv} \qquad \textbf{3.1}$$

$Where$

$BD = Bulk\ Density\ (kg/m^3)$

$Mt = Total\ mass\ (kg)$

$= Mass\ of\ Material\ (kg) + Mass\ of\ Vessel\ (kg)$

$= 2.5845$

$Mv = Mass\ of\ Vessel\ (kg) = 1.25$

$Vv = Volume\ of\ Vessel\ (m^3) = 0.0015$

$$BD = \frac{(2.5845 - 1.25)}{0.0015} = 890 kg/m^3$$

3.2.4 Particle Size Distribution for Sampling Sublots

Another key value for determining the size of the sample required to ensure representativeness is particle size distribution (PSD). The maximum particle size is important as this has a direct effect on the particle count required in the sample sublot. The values for PSD were also used to compare the morphology of the particles collected from the dry abatement against the particles from the wet abatement. Based on the work by Di Zhao outlined in section 2.10.3, coal-originating carbon contributed to changes in particle size distribution in the dust, hence the data from the mastersizer was compared against LOC within blast furnace dust as a potential replacement for the current techniques of quantifying LOC. PSD samples were dispersed in 100% methanol for maximum dispersion and analysed using a Malvern Panalytical Mastersizer 3000. The Mastersizer 3000 employs a laser diffraction method for determining the size and size distribution of particles within a suspension. It does so by assessing the strength of light scattered as a laser beam passes through a dispersed particulate sample. The system then analyses this information to determine the size of the particles that caused the scattering pattern. The instrument is capable of measuring particles within the range of 0.01µm to 3500µm which is suitable for blast furnace dust material where the top size appears to be around 800 micron. The instrument calibration is checked once every 7 days using CRM0016 the expected values were as per Table 8. The acceptance criteria for the dispersion units are set at ± 2.5% for the Dv50, ±3% for the Dv10 and ±4% Dv90. Magnetic stirring was used to ensure homogeneity and the instrument was completely cleaned between samples to prevent any cross-contamination. The maximum particle size of this sample appeared to be 751 micron according to Figure 50. This value was used in the measurements for the representativeness of the sampling technique.

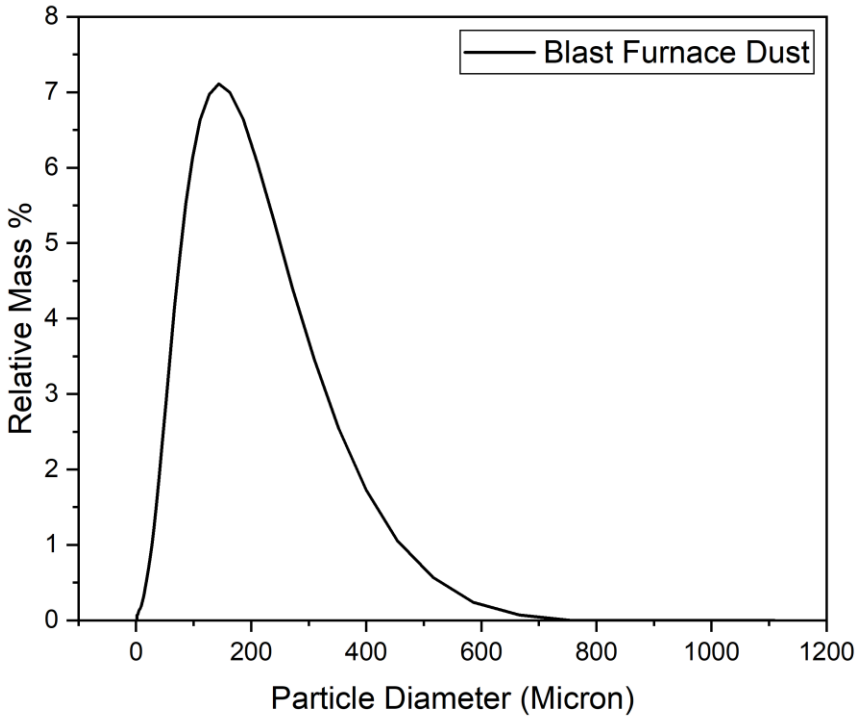

Figure 50 Particle size distribution of blast furnace dust

Table 8 Upper and lower control limits for CRM0016

	Dv10 / µm	**Dv50 / µm**	**Dv90 / µm**
Lower Limit	35.597	60.054	85.928
Target Value	36.698	61.594	89.508
Upper Limit	37.799	63.134	93.088

3.2.5 Stockpile Sampling

When sampling any type of aggregate, it is important to follow recognised standards to ensure the process is repeatable and the results produced are credible. The method of obtaining a sample will vary depending on the infrastructure available and key critical material properties such as the mass of the sample, maximum grain size and the loose bulk density of the material. Equation 3.2, for determining the sampling increment has been devised from experience with sampling similar aggregates. All the information required to representatively take a sample from a stockpile can be found in the British standard BS EN932-1:1997.

$$M = 6 \times \bar{D} \times \rho_b \quad \textbf{3.2}$$

M = Mass of the sample, in kg

$\bar{D}$ = Maximum particle size in mm

ρ_b = Loose bulk density in Mg (Megagrams)

The bulk density of the material was measured to be 890kg/m^3 or the equivalent of 0.89Mg/m^3, and the average dump size under BF5 was 52 tonnes based on the process data for T/day flue dust output. The maximum particle size was 0.75mm as determined using the Malvern Mastersizer 3000. Therefore, the required sample size was 4.01kg, to ensure a representative sublot was taken for analysis.

According to the standard, these sample increments should be taken across specific regions of the stockpile itself. Figure 51 depicts the regions from where the sample increments should be taken, this takes into account the natural flow of the material and distribution as it is deposited onto the ground. Generally speaking, the larger size fractions will be concentrated towards the bottom of the pile, whereas the smaller, finer material will concentrate towards the peak of the stockpile. The mass of the sample required to be taken at each increment from the top, middle and bottom of the pile, was 0.1602kg, 1.041kg and 2.804kg respectively. It is certainly not practical in the field to measure these increments out accurately. To compensate for the practicality, a 500g scoop was used. Ensuring to leave equal space between sample sites, scoops were taken from the surface of each layer of the pile. 1 scoop was taken from the top third of the pile. 2 scoops were taken equally spaced around the middle third of the pile. Finally, 5 scoops were taken from the bottom third of the stockpile[70].

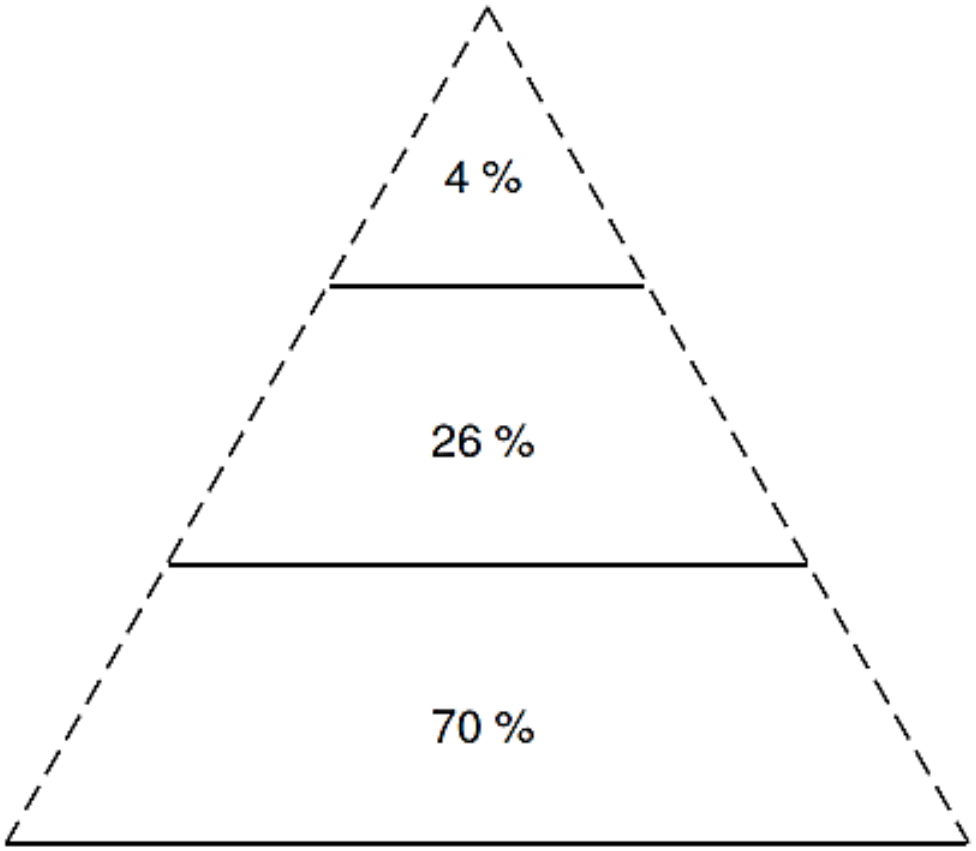

Figure 51 Sampling regions of a round-based aggregate stockpile[70]

3.2.6 Splitting Down Sublots

In total 8 scoops, each containing 500g of material were sampled from each pile of material. This equates to roughly 4kg of material. This was far too much material for storage, as very little was required for analysis. For this reason, the sample was reduced to a more manageable size for storage and analysis. There are many ways to do this, but a recognised method was followed to ensure the sample remains unbiased. The sample was mixed thoroughly to ensure homogeneity throughout the sample. The technique used in this case was cone and quartering, other techniques include riffle boxes where the material is fed into a hopper and drops onto dividing fingers which alters the direction of a weighted portion of the material. And spinning splitters, where jars rotate around a chute and are filled in order around the chute. The cone and quartering method was adopted, the material was piled onto a flat steel mixing plate. It was shovelled completely to form a new pile. This process was repeated a minimum of 4 times to ensure the sample was mixed sufficiently. Once mixed the pile was flattened into a circle as per Figure 52, and the circle was divided into 4 equal quarters. 2 quarters were discarded and 2 formed the sample. In this case, the whole process was

repeated until 500g of the sample remained. This meant mixing and splitting the sample twice until roughly 500g of the sample remained. This technique gave confidence in the sample ensuring that it was homogeneous for any subsequent analysis.

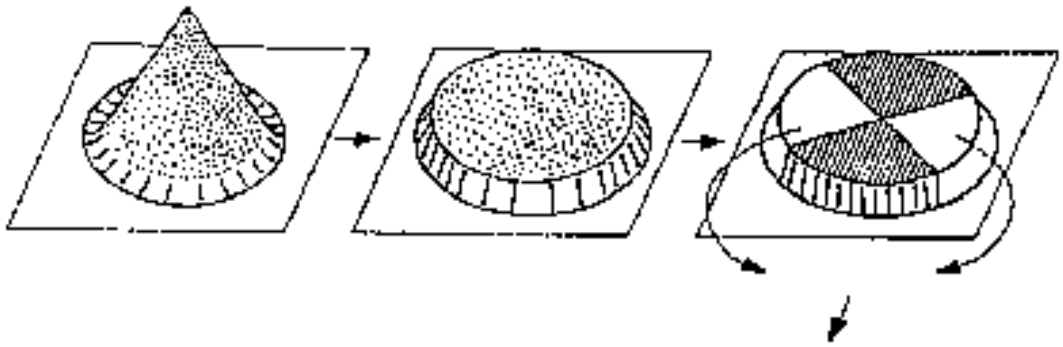

Figure 52 Cone and quartering technique for sample splitting[70]

3.2.7 Catalogue of Blast Furnace Dust

Dust

Dust samples were obtained from the dry and wet abatements as per sections 3.2.5 and 3.2.6. 45 samples of dust from each abatement were considered in the thesis. These were from a period spanning 9 months to allow for enough variation in the process conditions and raw material types, for a good representation of natural variation within the process. The dust from the dry and wet abatements was taken within 15 minutes of each other to allow for representativeness and a reasonable comparison allowed to be drawn between the material types. A catalogue of 90 samples was sampled in total, selected using process data, to determine when the furnace was operating "normally." This catalogue of samples has been analysed throughout the thesis particularly when comparing the dusts to process parameters. Samples from the days where injection rates of <100 kg/tHM were not considered among these samples because these are indicative of operational problems or periods of reduced production[65].

Float Material

During a large dust release event at Tata Steel Port Talbot, excess dust was deposited into the wet cleaning system, leaving material at the surface of the clarifying pond. This material was collected into a 5l vessel. 1l of water containing float material was dried until constant mass at 105^{o}C. The resultant material was characterised to determine the root cause of the incident.

Slurry

45 samples of slurry in the water flow from the water tower of the second gas cleaning abatement were taken coincidentally with the dust samples, for suspended solid instrument validation and characterisation of the blast furnace dust. The samples were filtered using Glass Fibre Circle's (GFC's) and the remaining dust samples were retained for analysis.[65]

3.2.8 Blast Furnace Raw Materials

To determine which material constituents are present within the dust and therefore contribute to its generation, samples for comparison were obtained from the stock house of BF4 of each raw material, following the principles in the British standard for sampling outlined in section 3.2.5[70]. Samples of limestone, iron ore pellet, sinter and iron ore lump were obtained and prepared for analysis as discussed in section 3.2.6.

3.2.9 Coke

Coke was obtained from the Morfa Coke Ovens at Port Talbot for the use of normalisation and synthetic char doping trials for the validation of the CET method. 1 sublot was obtained following the procedure outlined in section 3.2.6 of this thesis. The coke was dried and sieved to remove any under-carbonised material, before being crushed in a BJD Crushers jaw crusher. The small lumps were pulverised using a swing mill for 20 seconds to reduce the thermal effects on the carbon.

3.2.10 Coal Char

Synthetic char was obtained collaboratively, to mix with coke to make synthetic doped coke samples[71]. A sample of coal was combusted using the DTF. Normally the DTF is used to analyse the burnout of coals, but in this case, the char was retained for analysis. Coal particles were fed into the top of the tube furnace at a feed rate of 30 g/h at 1100^{o}C. The particles were entrained in a 20 l/min laminar airflow and the ash was collected at the bottom using a cyclone collector. The particle residence time was set to 35ms by altering the distance of the mobile water-cooled collection probe from the water-cooled inlet feeder. The coal used to produce the char was low-volatile injection coal, the properties are outlined in Table 9.

Table 9 Proximate analysis of coal used for char produced in the DTF

	Ash (%)	Volatile Matter (%)	Fixed Carbon (%)
Synthetic Char	7.7	13.2	79.1

The synthetic char and coke blends for CET validation were blended by weight% using a balance to measure out quantities of char and coke as per Table 10. The resultant mixes were agitated in a centrifuge tube to ensure homogeneity.

Table 10 Blends of synthetic chars with coke for CET validation

	Char (wt%)	Coke (wt%)
1	100	0
2	80	20
3	60	40
4	40	60
5	20	80
6	0	100

3.2.11 Coal

A stock of coal was required to reproduce the blends in operation on each of the days that dust samples, were collected from the silos as described in section 3.2.8. The coals were collected pre-crushing therefore were required to be granulated using a BJD crusher's hammer mill. The coals were reduced to 95% <1mm and blended by the mass fractions outlined in Table 11. For homogeneity, blends of 5kg were produced and each analysis portion was used from this sublot subsequently.

The blends of coals and individual coals that were used were analysed for their chemical properties. Often coal blends are selected based on cost and availability, but for stable operation, it is common to make incremental changes to blends as opposed to macro changes[72]. Coal B was low-volatile bituminous coal and was a component of all the blends. The availability of this coal and coal E was good, hence the blends

appear to be based on these coals. Blends tend not to change often and therefore present problems with data resolution which should be considered when analysing the data.

Table 11 Coal blend per mass fraction of coal

	Coal A	Coal B	Coal C	Coal D	Coal E
	%	%	%	%	%
Blend 1	11	11	-	-	78
Blend 2	17	17	-	-	66
Blend 3	12	23	-	-	65
Blend 4	-	50	-	50	-
Blend 5	-	33	17	50	-
Blend 6	-	66	-	-	34
Blend 7	-	33	-	-	67
Blend 8	12.5	37.5	-	50	-
Blend 9	-	40	-	60	-
Blend 10	-	1	-	-	99
Blend 11	-	25	-	-	75
Blend 12	-	40	-	-	60
Blend 13	7	36	-	-	57

3.3 Characterisation Methods

3.3.1 Scanning Electron Microscopy

SEM and energy dispersive spectroscopy (EDS) analysis was conducted on the material for characterisation of each of the raw material constituents. It was also used as supporting analysis for each stage of the alternative combustion technique outlined later in this thesis in section 3.4.3 to check the morphology of the material and the corresponding chemical composition. It was also used to explain the differences between the effect each stage of the technique had on the dust material. Samples of float material we also characterised using the SEM and EDS to compare the morphology with a typical BF dust and compare analysis from the EDS to determine the cause of the dust on the clarifying pond incident outlined in section 3.2.7.

Samples were mounted using pin stubs with carbon stickers to promote conductivity. The selected samples were dried at 105^{o}C for 4 hours to ensure total dryness. The pin stub with the carbon sticker was introduced to the dry material so that a single layer of particles adhered to the surface. Any loose particles were removed with a jet of compressed air, to prevent any problems in the vacuum of the chamber in the SEM. The SEM used was a Zeiss Evo LS25. The stubs with the material were mounted onto the carousel of the instrument for analysis. For investigation purposes,

the samples were observed under magnifications of 25x, 50x and 150x of each setting. Backscatter was used to help with contrast, as the material contained elements mainly of a lower atomic mass, resulting in charging under secondary electron. The backscatter was also the justification for using SEM coincidentally with optical microscopy, the contrast between material of different atomic weights helps inform the origin of each of the particles. The current was set to 300pa, and the voltage (EHT) was set to 20kV. SEM was a good technique to use for the general investigation of the sample and for detecting the presence of charcoal. EDS was also carried out on the samples to give an overall chemistry of the material. The EDS was relatively subjective, therefore absolute chemistries should not be determined, but it gave a qualitative analysis and elemental distribution and reinforced the chemistries derived using other methods.

3.3.2 Optical Microscopy

To ascertain the presence of char cenospheres in the blast furnace dust samples and generate images suitable for ImageJ manipulation for carbon particle counting, samples were hot mounted in polyvinyl formal resin. This resin best suited this dust material due to enhanced contrast colour to the sample as opposed to phenol formaldehyde resin, which is dark in colour. Polyvinyl formal also has a superior ability to hold on to dust during grinding and polishing, because the material shrinks during cooling. The polished specimens were imaged using a Zeiss Primotech light microscope. Different degrees of light polarisation were used to achieve the best-quality image. This was particularly useful when using software such as ImageJ or Zen Intellisis to differentiate between material types within samples.

3.3.3 Proximate Analysis

Proximate analysis was used to characterise coal and coal blends used throughout the thesis, proximate analysis was also used to quantify the degree of highly reactive particulates that remain within the dust along with LOI as described in 3.3.9. The analysis from this combination of techniques was aimed at identifying the sources of the particulates within the dust and determining the degree of variation between the samples and sample types.

Proximate analyses were carried out manually per the publication of the British standard for the proximate analysis of coal[53]. Moisture analysis was carried out using

a Memmert UN30 drying oven at 105°C until constant mass to ensure dryness. 10g of the sample was weighed into a metal drying tray. The mass loss was divided by the total mass to calculate the moisture portion of the material.

Volatile Matter Content (VM) was carried out in air, in a volatile crucible with a lid inside a muffle furnace set at 900°C for 7 minutes. The sample was weighed before and after and the VM was determined as the mass-lost portion of the sample.

A swelling test was carried out in a specialist Carbolite swelling number furnace. The test was carried out in a swelling crucible at 900°C for between 3 and 5 minutes in an air atmosphere. The resultant swelling button was compared to a standard reference chart as per Figure 53[73]. The result was a number relating to the degree of swelling and was relative to the carbonisation properties of the coal.

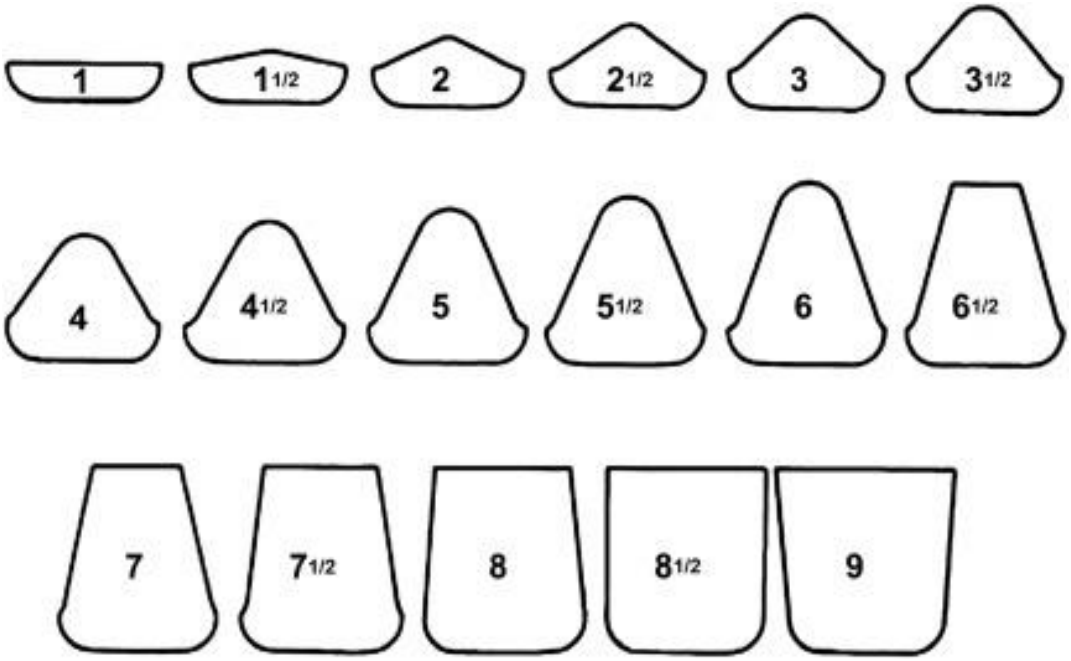

Figure 53 Chart of swelling buttons for comparison[73]

Ash analysis was carried out in an ashing furnace at 815°C for 1 hour in an air atmosphere, the mass remaining per the total mass is relative to the ash constituents of the sample including alkali and refractory compounds that remain after the combustion of coal.

3.3.4 Carbon and Sulphur

To normalise the carbon types derived from the carbon type analysis chapter, an Eltra CS500 C/S analyser was used to quantitatively measure carbon and sulphur in the BF dust. The carbon measurement was also used to validate the carbon type differentiation

technique to ensure the total carbon determined by the alternative technique was equal to the total carbon of the sample. Al_2O_3 combustion boats with 200 mg of powdered material were precisely weighed and charged into the analyser's horizontal tube furnace. The furnace was preheated to 1450°C and purged with a 4 l/min O_2 purge to allow for the oxidation of carbon and sulphur into CO_2 and SO_2 respectively.

3.3.5 Ultimate Analysis

A Costech elemental combustion system was used to determine the oxygen, nitrogen and hydrogen content of the coal samples. This analysis was important in determining the amount of coal than can replace coke within a blast furnace. This has been outlined in section 0. Between 1.8 and 2.2mg of sample was weighed into a tin capsule with 5-6mg of vanadium pentoxide for combustion acceleration. The capsule was loaded into the instrument and combusted under pure oxygen. The off gas was transported to gas chromatography for separation using helium inert carrier gas. Followed by off-gas detection by thermal conductivity.

3.3.6 Powder X-Ray Diffraction

XRD was utilised coincidentally with the SEM to check remaining constituents post-digestion *and* combustion, during the digestion and combustion trials outlined in section 3.4.3. It was also used to measure the changing morphology of the amorphous carbon peak to determine the impact of the acid on it. Phase identification techniques using the XRD were used to investigate the key differences between the float material outlined in section 3.2.7 and typical BF dust phases. The shape of the amorphous carbon peak was used to identify the dominant carbon layering and degree of graphitisation as an attempt to differentiate between carbon types in blast furnace dust.

XRD analysis was used to determine carbon stacking parameters and mineral identification. It was performed using a Panalytical Empyrean S3 (Co-Kα1 $\lambda = 1.78901$ Å, 10 – 120 °, s = 0.066 °, t = 20 s). A rotating stage was used to improve the data and bias from the preferred grain orientation[74]. The diffraction patterns were interpreted using Bruker Diffrac Eva software with access to the crystallographic open database.

3.3.7 X-ray Fluorescence

To determine any carbon to ash constituent relationships, X-Ray Fluorescence (XRF) analysis was carried out on the blast furnace dusts. XRF analysis was also used to

characterise the coal and the subsequent blends as ash content is thought to influence coal burnout as outlined in the literature review. 20g of material was ashed in an ashing furnace at 815^{o}C for 10 hours. On removal from the furnace, the ash was stirred to ensure the whole sample had turned to ash. Around 0.3g of ashed sample was mixed with Fluore-x 65 Flux in a ratio of 1:17. The mix was transferred to a platinum crucible for fusion into a glass bead using a phoenix bead maker.

The cooled bead was suitable for measurement using a Panalytical Axios Fast WDXRF Spectrometer. Standard reference material of sinter, iron ore and BF dust was used to develop the calibration required for the analysis of metal oxides. This technique was used to quantify the refractory elements present within blast furnace dusts.

3.3.8 Inductively Coupled Plasma – Optical Emissions Spectroscopy (ICP-OES)

Inductively Coupled Plasma – Optical Emissions Spectroscopy (ICP-OES) was used to determine the difference in metals analysis between typical BF dust samples and the event material described in section 3.2.7, The difference in metals was aimed at determining the root cause of the float material incident and the material properties of the constituents of the material. The ICP-OES was also used to quantify the degree of metallic element removal when trialling various acids for the modification of the digestion and combustion techniques as detailed in section 3.4.3. To determine the metals and alkali content of the blast furnace dust, samples were digested in 13cm^3 aqua regia for 180 minutes using the DigiPREP jr. block digester at 120^{o}C. A watch glass was added to the top to allow for reflux. The refluxed samples were made up to 50cm^3 with deionised water before being centrifuged and analysed using an Agilent 5100 ICP-OES with an SPS 4 autosampler, Plasma gas flow set at 12.0 l/min, Plasma Gas was Argon, Nebuliser flow rate was set to 0.7 l/min, Sample up take was for 30s with the pump at 12 rpm and the RF Voltage used was 1.2 kW 240 V. Multi-element standards were created with a calibration range between 0.5-100ppm with the same matrix as the samples. The regression of the calibration curve exceeded 0.9990 which was deemed to be in the acceptable range for accuracy.

Preparing a sample for ICP requires the dust to be digested into an aqua regia solution consisting of 10cm^3 HCl and 3cm^3 HNO_3. This extra step can potentially lead to loss of material particularly if the metals required to be analysed do not go into solution readily. To ensure this was not an issue for this particular type of sample, a

calibration standard was used consisting of furnace dust[75]. Certified Reference Material (CRM) 884-1 was used because it was the closest matching material to the dust materials used for analysis. The expected values for the CRM can be seen in Table 12.

Table 12 Certified reference material 884-1, expected analysis versus recovery

Certified Analyte	Certified Composition (Wt%)	C(95) Error	Actual Composition (Wt%)	Recovery (%)	Standard Deviation (%)
Fe	31.67	0.13	31.42	99.21	0.50
Zn	17.5	0.07	17.42	99.54	0.25
Cr	1.86	0.04	1.81	97.31	0.12
K	0.979	0.014	0.952	97.24	0.08
Pb	0.442	0.006	0.433	97.96	0.05
Ni	0.197	0.006	0.190	96.44	0.02
Cu	0.156	0.002	0.149	95.51	0.02
Ba*	*	*	0.081	*	0.01
V	0.0303	0.0013	0.029	95.70	0.01
Na	0.585	0.015	0.587	100.34	0.06

* Not certified but detected and determined

All the measured recoveries of each of the analytes were above 95% and the technique for digestion was determined suitable for this particular dust[76]. The potential sources for error can include measurement errors from the glassware and the balance. The material itself will have a degree of uncertainty hence the presence of C(95) values. It is clear from the data that Iron is the most uncertain measurement but is still within a reasonable degree of uncertainty.

3.3.9 Loss On Ignition (LOI)

Similar to the VM from the proximate analysis section 3.3.3, loss on ignition (LOI) analysis was carried out in an ashing furnace at 1000^{o}C for 3 hours in an air atmosphere, the mass loss per the initial mass is a measure of combustible materials and the degree of loss on ignition of the sample. The values for LOI are important to

compare against the carbon values in blast furnace dust, this will determine if there is a relationship between the combustibility and carbon type of each dust.

3.4 Carbon Type Differentiation Methods

Where carbon type differentiation of blast furnace dust was explored, the following techniques were utilised following a similar methodology for all blast furnace dust and sludge samples.

3.4.1 Thermogravimetric Analysis - CET

TA Instruments SDT Q600 was the analyser used to recreate the CET outlined in section 2.10.3 and subsequent TGA techniques. The CET was used to quantify the presence of LOC within the blast furnace dust which is indicative of the presence of coal char, as explained in section 2.10.2. 20 mg ±0.5 mg of the sample was weighed into Al_2O_3 crucibles. 100ml/min of compressed air was used as a reaction gas to promote oxidation of the carbon within the dust. The program for testing included 1^{o}C/min ramps between a 30 minute isotherm at 175^{o}C, 390 minute isotherm at 475^{o}C, 330 minute isotherm at 600^{o}C and a 30 minute isotherm at 1000^{o}C. As outlined by Wing *et al.*, two isothermal holds were introduced at 475^{o}C and 600^{o}C to allow for the LOC and HOC to respectively oxidise and the ramp rate was fixed at 1^{o}C/min. The length of the holds was defined to minimise the overlap in oxidation between these two carbon types[55]. According to Wing *et al.,* the suitability of this method for industrial samples has been established using synthetically doped coke and chars [55,61].

Repeatability

Some of the analysis was carried out at the Materials Processing Institute (MPI) using the Netzsch STA 409 PC Luxx. The data from the MPI instrument was compared to the TA Instruments SDT Q600. Challenges of equipment availability were overcome by carrying out the repeat and check analysis using the TGA at MPI. To remove any doubt from any potential errors caused by using different analysers a repeatability study was completed on 10 samples. The previous CET work assessed blast furnaces that use only PCI systems as opposed to GCI systems. The difference between the two was predominately size fraction. PCI aims for 60% of the material to be less than 65 micron, as opposed to GCI which was coarse, measuring up to 2-3mm[36,77]. A larger

PSD was therefore attributed to GCI which was thought to result in a greater variation in combustion as per the effects of PSD reviewed in section 2.8.3. It was therefore important to analyse if the CET was suitable for dust samples from GCI systems. An initial programme of ten repeatability tests was conducted on dust apportioned from Sample 1 to ensure that the variation in PSD did not result in significant test variability during TGA and that the data was within the 6σ range. The variation within the sample remained within the control limits for all the calculated constituents including LOC, HOC, soot, ash and moisture as per Figure 54. With satisfactory repeatability as all datapoints fell within the upper and lower control limits of the 6σ chart, TGA was subsequently conducted on all of the BF dust samples.

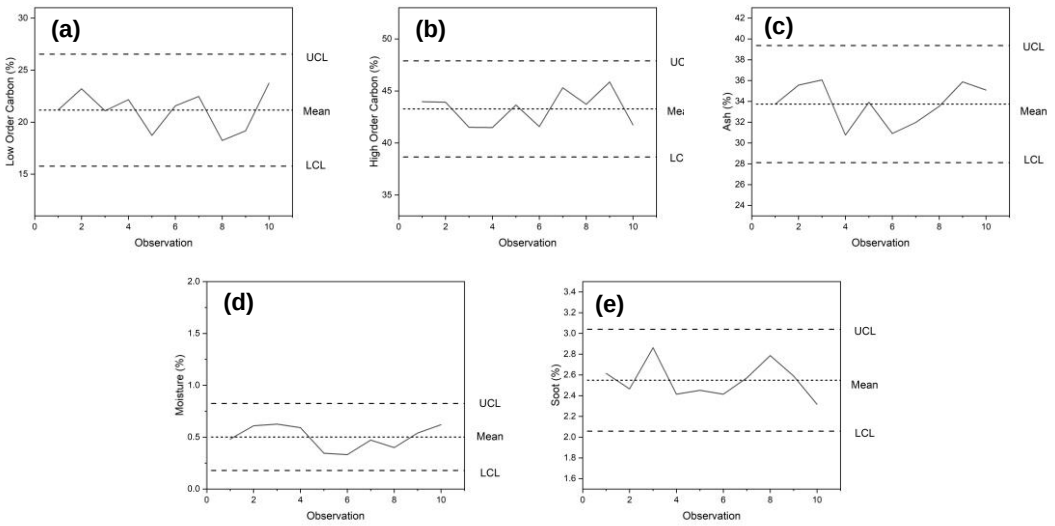

Figure 54 Control charts for the repeatability of BF dust samples a) low order carbon b) high order carbon c) ash d) moisture e) soot

To confirm the work of Wing *et al.* and investigate the suitability of the coke from this trial and the char developed by the DTF[61]. A char in coke doping trial was completed as described in section 3.2.10. The resultant Thermogravimetric (TG) and Differential Thermogravimetric (DTG) curves can be seen in Figure 55, where the char peak was strongly pronounced in the top left graph of 100% char. The char peak diminishes with the increasing coke peak as the samples evolve from a to f of Figure 55. It was clear to see the effect of the LOC and HOC in the data, hence the CET was suitable for detecting and quantifying char in dust samples.

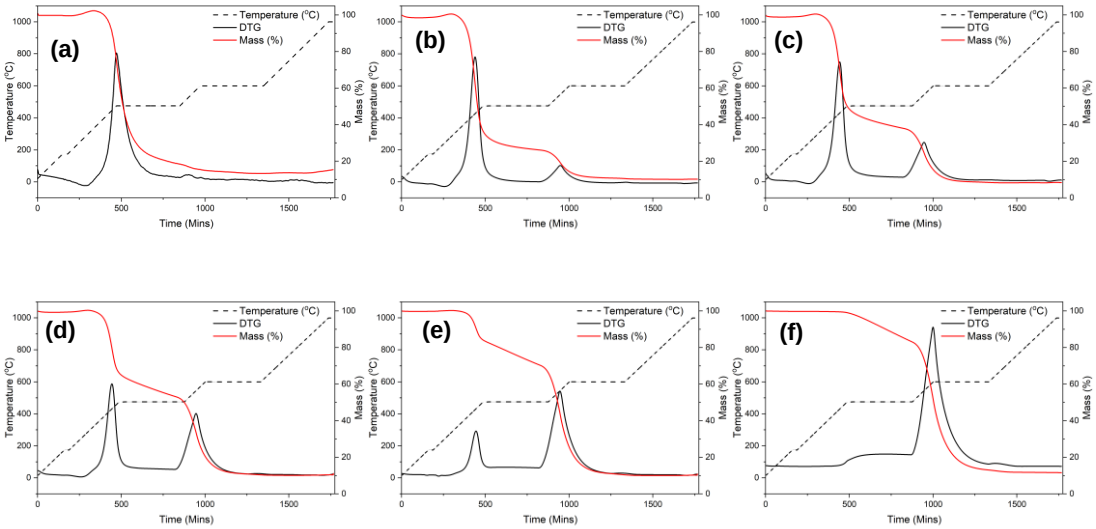

Figure 55 DTG and TG curves for various char-doped coke samples a) 100% char b) 80% char and 20% coke, c) 60% char and 40% coke d) 40% char and 60% coke e) 20% char and 80% coke f) 100% coke

The regression chart was analysed as per Figure 56, where the relationship between the %LOC detected using the CET was plotted against the actual %char in the coke and likewise for the %HOC and the %char in the coke. The R^2 was 0.98 and 0.99 respectively demonstrating the ability of the test to accurately determine char quantity in samples from Port Talbot.

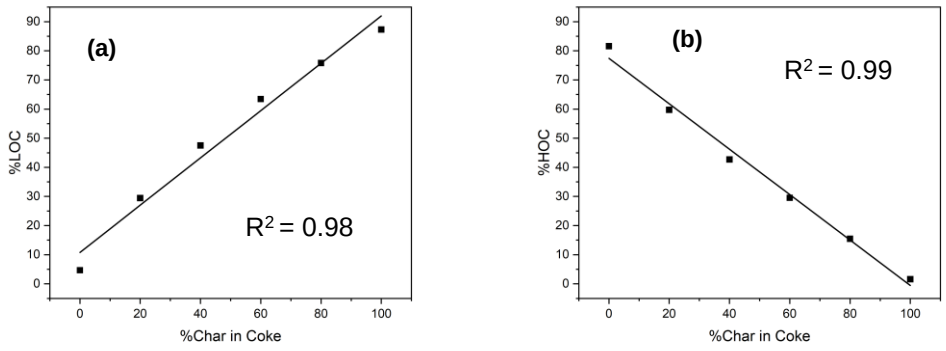

Figure 56 Regression graphs for the char doping trial a) LOC% versus %char in the coke b) HOC% versus %char in the coke

Normalisation

The CET produces resultant peaks such as in Figure 57a when analysing BF dust. In Figure 57a, the left peak refers to the concentration of LOC and the area beneath the right-hand peak was a reference to the concentration of HOC in the sample. Despite the lengthened isothermal hold at 475ºC to allow for complete oxidation of the LOC,

the DTG in Figure 57a doesn't return to zero, indicating some overlap in carbon types. According to the procedure outlined in the literature review section 2.10.3, sieving the materials with a 150-micron sieve to remove HOC contamination should minimise this issue. To remove this factor an attempt was made to normalise the HOC data to remove this effect. By subtracting the coke HOC peak Figure 57b, which was analysed separately, from the DTG of the sample. The resultant DTG was given in Figure 57c. The LOC and HOC from the resultant peak are therefore the normalised analysis without the influence of coke HOC. This work aims to remove the overlap of the carbon types within the dust samples to improve the CET and the values for LOC.

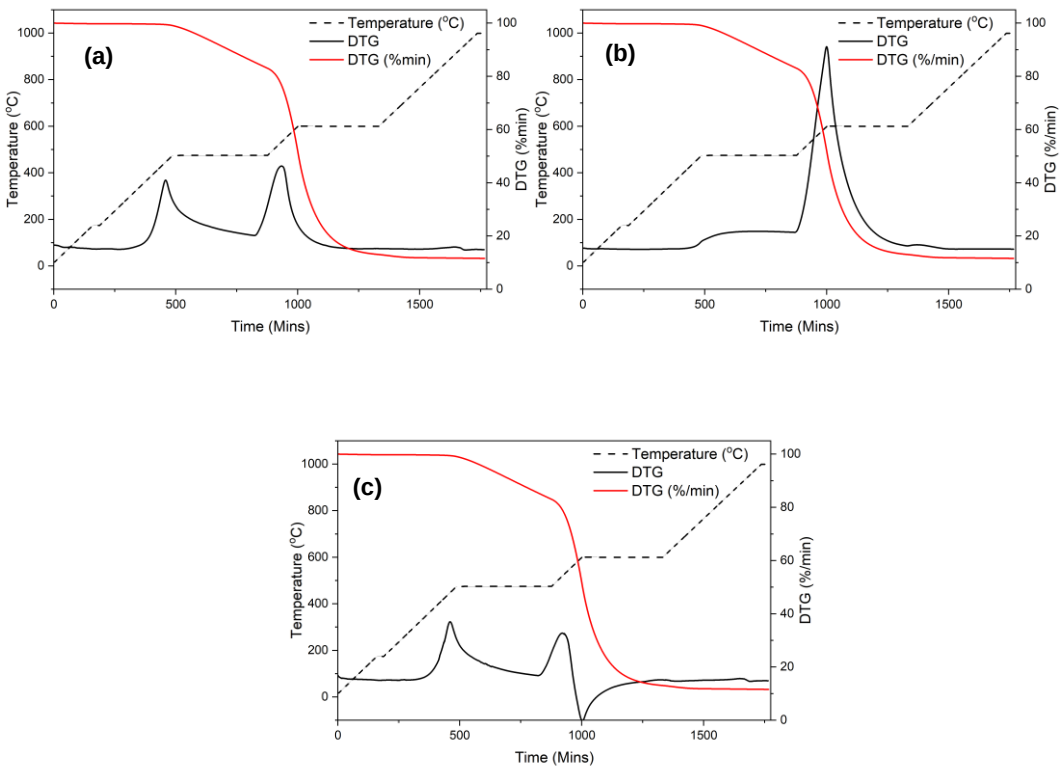

Figure 57 DTG Graphs a) raw dust sample b) raw coke sample c) raw coke DTG subtracted from raw dust

Low Order to High Order Carbon Ratio

The low-order to high-order ratio (LO:HO) was an technique used to determine the amount of LOC, normalised to the total carbon within the sample, thus removing the influence of ash constituents within the dust on the LOC. This ratio was calculated as per equation 3.3, by dividing the LOC determined by the test, by the HOC.

$$LO{:}HO\ Ratio = \frac{\%\ Low\ order\ carbon}{\%\ High\ order\ carbon} \quad \textbf{(3.3)}$$

Cross Instrument Comparison

Due to the impact of Covid-19 and equipment availability in Swansea University some of the TGA testing was carried out at the Materials Processing Institute (MPI). Raw data files from the instrument were collected and a cross comparison carried out. The results of the comparison between instruments at Swansea University and MPI, can be seen in Figure 58 and Table 13. For each of the tests, the regression was good, including the LOC and HOC for which the R^2 values remain above 0.98. The moisture calculation of the test was not compared as it was irrelevant to the overall analysis using the CET and moisture was inevitably lost or gained during the transport and storage of the samples.

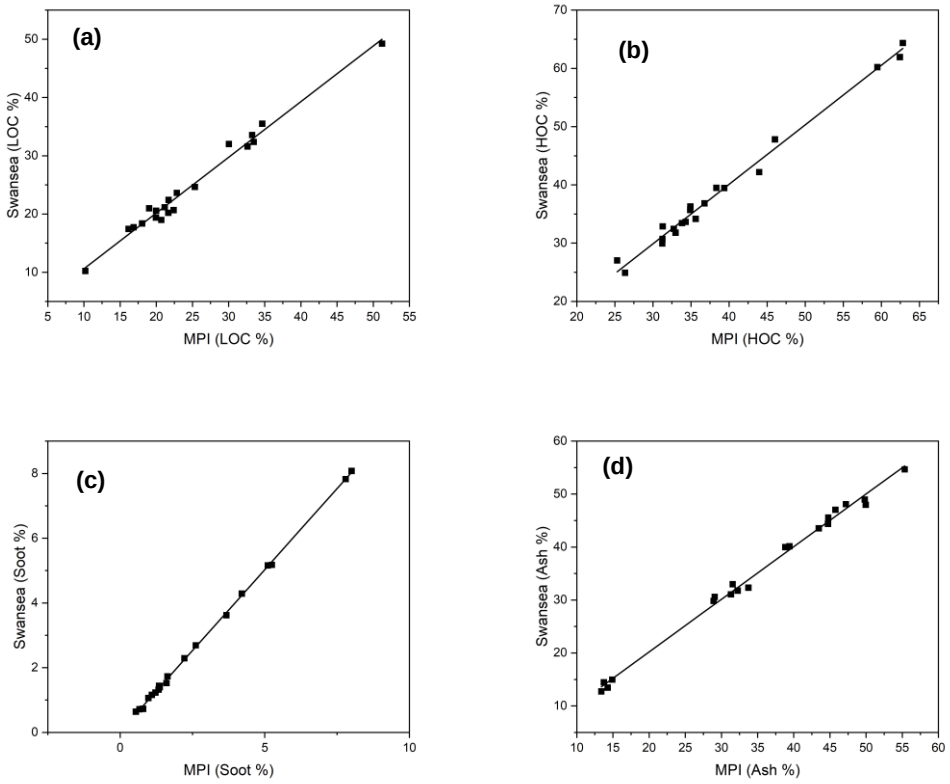

Figure 58 Regression charts for TGA analysis round robin between Swansea and MPI a) LOC % b) HOC % c) Soot % d) Ash %

Table 13 R^2 values for round-robin validation between Swansea University and MPI

	%LOC	%HOC	%Soot	%Ash
R^2	0.983138	0.989358	0.999272	0.994239

3.4.2 Modified CET

The current CET profile takes more than 1600 minutes to analyse a single sample, meaning it was not possible to analyse coal combustion daily, and therefore no capability to respond to any change in furnace condition on plant. The first technique attempted was to modify the thermal profile for the CET. The aim here was to therefore suggest a new thermal profile for TGA, to reduce the overall testing time to allow rapid response carbon type differentiation, enabling at least one sample to be characterised per day. Following optimisation trials of the thermal profile, the final modified CET condition comprised of increasing the ramp rate from 1°C/min to 20°C/min, while the isotherms were held at similar temperatures and durations as per the CET to minimise the overlap between the carbon types. The overall duration of the test was approximately half that of the original CET at around 16 hours meaning at least one test could be carried out daily.

3.4.3 Combustion and Digestion

Research conducted by Winkler in 1984, outlined a technique for quantifying charcoal in soil sediment samples, which consisted of nitric acid digestion and ignition to measure the relative frequency of charcoal in lake and bog sediment. It was discovered that the technique returned similar values of charcoal to when charcoal particles were manually counted under a microscope and the analysis was completed in less than half the time[78]. Soil can be relatively complex, soil and blast furnace dust are chemically different substances. Soil is a natural mixture of minerals, organic matter, water, and air, and typically contains a variety of elements such as silicon, aluminium, iron, calcium, potassium, magnesium, and others in varying amounts, depending on the type of soil and its location[79,80]. Blast furnace dust, on the other hand, is a by-product of the steel-making process, composed of fine particles of iron oxides, primarily Fe_2O_3 and Fe_3O_4, as well as smaller amounts of other metals such as zinc, lead, and cadmium[81]. It also contains carbon, which is a component of the coke used in the blast furnace. Overall, the chemical composition of soil and blast furnace dust is very

different due to their distinct origins and properties. Both have very different constituents which would react differently to nitric acid digestion. The work by Schwalbe described in the literature review section 2.10.3 helped direct which acids would be used. This aspect of the experimental methodology aimed to assess the applicability of the Winkler method for carbon type differentiation, a novel concept which has not yet been trialled. An investigation was undertaken to assess the suitability of alternative acid digestions to replace the chemical oxidation stage and evaluate the effectiveness of the acid, for removing elements without impacting the carbon remaining, similar to the work of Schwalbe. The acid solutions used for investigation were iterations of aqua regia as per Table 14.

Table 14 Iterations of aqua regia for replacement of digestion stage

	HNO_3 (cm^3)	**HCL (cm^3)**	**H_2O (cm^3)**	**H_2O_2 (cm^3)**
Acid 1	13	0	0	0
Acid 2	10	3	0	0
Acid 3	5	1.5	6.5	0
Acid 4	3	10	0	0
Acid 5	1.5	5	6.5	0
Acid 6	3	7	0	Dropwise until residual organic matter digested

The aim of this technique was to enable batch processing of samples to reduce the time for analysis significantly.

3.4.4 X-Ray Diffraction Carbon Parameters

The morphology of the amorphous carbon peak in the XRD spectra was compared with the data from the CET to highlight an opportunity to replace the CET with a fast XRD technique. XRD was a useful tool for identifying crystallite phases, particularly in complex materials such as furnace dust. One of the limitations when analysing BF dust is an amorphous region of carbon present between 25^o and 33^o[82]. This can often hide peaks such as graphite and Fe_2O_3. This broad region can be used to identify some key parameters and characteristics of the carbon itself. Similar to the work of Di Zhao discussed in section 2.10.3. By deconvoluting two gaussian peaks around 28^o and 31^o

named alpha (α) and beta (β) respectively, the following parameters can be calculated using iterations of Scherrer's equation as per equation 3.4[83].

$$\text{Aromaticity} = \text{fa} = \frac{Car}{(\text{Car} + \text{Cal})}$$

$$\text{Rank} = \text{I}\beta/\text{I}\alpha$$

$$\text{Crystallite Lateral Size (nm)} = \text{La} = 1.84\lambda/\text{Ba}\,\text{Cos}\varphi\text{a}$$

$$\text{Degree of Crystallinity} = \text{Lc} = 0.89\lambda/\text{B}\beta\,\text{Cos}\varphi\beta \quad \textbf{(3.4)}$$

$Where$

$Car = Area\ under\ \alpha\ peak$

$Cal = Area\ under\ \beta\ peak$

$I\alpha = Intensity\ of\ \alpha\ peak$

$I\beta = Intensity\ of\ \beta\ peak$

$\lambda = X - Ray\ Wavelength$

$Ba = FWHM\ of\ \alpha\ peak$

$B\beta = FWHM\ of\ \beta\ peak$

$\varphi a = Bragg\ Angle\ of\ \alpha\ peak$

$\varphi\beta = Bragg\ Angle\ of\ \beta\ peak$

Bragg's law can be used to calculate interlayer spacing as per equation 3.5[84].

$$D\beta = \frac{n\lambda}{2Sin(\varphi\beta)}$$

Where

$D\beta = Interlayer\ Spacing$

$n = order\ of\ diffraction$ **(3.5)**

$\lambda = X - Ray\ Wavelength$

$\varphi\beta = Bragg\ Angle\ of\ \beta\ peak$

3.4.5 Kinetics

Common iso-conversional techniques for calculating kinetic variables, especially activation energy (Ea), include the Friedman approach[85], the Flynn-Wall-Ozawa method (FWO)[86], and the Kissenger Akahira Sunose method (KAS)[87]. The paper written by Sima-Ella outlined in section 2.9 of the literature review used Coats Redfern, as a technique for characterising char in dust, but this was a model-based technique which is simplified and relies on curve fitting techniques to determine the activation energy, hence alternative kinetic parameters were sought. It has been demonstrated that the reaction energy for the oxidation of carbon compounds varies significantly with the conversion degree[88]. The FWO and KAS methods are derived from systems whose activation energy does not change with reaction progress, hence the Friedman approach was chosen as a replacement, as changes in the mechanism can be factored into the model-free method used. To compare the reactivity of each of the blast furnace dusts against the LOC value derived using the CET, kinetic analysis was applied to the blast furnace dust samples. It is thought that with increasing LOC the activation energy will decrease due to the increase in reactivity of LOC.

Equation 3.6 gives the generalised kinetic expression for decomposition gas-solid reactions, where t is time, k(T) is the temperature-dependent kinetic constant, f(α) is the expression of the reaction model, dα/dt is the rate of conversion with respect to time and α is the conversion degree. Equation 3.7 gives the generalised kinetic expression for conversion degrees, where m0 is the initial mass of the sample before reaction initiation, mt is the mass of the sample at time t and mf is the final mass of the sample.

$$\frac{\mathrm{d}\alpha}{\mathrm{d}t} = k(\mathrm{T})\mathrm{f}(\alpha) \tag{3.6}$$

$$\alpha = \frac{\mathrm{m0} - \mathrm{mt}}{\mathrm{m0} - \mathrm{mf}} \tag{3.7}$$

By substituting the Arrhenius equation into Equation 3.6, a general expression to calculate kinetic factors Ea and A is given in Equation 3.8, where A is the preexponential factor (min^{-1}), Ea is the activation energy of the conversion ($kJmol^{-1}$) and T is the absolute temperature (K).

$$\frac{d\alpha}{dt} = f(\alpha)A \cdot \exp\left(-\frac{Ea}{RT}\right) \quad \textbf{(3.8)}$$

The expression as proposed by Friedman involves taking the natural logarithm of Equation 3.8 to yield Equation 3.9[85].

$$ln\left(\frac{d\alpha}{dt}\right) = \ln[Af(\alpha)] - \frac{Ea}{RT} \quad \textbf{(3.9)}$$

The slope of each iso-conversional line from the plots of ln(dα/dt) versus 1000/T at a particular conversion value for several experiments varying the heating rate β (°C/min) each time, can be used to obtain -Ea/R.

3.4.6 BET Surface Area

The Brunauer Emmett Teller (BET) analysis technique was used for determining the surface area of solids from the nitrogen sorption isotherm at liquid nitrogen temperatures[89]. Based on the work of Pohlmann *et al.* and the Charfoco report outlined in section 2.9 of the literature review, surface area is a key driver for char burnout. Hence there should be a relationship between the surface area of char and other constituent materials. The analysis was carried out using a Nova 2000E analyser, where a known mass of blast furnace dust was degassed to ensure total dryness and evacuation of pore moisture. The gas sorption data from the reintroduction of nitrogen to the vessel can be analysed and converted into data such as pore size and specific surface area. Samples were degassed for 4 hours at 130^{o}C to avoid physical alteration of the material. The test was run to totality and the volume adsorbed and relative pressure was plotted by the instrument.

3.4.7 ImageJ

To process and automate images for char cenosphere identification similar to the work of Pohlmann *et al.* outlined in section 2.9, who explained the source of cenospheres in BF dust, thresholding techniques were adopted using software called ImageJ. The optical micrographs of dust samples were thresholded to isolate the cenospheres from the background and flux materials. The subsequent information attained using the processing software such as the surface area of cenospheres and a count of the number of cenosphere particles was carried out on the processed images as a method of

quantifying the carbon type within the micrograph for comparison against the LOC derived by the CET.

Cenosphere particles were thresholded using the software and particle counting was carried out using resultant images. The aim of this was to automate the char cenosphere counting technique previously carried out by Nyanin[12]. To successfully threshold an image for the quantification technique, the following steps were undertaken. The image was calibrated using the scale bar which allows the software to reference the correct size for pixel quantification. The image was converted to 8-bit to allow for greyscale thresholding across 225 grey levels. This allowed for the background to be negated from the image as per Figure 59.

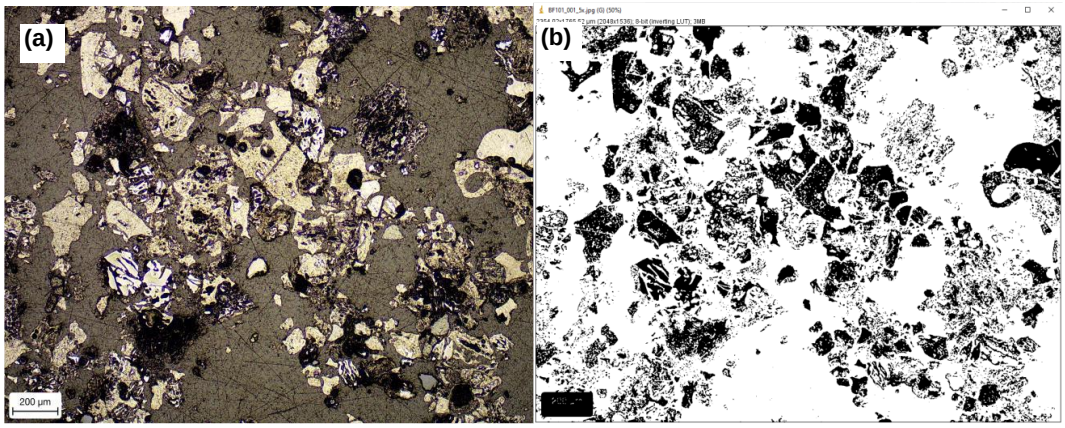

Figure 59 a) Raw dust optical image b) greyscale thresholding for background removal

The cenosphere type could be further thresholded out as per Figure 60, by increasing the threshold limit.

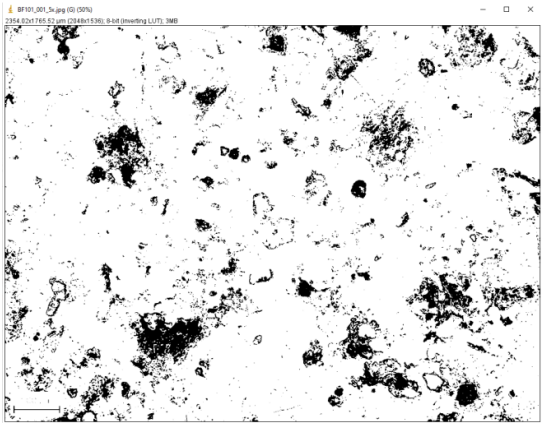

Figure 60 Dust imaged threshold for only cenosphere particles

Salt and pepper noise, as described by Zhang *et al.*, was removed by despeckling, replacing each pixel with the median value in a 3x3 neighbourhood[90]. The resultant image was filtered for particles over 10 pixels in size to remove false data from the salt and pepper noise remaining. All particle circularities were counted including holes to ensure all remaining thresholded cenosphere particles were counted. The results were deduced from the images, as shown in Figure 61, where the total cenosphere particle count was calculated to compare against the data from the CET. The value used to compare against the CET was the number of counted cenospheres over the total particle count as a percentage of cenospheres per total particles. This value was thought to be relative to the LOC value derived from the CET.

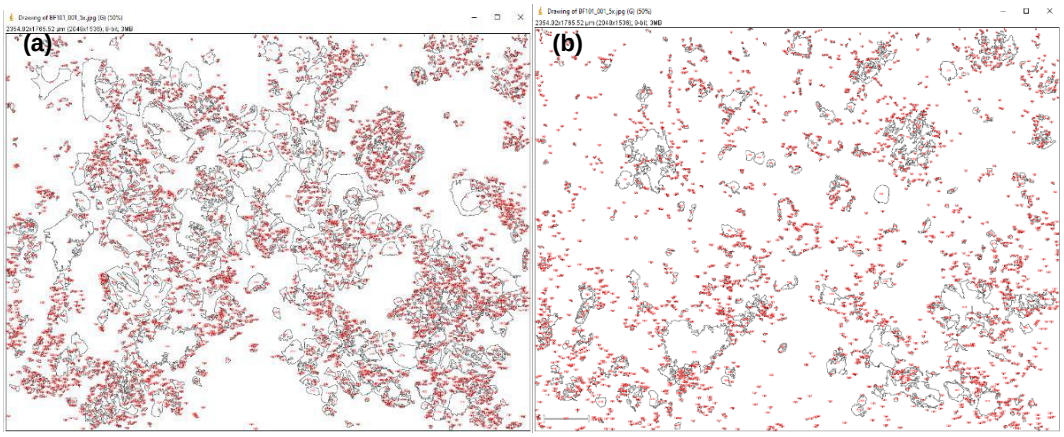

Figure 61 a) particle count all particles considered b) particle count all cenosphere particles considered

3.4.8 Raman Spectroscopy

To compare the Raman spectra of blast furnace dust against the LOC quantified by the CET with the aim to use it as a replacement methodology, the Renishaw inVia confocal

Raman microscope using a backscattering configuration was used. 50x magnification was used to collect Raman spectra from randomized points across the dust sample. All measurements were conducted under a nitrogen inert atmosphere. The laser spot size used was ~10 micron and the spectra were collected at wavelengths (457, 488, and 514 nm) using an argon ion laser. Acquisition times and laser powers were optimised as described later in the text in results chapter 4.2. Calibration was conducted using a silicon reference sample, and background photoluminescence was subtracted using a polynomial fit. The spectra from random points in the sample were used to determine the degree of low-order and high-order carbon types in the dust.

Each of the peaks from the Raman spectra can be referenced to different characteristics of the carbon type in the material. It was hypothesised that samples exhibiting low-order forms of Raman spectra will naturally contain more LOC when comparing the data to the CET. The "G" peak refers to the peak around 1582cm^{-1} on the spectra which was indicative of the sp2 C-C type bonding[91]. Increased intensity of this peak indicates the increased ordering of the carbon type. The "D" Peak around 1350cm^{-1} was indicative of impurities in the carbon stacking structure, higher values for this indicate less order in the carbon structure[92]. Hence the D/G ratio was calculated based on the heights of the peaks to determine the degree of carbon order. Lower values for D/G indicate more ordered carbon and therefore it was appropriate to consider using Raman as an alternative technique to the CET as lower order within the carbon type may return lower values for LOC from the CET[93].

3.4.9 Micro Computed Tomography

Micro Computed Tomography (Micro CT) was used to provide 3-d images of the dust for char counting. It is thought that the amount of char particles found can be compared to the LOC from the CET to improve upon it. Samples were mounted into plastic straws to prevent excessive movement interference with the final images. The mounted samples were scanned using an Xradia Zeiss 520 Versa X-Ray microscope. The data was reconstructed with XMReconstructor software, and the images were used for identifying char presence within the samples.

The aim of this work was to produce a 3D representation and dataset for char or cenosphere counting. The main limitation of microscopic techniques was the objective size and representativeness of a batch of material. This technique aims to

provide increased image surface area and increase the visualisation aspect of each particle available in slices.

3.4.10 XPS

To determine surface chemistry, XPS was carried out to compare differences in the C1S and O1S spectra of the dust samples to the results from the CET[94]. The focus was on these specific peaks because these peaks best describe the bonding between carbon types. The XPS analysis was selected based on the research by Steer *et al.* in section 2.8.3 who identified changes in surface chemistry within coal and char depending on the thermal history. This technique was selected to highlight changes between dust samples to tie back to the changing thermal history of the carbon within the dust.

To identify carbon bonds and types within the dust samples a Kratos Axis Supra XPS was used. The instrument used a monochromatic Al Kα X-ray source at 225W and a 15mA emission current. Multiple wide scans at pass energy of 160 eV across the range of binding energies 1200-0eV were used on each sample to identify all the bonds and elements present. A step size of 1eV was used for this. For the high-resolution spectra, a pass energy of 40eV with a step size of 0.01eV and a multi-sweep dwell time of 2000ms was used to reduce noise ratios. The binding energy was charge correct to the C-C component of the carbon peak at 248.8eV. Gauss-Lorentz peak models and Shirley backgrounds were used to quantify the peaks using Casa XPS software with a Kratos sensitivity factor library to quantify the data.

3.4.11 Petrography

Samples were analysed using a novel automated petrography technique in a collaborative programme of work with Nottingham University[95]. The work looked to identify links between optical analysis and the CET. The technique focused on identifying the different carbon types and using computer-based thresholding to automate the identification and particle counts.

Mounted samples were polished to maximise the resolution of the structures within the sample. A Zeiss Image M1 microscope was used with a 50x oil immersion objective and a 10x lens amounting to 500x magnification. An automated stage was used to generate a 20x20 mosaic totalling 400 images across the surface. Thresholding

was applied to the images to separate the different carbon types, including, coke, green coke, coal and mineral matter.

Manual analysis was used to identify the relevant macerals such as vitrinite, liptinite and inertinite to identify which parts of the image to threshold into each carbon type[96].

3.5 Coal Combustibility Analysis

3.5.1 TG Parameters

To identify the thermal properties of each coal used and their subsequent blends, the SDT Q600 was used to create TG and DTG profiles. The aim of this work was to ascertain which of the coals and the coal blends would be most likely to burnout in the raceway of the blast furnace. 20 mg ±0.5 mg of coal or blend was weighed into an Al_2O_3 crucible and heated in 100ml/min of flowing air to 1000^{o}C at a rate of 10^{o}C/min. The resultant TG and DTG profiles were used to compare burnout characteristics and TG parameters. According to Wang *et al.*, Initiation Temperature (Ti) was the temperature where the DTG elevates to > 0.1%/min, indicating the start of the oxidation process. Peak temperature (Tmax) was the highest point of the DTG curve, indicating the temperature with the maximum rate of oxidation. T-half (T0.5) according to the TG curve was the point at which half of the material has oxidised. Burnout temperature (Tb) relates to the temperature where the DTG falls to < 0.1% min, an indication of the end of the coal burnout stage. The combustibility index (s) describes the effect of oxygen concentration on the combustion characteristics of the coal, this was calculated as per equation 3.10 and ensures that both ignition and burnout temperatures are considered in the same index[97]. Figure 62 best describes the location of each of the parameters on the DTG and TG curves respectively.

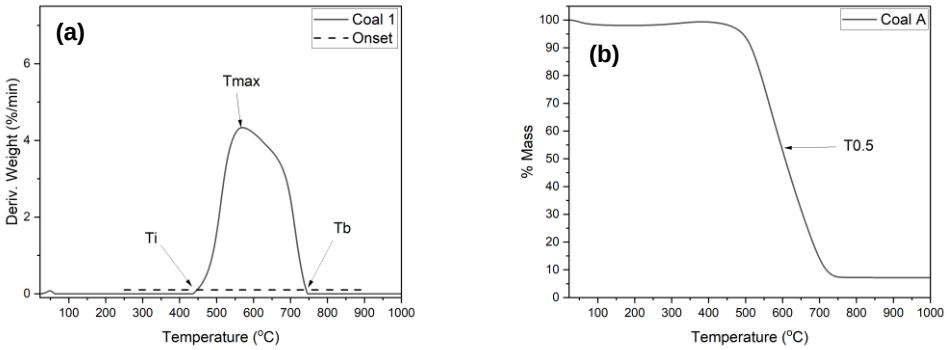

Figure 62 Temperature locations from which TGA parameters are derived a) DTG curve coal 1 b) TG curve coal 1

$$Combustibility\ Index\ (S) = \frac{(\frac{Dw}{Dt})max(\frac{Dw}{Dt})mean}{Ti^2Tb} \quad \textbf{(3.10)}$$

$Where$

$\frac{Dw}{Dt} = The\ rate\ of\ change\ in\ Weight\ and\ Temperature$

3.6 Plant Analysis Methods

3.6.1 Process Data

Many of the process parameters for blast furnace ironmaking have been optimised for iron quality and production maximisation. Parameters such as blast pressure, temperature, volume, oxygen enrichment, fuel rates and steam are used to maintain the environment within the blast furnace to ensure the stable manufacture of iron[98]. These conditions are suspected to influence the dust generated by the blast furnace. In this work, each parameter was investigated to understand their influence. Whilst macro changes in process parameters may be detrimental to the manufacture of iron, an understanding of the leading influences on coal combustion can help drive data-driven decision-making, with a focus on the reduction of dust generation.

Process information (PI) data was obtained from sensors placed strategically around the blast furnace to monitor conditions and processes. The aim of this work was to compare the process parameters against the LOC in the dust, for any given time, in an attempt to ascertain which parameters should be the focus for diagnosing the presence of coal char in the raceway. The information was stored on a central system

named PIWeb. The information retrieved was in 30-second intervals, averages have been calculated for each process parameter spanning 12 hours before the samples were obtained. Each set of process parameters has been checked to ensure no major process deviations occurred within the 24-hour period leading up to sampling and only natural variation was observed.

Vast quantities of information can be observed using the sensors alone. But to gain a deeper understanding of the complex nature and combined effects of process parameters, the following parameters have been calculated. Raceway adiabatic flame temperature (RAFT), total oxygen enrichment, oxygen mass flow, permeability, moles of carbon per moles of oxygen ratio (CPO), coal mass per oxygen mass and coal flow.

RAFT was a theoretical combination of heat supplied from the blast and heat generated by coke and coal combustion in the raceway. This allows the temperature to rise above the melting point of the burden. In the raceway coal reacts with oxygen to produce carbon monoxide and water is converted to hydrogen in the presence of carbon. The RAFT is the temperature in the raceway as soon as the gas has fully converted to CO and H_2 respectively. The RAFT can be calculated as per equation 3.11 and is dependent on hot blast temperature, oxygen enrichment, blast oxygen and changes in reductant rates[99]. A criticism of this calculation is that it doesn't account for the moisture in the coal. This can have a large impact on the RAFT and the conditions wouldn't be known to the operator as this is a theoretical value. Large parts of the equation are redundant in many blast furnaces that don't inject tar, oil or natural gas. The calculation shows a heavy reliance on natural gas and oil injection as these would be the most energy intensive influences on it.

$$RAFT = 1489 + 0.82BT - 5.705BM + 52.778(OE) - \frac{18.1Coal}{100WC} - \frac{43.01Oil}{100WC} - \frac{27.9Tar}{100WC} - \frac{50.66NG}{100WC} \quad \textbf{(3.11)}$$

Where

$BT = Blast\ Temperature\ in\ °C$

$BM = Blast\ Moisture\ in\ gr/m^3\ STP\ dry\ blast$

$OE = Oxygen\ enrichment\ (\%\ O2 - 21)$

$Oil = Dry\ Oil\ injection\ rate\ in\ kg/tHM$

$Tar = Dry\ Tar\ injection\ rate\ in \frac{kg}{tHM}$

$Coal = Dry\ Coal\ injection\ rate\ in\ kg/tHM$

$NG = Natural\ gas\ injection\ rate\ in\ kg/tHM$

$WC = Wind\ consumption\ in\ m^3/tHM$

Permeability was calculated to combine the volume of the blast furnace with the pressure from the bottom and the top of the furnace. The known volume, blast volume and changing pressure provide an index for determining permeability provided by the descending burden. Higher values for permeability suggest increased channels and pores within the burden for gas to ascend the furnace. The permeability index was calculated as per equation 3.12. The limitation of using formulas such as these is that they are derived collaboratively. All blast furnaces are different and hence the shape of the furnace as opposed to the working volume and height may be more influential than this calculation accounts for. The pressure is considered here but there is a large reliance on the furnace height.

$$Permeability = \frac{FH^{1.5} \times 1000BV}{WV \times (BP - HTP)^{1.5} \times (BP + HTP + 2)^{0.36}} \quad \textbf{(3.12)}$$

Where

$FH = Furnace\ Height\ (m)$

$BV = Blast\ Volume\ (\frac{km^3}{hr})$

$WV = Working\ Volume\ (m^3)$

$BP = Blast\ Pressure\ (Bar)$

$HTP = High\ Top\ Pressure\ (Bar)$

Oxygen volume was a parameter focused on oxygen enrichment in the raceway. To account for the oxygen present within the blast air, equation 3.13 was derived. Oxygen mass flow was also derived as per equation 3.14. This was to convert the oxygen volume into a mass flow for later conversion into coal parameters.

$$\boldsymbol{Total\ Oxygen\ Enrichment\ (TOE)\left(\frac{m^3}{hr}\right) = (BV \times 0.21) + OV} \quad \textbf{(3.13)}$$

$$\boldsymbol{Oxygen\ Mass\ Flow\ \left(\frac{kg}{hr}\right) = TOE \times 0.385} \quad \textbf{(3.14)}$$

Where

$\boldsymbol{BV = Blast\ Volume\ (\frac{m^3}{hr})}$

$\boldsymbol{OV = Oxygen\ Volume\ (\frac{m^3}{hr})}$

The carbon present within the raceway can be quantified using the coal rate and coke rate from the PI data. However, to further identify the conditions within the furnace, coal flow was a direct measure of coal flowing in kg/hr into the furnace as opposed to the coal rate which was dependent on the production rate of the blast furnace, coal flow can be calculated as per equation 3.15. With depleted oxygen conditions in the raceway, combustion is less favourable[100]. Coal per oxygen mass flow (CPM) derived in equation 3.16, was calculated based on the mass of oxygen and coal flowing into the furnace at any given time. Similar to the CPM, the moles of coal

per unit oxygen CPO as per equation 3.17, was a good indication of the abundance of coal in comparison to oxygen on a molecular level in the raceway. These calculations were based on improved calculations for O/C outlined in the work by Schwalbe in section 2.11 of the literature review.

$$Coal\ Flow\ (CF)\ (\frac{kg}{hr}) = PR\ \times\ CR \tag{3.15}$$

$$Coal\ per\ Oxygen\ Mass\ Flow\ (CPM)\ = \frac{CF}{OMF} \tag{3.16}$$

$$Moles\ of\ Coal\ Per\ Moles\ of\ Oxygen\ (CPO) \tag{3.17}$$

$$= \frac{\left(\frac{0.8CF}{12.011}\right)}{\left(\frac{0.8CF}{12.011} + \frac{OMF}{31.9988}\right)} \Big/ \frac{\left(\frac{OMF}{31.9988}\right)}{\left(\frac{0.8CF}{12.011} + \frac{OMF}{31.9988}\right)}$$

Where

$PR = Production\ Rate\ (\frac{t}{hr})$

$CR = Coal\ Rate\ (\frac{kg}{tHm})$

$OMF = Derived\ in\ Equation\ 4.2$

To determine which operating parameters and variables had the largest influence on dust generation, the data from the process itself was required. Blast furnace PI was used to determine the parameters at the time of sampling and before the sample. The data helps visualize changes in process conditions that led to a sample containing more or less LOC. The data types used are outlined in Table 15.

Table 15 Process parameters from PIWEB

Parameter	Unit	Descriptor
Total Suspended Solid	g/l	Dust concentration in the water from the wet abatement
Dust Output	g/s	Dust mass flow from the wet abatement
Water Flow	m^3/hr	Flow of water used for gas cleaning out of the wet abatement

O_2 Setpoint	%	Operator-controlled parameter to increase oxygen enrichment
O_2 Volume	m^3/hr	Output of the change in Oxygen setpoint. This is the flow of oxygen into the blast furnace
Total Oxygen	m^3/hr	Oxygen enrichment including the oxygen from the blast air. This is the flow of oxygen into the blast furnace inclusive of the oxygen in the blast air.
Oxygen Mass Flow	kg/hr	Molecular oxygen flowing into the furnace
Steam	t/hr	Process used to control the temperature of the flame has a cooling effect
Raceway Adiabatic Flame Temperature (RAFT)	^{o}C	Calculated temperature at the tip of the tuyere
Blast Volume	km^3/hr	Volumetric flow of hot air blasted into the furnace.
Blast Pressure	Bar	Pressure of hot air blasted into the furnace
Blast Temperature	^{o}C	Temperature of the air blasted into the furnace
Delta Pressure	Bar	Change in pressure from the top and bottom of the furnace
Production Rate	t/hr	Rate of manufacture of iron
Hot Metal SiO_2	%	Related to the composition of material produced
Mole Carbon Per Mole Oxygen	%	Calculated based on molecular oxygen and coal in the furnace at any given time
Coal per Oxygen	kg/hr	Flow of coal per unit oxygen at any given time
Coal Flow Rate	kg/hr	Flow of coal based on the original production rate of the furnace
Coal Rate	kg/tHM	Mass of coal used per tonne of hot metal produced
Coke Rate	kg/tHM	Mass of coal used per tonne of hot metal produced

Max Differential Pressure	Bar	Difference between the top and bottom pressures in the furnace, related to permeability
High Top Pressure	Bar	Pressure of gas exiting the furnace
Top Temperature	^{o}C	Temperature of the gas exiting the furnace
CO	%	Concentration of CO in the top gas at the first analyser
CO_2	%	Concentration of CO_2 in the top gas at the first analyser
H_2	%	Concentration of H_2 in the top gas at the first analyser
N_2	%	Concentration of N_2 in the top gas at the first analyser, the difference between the other measured gases
CO b	%	Concentration of CO in the top gas at the second analyser downstream
CO_2 b	%	Concentration of CO_2 in the top gas at the second analyser downstream
H_2 b	%	Concentration of H_2 in the top gas at the second analyser downstream
N_2 b	%	Concentration of N_2 in the top gas at the second analyser downstream, the difference between the other measured gases
Gas Efficiency $Co_2/(Co+Co_2)$	%	Calculated based on the output from the top gas analysers
Permeability	Index	Indices based on blast volume, working volume and changes in pressure across the furnace

3.6.2 Replacement Ratio

To combine several coal properties into a single figure for comparison to the LOC in the dust output at any given time, the replacement ratio was considered. It is widely accepted that coal is used to substitute coke as a fuel in blast furnace iron making. The ratio of how much coal can be used to offset coke is highly dependent on the morphology, surface area, phases present and chemistry of it. The analysis to satisfy the equation for replacement ratio was carried out, according to the ultimate analyser

and proximate analysis procedures outlined in section 3.3.3. The formula for calculating the replacement ratio of a particular coal or coal blend was as per equation 3.18[99]. This formula considers the energy required to crack the coal structure including C-H bonds, evaporating the moisture within the particle, and minimising the ash levels within the furnace to determine a suitable ratio to inject the coal offsetting coke as a fuel. The output of this calculation was a value indicating the amount of coke in kg/tHM each 1kg/tHM of coal blend or coal can replace. A replacement ratio of 0.98 would essentially mean that 1kg/tHM of coal will offset 0.98 kg/tHM of coke. The coal goes through a drying stage on the plant, hence the moisture was assumed to be 1.5% due to moisture pick up from the GCI plant to the furnace tuyeres. In terms of coal combustion. A higher value for replacement ratio means that more carbon is available for the boudouard reaction and more hydrogen is available in the furnace. This will decrease the energy demand of the furnace.

$$\boldsymbol{RR = 2C\%(Coal) + 2.5 \times H\%(Coal) - 2 \times Moisture\%(Coal) - 86 + 0.9 \times ash\%(Coal)} \quad \textbf{(3.18)}$$

Where

$\boldsymbol{RR = Replacement\ Ratio}$

$\boldsymbol{C\%(Coal) = Determined\ by\ Ultimate\ Analysis}$

$\boldsymbol{H\%(Coal) = Determined\ by\ Ultimate\ Analysis}$

$\boldsymbol{Moisture\%(Coal) = 1.5\%}$

$\boldsymbol{Ash\%(Coal) = Determined\ by\ Proximate\ Analysis}$

3.7 Dust Output Monitoring

Manual Probe

To generate a data set for dust output, for comparison against process data, the dust output was monitored using a Royce Technologies suspended solids meter seen in Figure 63. This measures light transmittance across the bridge as per Figure 64, and converts it into grams per litre solids in water measurement[106]. The flow of water from the wet abatement was used to convert the value into a mass flow in kg/s. This value was used to compare directly with the process parameters of the blast furnace to determine which parameters have the largest influence on the dust output. The

handheld manual probe was used to validate the hypothesis that the dust output could be monitored and to justify the procurement of a fixed monitor.

Figure 63 Royce Technologies total suspended solids probe

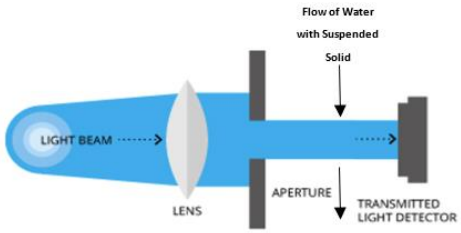

Figure 64 Working principle of the probe (Image adapted from Fondriest learning services)[106]

Sampling location was important for monitoring output, it was important to capture the most particles to ensure the sampling remains representative of the process. However, steelmaking is inherently fraught with hazards due to the nature of the process. A balance between representativeness and suitability was drawn to select the sampling point as per Figure 65. This was in the stream of water after the wet abatement before it enters the clarifying pond. Here the water was cool enough to protect the instrument, access was suitably safe, and the water flow was less turbulent here for the accuracy of the measurement.

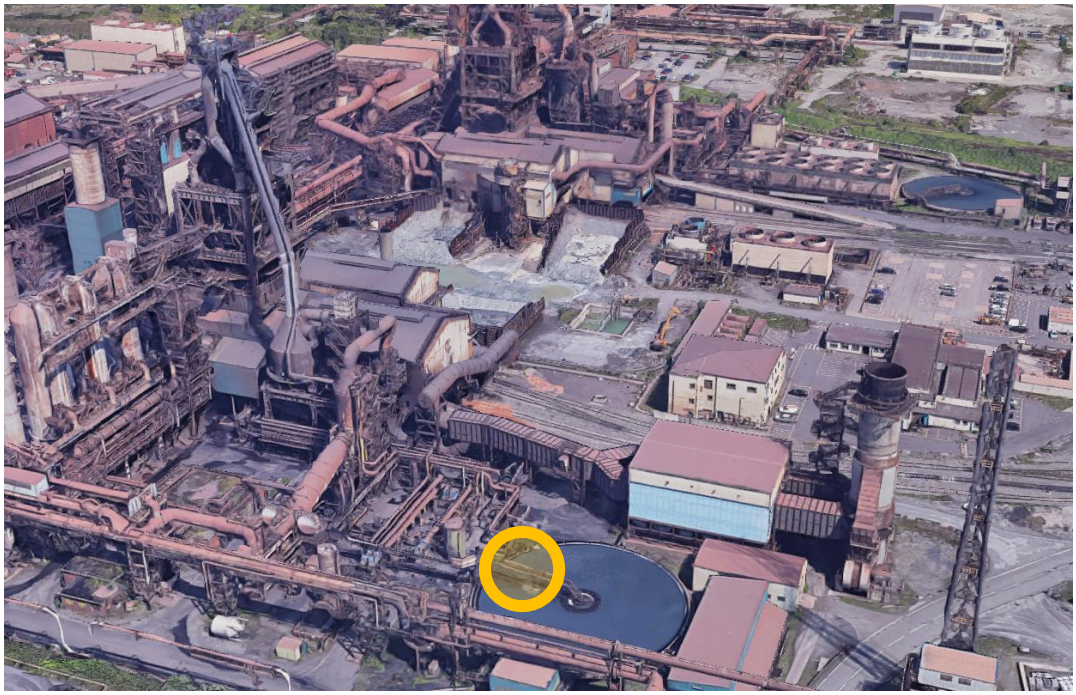

Figure 65 Google maps representation of sampling point on BF5 in TATA Steel Strip UK Port Talbot

3.7.1 Dust Monitor Validation

To calibrate the monitoring equipment and validate the technique, 1000cm^3 of process water was sampled from the centre of the stream to ensure representativeness. 100cm^3 of agitated water was filtered using a dried and weighed GFC. The filter containing the dust was dried until constant mass at 105^{o}C in a Memmert UN30 drying oven. The mass of dried residue and the filter were used to calculate the suspended solids concentration (TSS) of the water as per equation 3.19.

$$TSS = \frac{Wf - \wp}{Vw} \quad \textbf{(3.19)}$$

Where

$TSS = TotalSuspendedSolid$ (mg/l)

Wf = Mass of dried filtered material and filter paper (mg)

$\wp = Mass\ of$ dried blank filter paper (mg)

$Vw = Volume\ of\ water\ (l)$

The Royce Technologies instrument was sensitive to different solid morphologies and reflectance properties of the particles suspended in the water[107]. For this reason,

the instrument was calibrated using a sample taken from the source. The laboratory TSS technique was carried out on a sample of slurry water, this value was used to drift correct the instrument to ensure the accuracy of measurement. A series of comparisons were made on samples from different days and times to prevent condition bias. The comparison between measurements made using the probe versus the measurements of the samples taken and filtered in the laboratory was as per Figure 66. The R^2 for this technique was 0.86186. This was a good regression for comparing two techniques with the inherent sources of error, the measurement uncertainty for the laboratory technique alone is ±20%[108]. The uncertainty for the probe was ±5%, hence the R^2 was good for these processes[109]. Reverse validation was considered but the dust was partially soluble in the water hence a difference in the data would be observed and reverse validation was not possible with BF dust.

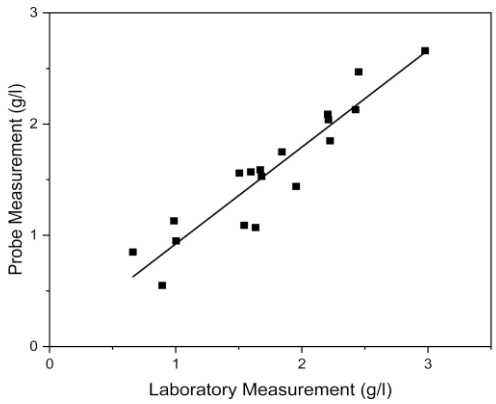

Figure 66 Regression data for validating the probe against the laboratory-accredited suspended solids technique

4 Results and Discussion

4.1 Understanding Blast Furnace Dust Formation

4.1.1 Introduction

To optimise the process of iron making for dust reduction, a comprehensive review of the material was required to understand how the dust was formed and which constituents can be reduced to minimise the overall volume of dust generated by the process. The quality and mechanical strength of the raw materials have a large influence on dust generation[101]. Coke, sinter, limestone and iron ore are the raw materials that are fed into the top of the blast furnace in layers, on route to the top of the furnace the materials are stacked in huge storage bunkers, dropped between conveyor belts and dropped into charge cars. The mechanical degradation of the raw materials was inevitable. The mechanically degraded raw material, when introduced to the pressure of top gas flow from the top of the blast furnace, any loose material fines will be dislodged from the surface of the macro particles and enter the gas stream[81].

Dust generation in a conversion process such as this will also be inevitable. Typically, 80 tonnes of dust is generated daily per furnace, as per Figure 67. Although this value is rather variable due to the measurement technique. Lorries containing dust are measured using a weighbridge and the value is totalled for the daily output. The accuracy of this measurement was only sensitive to the resolution of the weighbridge, to the nearest tonne. Prior to this investigation, the only benefit of the measurement was to calculate the growth rate of a legacy stockpile of material and to ensure the use remains greater than the generation. But as per Figure 67, the output of the furnace is very variable, if this variability can be reduced through a tighter control of the blast furnace process conditions then the focus can be to reduce the daily dust output.

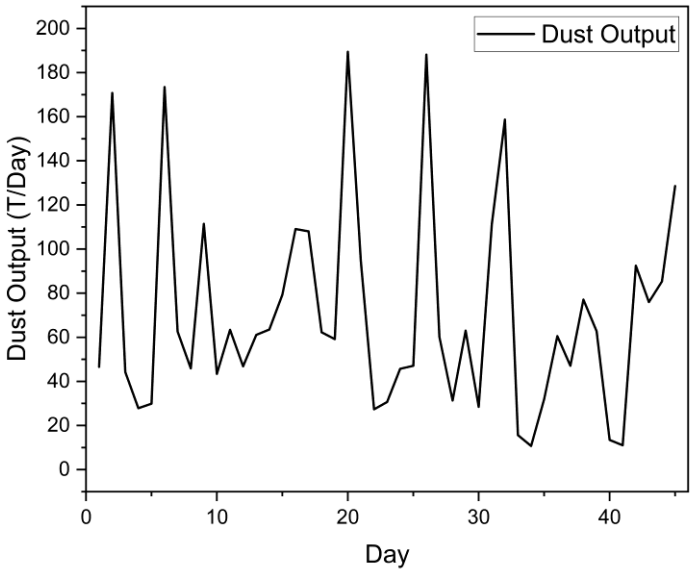

Figure 67 Daily BF dust output in tonnes per day

The scope of this work meant the dust from the dry and wet abatements was analysed from different days, spanning 9 months to allow for a good variety of process conditions and dust types to be represented. The aim of this work was to first identify the materials present in the dust and discuss the potential origins, using analyses from each of the raw materials for blast furnace ironmaking. The second was to determine the key differences between the samples from the wet and dry abatements to determine which sample type is most representative of the dust as a whole, the third was to identify the degree of variation in analytes between dust samples and slurry samples, finally to identify any relationships between the carbon in the material with the other analytes.

4.1.2 Constituents of Blast Furnace Dust

The SEM image in Figure 68, shows the presence of multiple particle types within the dust itself. The presence of each of the raw material constituents was expected based on the work of Schwalbe from the literature review, who said that flue dust is made up of both carbon and non-carbon-bearing materials such as gangue and fluxes, but within this particular sample, examples of each raw material present can be seen, the source of each is not definitive based on this SEM image but these are the most likely source of each. The likely presence of each material was confirmed using EDS, which quantifies areas of element concentration and allows for accurate particle

identification. Limestone was identified due to the bright colour using the backscatter detector (BSD) and the globular morphology. The EDS data in Table 16 shows these particular particles to be high in calcium, indicative of CaO known as lime[124]. With EDS analysis consideration to accuracy should be made. The values are relative analyses and should be treated as an indication only. Iron ore was also clearly present, these iron-rich particles glow much brighter under backscatter due to the density difference of iron to the carbon circle background. The Fe_2O_3 appears globular in morphology but was differentiated between CaO using the data from the EDS[125]. Sinter identification was more difficult because the iron content around 56% was lower but similar to that of iron ore at around 65%, the BSD shows colours that are similar between the materials. The shape of the particle was a good indicator that the particle was sinter, sinter was a synthetic product of the agglomeration of waste materials around the site. The process of manufacture through sintering means that the product morphology was more angular than the naturally occurring iron ore which was more globular in nature[126]. The coke can be characterised by a large flake-like morphology, the backscatter gives a darker colour to this particulate because it is predominately carbon and is less atomically dense than iron bearing materials, the angular morphology differentiates it from other carbon sources within the dust[127]. The presence of coal or coal char as seen in Figure 68, was the most interesting. The coal is initially injected into the bottom of the blast furnace and for this reason, it travels through the hottest and most oxygen-rich zones of the furnace before exiting the furnace. Coal should be fully gasified, before leaving the raceway[99], however the presence of char in the dust means that it is not fully gasifying. Char in the dust can be identified in globular particles with pores also known as cenospheres as identified by Pohlmann *et al.* in the literature review section 2.9. The black colour was indicative of the atomic density in comparison to the other materials present[12].

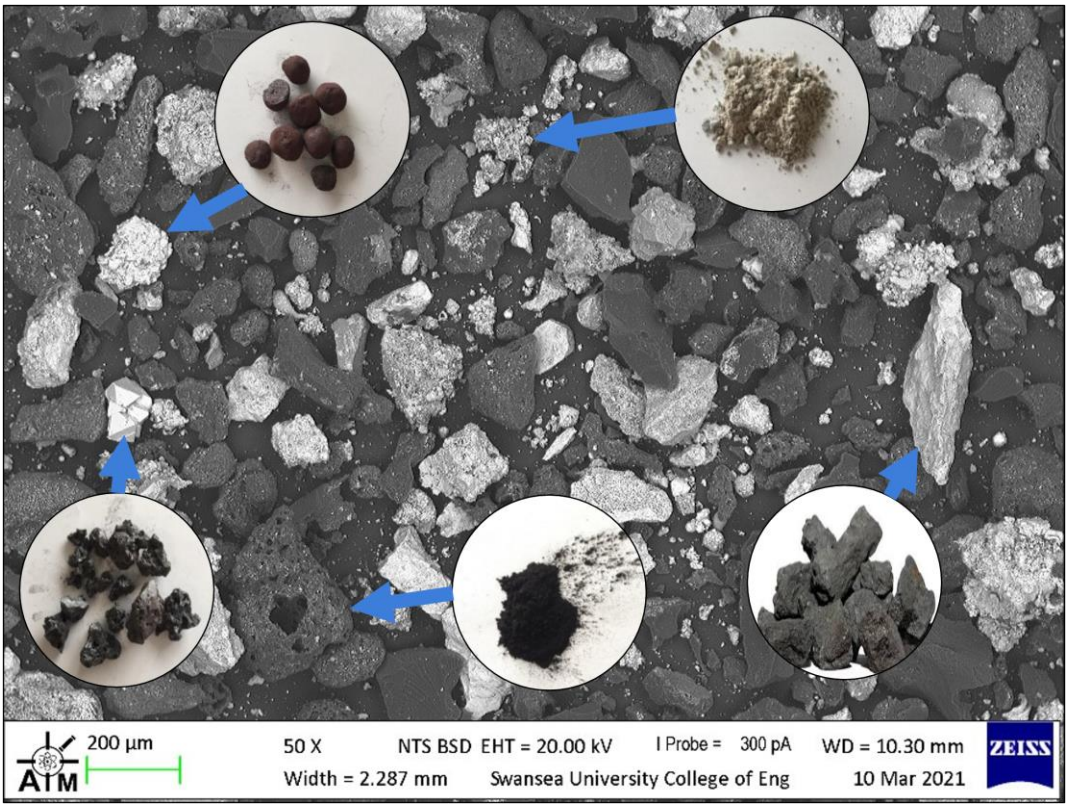

Figure 68 SEM micrograph showing the presence of each of the raw materials within the dust. From top left and in clockwise order these include, iron ore, limestone, coke, coal char and sinter

Table 16 EDS analysis of each of the particles identified in the SEM image in Figure 70

	Iron Ore Particle	Lime Particle	Coke Particle	Coal Char Particle	Sinter Particle
C Rel. wt%	3.7	12.6	88.2	51.2	4.5
Fe Rel. wt%	65.2	-	1.4	0.8	41.3
Ca Rel. wt%	1.1	22.8	1.8	8.4	33.7
Mg Rel. wt%	0.1	20.1	-	2.2	1.8
Si Rel. wt%	5.1	-	3.9	9.2	12.2
O Rel. wt%	24.8	44.5	4.7	28.2	6.5

XRD was used to identify the phases present within BF dust. Figure 69 shows the presence of magnetite, haematite, wustite and metallic iron. The presence of these phases was a strong indication of the presence of iron ore and sinter material. There appears to be a presence of calcite dolomite and silica in the form of quartz, indicating the presence of fluxes in the dust[128]. The presence of graphite phases and a large amorphous region between 25^{o} and 33^{o} indicates the presence of different carbon sources, likely to be from the coal and coke-originating carbon present in the SEM images[63].

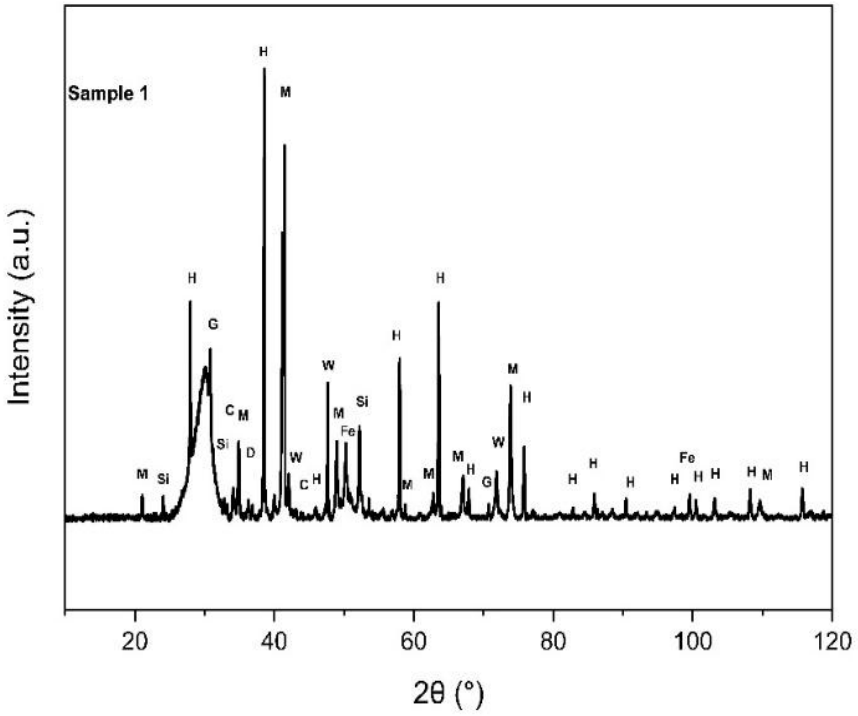

Figure 69 Powder XRD patterns for Sample 1. H = Hematite (Fe_2O_3 – COD# 9000139), M = Magnetite (Fe_3O_4 -COD# 1011084), W = Wüstite (FeO – COD# 9008636), C = Calcite ($CCaO_3$ – COD# 9016200), Si = Quartz High (O_2Si – COD# 1011200), G = Graphite (C – COD#9011577), D = Dolomite ($CaMg(CO_3)_2$ – COD# 9000885), Fe = Iron (Fe – COD# 4113941)

The typical size distribution of n=3 samples can be seen in Figure 70. The distribution was skewed towards the sub-400-micron average particle size, indicating that the vast majority of the dust was less than 1mm in size. Because the bottom size of each of the raw materials was >1mm, this data indicates that the dust was generated through mechanical degradation as opposed to prime macro particles of raw material being lost into the gas stream. Sample 3 appears to have 2 phases of material present, due to the presence of the second peak. Further chemical analysis showed an increase in CaO and MgO in sample 3, as opposed to the other samples. This second phase

could indicate that a particularly low-strength CaO was used as a flux on the day, as more of this broke down and entered the gas stream compared to the other samples. The mean value for each of the dust samples remained consistent indicating a relatively stable dust generation. This was beneficial to the process of optimisation as allows for a relatively good degree of predictability. The average particle size parameters and bulk density for dust can be seen in Table 17. This bulk density was between the bulk density of coke and iron at ~400 kg/m^3 and ~1200 kg/m^3 respectively, which indicates that the dust was a mixture of particulates and the value for bulk density was sensitive to changes in particle type.

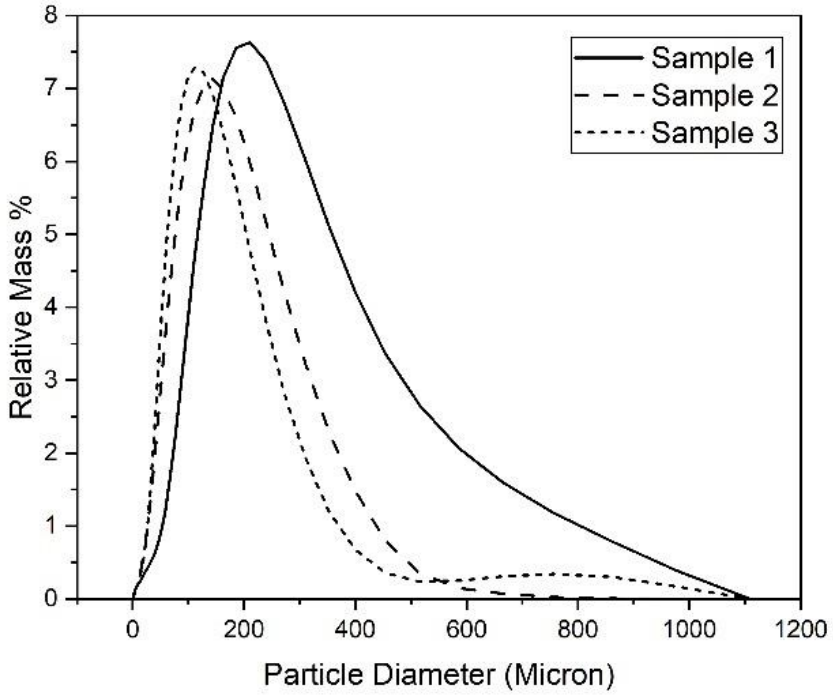

Figure 70 Histograms of the particle size distribution for samples 1, 2 and 3

Table 17 BF dust physical parameters

	Average of Dx (10) (Micron)	Average of Dx (50) (Micron)	Average of Dx (90) (Micron)	Average of Dx (99) (Micron)	Average of Dx (100) (Micron)	Bulk Density kg/m^3
BF dust	31.12	87.91	154.00	204.50	236.80	860.18

Table 18 shows the typical metals composition of BF dust. Metallic iron was the highest fraction at 20.61%. The presence of potassium, zinc and sodium was detrimental to blast furnace refractories and was tightly controlled in the raw materials to prevent the introduction of alkali metals into the furnace[129]. Zinc and potassium

are somewhat higher than sodium, mainly because zinc will concentrate in the dust as the iron within the sinter and iron ore are reduced. Some zinc will reduce with the carbon present in the furnace, but this reaction occurs much further down the process with higher temperatures, the zinc here was in the form of zinc oxides expelled from the top of the burden[130].

Table 18 Metals composition of BF dust as derived by ICP

	Fe %	Zn %	Cr %	K %	Pb %	Ni %	Cu %	Ba %	V %	Na %
BF dust	20.61	0.09	0.00	0.09	0.00	0.01	0.00	0.09	0.03	0.01

Table 19 shows the typical XRF analysis of BF dust and each of the raw materials present in the dust. The values for the XRF are the concentrations of each analyte within the ash portion of the sample, ashing of the dust was carried out to protect the platinum crucibles during the preparation of the glass bead procedure in the XRF. The SiO_2 in the dust appears to originate from carbon-based raw materials, as does Al_2O_3, TiO_2, phosphorous and manganese. The CaO was clearly from the limestone with some potential contribution from the sinter, however, the sinter was more mechanically stable compared to limestone therefore was less likely to contribute to the dust. The iron-bearing analytes are contributed from the iron ores and sinter, except for FeO which may be contributed to by coke.

Table 19 XRF analysis of the dust and raw materials present within the dust itself

	SiO_2	Al_2O_3	TiO_2	CaO	MgO	Fe	Fe_2O_3	FeO	P	Mn
	% in Ash	% in Ash	% in Ash	% in Ash	% in Ash	% in Ash	% in Ash	% in Ash	% in Ash	% in Ash
Flue Dust	**13.51**	**6.65**	**0.28**	**6.47**	**1.20**	**8.00**	**48.22**	**9.00**	**0.86**	**0.78**
Coal	50.80	29.65	0.99	2.22	1.08	6.35	-	-	0.44	0.12
Coke	13.06	7.48	0.15	7.69	2.24	8.62	47.29	8.80	0.52	1.04
Iron Ore Pellet	2.83	0.58	0.15	0.54	0.41	66.78	95.00	0.45	0.012	0.04
Iron Ore Lump	4.50	0.99	0.059	0.18	0	65.37	92.51	0.87	0.044	0.025
Sinter	5.73	1.17	0.15	10.53	1.59	56.48	71.88	7.97	0.037	0.40
Limestone	1.33	0.01	0	50.94	0.89	0	0.12	0	0	0

The alkali metals depicted in Table 20, as determined by ICP confirm the presence of coal or char in the dust, due to the high K_2O concentration. Na_2O was

present both in coke and coal therefore it would be difficult to ascertain the contribution made by each to the dust. But it was clear that alkali metals originate from carbon-based materials, as opposed to ferrous-based materials.

Table 20 ICP analysis of alkali metals within the dust and the raw materials

	Na_2O	K_2O
	%	%
Flue Dust	**0.61**	**1.60**
Coal	0.61	1.88
Coke	0.68	0.18
Iron Ore Pellet	0.072	0.06
Iron Ore Lump	0.041	0.131
Sinter	0.060	0.065
Limestone	0.031	0.051

The carbon and proximate analysis in Table 21, was indicative of the presence of coal and coke, the carbon-based raw materials. The presence of coal here could be misleading, and it is important to note that under-carbonised material, which was inevitably present in coke was more likely to be present in the dust than raw coal itself. Prime quality coke typically has a volatile matter content of ~1%, therefore it is indicative that the material present in the dust was more reactive than coke because there was more volatile matter present in the dust itself.

Table 21 Carbon and proximate analysis of BF dust and ironmaking raw materials

	Carbon	Sulphur	VM	ASH	LOI
	%	%	%	%	%
Flue Dust	**64.26**	**0.52**	**4.78**	**35.21**	**53.43**
Coal	84.26	1.050	14.32	9.00	-
Coke	90.47	0.6	1.11	58.4	42.49
Iron Ore Pellet	-	0.011	-	-	0.06
Iron Ore Lump	-	0.016	-	-	0.63
Sinter	-	0.025	-	-	0.38
Limestone	12.09	0.001	-	-	42.98

Another influencing factor for the degree of dust generation was the moisture content of the material and weather conditions. Limestone is hygroscopic, meaning that it will naturally draw moisture from the atmosphere, which can be problematic for material handling and usage. On the contrary though, in terms of dust generation, a

theory could be that with increased moisture, particles will be more likely to adhere to the surface of the macro particle and less likely to exit the furnace in the form of dust. The counter effect of this though, is that increased moisture draws on the heat reserves of the blast furnace and requires increased energy use to process the raw materials into liquid iron. The moisture content of the materials was not considered in this study, as the moisture content of the dust itself was irrelevant, due to it being influenced on collection, water was present in the area round the dust catcher when the area was being cleaned and therefore would contaminate the moisture test. Also, obtaining samples of each raw material on a routine basis from the stock house was not practicable due to the safety constraints and the inherent process hazards.

Temperature conditions within the furnace work in collaboration with the moisture content of the material. Higher temperatures towards the top of the blast furnace will allow the materials to dry rapidly and discharge the surface particulates that were adhered to the macro particle, into the gas stream. Temperature conditions also influence the material utilisation towards the bottom of the furnace. The material that remains adhered to the macro particle descends to the bottom of the furnace, where conditions become more favourable for combustion and utilisation, due to increasing temperature and gaseous conditions. The material that is fed into the bottom of the blast furnace including injected reductants such as coal, is most likely to combust in the raceway at the point of entry to the furnace. But with conditions becoming less favourable for combustion towards the top of the furnace, the ascending coal is less likely to combust or gasify and will exit into the dust mainly in the form of char.

4.1.3 Comparing Samples from the Dry Abatement with Samples from the Wet Abatement

To determine whether the complexities and limitations of obtaining a sample from the wet abatement outlined in section 3.2.2, was necessary for the representativeness of the sample of the process, a comparative study was completed, to demonstrate the differences between the sample types and if the same information can be ascertained by analysing the material from the dry abatement only, it can be determined that this was representative of the process. The work of Wing *et al.* in the literature review section 2.10.3, states that the heavy coarser particles drop out during dry cleaning and the lighter finer particles are captured by wet scrubbing. The particle size distribution of the two materials can be compared in Figure 71. The average particle size of the

slurry was much lower than the dust. It is clear that the larger but less dense particles were separated in the dry abatement before reaching the wet abatement. The bulk density of the slurry was higher on average at ~900 kg/m^3 indicating that some of the less dense, likely carbon-based material was separated before the gas reached the wet abatement.

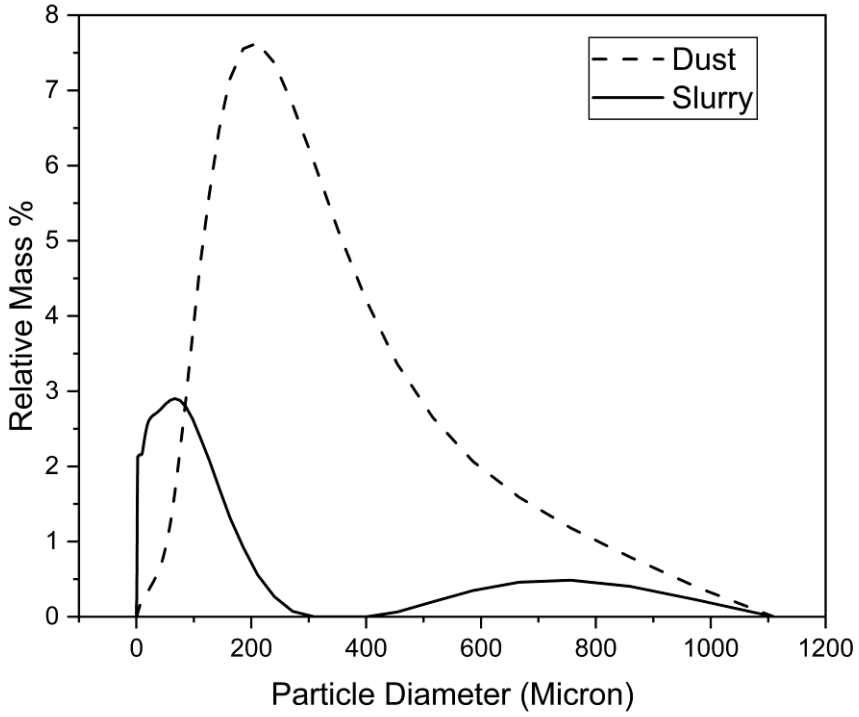

Figure 71 Particle size distribution of dust from the dry abatement and slurry from the wet abatement

The XRD spectra in Figure 72, also demonstrate an increased relative concentration of the iron-bearing constituents in the slurry as opposed to the dust. The amorphous carbon region remains present in the slurry which indicates some of the carbon-based material was still getting through to the wet abatement. However, the relative intensity of graphite present in the slurry was less than that of the iron oxides and metallic iron. There appears to be an increased presence of calcite and dolomite phases in the slurry, indicating the presence of the fluxes. The data from the XRD was relative to concentrations of each analyte within the dust, the volume of dust discharged into the wet abatement was not able to be quantified at this stage of the thesis. This data would provide insight into the mass of each constituent present in each dust type.

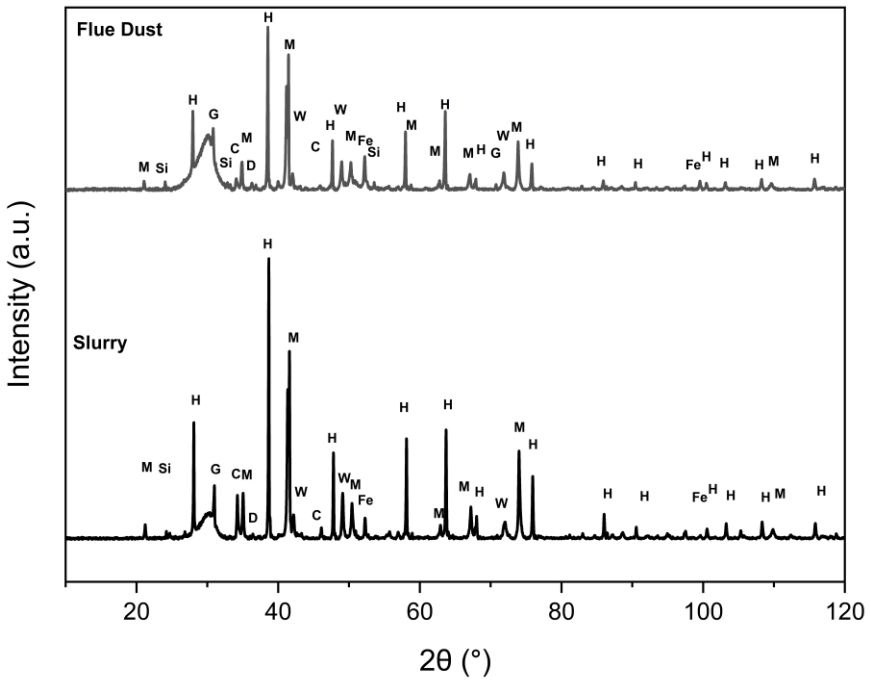

Figure 72 Powder XRD patterns for dust and slurry. H = Hematite (Fe_2O_3 – COD# 9000139), M = Magnetite (Fe_3O_4 -COD# 1011084), W = Wustite (FeO – COD# 9008636), C = Calcite ($CCaO_3$ – COD# 9016200), Si = Quartz High (O_2Si – COD# 1011200), G = Graphite (C – COD#9011577), D = Dolomite ($CaMg(CO_3)_2$ – COD# 9000885), Fe = Iron (Fe – COD# 4113941)

The XRD parameters of the amorphous region of carbon between 25 and 33^o were determined using the calculations outlined in section 3.4.4. Asymmetry within the amorphous region can be seen clearly in Figure 72, which was why there must be at least two bands of material within the same peak. The right-hand gaussian peak refers to aliphatic structures attached to the carbon crystal structure, but the left-hand peak can be attributed to the spacing of the aromatic ring layer. Graphite was also clearly present with a large peak present at 31^o[131].

Lc is the degree of crystallinity and is the measure of stacking height in nm of the carbon layer structure within the dust sample. With samples containing more coal-originating carbon, it can be expected to see lower values for stacking because the carbon present is more crystalline[82]. La refers to the average crystallite lateral size in nm. This is the lateral size from the left gaussian peak, referring to the aromatic carbon rings. For this reason, it is expected that lower values for lateral size will demonstrate more coke-originating carbon, because of lower aromaticity. Rank is simply a comparison between the intensities of the aromatic and aliphatic peaks of α and β. This is a crude measure for this type of sample due to sample complexity, the

many forms and sources of carbon present within the dust make the application of this technique challenging, rank is more suited to coal analysis with less variety in the carbon-based constituents[132]. It can be said that with increasing rank the intensity of the β peak is growing or the intensity of the α is shrinking, which would lend itself to increased crystallinity therefore a higher value for rank would be expected to represent more coke-originating carbon present in the sample. The interlayer spacing (D_{002}) can be considered a measure of the stacking quality, more perfected stacking structures are considered to be stacking towards a graphite structure, which would give a lower interlayer spacing. There is a known link between Lc and interlayer spacing as proven in the work of Manoj *et al.* With increasing stacking towards graphite, it is acceptable to say the carbon present is more likely to originate from coke because the interlayer spacing is decreasing. The aromaticity measure simply measures the area of the aromatic α peak per total area of both α and β peaks. The increasing aromaticity means a higher aromatic per aliphatic ratio, which would suggest decreased crystallinity. For these reasons it could be expected that with increased aromaticity, the carbon within the sample is more likely to originate from coal[133].

The range of aromaticity in the dust and slurry was compared in Figure 73. The mean aromaticity was lower in slurry than that of dust, indicating that less aromatic carbon was present in the slurry, hence coal and char-originating carbon was likely to dominate the dust. Similar observations are made for each of the parameters, however, the range of the La values appears smaller in the slurry. It was not clear that there was a significant change in the carbon types between the dust types but the larger range in La, demonstrates that more variety of material would be captured in the dry abatement.

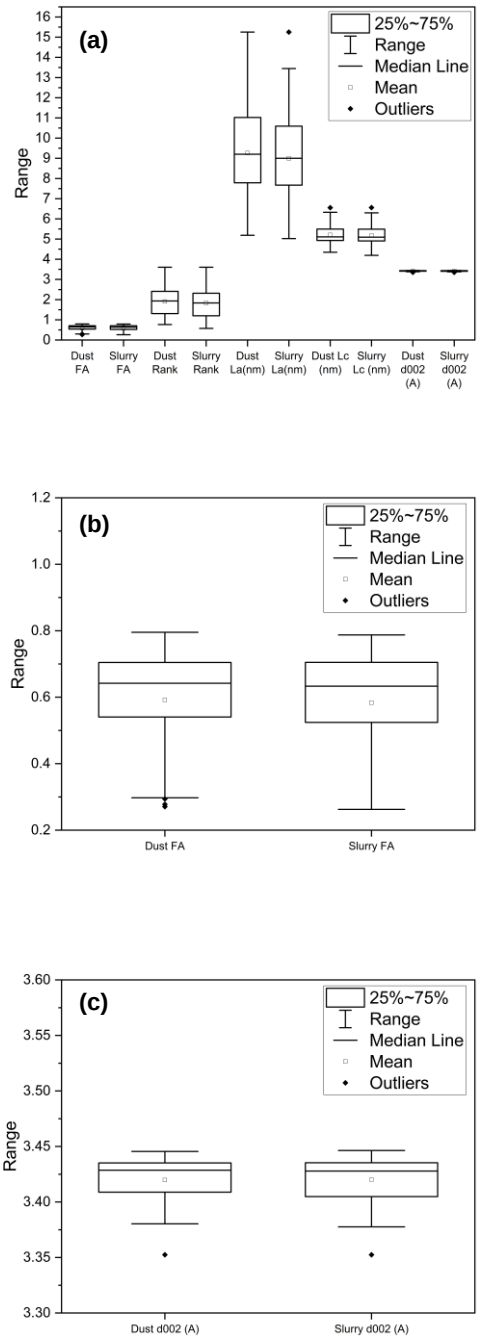

Figure 73 Box plots of XRD parameters of dust versus slurry a) All the XRD parameters of the dust b) aromaticity parameter the range was too small for the first graph c) the interlayer spacing range

The graphs in Figure 74, compare the differences in physical and chemical properties between the dust and slurry samples. Iron-bearing analytes in the top left graph of Figure 74 are higher in concentration in the slurry as are the metals from the ICP analysis. This confirms the observations from the XRD spectra comparison. The

LOI was increased in the slurry, meaning that the slurry contains more low-order reactive material than the dust, this could, however, be due to the particle size, smaller particles combust better during the LOI test due to the increase in surface area to volume ratio[134]. Ash was higher in the dust which indicates a higher presence of the refractory elements present within the flux raw materials. The carbon, volatile matter and alkali metals are all higher in the dust confirming that more carbon materials in general are scrubbed out of the gas, more than the iron-based materials at the dry abatement. For the subsequent chapters of the thesis, the focus on carbon-based materials requires this justification for the analysis of dust samples before slurries.

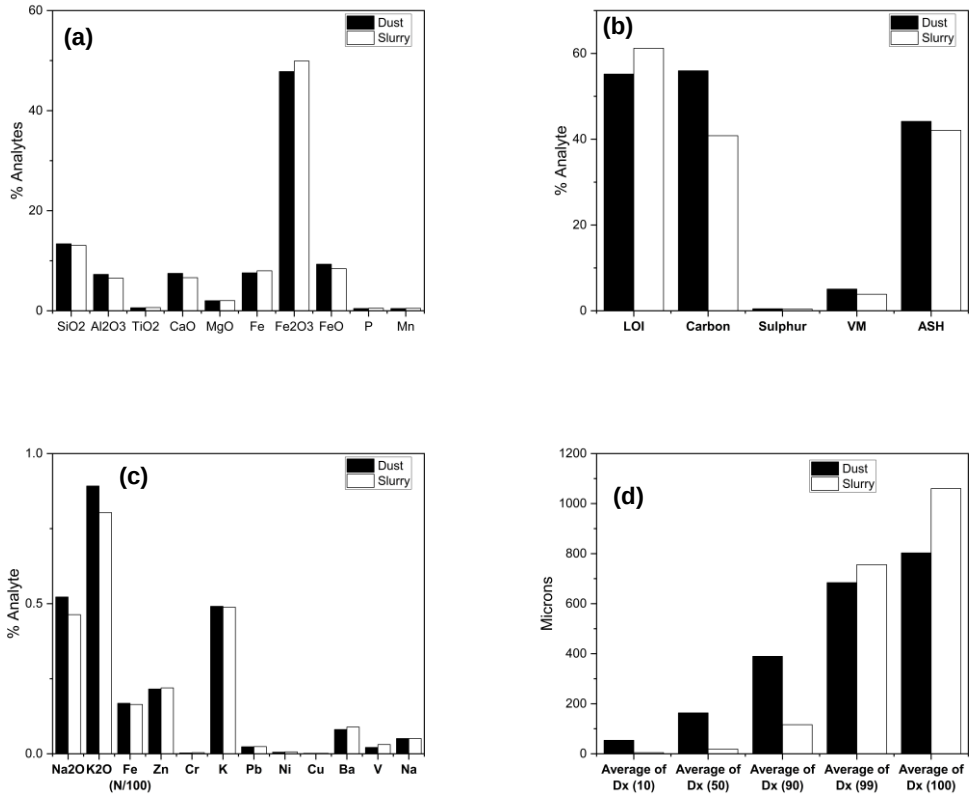

Figure 74 Bar graphs comparing average dust versus slurry analytes a) XRF data b) combustion-based analytes c) ICP derived analytes where the Fe has been normalised to 1% to bring in line with scale d) PSD comparison

4.1.4 Variation in the Dust and Slurries

Minimal process variation is a target of blast furnace ironmaking, a stable production rate allows for the predictable operation of downstream units. Oversupply of iron to the steel plant can be wasteful hence the drive for stability greatly outweighs the demand for increased production as the steel manufacturing process is designed to

operate at capacity. Despite the best efforts for stability, process variation and material variation is inevitable, however. The XRD spectra in Figure 75, show 5 different dust samples from samples taken on different days. The relative intensities of the various analytes can change drastically between samples, indicating variation in concentrations of the different analytes. The shape of the amorphous region varies also between the samples as can be seen in sample 13, with no graphite peak present, the overall amorphous region between 25 and 33^{o} dwarfs the peaks of the other phases present within the spectra. There was variation between the silica and calcium silicate phases as observed with increases in these specific peaks in sample 5 compared to the other dust samples. In sample 24 the intensities of the silica quartz peaks are less prominent, but the presence of magnetite was more prominent in this particular sample indicating more dust from iron-rich materials. Sample 25 was unique with the presence of Wollastonite, a calcium silicate peak present at around 15^{o} that does not appear in any of the other samples. This was coupled with a small amorphous carbon region, demonstrating this particular sample was lower in carbon-based phases. The degree of variation between the samples was clear to see and further justifies the focus on the dust samples from the dry abatement as there was ample variation to determine changes in the process.

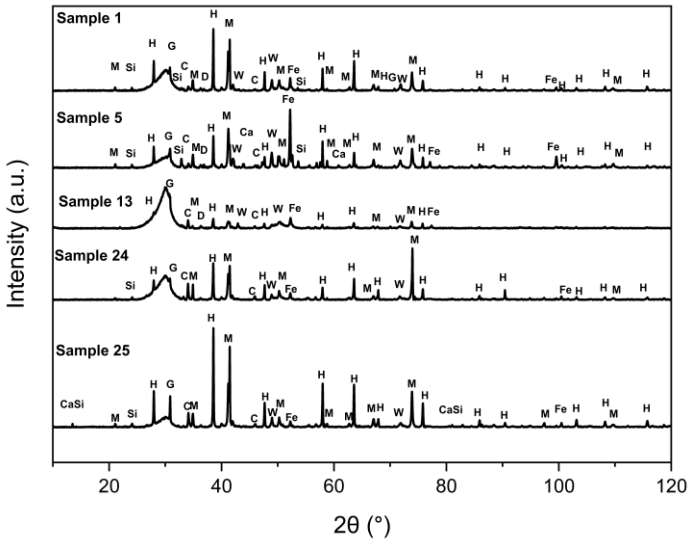

Figure 75 Powder X-Ray diffraction of 5 dust samples. H = Hematite (Fe_2O_3 – COD# 9000139), M = Magnetite (Fe_3O_4 -COD# 1011084), W = Wustite (FeO – COD# 9008636), C = Calcite ($CCaO_3$ – COD# 9016200), Si = Quartz High (O_2Si – COD# 1011200), G = Graphite (C – COD#9011577), D = Dolomite ($CaMg(CO_3)_2$ – COD# 9000885), Fe = Iron (Fe – COD# 4113941), CaSi = Wollastonite (Ca_3O_9Si – COD# 1011227)

Figure 76, shows the ranges for the combustion-based parameters of dust samples are larger than that of the slurries. The carbon and ash ranges are significantly lower in the slurry, indicating that the type of ash constituent and carbon constituent passing through the dry abatement and being scrubbed in the wet abatement was more consistent than the dust. The volatile matter range was also smaller in the slurry, but because this test was only 7 minutes long under combustion conditions, the size of the particle may impact the output of this value[134]. Although the opposite of the observation seen in Figure 76 would be expected. The slurry was smaller in size comparison and therefore should combust more readily during the test. The range was smaller in the volatile matter of the slurry indicating that if only the observations from the slurry were made, much of the information of the sample would be missing because the variation was captured in the dust sample. The ranges indicate the importance of the dust sample in comparison to the slurry sample for carbon-type analysis.

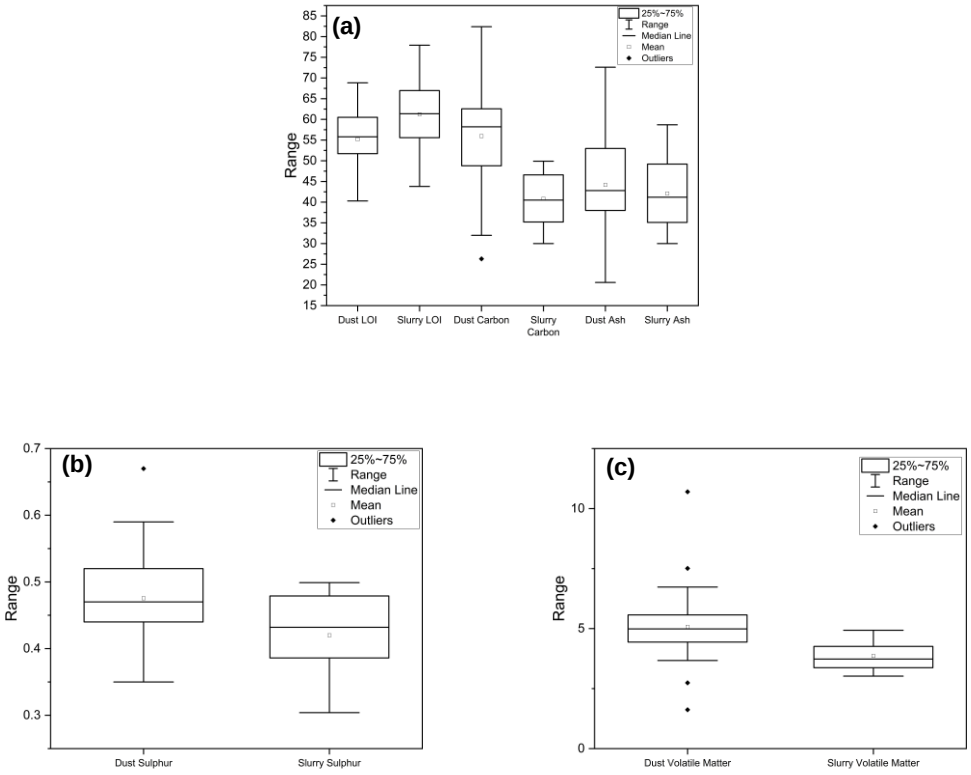

Figure 76 box plots comparing the ranges of the combustion-based analysis of dust versus slurry a) proximate analysis b) sulphur analysis c) volatile matter

Similar observations are made in the ranges in the XRF chemistry of the dust versus the slurry as per Figure 77. The largest change between the sample types was observed in the Fe_2O_3, and a large increase in range and average was observed in the slurry. This indicates that the iron-bearing portion of the material was getting through the dry abatement more than the carbon-based materials. Another observation to note was the decrease in FeO between the dust and slurry samples, which was the inverse of the changes in the other iron-based constituents. The FeO portion of the dust was a result of coke ash or sinter present in the dust, as opposed to iron ore as per previous observations in the constituents of blast furnace dust section 4.1.2. This indicates that the coke was being captured in the dry abatement more effectively than the iron ore which bares the iron and Fe_2O_3 fractions of the dust.

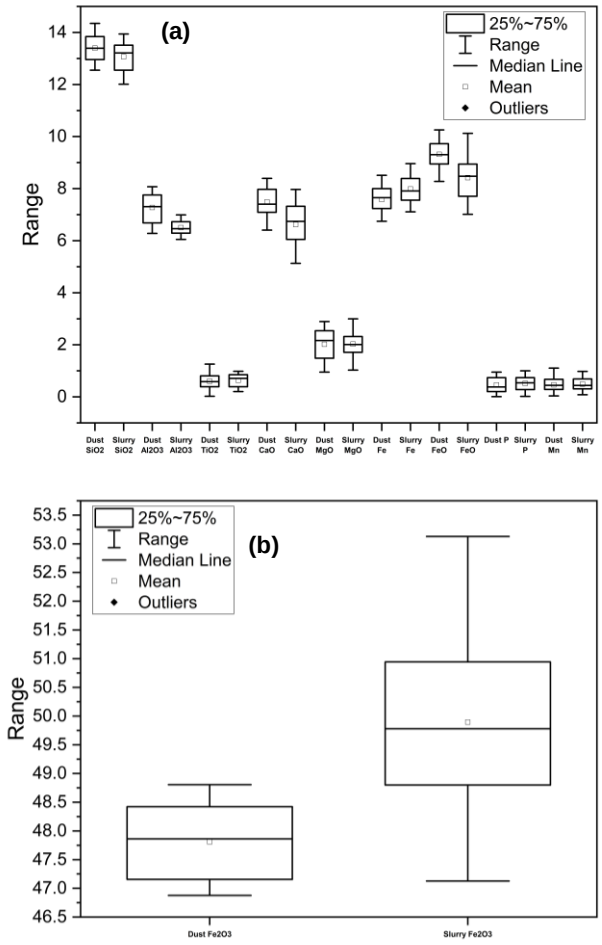

Figure 77 Box plots of the XRF chemistry comparing the ranges of dust versus slurries a) all analytes b) Fe_2O_3 specifically to show within the range

The ICP analysis for metals and alkali metals was consistent between dust and slurry as per Figure 78. The observations to note are the increasing range of Fe in the slurry. This technique measures the iron in the sample as a whole and not just the ash concentration, this follows the observations in the XRF data with increasing iron present in the slurry. The other observations to follow this trend are vanadium and chromium. The range in copper was minuscule and therefore a reliable comparison was not possible. The change in vanadium and chromium could be due to the increased density similar to the Fe materials compared to the carbon-based analytes.

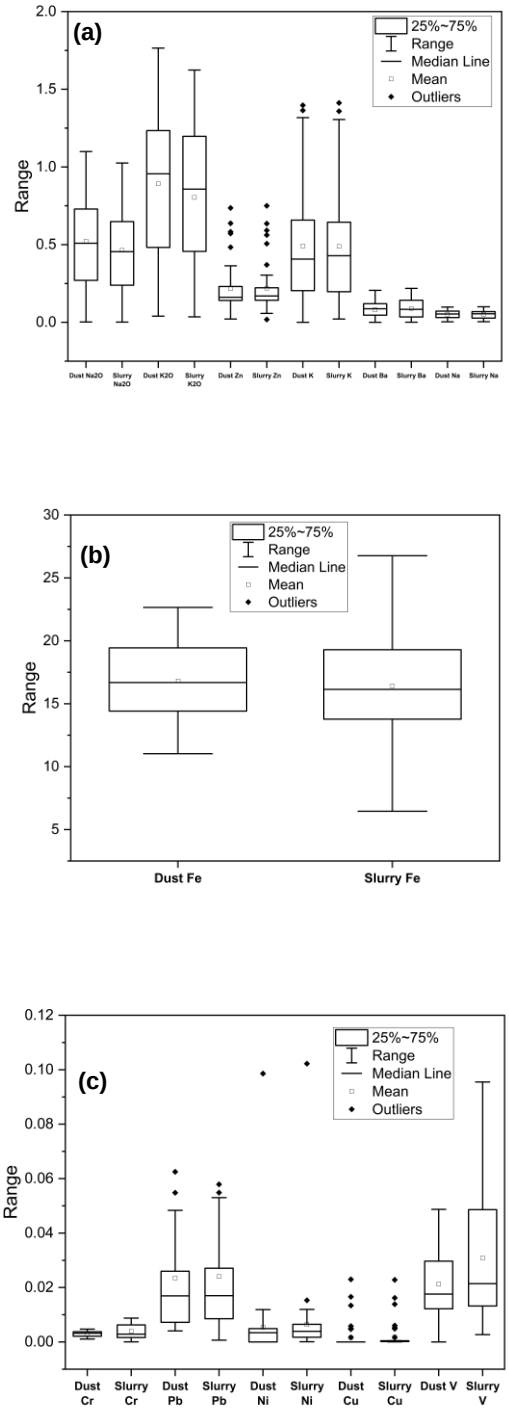

Figure 78 ICP box plots of dust versus slurry a) mid-range analytes b) high range Fe c) ultra-low range analytes

The range in physical properties appears in Figure 79, as expected it varies between the dust and the slurry. The majority of particles are stripped from the gas in the first abatement according to the work of Winfield *et al.*[68]. The decrease in the

range between the physical properties of slurry indicates just this. It can be observed that the material getting through to the wet abatement was much more consistent than the dust due to the decrease in range. This increase in range would indicate that material more representative to the process would be captured within the dry abatement. If only the wet abatement was sampled, many of the variable particles will have been filtered out already and would therefore be less representative. For this reason and ease of sampling of the dry abatement, the focus on dust for carbon-based analysis in the subsequent chapters was justified.

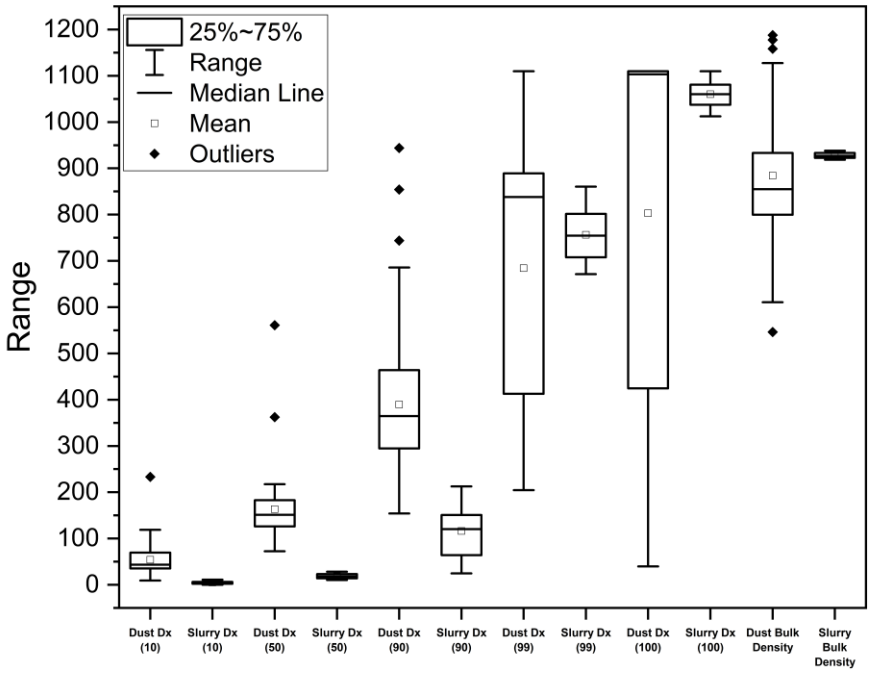

Figure 79 Box plots of the physical properties of dust versus slurry

4.1.5 Determining Carbon Relationships

To determine relationships between the carbon constituents and the other analytes of the materials, simple Pearson's correlations were drawn as per Table 22. None of the correlations observed were strong enough to determine any relationship, to confirm this the scatters can be observed in appendices 1-8 in section 7.1. In dust samples, there appear to be positive weak relationships between carbon and LOI, Mn, Pb, S and Dx (100). The carbon and LOI relationship can be explained because the two tests are combustion-based analyses therefore similarities are expected. Inverse relationships include Fe_2O_3, volatile matter, ash and bulk density. The bulk density relationship helps demonstrate that increasing carbon-based constituents will decrease the overall density of the material because carbon is less dense than iron. The same relationships are not necessarily observed in the slurry data with Fe, Dx (50) and Dx (90) demonstrating positive relationships with carbon. Cu, Dx (10) and Dx (99) have weak inverse relationships with carbon, with decreasing particle size as observed in increasing Dx (10) with increasing carbon confirms the work of Wing *et al.* in section 2.10.3 of the literature review because the finer particles are reaching the wet scrubber. Because of the lack of correlations it can be said that carbon is independent of the other analytes. There is a small improvement in correlation in the dust samples which may indicate the representativeness of the dust over slurry, but any potential relationships appear simply circumstantial or randomly scattered and it cannot be determined that correlation or causation is true in this case. With this information it can be determined that the focus on carbon analysis in the subsequent chapters is independent of any of the other analytes.

Table 22 Pearson's correlation and R^2 values for carbon versus alternative analytes in dust and slurries

Flue Dust Carbon	Pearson's Correlation	R^2	Slurry Carbon	Pearson's Correlation	R^2
LOI	0.32	0.10	**LOI**	0.19	0.04
SiO_2	0.15	0.02	**SiO_2**	0.14	0.02
Al_2O_3	0.09	0.01	**Al_2O_3**	-0.16	0.03
TiO_2	0.07	0.00	**TiO_2**	0.00	0.00
CaO	0.05	0.00	**CaO**	0.03	0.00
MgO	0.16	0.02	**MgO**	0.12	0.02
Fe	-0.19	0.04	**Fe**	0.27	0.07
Fe_2O_3	-0.24	0.06	**Fe_2O_3**	-0.10	0.01
FeO	0.10	0.01	**FeO**	-0.10	0.01
P	-0.07	0.00	**P**	-0.13	0.02
Mn	0.23	0.05	**Mn**	0.16	0.03
Na2O	0.02	0.00	**Na2O**	-0.03	0.00
K2O	-0.05	0.00	**K2O**	-0.04	0.00
Fe	0.04	0.00	**Fe**	-0.13	0.02
Zn	0.17	0.03	**Zn**	-0.14	0.02
Cr	0.02	0.00	**Cr**	0.02	0.00
K	-0.08	0.01	**K**	0.13	0.02
Pb	0.21	0.04	**Pb**	-0.03	0.02
Ni	-0.03	0.00	**Ni**	-0.19	0.04
Cu	-0.16	0.03	**Cu**	-0.24	0.06
Ba	-0.01	0.00	**Ba**	-0.20	0.04
V	0.13	0.02	**V**	-0.09	0.01
Na	0.15	0.02	**Na**	-0.08	0.01
S	0.30	0.09	**S**	0.05	0.00
V.M	-0.30	0.09	**V.M**	0.00	0.00
Ash	-0.34	0.11	**Ash**	-0.06	0.00
Dx (10) Micron	0.12	0.01	**Dx (10) Micron**	-0.29	0.09
Dx (50) Micron	-0.01	0.00	**Dx (50) Micron**	0.24	0.06
Dx (90) Micron	-0.09	0.00	**Dx (90) Micron**	0.28	0.08
Dx (99) Micron	0.10	0.01	**Dx (99) Micron**	-0.32	0.10
Dx (100) Micron	0.24	0.06	**Dx (100) Micron**	-0.18	0.03
Bulk Density	-0.47	0.22	**Bulk Density**	0.00	0.00

4.1.6 Summary

The scope of this chapter was to characterise the dust from blast furnace ironmaking, to understand the constituents of the dust and where the particulates may originate from. It was clear from the SEM micrographs that each of the raw materials used for ironmaking will inevitably contribute to dust formation. This was confirmed by the phases of each raw material being identified in the XRD spectra of the dust. The particle size distribution was a good indicator that the material in the dust originated from the degradation of the raw materials. The chemical analysis shows where most of the constituents were likely to originate from in the dust. There appears to be a good

representation of each of the raw materials contributing to the dust itself as outlined in the various analysis of each of the raw materials. The quantifiable presence of each of the constituents allows for changes to be detected in the dust through time, thus allowing for the diagnosis of combustion conditions in the blast furnace. This work showed that the hypothesis presented in section 1.2 was correct, 'The raw materials that feed the blast furnace are expelled into the gas stream and all influence the blast furnace dust.'

When comparing the different types of BF dust, it appeared that the dry abatement was capturing the majority of dust particulates. A clear representation of the process variation can be obtained from this particular sample type in comparison to the slurry data. Some of the key differences observed can be related to the type of material that was carried over being carbon-based or iron-based, this appears to influence where the material was scrubbed from the gas. Much of the constituents within the dust from the iron ore can be found more concentrated in the slurry than the dust, the inverse can be observed with the carbon-based constituents. The dry abatement appears to be more efficient at removing the carbon-based materials as observed when comparing the chemistry and ranges of each analyte in both the dust and the slurry. The only iron-based compound not increased in the slurry was FeO, the source of which appears to be coke or sinter which would support the observations in segregation.

Data on dust variation and drawing comparisons with the slurry variation show that the analytes are more variable in the dust than in the slurry. This indicates that a more representative material of the overall dust output was being collected by the dry abatement. This was another indication that dry abatements are effective at removing dust from the gas stream. The consistency of the slurry indicates that much of the process variation was absorbed in the dust extracted in the dry abatement and provides justification for the samples used in subsequent chapters to be taken from the dry abatement. The efficiency of the abatements has only ever been modelled previously and hence this work is a step towards representing efficiency using live data.

When identifying relationships between the carbon and the other analytes of the dust and slurries, only weak correlations could be observed and most scatters appear circumstantial even randomly scattered. The relationships noted in the dust samples were weak but were stronger than the carbon-to-analyte relationships in the slurries.

The increased presence of relationships albeit minute, between the dust carbon versus the slurry carbon could provide further justification for the focus on dust in the subsequent chapters. The lack of relationships between carbon and the other analytes indicates the independence of carbon compared to the other analytes and was yet another justification for the focus on carbon analysis for diagnosing coal gasification issues. The carbon analysed in this chapter was based on the total carbon of the dust itself, further analysis into the sources of carbon was justified due to the clear presence of both coke-originating and coal-originating carbon present in the SEM micrograph and the subsequent chemical analyses. In terms of dust output reduction, the presence of carbon from coal and coke means there was an opportunity to reduce the output of carbon-based dust through the optimisation of the utilisation of these materials.

4.2 Carbon Type Differentiation in Blast Furnace

4.2.1 Introduction

Complete combustion of coal in the raceway of a blast furnace, due to the low residence time and fast-paced reaction zone, is highly unlikely. The depleting temperatures and evolving gaseous conditions throughout the furnace means that coal char will inevitably be present within the flue dust. Optical and scanning electron microscopy techniques have been used to confirm the presence of coal char in the form of cenospheres in the dust[12], but quantifying the char has been a challenge. Due to the multiple constituents and carbon types present within the dust, there is a degree of overlap and uncertainty when quantifying LOC.

To assess coal combustion effects within the blast furnace, in the laboratory, studies have been completed on the off-gas dust to quantify the sources of carbon present within the dust itself, as a method of diagnosing issues with coal gasification in the raceway in terms of the degree of coal burnout. A carbon-type differentiation technique outlined by Schwalbe *et al.* included deconvoluting the ion current peaks from a mass spectrometer coupled with a thermoanalyser[63]. The peaks present from the off gas created by increasing the temperature in the thermoanalyser with a BF dust, could be integrated into carbon from coal, coke and soot respectively. Further peroxide and mineral acid digestion of the sample was carried out to calculate the graphite portion of the sample using X-Ray Diffraction[63]. An alternative technique, developed by Wing *et al.*, known as the CanmetEnergy Technique (CET), makes use of a specifically designed temperature profile using a thermogravimetric analyser to quantify moisture, LOC, HOC, soot and ash content of BF dust samples. The technique has been validated using char and coke mixes of known quantities and the technique returns the correct LOC portion in each case. The LOC in this context refers to predominately coal-originating carbon as per section 2.10.2, but due to the complex nature of BF dust, there will inevitably be an overlap in the temperature of ignition of LOC and HOC in the material[55,61]. The work of The *Charfoco* report in section 2.9 of the literature review says that the technique had taken into account the higher reactivity of coal char, compared to coke making it useful for carbon type differentiation. The fact that this technique has been validated using synthetic mixes, makes it attractive for use as an industrial diagnostic tool. It was hypothesised that an

increase in LOC indicates an increase of coal char present in the dust itself, and therefore less combusted coal in the raceway.

While the CET was successful in terms of result output, the requirement to conduct rapid assessments in response to the ever-fluctuating conditions of the blast furnace remains a challenge. Similarly, this technique has not been validated for dusts from blast furnaces that use GCI as opposed to PCI. Moreover, as environmental considerations are increasingly prioritised, it was important to be able to identify critical process and raw material variables that may result in incomplete coal combustion and unwanted particle matter in blast furnace off-gas. This chapter aims to assess the applicability of existing techniques to understand coal combustion before exploring alternative methods to conduct rapid response carbon type differentiation. Advanced characterisation will be utilised alongside quantification methodologies to provide additional qualitative information and validation of the experimental methods trialled. Image processing technologies have been utilised to attempt to automate the counting of char particles and thermal analysis techniques, to exploit the thermal properties of different carbon types to quantify the differences within this chapter. The power of X-Ray analysis has been explored alongside simple analytical techniques such as particle size distribution and bulk density. All of these techniques are aimed at discovering the best available technique, with the accuracy of the CET, but with a smaller analysis time to allow for rapid analysis in line with ever-changing blast furnace conditions. To assess the suitability of each carbon type differentiation analysis technique, 18 samples of BF dust, 9 from each furnace were used from the catalogue of samples discussed in section 3.2.7. Samples from the high, medium and low events of production rate, oxygen conditions and coal rate were used to ensure a wide variety of LOC was likely.

4.2.2 Identifying Coal Originating Carbon in Blast Furnace Dust

Optical and SEM characterisation was conducted on the BF dust samples for baseline analysis, examples of which are shown in Figure 80. Figure 80 a and b provide optical microscopy cross-sections of the dust, highlighting the presence of cenospheres[56]. The presence of cenospheres in BF dust was therefore indicative of coal-char particles, and thus suggests incomplete combustion of the coal[12,56]. Figure 80 c and d show examples of typical SEM micrographs obtained from the dust samples. The SEM micrographs highlight the presence of char which appear as dark particles with visible

surface pores. These differ from metallurgical coke particles, which appear flaky and lighter in colour[135].

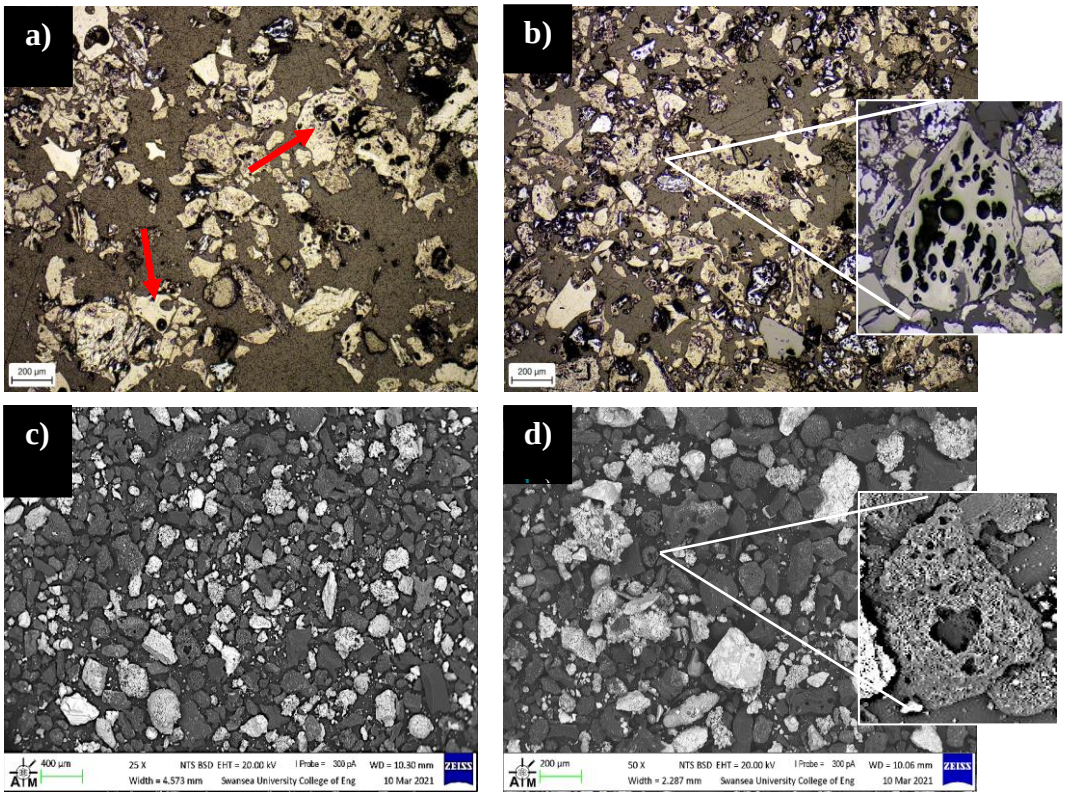

Figure 80 a) and b) optical micrographs of BF dust mounted in Polyvinyl Formal resin. c) and d) SEM micrographs showing the presence of coal char cenospheres

4.2.3 CanmetEnergy Technique

TGA analysis of the dust samples was carried out as set out by the CET. The thermal profile utilised, described in section 3.4.1, was shown in Figure 81, alongside the DTG curve for Sample 1. Each section of the curve represents a different stage in the gasification of the samples. Initially, moisture losses are calculated as the mass lost from the beginning of the test to the end of the 175^{o}C isotherm. The area under the DTG curve, between the minimum points before and after the respective isotherms, was relative to the quantity of LOC and HOC as validated in section 3.4.1. The small peak at ~1400 minutes refers to the soot portion of the carbon in the sample and ash can be calculated from the mass lost after carbon. The differences between the reactivity of the carbon types were discussed in the literature review section 2.10.3, where it was stated that cenospheres form within the particle which will not only combust readily but provide extra surface area for oxidation reactions. When coal

volatile decreases, exinite and liptinite levels within coal decrease, and the remaining vitrinite will convert into a coke-like structure rather than forming cenospheres. These coke structures are less combustible than cenospheres, based on the surface area[55].

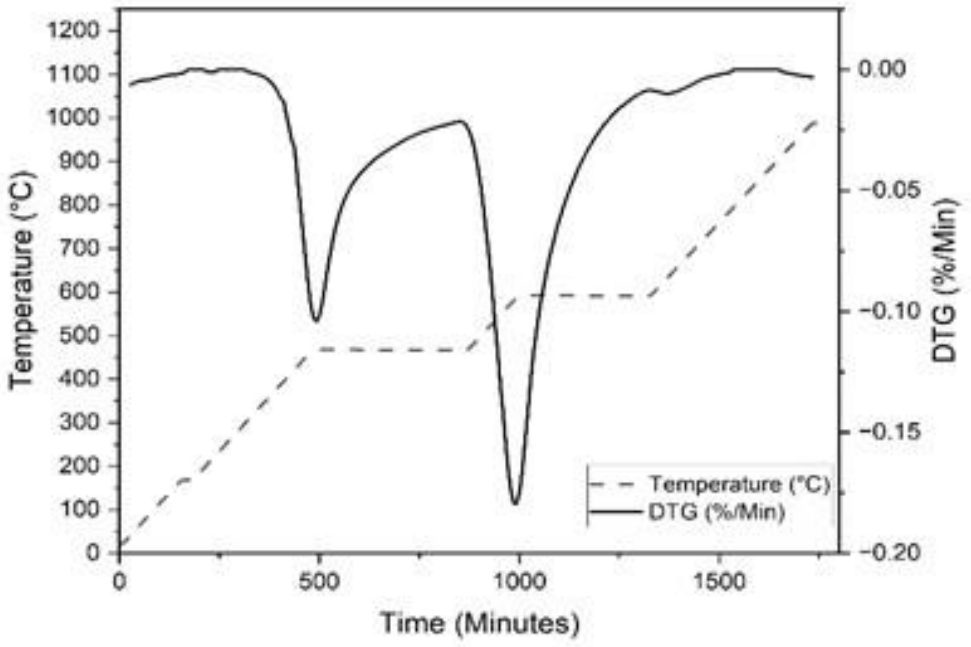

Figure 81 Thermogravimetric analysis of a BF dust (sample 1). DTG and temperature plotted against time.

Normalised versus Non-Normalised LOC

The final values for CET versus normalised CET are seen when comparing the data in Figure 82. When looking at each sample it was clear that the CET and normalised CET values are similar. There appears to be a large difference in sample 35 compared to the others inferring that higher values for LOC are more susceptible to carbon type overlap. The combustion stage will inherently take longer if there was more LOC to combust and hence the overlap will be greater. Sample 62 had the same values for normalised and non-normalised LOC, this indicates a high value for LOC present as the overlap for LOC and HOC will be significantly reduced with a larger difference between carbon types.

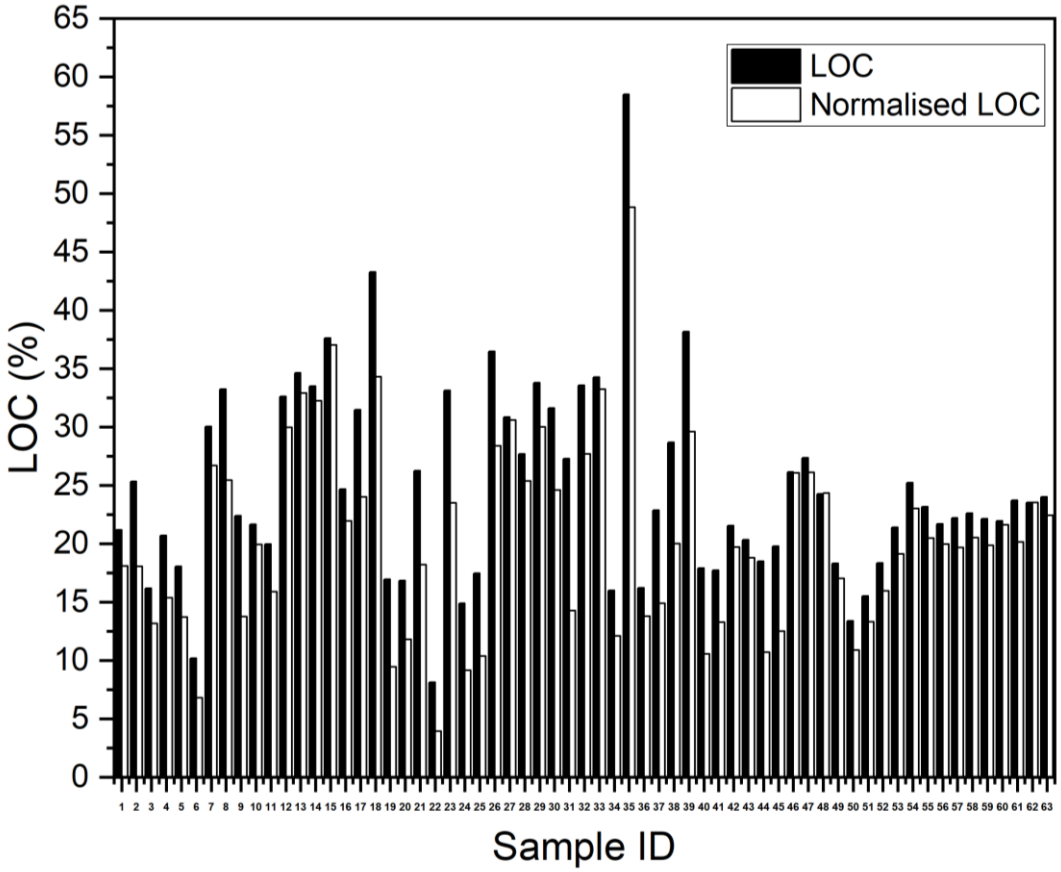

Figure 82 Bar chart comparing LOC and normalised LOC values

When comparing the values for LOC and LOC normalised in a line graph, it can be observed that the normalised LOC was always lower than LOC. The values track each other very well, but the spread can be observed more clearly in Figure 83, particularly around sample 32 which was the point with the largest difference. Indicating a large overlap in carbon type in that particular sample.

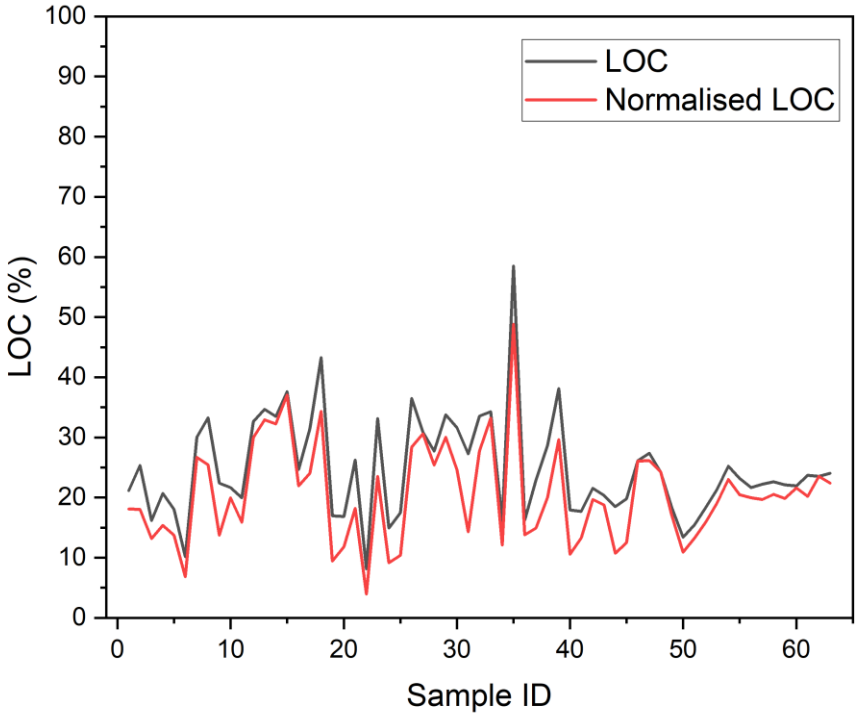

Figure 83 Line graph comparing the values for LOC and normalised LOC

The box plots in Figure 84 show the increase in the range of data from the LOC compared to the normalised LOC of 50.38% and 44.91% respectively. This with the increased standard deviation of the LOC of 8.39% versus the 8.17% from the normalised dataset, indicates the degree of variation increased without the normalisation stage. It was decided that the normalisation stage should be excluded from the data analysis, because of the lack of range, the normalised dataset was not a true representation of the actual data. Since comparisons were needed against process data in later chapters of this thesis, variation in each variable was essential for the true representation of relationships between the LOC and the blast furnace parameters. The extra normalisation step would also compromise any potential relationships drawn between analysis techniques for carbon type differentiation that are explored in this chapter.

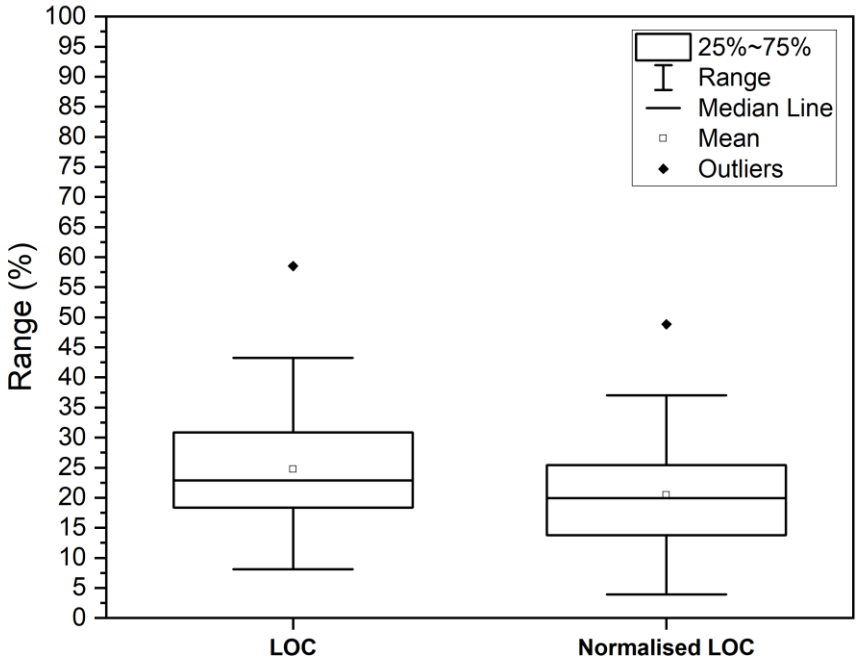

Figure 84 Box plot of the range of data comparing LOC and normalised LOC

Comparison with Eltra Carbon

The TGA CET method was used to calculate the total carbon within each sample by simply determining the sum of LOC and HOC for each test. The data calculated from the sum of LOC and HOC was compared to the total carbon data obtained from the Eltra C/S 500 and shows a good tie up, with less than 3% variation between TGA-calculated and measured carbon, as shown in Figure 85. Table 23 shows the error statistics for the carbon types, the low error values support the comparison. This data comparison provides additional confidence and validation that the TGA method provides a good representation of the total carbon types within the BF dust samples and that the method was a suitable comparison and diagnostic tool.

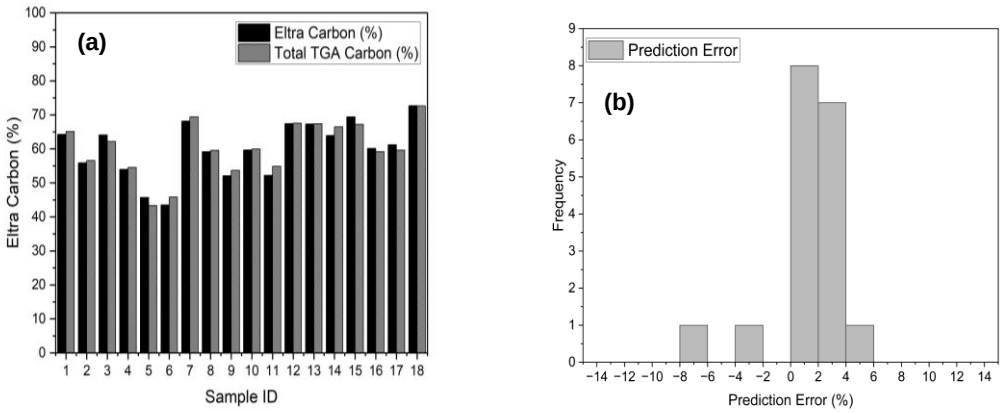

Figure 85 a) Total carbon from Eltra C/S 500 versus total carbon calculated from CET b) prediction error histogram

Table 23 Error of carbon from Eltra C/S500 versus total carbon calculated from CET

Mean Error (%)	1.25
Mean Squared Error	2.35
Max Error (%)	2.66
Root Mean Squared Error	1.53

4.2.4 Raw Coal in the Dust

Evidence of LOC in the BF dust was indicative of coal char leaving the raceway and exiting the furnace as a solid as opposed to a gas. When analysing the TGA graphs of the dust samples there was evidence of coal as well as coal char, also reaching the dust. The small hump in the TG and DTG graph around 500 minutes was indicative of the oxygen adsorption step outlined by Niroj *et al.* and Avila *et al.* where the temperature of 272^{o}C was the onset of this stage of coal combustion[136,137]. The temperature of the hump in the TG curve in Figure 86 was around 270^{o}C, indicative of this oxygen adsorption stage and the presence of raw coal in the dust[138].

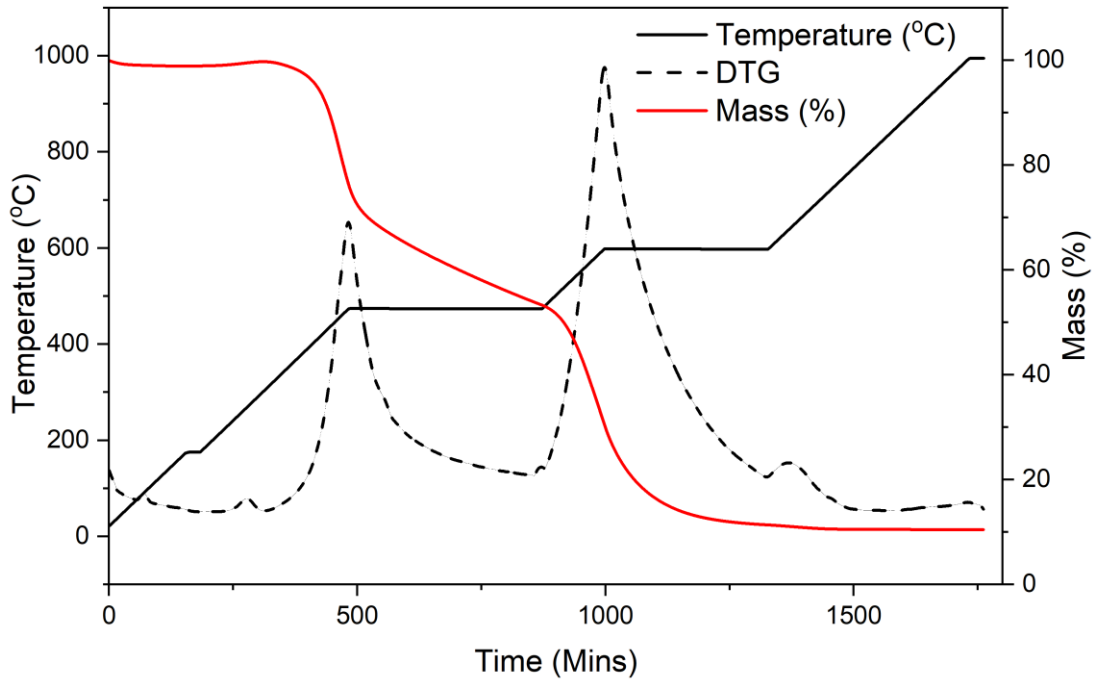

Figure 86 DTG and TGA graph of BF dust containing coal presence

Further evidence of coal in the dust can be found in the SEM micrograph of BF dust in Figure 87. The darker particles are atomically lighter due to the use of backscatter detection[139]. Coal particles such as those circled in Figure 87, mean that some coal injected in the bottom of the furnace moves through the raceway before it has the chance to combust. These coal particles are like those found in the work of Asif *et al.*[140]. It is important to note that some under-carbonised material was possibly ejected from the surface of coke due to the inefficiencies of coke manufacturing, however this would appear a different density in the BSD.

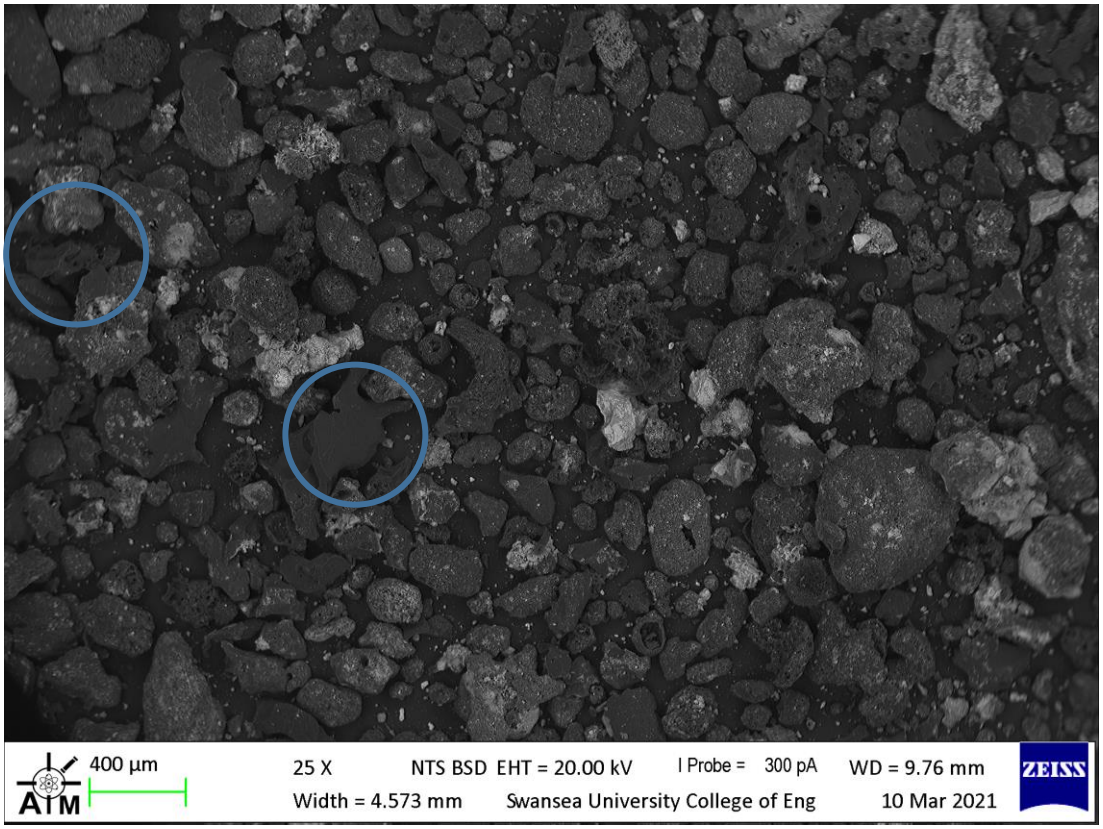

Figure 87 SEM micrograph of BF dust highlighting coal particles

To further determine the presence of coal in the flue dust, the amorphous carbon region on the XRD spectra was examined. The results shown in Figure 88, demonstrate the inverse relationship between coal La and dust La. This relationship shows that the carbon morphology changes with heating. Higher degrees of La in the coal leads to lower degrees of La in the dust. This means the morphology of the carbon peak becomes more ordered in the dust as the lateral crystallite size decreases[115]. Many factors could influence the shape of the amorphous peak, but the increased aromaticity in the Dust Fa relating to the Coal Fa shows that some coal or aromatic carbon, was getting through to the dust. Appendix 9 shows the strength of the relationships, the La was the strongest at -0.38 and this was considered weak along with the R^2 that was relatively low at 0.14. The aromaticity (Fa) shows no relationship, but visually a relationship appears more strongly in higher levels of dust aromaticity.

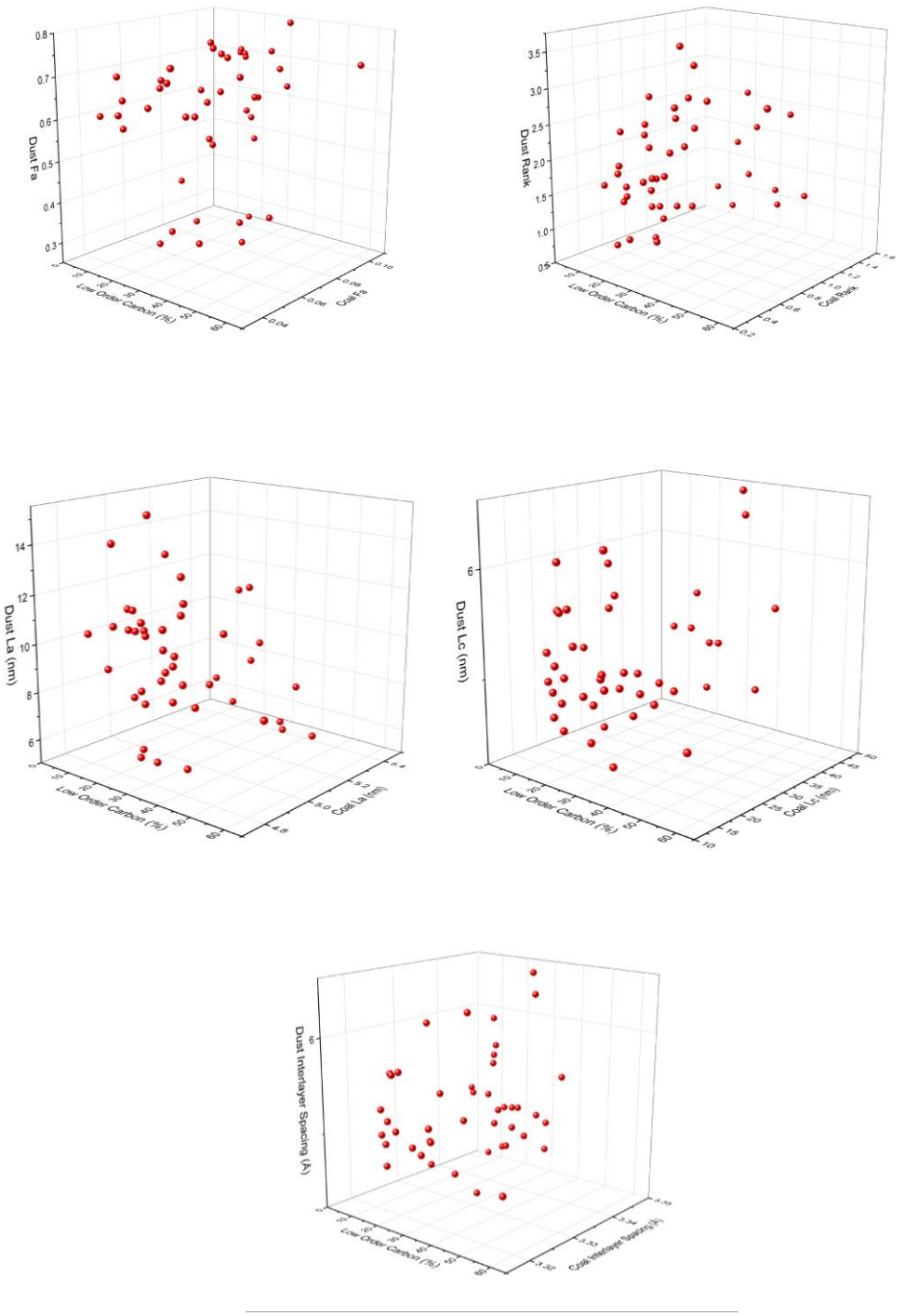

Figure 88 Scatter graphs of LOC versus XRD parameters of coal blend and the dust samples, top left to bottom right, dust Fa and coal Fa, dust rank and coal rank, dust La and coal La, dust Lc and coal Lc, dust interlayer spacing and coal interlayer spacing

With depleting oxygen and lower temperatures on the ascent to the top of the furnace, it was unlikely that coals will further combust once the coal has left the raceway. BF dust samples from blends 1 and 9 displayed signs of coal present in the dust, caused by lack of combustion or process conditions. Gasification studies have been completed by various people using a TGA with CO_2 as a reaction gas such as Liu

et al.[141]. The work of Pohlmann *et al.* was discussed in section 2.9, where he attempted to quantify the degree of stack burnout of char or coal that leaves the raceway. Although this was experimentally representative of coal gasification, it was not truly representative of blast furnace gas. As a recommendation, the blast furnace gas compositions outlined in chapter 6, are based on the work by Hou *et al.* and Grammelis *et al.* and should be used to determine true coal gasification higher in the blast furnace[142,143]. The impact of controlling the raceway combustion and combustion throughout the whole furnace would provide better information on coal selection for maximum combustion performance.

4.2.5 Modified Techniques

Canmet Fast

Following optimisation trials of the thermal profile outlined in section 3.4.2, the final *modified CET* condition comprised of increasing the ramp rate to 20ºC/min, while the isotherms were held at similar temperatures and durations as per the CET to minimise the overlap between LOC and HOC. The overall duration of the test was approximately half that of the original CET as per Figure 89.

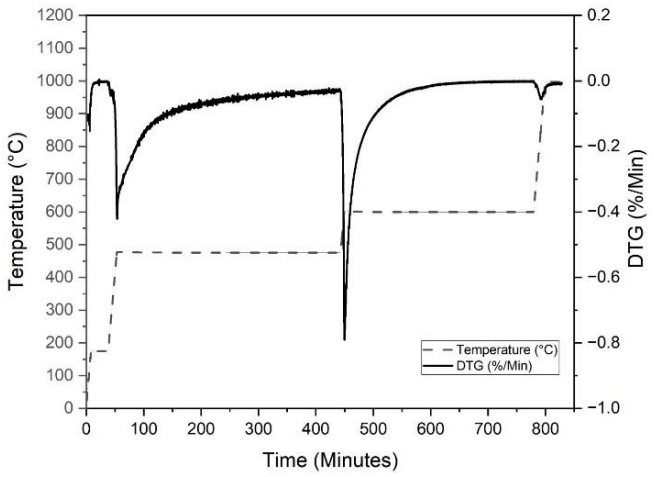

Figure 89 Modified CET profile with 20ºC/min ramp rate and total test time of ~800 mins. DTG for sample 1 is shown.

Each of the constituents including LOC, HOC, soot, ash and moisture were calculated in the same way as the original technique, adjusting the minimum points to the beginning and end of the new isotherms. Tests were completed on all 18 samples and Figure 89 shows an example DTG produced for Sample 1, which was typical of

all the tests. Despite decreasing the overall time to complete the test, the degree of overlap remains minimised, and the peaks are relative to the original technique.

Figure 90 shows the values for LOC produced by the faster technique, which correlates very well with the original and the coefficient of determination shows that the data fits the regression well. The other constituent comparisons appear to correlate to a lesser extent, with moisture correlating lowest of all according to Appendix 10, the error data also shows a close relationship between the actual values from the CET and the modified CET. The rapid heating and short isotherm time here appear to be too short for moisture determination and would require an extended hold at 175^{o}C to ensure complete moisture removal for improved accuracy. The soot portion appears to be a weak correlation, however, the value for soot was <1% in all cases, which was likely to be influenced by the resolution of the equipment. According to Figure 90, the results for each sample appear to correlate well with the original CET. This technique could be used in the context of comparing daily LOC quantities with a relatively high degree of confidence and this test can be completed in just 16 hours, hence accomplishing the requirement of testing one sample per day.

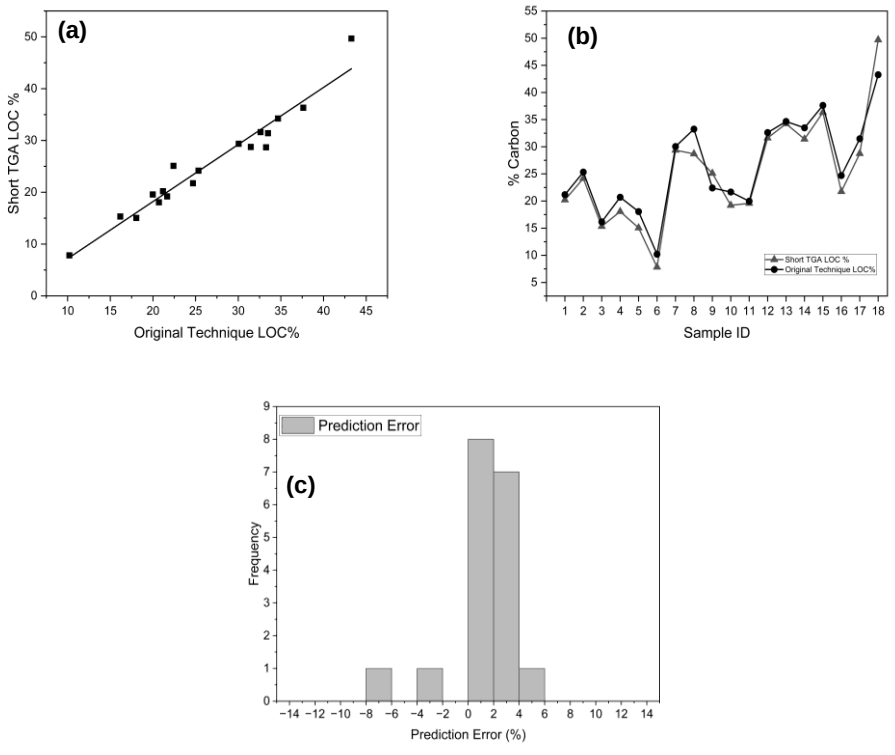

Figure 90 a) Correlation of LOC for modified TGA and original CET (b) %LOC for both techniques per sample c) histogram of error for modified TGA and original CET

XRD Parameters

The XRD spectra for sample 1 can be seen in Figure 91. One of the limitations when analysing the BF dust was that an amorphous region of carbon exists between 25º and 33º[82]. This can often hide peaks such as graphite and Fe_2O_3. This broad region, as per Figure 91, can be used to identify some key parameters and characteristics of the carbon itself, by deconvoluting two gaussian peaks around 28º and 31º named alpha (α) and beta (β) respectively.

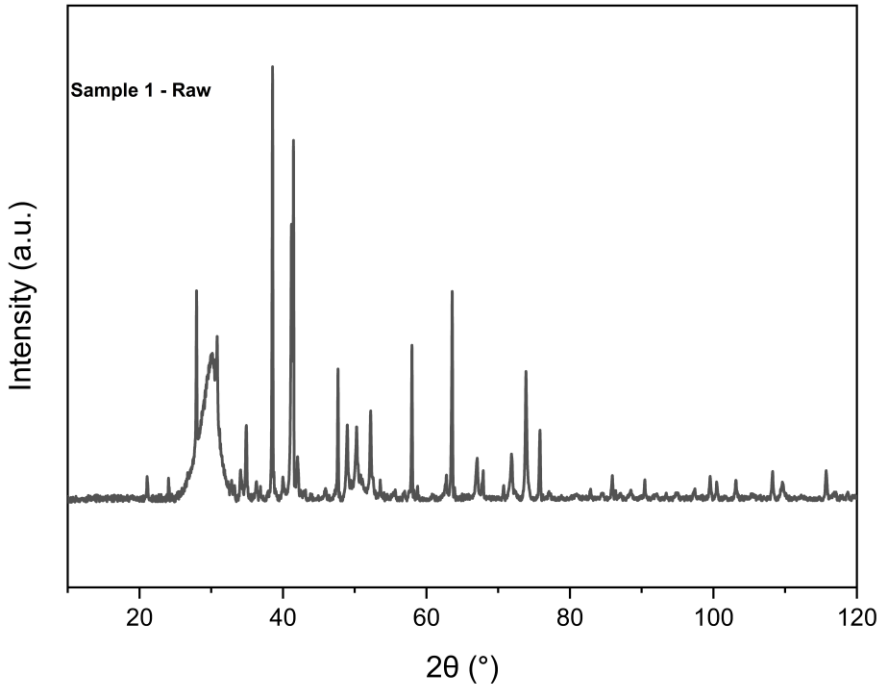

Figure 91 X-ray diffraction pattern for sample 1 BF dust

Asymmetry within the amorphous region has been discussed to deem that two peaks are present within the peak in section 3.4.4[131]. Higher values for Lc are hypothesised to contain less LOC due to the increased crystallinity discussed previously[82]. It was expected that lower values for lateral size (La) will give higher values for LOC, because of higher aromaticity. Rank was less likely to correlate because it is more suitable for coal products as opposed to complex dust samples[132]. Although it was hypothesised that higher values for rank are more crystalline hence lower LOC was expected in higher-rank dust samples. With increased interlayer stacking, a more perfect stacking structure was expected, therefore lower values for

LOC are expected. With increasing aromaticity, there was hypothesised an increase in LOC[82,117,131,133].

The XRD results were correlated against the original CET, shown in

Appendix 12. The correlation between XRD parameters and LOC measured using the CET shows a very weak relationship and one that appears circumstantial, which was observed in the data, although this was hardly surprising because of the highly amorphous nature of the carbon present and the difficulty of XRD to quantify amorphous phases. An improvement was seen for the interlayer spacing and LOC also witnessed in the data, although the relationship doesn't appear to be linear hence the low value for R^2, as per

Appendix 12. Despite the improved inference of correlation, the sensitivity of the interlayer spacing was high, with the entire span being just 0.05Å, and was therefore unable to track well with the CET LOC measurements, as per Figure 92. While XRD would be a fast technique, with samples being analysed in 25 minutes, the data shows too little correlation to be comparable.

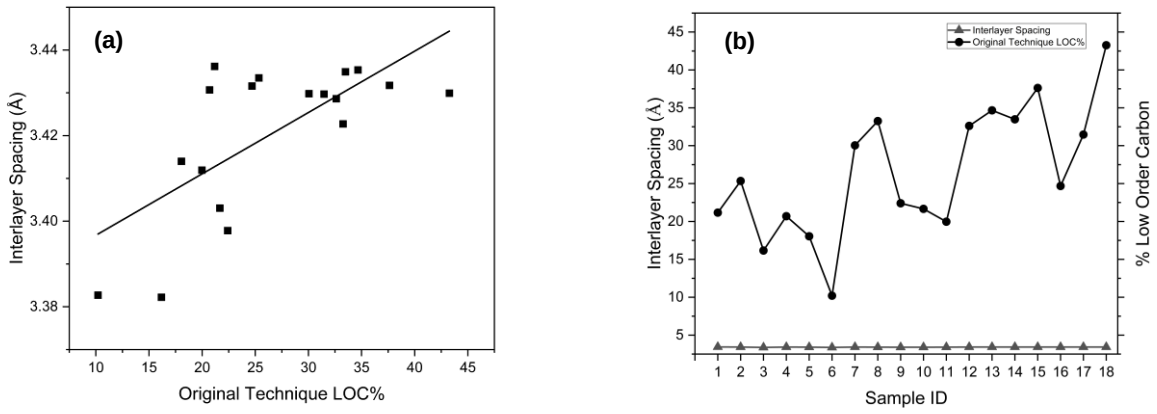

Figure 92 a) Correlation of LOC for XRD interlayer spacing and original CET b) %LOC for both techniques (XRD and CET) per sample

The relationships were randomly scattered, with the other carbon parameters and the LOC as seen in Appendix 11, this shows that only the interlayer spacing was potentially related supporting the findings in Appendix 12. This confirms that the XRD could not be used as a replacement for the CET.

Digestion and Combustion Technique Winkler

The following calculations in equation 4.1 were used to calculate the charcoal and organic constituents of the dust following the digestion and combustion steps, as per the Winkler Method outlined in section 3.4.3 of this thesis.

$$\% \text{ Charcoal} = \frac{(\text{NW} - \text{IW}) \times 100}{\text{DW}}$$
$$\% \text{ Organic Matter} = \frac{(\text{DW} - \text{NW}) \times 100}{\text{DW}} \quad \textbf{(4.1)}$$

Where

NW = weight after digestion

IW = weight after ignition

DW = weight after drying

The linear fit from the %Charcoal versus CET LOC was used to generate values for predicting the LOC using the 'Winkler Method', from initial inspection there appeared to be a moderate correlation. A correlation coefficient of 0.7946 was observed with an R^2 of 0.6313 as per Figure 93. The values appear to resemble the original CET well which shows that the difference in LOC between samples was more important than the absolute values when comparing samples.

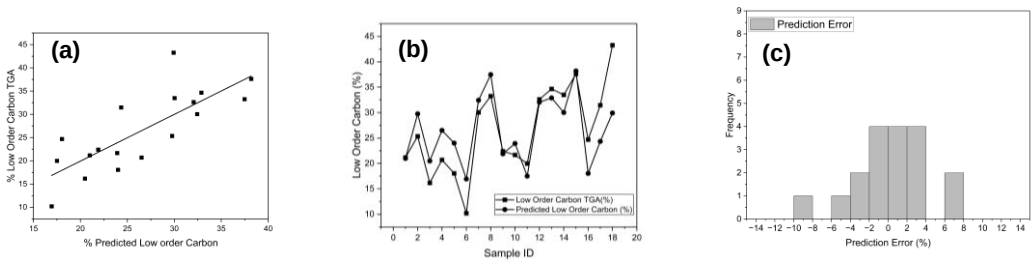

Figure 93 a) Correlation of predicted LOC obtained through Winkler Method and Original CET b) %LOC for both techniques (Winkler and CET) per sample c) Prediction Error Histogram

The values of total carbon obtained from the Eltra C/S500 have been used to normalise the carbon value into a %charcoal per carbon value. Figure 93 shows both the coefficient of correlation and determination have improved, with a tighter fit of the data evident at 0.88282 and 0.76558 respectively. This technique removes the effect of changing ash values which can influence the predicted LOC.

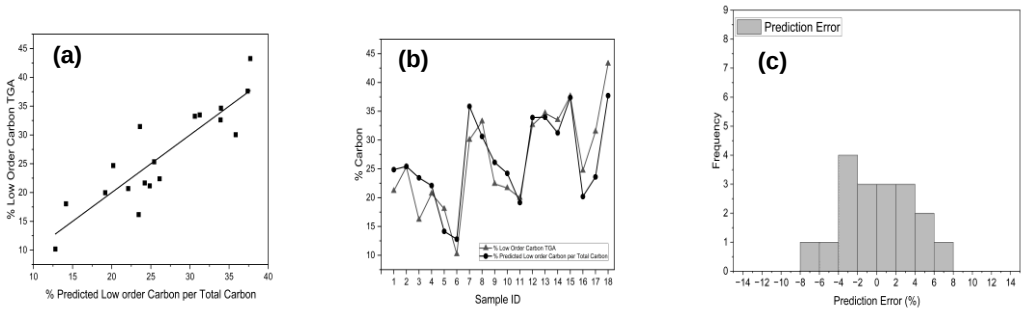

Figure 94 a) Correlation of predicted LOC/total C, obtained through Winkler method and Original CET b) %LOC for both techniques (Winkler and CET) per sample c) prediction error histogram (predicted carbon has been normalised per total carbon)

Except for sample 3, the results appear to trend with each other across the 18 samples. It appears from this data alone, that using this technique could be a suitable tool for monitoring the changes in LOC within the BF dust. This test appears to be time-consuming, with a digestion step that takes 3 hours and a combustion step that takes 12 hours. This analysis, however, can be run in batches, limited by the size of the digestion block and the furnace size. In this case, 24 samples can be analysed in the same time frame as 1 sample per the original CET.

Figure 95 highlights how the ash was broken down into respective constituents following the application of the Winkler Method. The total ash from the CET would be different because the digestion stage was not in place before the combustion.

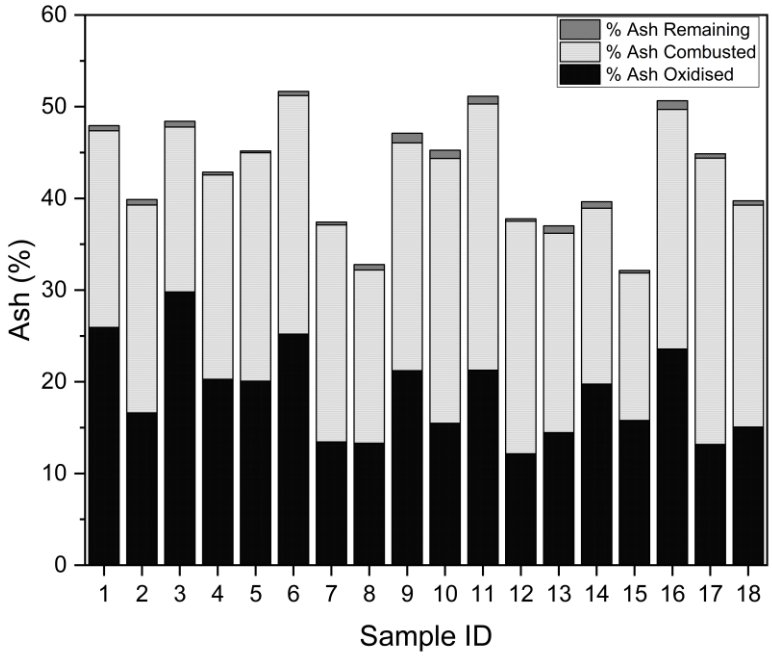

Figure 95 Breakdown of ash constituents per the derivation of ash

Further investigation into each of the stages, applying the new technique, was carried out to ensure the hypothesis was correct. To confirm if the nitric acid stage was indeed removing the organic material, the samples were investigated using XRD. Samples were analysed before and after digestion. XRD was also completed on the ash after ignition to understand what changes can be observed at each stage. As can be seen in Figure 96, the acid has a significant effect on haematite, magnetite, silica, metallic iron, calcite and dolomite. The acid was not effective enough to strip it completely of the organic materials and some materials remain. After combustion, these spectra show that the organic matter has become more concentrated in the ash, therefore much of what remained initially has not been impacted by the ignition cycle. This shows that it was likely the carbon was selectively combusted.

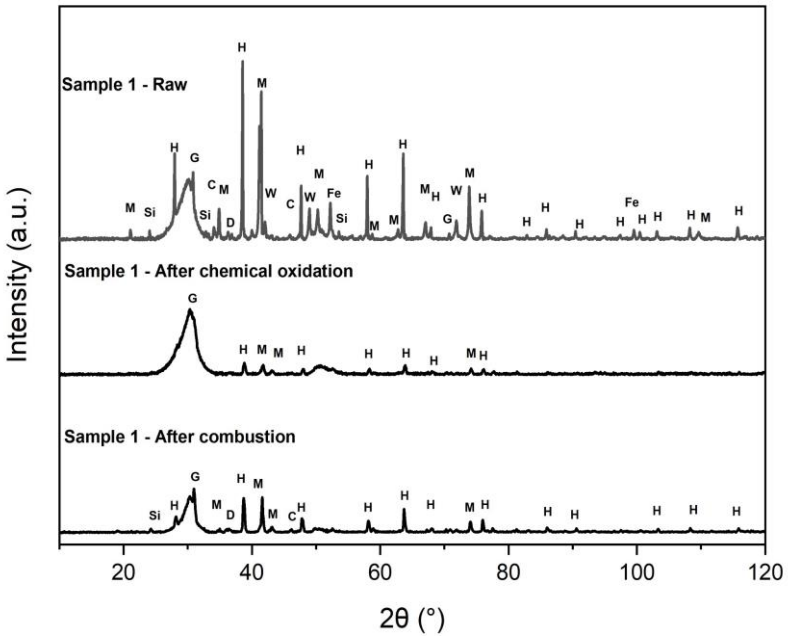

Figure 96 Powder XRD patterns for sample 1 – raw, sample 1 – after chemical oxidation and sample 1 – after combustion. H = Hematite (Fe2O3 – COD# 9000139), M = Magnetite (Fe3O4 - COD# 1011084), W = Wustite (FeO – COD# 9008636), C = Calcite (CCaO3 – COD# 9016200), Si = Quartz High (O_2Si – COD# 1011200), G = Graphite (C – COD#9011577), D = Dolomite ($CaMg(CO_3)2$ – COD# 9000885), Fe = Iron (Fe – COD# 4113941)

The SEM/EDS images in Figure 97 also show the changes in chemistry and morphology between each stages as did the XRD data. EDS analysis highlights that following digestion, when the samples are oxidised, the concentration of Fe was reduced and the carbon appears to be more concentrated. Carbon remains present in the post-combustion sample also but was slightly less concentrated due to the combustion of LOC at 475^{o}C. The remaining ash constituents include HOC, observed as grey flakes in the SEM image, SiO_2, Al_2O_3 and MgO, which are all more concentrated in the ash, supporting the theory that the carbon was selectively combusted.

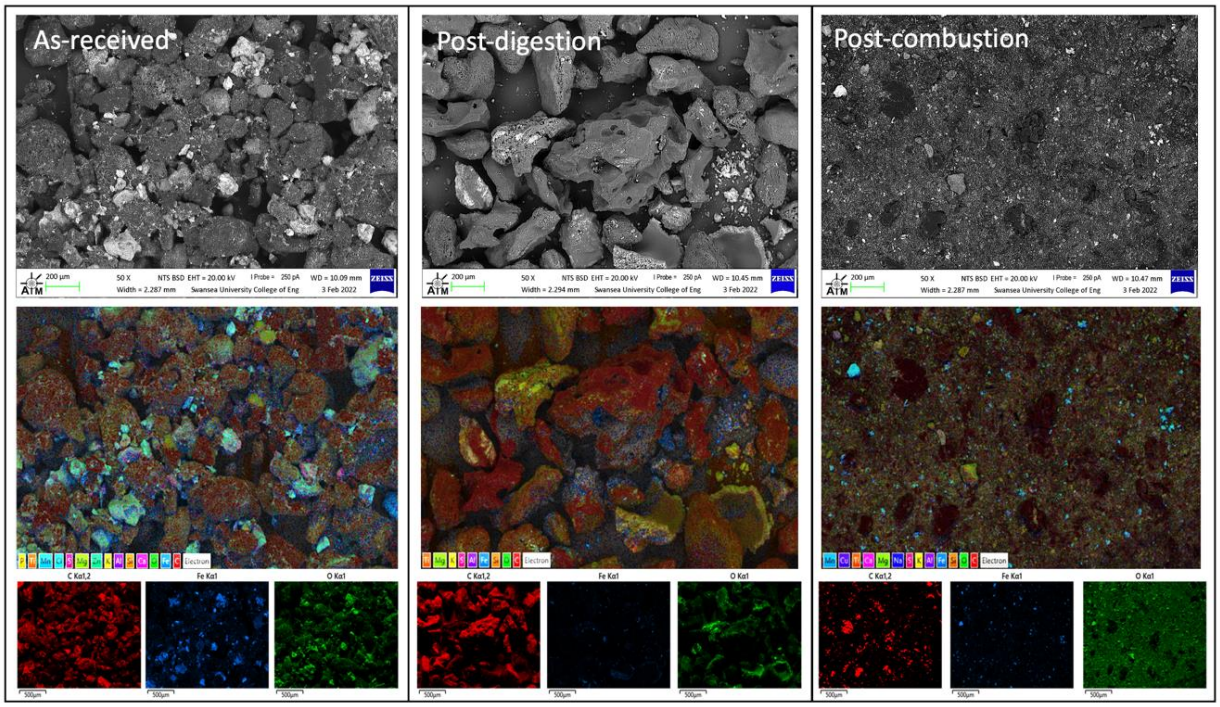

Figure 97 SEM/EDS analysis of sample 1 in the as-received (pre-tested) condition, the post-digested condition and the post-combusted condition. SEM micrograph, full EDS map and C, Fe and O spectra highlighted.

Improving the Method

By trialling various acid solutions on samples 1-3, the ICP-OES analysis in Figure 98 suggests that Acid 4 was the most effective at removing Fe. However, Acids 1 and 6 had the best overall effect when removing all of the metals, particularly Acid 6, with the addition of peroxide. Low-level elements such as Zn, Cr, Ni and Na were stripped relatively easily to below the levels of detection for the instrument in all cases, however, the nitric acid alone appeared to be gentle in removing elements, particularly Cr and Ba which were not digested at all. Potassium appeared to not reduce well with the acids in question, but this appeared to be a similar case for nitric acid.

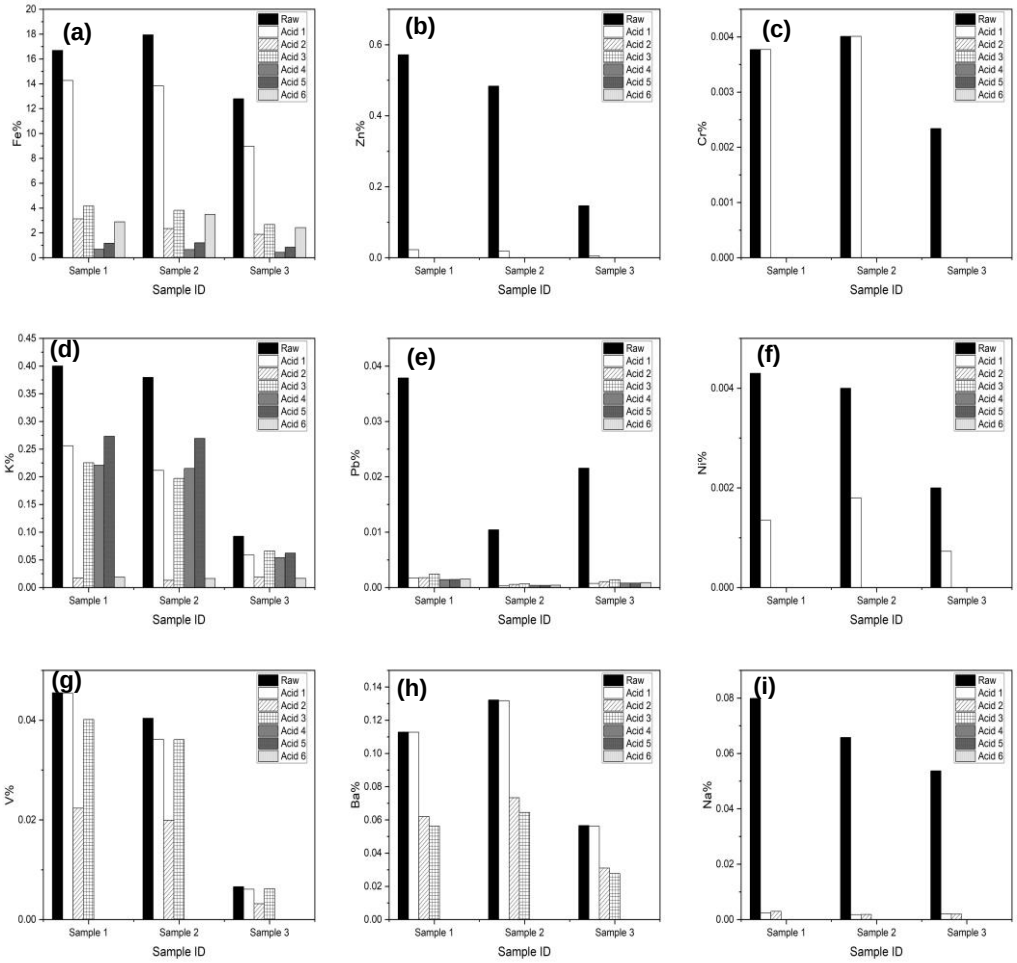

Figure 98 ICP-OES analysis of raw BF dusts compared to dust samples digested in various mineral acids outlined in Table 24 a) Fe b) Zn c) Cr d) K e) Pb f) Ni g) V h) Ba i) Na

One of the key considerations when digesting materials for selective carbon combustion was the effect of the acid on the carbon. It was important to minimise the number of residual elements before combustion, to avoid any contamination during the ignition stage, but it was equally important not to physically alter the carbon, which *was* possible when different acids in varying degrees of strength are used for digestion. Figure 99 has been developed to show the changes in XRD parameters with the various acids. When examining the aromaticity and rank parameters, all of the acids have altered the aromaticity from the raw sample. But it appears Acid 6 has had the least effect over the 3 samples. In terms of La and Lc, Acid 2 has the least effect on carbon. The interlayer spacing was relatively consistent with all acids. Overall either Acids 2 and 6 perform better in terms of digestion as these have the lowest aggregated effect on the carbon during the reaction. It was clear though that the effect on the XRD

parameters was within a minuscule scale. Therefore, the impact of all of the acids was minimal.

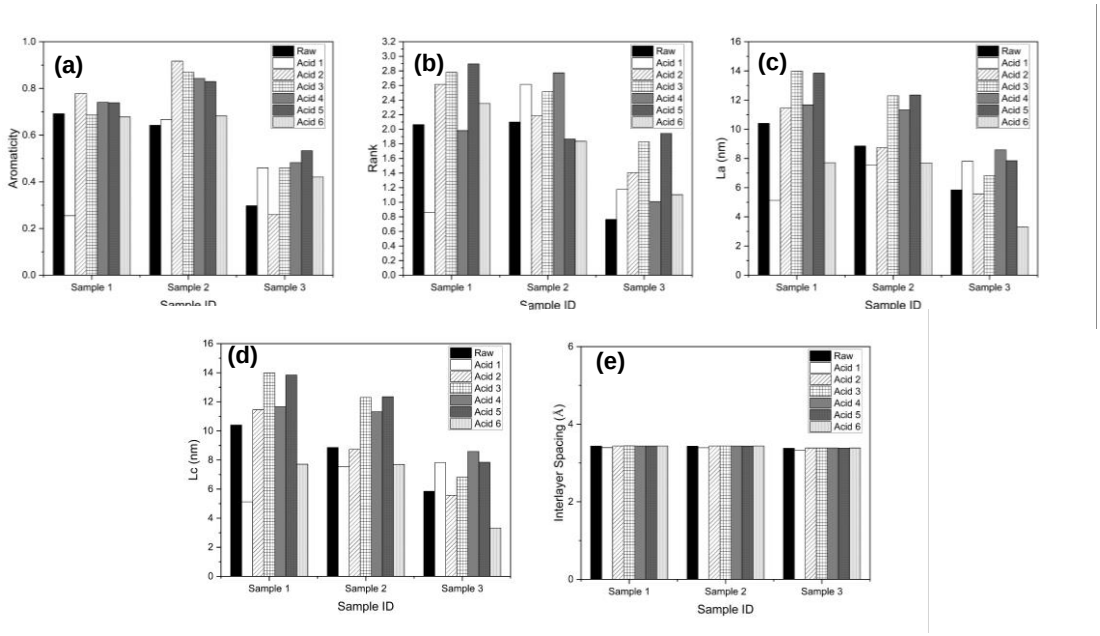

Figure 99 Graphs to show evolving XRD parameters with varying digestion acids as per Table 24 a) aromaticity b) rank c) La d) Lc e) interlayer spacing

The XRD spectra in Figure 100 show that all acids have reduced the residual elements, but Acids 1 and 5 appear to be most effective because the peaks diminish after the large amorphous carbon peak referenced in the section 3.4.4. It also shows the change in the amorphous carbon peak that the parameters are referring to. It can be seen that dust digested in Acid 1 retains a similar peak shape, only losing the haematite and graphite spikes, whereas the other acids have either elongated or altered the overall shape of the carbon peak. The observations thus far, suggest Acid 2 and Acid 6 appear to be the best performing overall, for both element reduction and the lowest effect on the carbon itself. Acid 4 performed best in terms of the removal of residual elements but had more of an effect on the carbon peak.

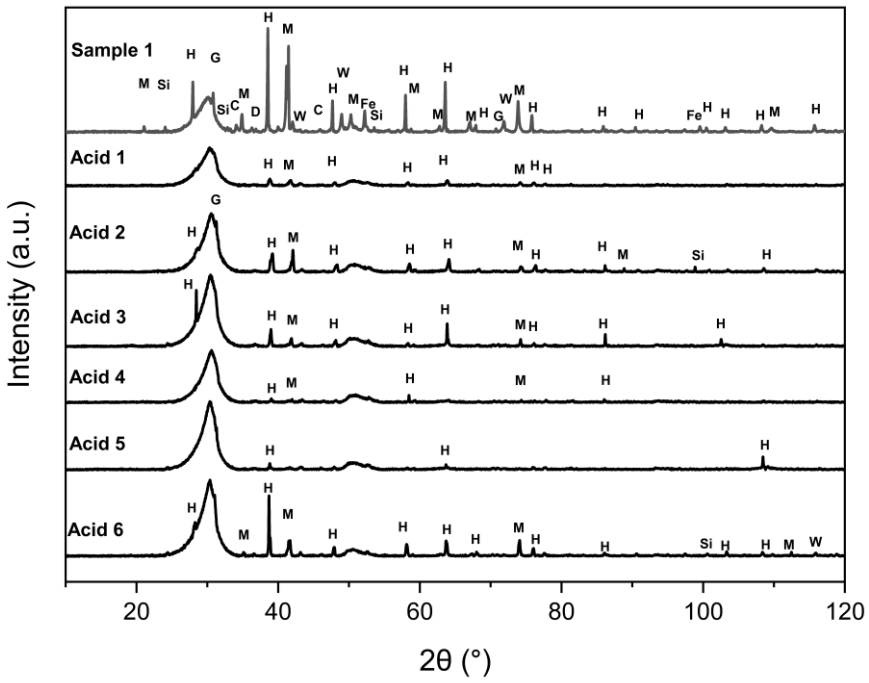

Figure 100 XRD spectra showing sample 1 after chemical digestion with acids outlined in Table 24

Each of the digested samples from the experiment was subsequently subjected to the same combustion stage as the 'Winkler Method'; 12 hours of combustion at 475^{o}C to assess the techniques' correlation with the original CET method. The values for low-ordered carbon from the technique were calculated using the linear fit for each of the acid trials against the LOC value from the original CET, the correlation can be seen in Appendix 13. At this stage, the sample digested in nitric acid (Acid 1) appears to be most effective despite having inferior metal digestion properties and carbon influence. Acid 2 also performed well with a good correlation to the CET, but Acid 6 performed relatively poorly with the peroxide addition, according to the XRD spectra in Figure 100, which was likely due to the digestion of some of the aromatic carbon, leaving the remaining carbon more crystallised and more graphitic in structure.

It was clear from Figure 101 that acid 1 still tracks the original TGA CET well. This was supported by the error data. Both acid 1 and acid 2 could be used within a reasonable degree of confidence however as can be seen in Figure 101, acid 2 tracks the CET well with a reasonable degree of correlation.

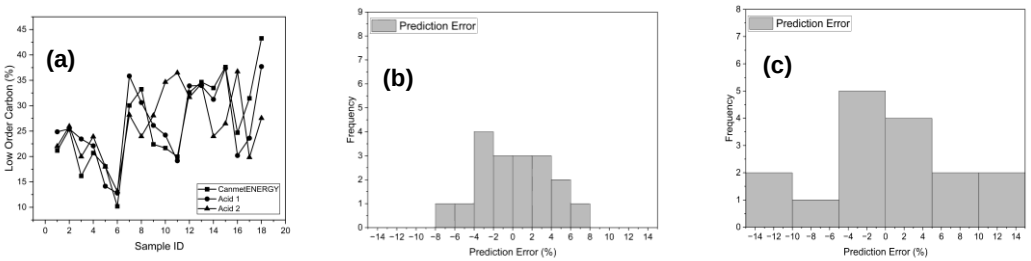

Figure 101 a) Line graph showing the results for each sample from the CET versus acid 1 versus acid 2 b) prediction error histogram acid 1 c) prediction error histogram acid 2

Eltra Carbon

Carbon analysis was initially completed to check that the values for total carbon derived by the original CET were correct. However, the instrument was also capable of measuring sulphur in the dust. Although sulphur was not necessarily an area of interest for this research, if a good correlation was proven, this analysis would be complete in less than 5 minutes per sample and would therefore be a good alternative measure for the changing LOC. This was not the case and the sulphur was found not to be relative to the carbon based material.

According to Figure 102, the results for the carbon from the Eltra versus the LOC carbon from the original technique show a moderate correlation at 0.78633. However, the coefficient of determination was low at 0.59445. It cannot be determined with sufficient confidence using the carbon value from this instrument could replace the CET, even though the results from each sample appear to track each other in the second graph, the changes are not relative. The error data can be seen in Appendix 14.

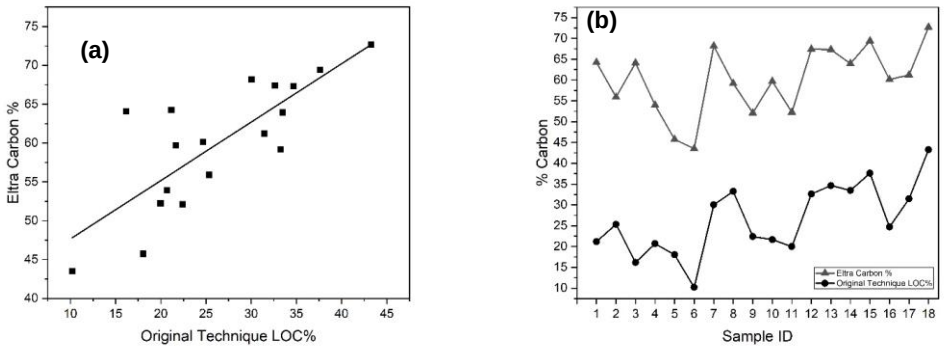

Figure 102 Graphs of Eltra carbon versus LOC using the CET a) Scatter Graph b) Line Graph

Particle Size Distribution

The particle size distribution of the material can help characterise the material itself but as work by Trinkel shows, there appears to be a correlation with dust samples bearing higher iron contents appearing smaller in the particle size range and carbon-bearing materials more abundant in larger size fractions[144]. LOC or carbon in the form of char was also smaller in size because as the coal particle was combusted, the volatile matter leaves the particle[61]. Iron and carbon are the main constituents of BF dust, hence the work with particle size was trying to prove a correlation between LOC and the particle size parameters D10, which was a measure of fines in the material, D50 and D90, which refer to the bulk of the distribution curve and was a crude measure of average size, also D99 which was more sensitive to the oversize particles[145].

The histogram in Figure 103, of distribution between the samples, remains consistent for the first 3 samples with relatively small changes considering the large changes in LOC witnessed from the CET between these samples. It explains somewhat why the values for correlation and r-squared are very low for all the constituents. In order, D90 which was the maximum relative size of 90% of the particles from smallest to largest was sample 3, 2 and 1 respectively. It could be anticipated that the LOC would follow the same trend if a larger particle size referred to less LOC. However, it can be seen that this was not the case as per Appendix 15 and Appendix 16. This was primarily because of the complexity of the dust in question. The presence of fluxes and ashes, whose particles would be of a similar size to the carbon present would cloud the presence of LOC due to the relative concentration. Hence there is no correlation between particle size distribution and LOC as graphed in Appendix 15.

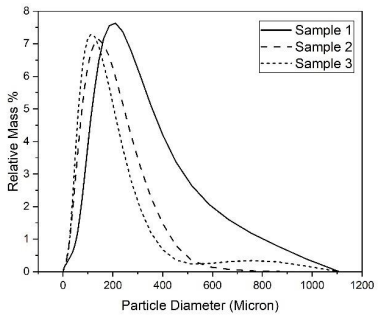

Figure 103 Histograms of the particle size distribution for samples 1, 2 and 3

Bulk Density

The bulk density of a material is relative to particle size, shape and density. In terms of loose bulk density, it was a measure of stacking density and was a good indicator of the constituents of the material[146]. If the dust contains more iron-bearing particles, the bulk density would increase, as the same volume of iron would be higher in mass than the same volume of carbon. The trend in Figure 104 shows a negative correlation which describes the inverse relationship as expected, increasing LOC leads to decreasing bulk density, however, the coefficient of correlation was relatively weak at -0.69778, with a low coefficient of determination at 0.45483 as shown in Appendix 17. The impact of this can be seen in the normalised values in Figure 104, where each sample appears to track the CET results but not with enough relativity to each other to warrant replacing the original technique with a measure of bulk density. Although it would be an improvement in testing time as the bulk density measure could take less than 5 minutes.

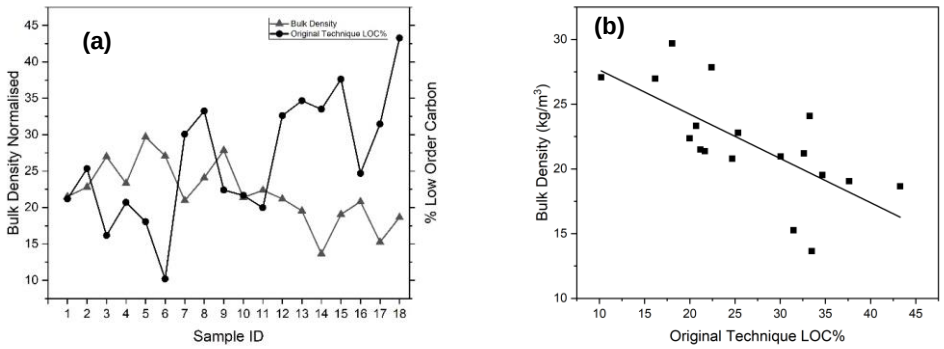

Figure 104 Graphs of bulk density versus LOC using the CET a) line graph b) scatter graph

BET

Pohlmann *et al.* used BET to analyse the surface area of pores within chars as explained in section 2.9, to follow on from this work BET was used to analyse the surface area of dust. The more porous nature of chars will increase the overall surface area of the dust. Hence the dust samples containing more char should also increase in surface area. Due to the nature of devolatilisation and combustion of coal, pore development increases. Particularly with partially burnt chars, the surface area was increased due to the increased number of pores developed. Studies by Chen *et al.* have shown that materials with increased volatile matter produce chars with higher surface area[147]. Char will have a higher surface area than coke and coal as per the work of

Yang *et al.* and it was therefore hypothesised that dust samples containing more char or LOC will have a higher surface area than those containing more HOC[148]. As can be seen in Figure 105 and Appendix 18, there was a correlation and a definite relationship between the two tests, however, the relationship was weak. It was certainly implied that with increasing LOC there was an increase in N_2 adsorption and therefore more pore structures in the dust. But there must be other material influence in the surface area, possibly from the limestone and iron ore. The complex structure of carbon types, in particular char, are subjective due to fragmentation as outlined in the literature review section 2.8.3, meaning that this technique should be applied with caution. The time improvement benefit was not reached with BET also, as for degassing there was a 12-hour stage and for testing was a 6-hour stage. With only 3 samples available per instrument at each time, even if this technique had a stronger correlation than the combustion and digestion technique, this technique would be less preferable.

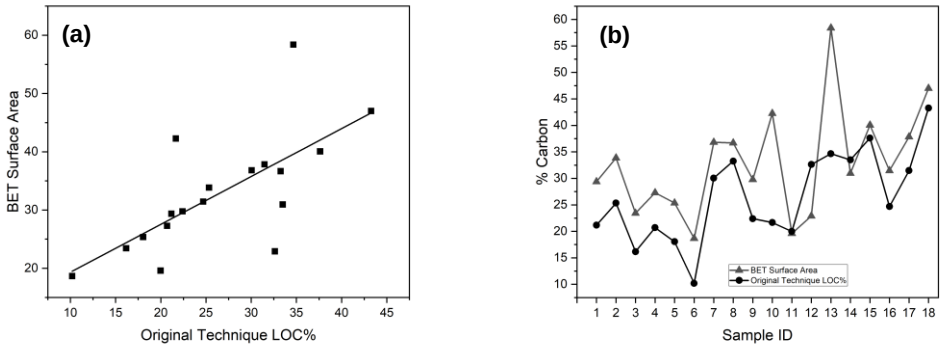

Figure 105 Graphs of BET surface area versus LOC using the CET a) line graph b) scatter graph

ImageJ

The use of ImageJ for counting particles was selected as a technique as it offers a practicable approach and fast turnaround time of analysis and ability to run samples in bulk. Once the samples were mounted and imaged, the analysis took less than 10 minutes per sample, a vast improvement on the CET. As can be seen in Figure 106 and Appendix 19, the amount of carbon counted using ImageJ was negatively correlated to the LOC using the CET. The difference between the data tracking in the line graph was significant and therefore the data was not reliable. Some of the limitations of this technique could help explain the differences in the data. Only the top surface of the image was analysed from a single image. This limits the sample size to an area not

representative of the whole sublot. Due to the nature of grinding and polishing, new pores in the material may have been opened, leading to the increased appearance of char particles. To improve this technique, multiple sites should be analysed and using machine learning techniques, a better threshold of the pore structure in char can be obtained for a more accurate count. Also, a more capable software package such as Zeiss Zen Intellisis could be used, which as per Figure 107, can be used to threshold the image based on colour matching. Machine learning was required on multiple samples but it was recommended in future work to pursue this and improve the algorithm to test the hypothesis.

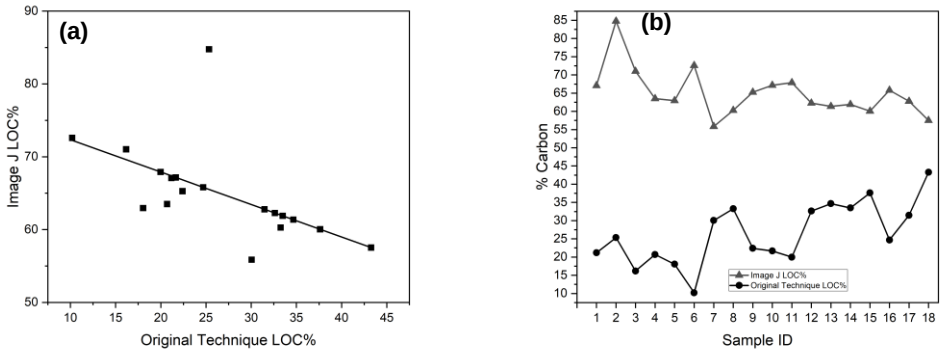

Figure 106 Graphs of ImageJ particle identification versus LOC using the CET a) line graph b) scatter graph

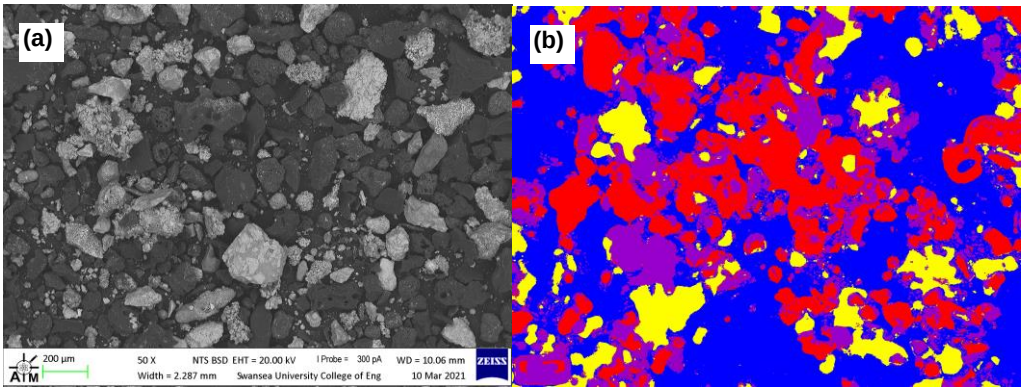

Figure 107 Image of a BF dust processed by Intellisis softwarea) raw SEM image b) segmented using Intellissis. Yellow is coal char, purple is coke, red is ash constituents, and blue is carbon background

Kinetics

The plot of α versus T and dα/dt versus T can be seen in Figure 108. The difference in conversion and reaction rate with air was clear between the different heating rates. Work by Al-Qayim *et al.*, Dadyburjor *et al.* and Ling Du *et al.* shows that char was more reactive than coal, and coal was more reactive than coke in terms of activation energy[149–151]. It can be hypothesised using this information that dust samples with lower activation energy (Ea), were higher in LOC. This was analysed by comparing the Ea of the dust with the LOC from the CET.

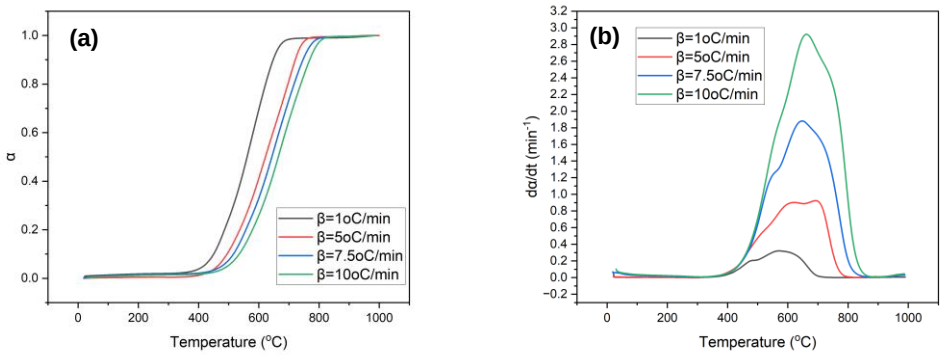

Figure 108 Plots of a) α and b) dα/dt against T (°C) for different heating rates for sample 1 BF dust

Friedman plots of ln(dα/dt) against 1000/T at iso-conversions of α = 0.1-0.9 and calculated activation energy at each α based on the iso-conversional line slopes can be seen in Figure 109. The range of Ea was quite small at each degree of α, in particular where α = 0.9. There appears to be a step up in activation energy between α = 0.2 and α = 0.3, indicating a shift in the reaction mechanism. This indicates the presence of two carbon sources present in the dust.

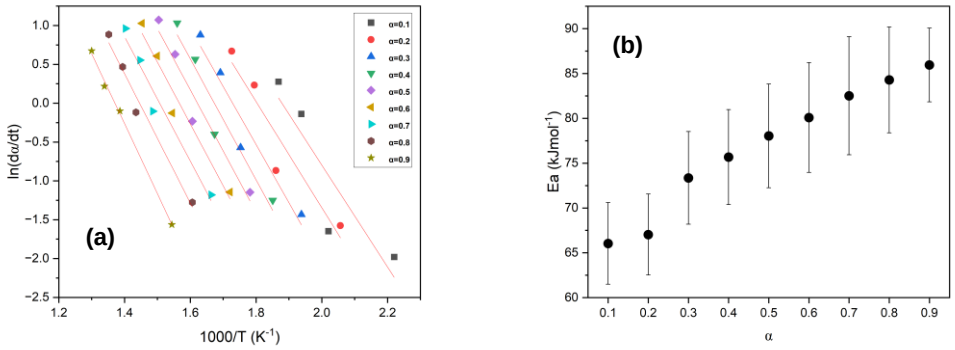

Figure 109 a) Friedman plots b) calculated activation energy (Ea) against α for all samples of BF dust

The results for average Ea versus LOC in the dust are shown in Figure 110, the apparent relationship fails to support the hypothesis that increased char in the dust leads to the increased activation energy. However there appears to be a relationship, according to Appendix 20, the correlation of 0.72 with a low R^2 of 0.52 means that this technique cannot be used to replace the CET. Also, the time to analyse including cooling time would be 30 hours, hence it would not be a good replacement for the CET.

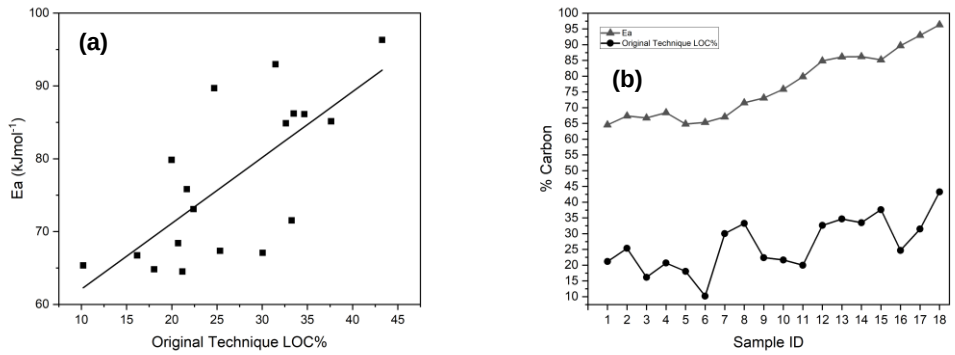

Figure 110 Graphs of calculated Ea versus LOC using the CET a) line graph b) scatter graph

Best Available Technique

As per Table 24, it was clear to see the original technique would not return one sample per day. The Eltra carbon technique was a good technique for comparing the carbon values but does not differentiate between LOC and HOC. The Modified technique was a good representation of the original CET with a high regression coefficient and low errors; however, the time was still excessive to test one sample. The digestion and

combustion techniques proved successful in quantifying the LOC portion of the carbon, the time to complete 1 sample applies when running the samples in batches. There was a good correlation and low root mean squared for both acids 1 and 2 which would be a good choice for a monitoring technique for LOC. When comparing the physical properties of the samples such as XRD parameters, particle size distribution, bulk density, and BET surface area, all the correlations were too weak to consider the techniques as a replacement for the CET, as was the activation energy as determined by Friedman's model free kinetics. Image segmentation and thresholding through ImageJ or other software show potential and it has been recommended to investigate machine learning and unlock the potential of image analysis to replace the CET and the subjectiveness of char counting.

Table 24 Pearson's correlation, coefficient of determination, mean error, mean squared error, max error, root mean squared error and time to test per sample for each of the analysed alternative carbon type differentiation techniques

		Pearson's Correlation	R^2	Mean Error (%)	Mean Squared Error	Max Error (%)	Root Mean Squared Error	Time to Complete 1 sample (hr)
	CanmetENERGY Technique	1	1	0	0	0	0	30
	Modified CET	0.97	0.94	2.14	6.88	6.43	2.62	16
XRD Parameters	**Aromaticity**	<0.10	<0.10	25.98	743.94	42.90	27.28	2
	Rank	0.13	<0.10	24.91	687.95	42.06	26.23	2
	La (nm)	<0.10	<0.10	18.86	440.89	37.99	21.00	2
	Lc (nm)	0.21	<0.10	21.21	516.55	37.77	22.73	2
	Interlayer Spacing	0.69	0.44	23.07	600.38	39.83	24.50	2
	BET	0.69	0.48	7.79	92.65	23.73	9.62	48
	Bulk Density	-0.70	0.49	853.96	757474.4	1169.91	870.33	0.5
	Carbon	0.79	0.61	33.57	1154.96	47.92	33.98	0.5

	Sulphur	0.14	0.02	26.01	745.03	42.84	27.29	0.5
Sizing	**D10**	0.68	0.46	22.77	750.06	53.92	27.39	1
	D50	0.65	0.43	116.16	14931.05	184.88	122.19	1
	D90	0.17	0.03	326.10	131730.7	718.56	362.94	1
	D99	0.45	0.20	553.94	391448.3	989.06	625.66	1
	Image J	-0.58	0.34	38.52	1653.88	62.38	40.67	10
	Kinetics	0.72	0.52	50.51	2604.51	65.01	51.03	30
Digestion and Combustion	**Acid 1**	0.88	0.77	3.17	15.06	8.26	3.88	1
	Acid 2	0.83	0.69	3.50	18.88	9.29	4.35	1
	Acid 3	0.65	0.42	5.03	37.11	12.60	6.09	1
	Acid 4	0.59	0.35	5.12	41.36	14.12	6.43	1
	Acid 5	0.50	0.25	5.84	49.44	15.15	7.03	1
	Acid 6	0.28	0.07	4.57	28.58	10.82	5.35	1

4.2.6 Potential Technologies

Raman Spectroscopy

Raman spectroscopy of particles within blast furnace dust was analysed, to determine the degree of carbon order and relate this to the LOC in the sample. The more ordered the carbon was, the less LOC was hypothesised to be present. 3 samples of dust, low, medium and high in LOC were used for the analysis. By analysing the D/G Ratio and looking at the spectra, it can be determined to what degree the carbon identified was ordered.

The spectra in Figure 111, show the ranging spectra from the different laser powers used on the same spot size. With increased laser power the spectra starts to change, this indicates the point at which the laser power is too great for the particle that the laser is focussed on. The increased height of the D peak in comparison to the G peak infers that the sample was less ordered and therefore more LOC. This was contradictory to the material though as there should be less LOC in the dust. However, this was a limitation of the analysis. Only a single particle was analysed in all cases due to the time limitations of the test. It relies on manually selecting particles and analysing each particle.

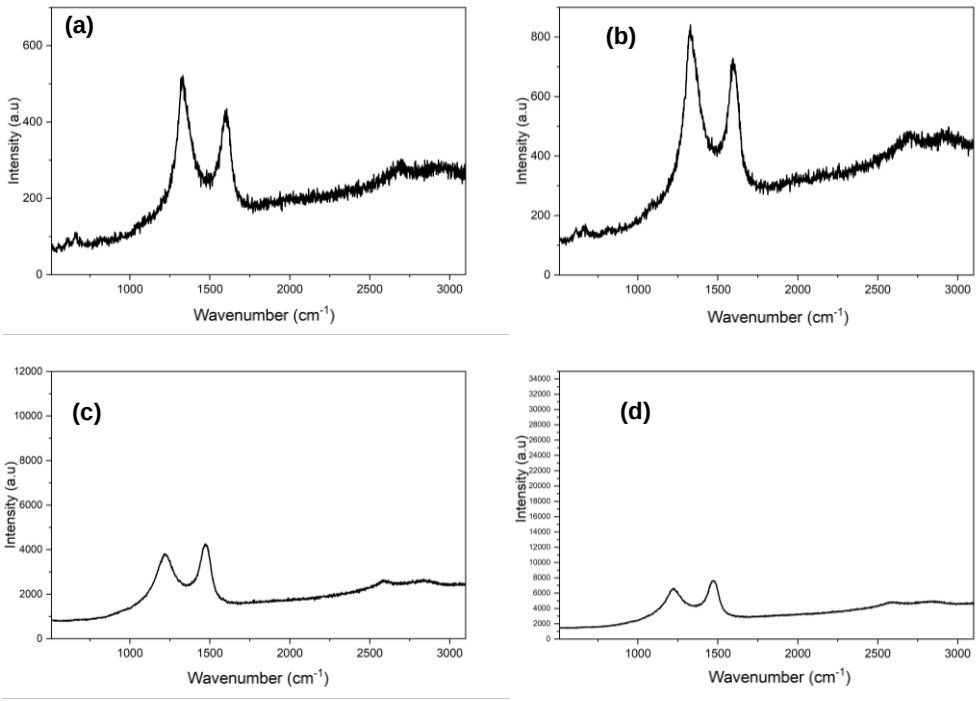

Figure 111 Raman spectra of low dust sample with different power lasers a) 0.5mW b), 1mW c), 5mW d) and 10mW

The spectra from the medium LOC in the dust sample are shown in Figure 112. The carbon layering was much less stacked here as can be seen in the laser power 5 spectra. The lack of a 2d peak indicates that the carbon type or laser power was not appropriate for the particular sample[152]. The D peak shows that the carbon particle identified in this sample was less ordered than graphitised in the G peak.

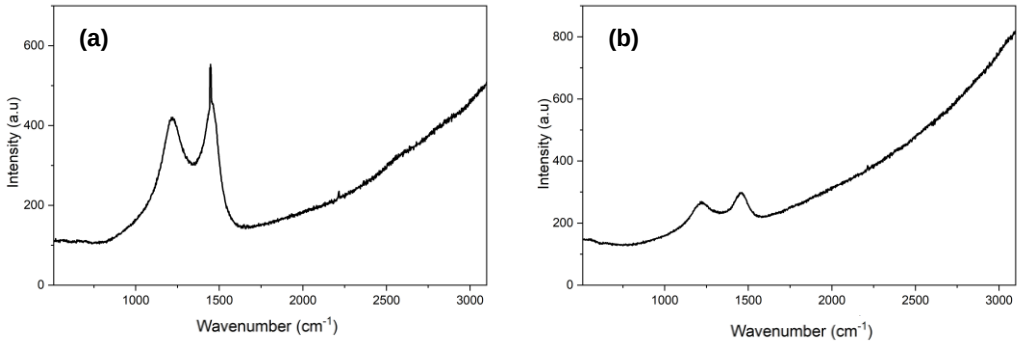

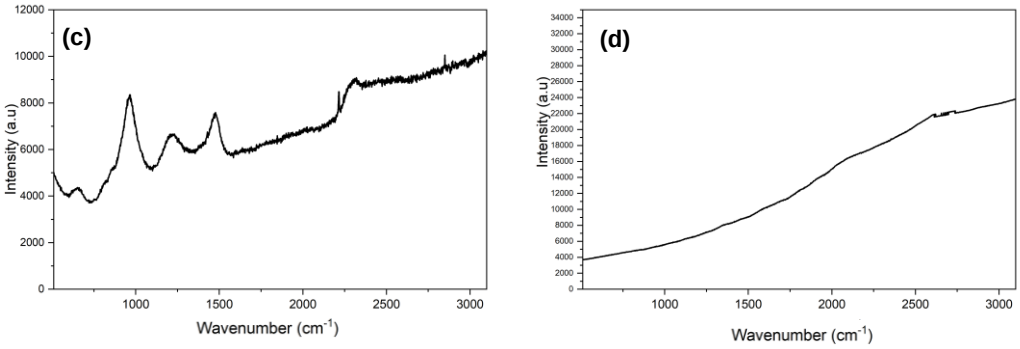

Figure 112 Raman spectra of medium dust sample with different power lasers a) 0.5mW b) 1mW c) 5mW d) 10mW

The spectra for the high LOC sample in Figure 113 show a significant 2d peak, that was not witnessed in Figure 111 or Figure 112. The carbon layers appear much thicker here due to the ability to use 10mW of laser power to obtain the spectra. The D peak was much lower than the G peak hence the material was more ordered here. This sample was particularly high in LOC in comparison to the low LOC sample which was contradictory to the Raman spectra. This was because the spectra are limited to one spot within the sample and this particular spot may have been considerably less ordered than the rest. Therefore, this specific technique gave LOC values that were not representative of the whole material.

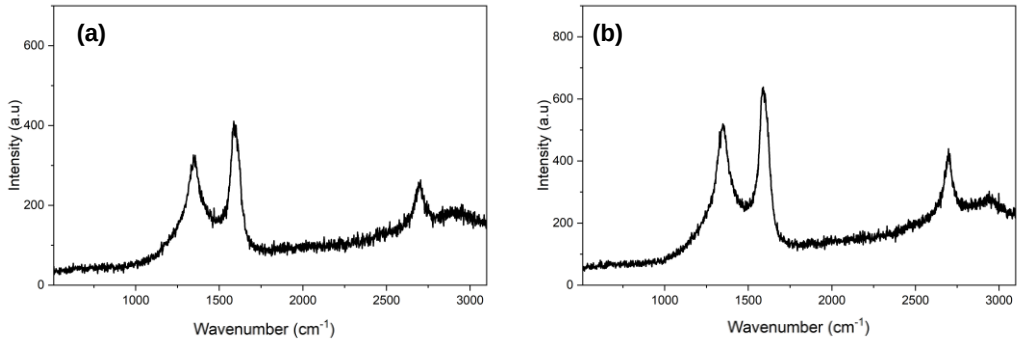

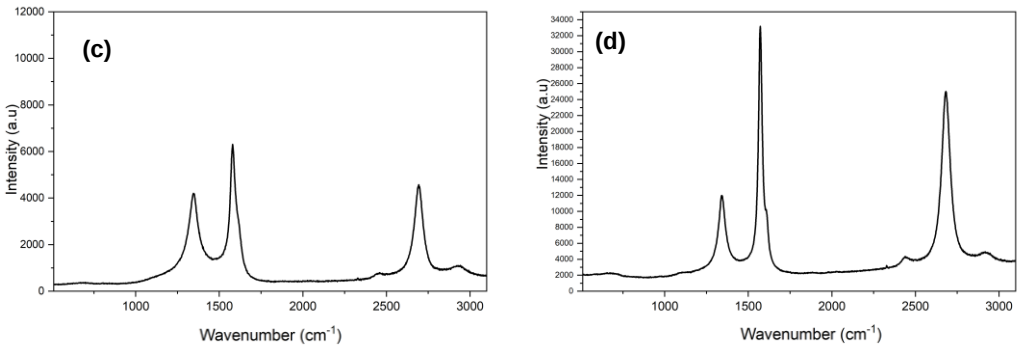

Figure 113 Raman spectra of high dust sample with different power lasers a) 0.5mW b) 1mW c) 5mW d) 10mW

Table 25 shows a comparison between the D/G ratio which indicates the degree of carbon order and LOC as determined by the CET. The lack of variation between the low and medium dust in the D/G ratio and the apparent inverse relationship between the D/G ratio and LOC indicates that this technique was not suitable. Raman spectroscopy was far more capable than this example shows though. There is potential with increased spot sampling and averaging that ratios could start to correlate with LOC. Another technique with potential, is Raman mapping. An automated process where multiple points of a sample are analysed and a map of carbon order is produced[153,154]. This information is potentially far more valuable and should be explored in future work.

Table 25 Comparing D/G ratio with LOC per sample type

	D/G Ratio				LOC
Laser Power	**0.5mW**	**1 mW**	**5 mW**	**10 mW**	%
Low LOC Dust	0.8	0.9	1.3	0	10.19
Medium LOC Dust	0.8	0.8	0.7	0.4	23.40
High LOC Dust	1.2	1.2	0.9	0.9	43.26

XPS

The resultant spectra from the surface chemistry, analysed by XPS are depicted in Figure 114. Each of the peaks was labelled on the top graph of spectra, however, the peaks of interest include the C1S and the O1S peaks which can be attributed to carbon types and bonding within the material. The C1S peak around 300eV can be seen to change depending on the sample. This peak was small in sample 1 in comparison to sample 3. The O1S peak at around 540 eV was however larger in sample 1 versus sample 3. The difference in peak height intensities was related to concentration but the whole spectra should be considered to accurately determine if the changes are relevant in terms of changing carbon type. Other peaks identified within the spectra do change but to a lesser extent. Another area of interest was the Cl2p peak at around 190eV, this was only prominent in samples 3, 5, 8, and 9. This could indicate the presence of iron-bearing constituents within the dust as opposed to the carbon-based LOC that was to be identified using this technique. The XPS technique was fast to analyse at around 30 minutes per sample. However, analysis of the data takes longer and was very sensitive to changing surface chemistry, because the surface of the particles was being analysed, sample storage and transport should be considered. Plastic bags have been known to transfer polydimethylsiloxane to the surface of the particles and impact the spectra generated for the sample[155].

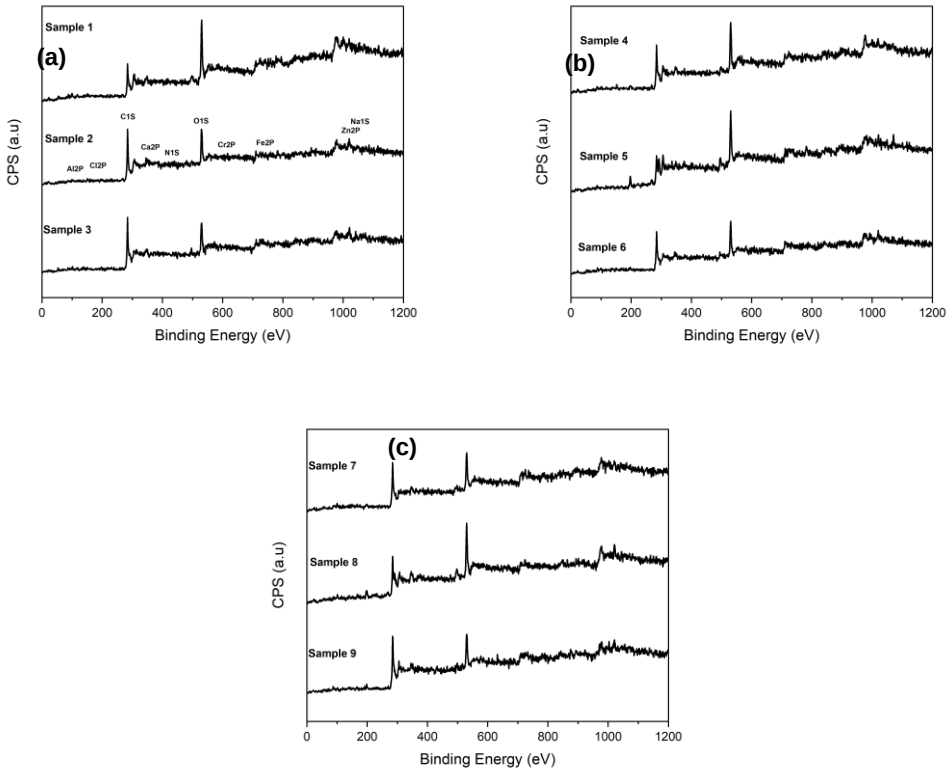

Figure 114 XPS spectra for each sample. a) samples 1-3 with the main peaks labelled b) samples 4-6 c) samples 7-9

The O1S and C1S peaks were deconvoluted as per Figure 115, to identify the concentrations of the bonds that are found within the overall peak. The concentrations of each deconvoluted peak can be used to compare with the analysis of LOC using the CET, to determine if the technique can be replaced. Each of the bonding types can be attributed to varying carbon types. The C-O and C-O-C bonds are indicative of LOC. The C1s carbonate bonds are indicative of fluxes such as $CaCO_3$. The C-C bonding can be attributed to HOC such as coke. The sensitivity of the analysis can be seen in Figure 115. The C1S peak was particularly narrow and contains lots of deconvoluted peaks, any deviation in this peak due to contamination could influence the result significantly.

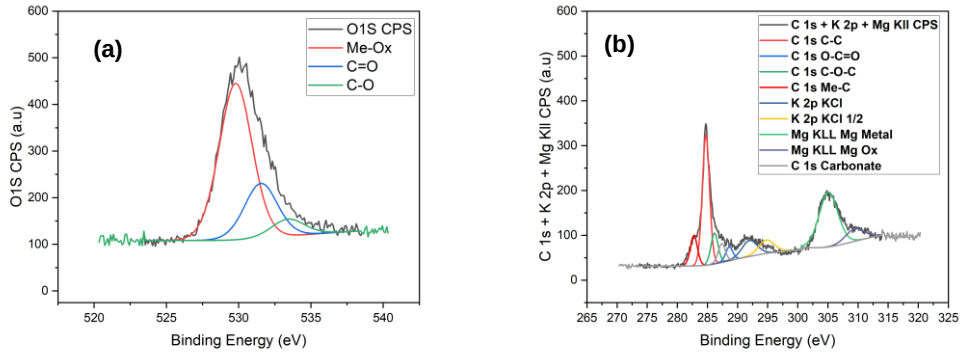

Figure 115 Deconvoluted peaks from the XPS spectra indicating the difference between bonds within the peaks a) O1S peak b) C1S peaks

Table 26 shows the correlation between each deconvoluted peak and the LOC% of each sample determined by the CET. The C1S carbonate has the strongest relationship with LOC, but this was still relatively weak. The inverse relationship with the C=O peak found in the O1S peak supports the hypothesis that more ordered carbon bonds present in the spectra correspond with less LOC in the dust as found by the CET. Despite these findings, all the correlations were too weak to consider the XPS a suitable replacement for the CET. Only 9 samples were analysed in this case, but further analysis of the C1s relationship may be more apparent with increased testing.

Table 26 Pearson's correlation and coefficient of determination for results from XPS peak deconvolution versus CET

	O 1s Me-Ox	O 1s C=O	O 1s C-O	C 1s C-C	C 1s O-C=O	C 1s C-O-C	C 1s Me-C	K 2p KCl	K 2p KCl 1/2	Mg KLL Mg Metal	Mg KLL Mg Ox	C 1s Carbonate
Pearson's correlation	0.40	-0.40	0.20	0.21	0.15	-0.32	-0.34	-0.09	0.02	-0.18	-0.41	0.63
R^2	0.16	0.16	0.04	0.04	0.02	0.10	0.12	0.01	0.00	0.03	0.17	0.39

Petrographic analysis

Green coke and coal were identified and thresholded out of the dust samples using the techniques outlined in section 3.4.11. Petrographic analysis has been used to confirm the source of carbonaceous materials in dust samples previously, as outlined in the literature review works by Di Zhao in section 2.10.3. The histograms and particles of

green coke and coal can be seen in Figure 116 and Figure 117 respectively. The greyscale histograms show a large concentration of green coke in sample 4 as compared to the others. Sample 1 contained more coal particles than the others. The wide range in greyscale value for the green coke in sample 4 was a reference to the different topography seen in the material in each particle. Green coke topography was not consistent when compared to coal, hence the wider greyscale bands.

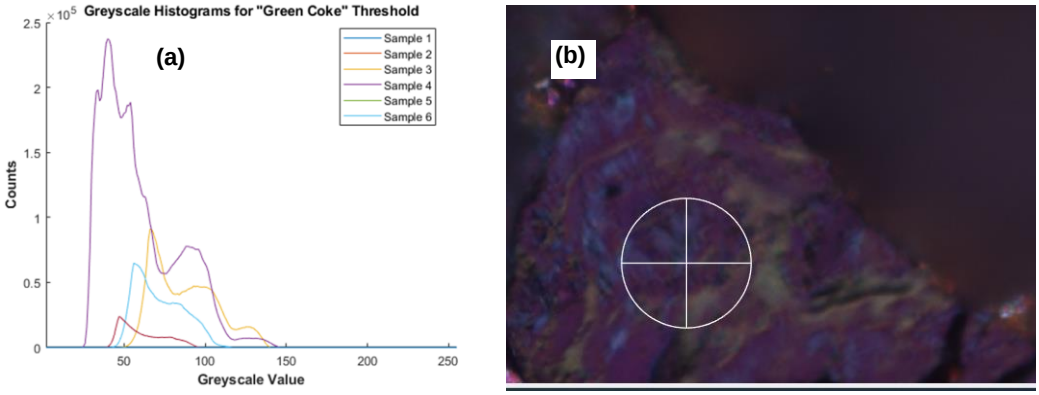

Figure 116 a) Histogram of colour thresholding b) image of green coke using oil objective in BF dust

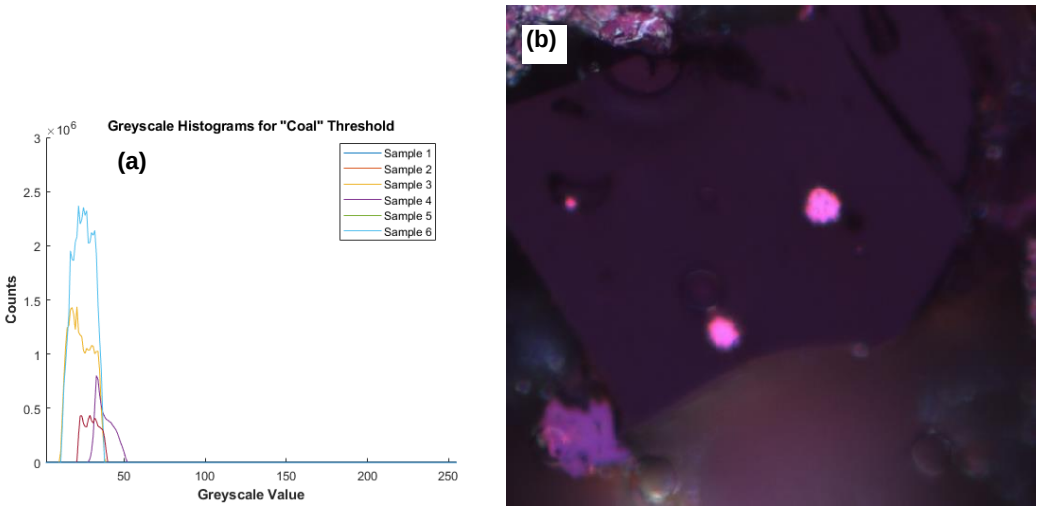

Figure 117 a) Histogram of colour thresholding b) image of coal using oil objective in BF dust

Figure 118 and Table 27 show any potential relationships between LOC and the identified petrographic constituents. The samples don't tend to track well in Figure 118 with each other, the variation in the LOC from the CET was far more significant than the petrography data. In Table 27, the strongest relationship was between LOC and the mineral matter identified in the dust. This was purely coincidental as the data set was only based on 5 samples. It was hypothesised that with increased data size, petrography could be a good replacement for the CET. Historically, petrographic

analysis has been time-consuming and very subjective. New techniques for automating analysis can lead to faster turnaround times and accurate representation of each carbon type[156]. Similar to the use of Intellisis as discussed previously. With machine learning the power of microscopy should be investigated further as the potential for carbon type differentiation is huge, once the subjectiveness and time constraints are removed.

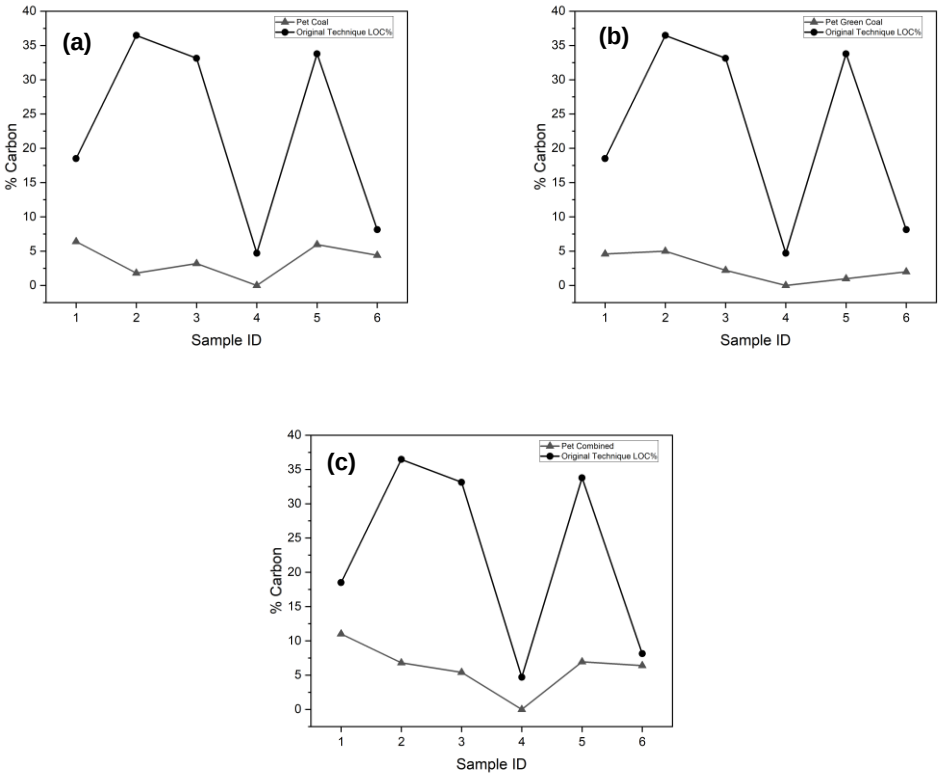

Figure 118 line graphs of petrography parameters versus LOC% from the CET. a) coal particles b) green coke c) petrography parameters combined

Table 27 Pearson's correlation and coefficient of determination for results from petrographic analysis versus CET

	Coke	Green Coke	Coal	Char	Mineral Matter	Resin	Combined
Pearson's Correlation	-0.25	0.42	0.22	0.64	0.84	-0.22	0.39
R^2	0.06	0.18	0.05	0.41	0.71	0.05	0.15

MicroCT

The applications of MicroCT are growing, from medical applications to the research of ancient Egypt. Samples of dust were imaged using the MicroCT and the results can be seen in Figure 119 and Figure 120. Char cenosphere counting has historically been limited to counting on a 2-dimensional plane. The images below are slices from a 3-Dimensional scan of the material. Without the requirement to mount and grind materials, the analysis time can be reduced to 30 minutes per scan. The char particles circled in Figure 120 are easily identified and due to the contrast in brightness between the char and the pores, this allows these materials to be thresholded relatively easily. A thorough scan of a large cross reference of material can be carried out and the resultant slices analysed for char count. This could give a much better representation of the material than 2-dimensional methods that have been a limiting factor. With increased capability now available and improved image analysis, this technique should be further explored. Multiple images containing multiple slices can be used to train the image analysis software and develop an Artificial Intelligence (AI) system capable of counting the particles in a large volume of images. The increased magnification can be used to identify individual particles, however, the resolution available at 10x magnification appears to be enough. If this was increased to 25x magnification, sample identification and pore-to-char colour differentiation would be improved.

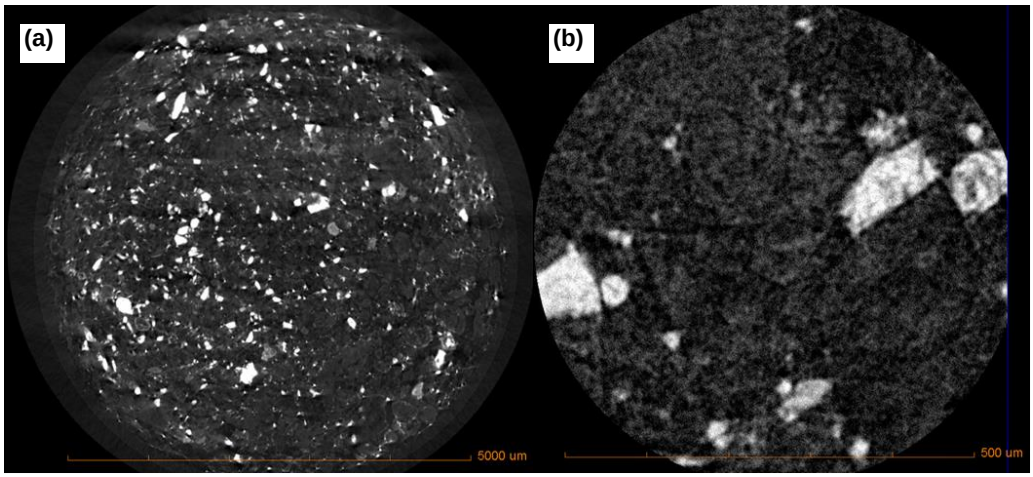

Figure 119 Sample 1 MicroCT scan a) image at 10x magnification b) image at 100x magnification

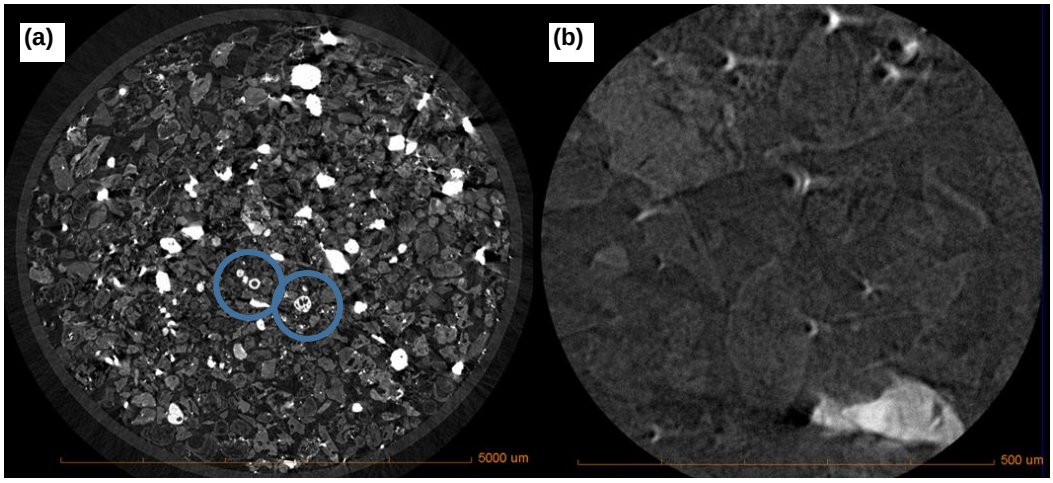

Figure 120 Sample 2 MicroCT scan a) image at 10x magnification b) image at 100x magnification

4.2.7 Summary

The evidence of coal char in furnace dust means that coal was not being fully combusted in the raceway, with residence times often less than 70ms, this was expected. Evidence indicates that coal as well as coal char was reaching the dust. The TGA spectra indicate a small peak at 270^{o}C indicative of the oxygen adsorption peak commonly found in the literature of coal TGA and the TGA spectra in section 4.2.4. Coal particles were identified in the SEM micrograph of BF dust. Further evidence was found in the relationship between the dust La and Coal La. There were also similarities recognised in the dust samples with high levels of aromaticity. The similarities in the parameters of the XRD amorphous carbon peak indicate the presence of coal within the dust samples.

Following a comprehensive study where the application of several techniques were trialled and the outputs compared against the values produced with the CET, it was found that the CET shortened approach, appeared to give the best correlation with the original technique with a correlation coefficient of 0.9713. As a replacement for the CET this could be used with a reasonable degree of certainty. This also came with a vast improvement in time to test reducing the test time by >50%. This informed the hypothesis that 'Thermal techniques can be used to differentiate carbon sources in dust generated in blast furnaces that use granulated coal injection.'

The analytical techniques including carbon and sulphur via Eltra C/S500, bulk density and sizing were all relatively fast techniques to analyse the samples, but the correlation to LOC was weak and would therefore not be a suitable replacement to the

CET. In this context, these techniques don't provide the information required, but can be useful for determining carbon content overall. The BET analysis showed a moderate to weak correlation but there were no time savings identified compared to the CET. Similarly, the Friedman Kinetic model-free analysis showed a moderate correlation, but the time taken to analyse 4 separate heating rates would exceed the time taken to carry out the CET.

The XRD was a useful tool for analysing BF dust samples, the parameters are useful in terms of characterising the material itself but bear little resemblance to the CET. The XRD would return a result in less than 20 minutes, which was useful for tracking phase changes, but the information can't be used for quantifying the LOC in this dust.

The acid digestion and ignition technique proved to be relatively successful in predicting the LOC within BF dust. A simple technique that can be used to analyse batches of samples. This has an advantage where 24 samples could be analysed each time and results returned within 15 hours including drying. The acid stage appeared to be effective in selectively oxidising the residual elements whilst ensuring the carbon remained relatively unimpacted. Some of the refractory elements remained as could be seen in the SEM-EDS data.

When investigating the use of alternative acids to replace the nitric acid digestion in the original digestion and combustion technique, it was clear that all of the acids were effective in removing residual elements. The XRD spectra showed that the nitric acid had the least amount of impact on the carbon structure, despite being not as effective in removing the metals. When each of the samples was combusted from the acid trials. Both nitric and Acid 2 had good correlations with LOC from the original Winkler technique. But the original Acid 1 from the Winkler technique was superior and this formed the foundation for the new replacement test. Acid 6 appeared to have performed the worst, from the XRD spectra the carbon structure was more graphitised and therefore more ordered. This work had not been explored previously using blast furnace dust, so the correlation had a marked impact on the body of knowledge.

Image analyses such as ImageJ, Petrography and MicroCT scanning show large potential with new technologies for machine learning available. This should be explored further as part of future work on similar projects. The limitations identified

in the ImageJ and Petrography would be addressed with the use of Artificial Intelligence and the increased imaging potential of MicroCT scanning.

The XPS analysis was subjective to sample storage and transport, the analysis was limited to 9 samples, but a relationship was identified with the C1S Carbonate deconvoluted peak. With further sampling and analysis, this may be a useful technique to replace the CET, only further analysis is required to support any potential relationship.

The Raman spectroscopy work initially appeared to fail to quantify each of the carbon types. However, the limitations of this technique such as sample size and single spot analysis were outlined. With improved Raman mapping, multiple points and particles within the sample could be analysed and mapped. The concentration of each carbon type can be mapped and quantified, unlocking the potential of Raman spectroscopy.

Suitable replacements for the CET have been found in the form of the digestion and combustion technique and the modified CET analysis. There was no short turnaround in analysis, an alternative technique was found with the ability to batch analyse multiple samples, using the combustion and digestion technique would allow for increased sampling frequency, but with a 24-hour delay on the results. Despite this delay the benefits to increasing testing capacity are significant.

4.3 Impact of Process Conditions on Coal Char Presence in Blast Furnace Dust

4.3.1 Introduction

With an established carbon type differentiation technique deemed suitable for the evaluation of BF dust generated by GCI injection system blast furnaces determined. The recognised LOC quantification technique has been used as a tool to identify changes in LOC and to determine the process conditions that could have influenced the dust generated. This technique was selected over the digestion and combustion technique, to allow for future research into comparing dust samples from various steel plants. The industrially recognised technique has been applied in other steel plants according to Wing *et al.*[61]. Therefore, if dust samples can be compared in future work, utilising this technique gives a larger data set. The aim of this work was to identify which coal properties, process parameters and conditions relate to the LOC generated. Each of the coal properties and process parameters were investigated to determine the influence on LOC within the dust. As discussed previously, LOC presence within the dust indicates the lack of coal gasification and conversion within the process[61]. Hence the desired outcome was to maximise the coal utilised in the furnace in place of prime fuel metallurgical coke but maintain the dust generation to a minimal level. To evaluate the LOC, 63 dust and slurry samples were investigated from the catalogue of samples outlined in section 3.2.7. The sample dates were checked against the process parameters initially to ensure all the samples selected for investigation, were from dates when the furnace was operational. Samples, where blast volume was >100 km3/hr, were considered to ensure a wide variety of process conditions could be observed.

4.3.2 Coal Blending for Consistency

Chemical analyses of the coals were carried out and compared to the LOC in the dust to determine the contribution of each. The alkali metals, proximate analysis and ultimate analysis for each coal and the blends are outlined in Table 28. The ash content of the final blend of coal should be maintained between 7 and 9%. This was to prevent issues with residue after combustion clogging the furnace, or the ash constituents drawing on heat reserves of the furnace caused by high levels of ash content of the coal[110]. Coals A and B are low in ash content and are blended with high ash coals,

to lower the ash content of the blend with high ash coals such as Coal E, which was above the limit for ash to be used in isolation. Volatile matter was a balance between high volatile coals which burnout better leaving less residue, but low volatile coals which provide more heat but burnout slower and are more likely to be found in the flue dust. The blend of coal was designed to produce a final volatile matter of 12-15%[111]. Sulphur and phosphorous should be minimised, as excess sulphur and phosphorous increases the tramp elements in the hot metal. Iron requires desulphurisation before the steel-making process as increase sulphur is detrimental to steel quality[112]. Alkali metals and zinc found in injection coal, are harmful to the refractories of the furnace and should therefore be maintained at a minimal level, the high levels of these residuals in coal B restrict the use as a singular injectant[113]. Moisture and the ultimate analytes, including carbon, hydrogen, nitrogen, and oxygen, are important characteristics of the replacement ratio. High values for carbon and low moisture levels allow for increased use of coal. Energy is required to crack the C-H bonds to combust the coal[99]. Moisture in this case was measured before the material was dried for injection, high moisture contents will require longer times for drying and slow the process down, also when shipping the coals around the world, the valuable commodity is the coal, any water above an acceptable tolerance is deducted from the cost of the cargo. As can be seen in Table 28, although there was considerable variation in the individual coals, the difference between the blends was minimal for consistency.

Table 28 ICP-OES, proximate and ultimate analysis of coals and blends

	ICP – OES				Proximate Analysis				Ultimate Analysis			
	Na_2O	K_2O	Zn	P	H_2O	Volatile	Ash	S	C	H	N	O
	wt%	wt%	wt%	wt%	wt%	wt%	wt%	wt%	wt%	wt%	wt%	wt%
Coal A	0.85	2.10	0.01	0.010	13.10	6.80	4.80	0.87	87.94	3.48	1.44	1.44
Coal B	0.93	2.30	0.02	0.046	10.80	14.60	6.40	1.13	85.83	3.99	1.30	1.32
Coal C	0.62	1.77	0.00	0.009	10.80	33.60	10.00	1.10	76.63	4.86	1.66	5.70
Coal D	0.30	1.50	0.01	0.024	10.20	13.30	8.90	0.49	82.59	3.87	1.81	2.30
Coal E	0.78	1.37	0.01	0.049	8.20	13.50	9.90	0.32	83.03	3.26	2.03	1.94
Blend 1	0.61	1.88	0.02	0.031	10.79	12.98	7.45	0.78	84.47	3.87	1.57	1.83
Blend 2	0.55	1.82	0.02	0.033	10.44	13.82	7.90	0.75	83.89	3.92	1.61	1.91
Blend 3	0.78	1.38	0.01	0.049	8.23	13.51	9.87	0.33	83.06	3.27	2.02	1.94
Blend 4	0.82	1.60	0.01	0.048	8.85	13.78	9.03	0.52	83.73	3.44	1.85	1.79
Blend 5	0.84	1.74	0.01	0.048	9.24	13.94	8.50	0.64	84.15	3.55	1.74	1.69
Blend 6	0.84	1.76	0.01	0.045	9.48	13.43	8.28	0.65	84.38	3.54	1.73	1.68
Blend 7	0.80	1.55	0.01	0.044	9.03	12.88	8.95	0.47	83.88	3.36	1.88	1.82
Blend 8	0.82	1.65	0.01	0.042	9.48	12.55	8.44	0.55	84.34	3.42	1.81	1.75
Blend 9	0.82	1.67	0.01	0.044	9.39	12.95	8.48	0.57	84.26	3.45	1.79	1.74
Blend 10	0.62	1.90	0.02	0.035	10.50	13.95	7.65	0.81	84.21	3.93	1.56	1.81
Blend 11	0.56	1.81	0.01	0.029	10.50	17.18	8.26	0.80	82.65	4.08	1.62	2.56
Blend 12	0.88	1.98	0.02	0.047	9.92	14.23	7.59	0.85	84.88	3.74	1.55	1.53
Blend 13	0.83	1.68	0.01	0.048	9.06	13.86	8.75	0.59	83.95	3.50	1.79	1.74

Low ash is required to prevent issues with permeability, generally, ash consists of refractory materials that will not be utilised within the furnace. The elements in the ash are dissolved in the slag, the consideration here was that the slag should be basic to protect the refractories within the furnace. High ash injection coal is undesirable as there is a requirement to control the levels of Al_2O_3 and SiO_2 within the furnace to allow for better slag tapping. CaO and MgO help control slag basicity, a more basic slag will produce more slag, but is less corrosive on the refractories of the furnace that are already basic[114]. As per Table 29, Coal B will produce slags of lower basicity which was another justification for it to be blended with coals producing higher basicity slags. Coal is not the only influence on basicity, but each component that was fed into the blast furnace should be controlled with this consideration.

Table 29 XRF chemistry of the ash analysis of coals and blends

	SiO_2	Al_2O_3	TiO_2	CaO	MgO	Fe	P	Mn
	% in Ash	% in Ash	% in Ash	% in Ash	% in Ash	% in Ash	% in Ash	% in Ash
Coal A	44.51	29.98	1.15	3.47	1.73	7.11	0.216	0.077
Coal B	44.16	33.27	0.95	2.38	1.31	6.76	0.720	0.045
Coal C	39.61	27.44	1.14	6.13	1.66	12.80	0.091	0.075
Coal D	57.35	26.85	0.97	1.78	0.74	5.86	0.290	0.180
Coal E	50.10	24.50	0.84	5.45	1.83	5.48	0.498	0.170
Blend 1	50.80	29.65	0.99	2.22	1.08	6.35	0.442	0.117
Blend 2	52.07	29.42	0.96	2.02	0.97	6.22	0.462	0.126
Blend 3	50.04	24.59	0.84	5.42	1.82	5.49	0.500	0.169
Blend 4	48.62	26.69	0.87	4.68	1.70	5.80	0.553	0.139
Blend 5	47.72	28.01	0.88	4.22	1.62	5.99	0.587	0.120
Blend 6	47.57	28.04	0.90	4.21	1.64	6.06	0.558	0.119
Blend 7	48.83	26.07	0.89	4.89	1.76	5.80	0.491	0.146
Blend 8	48.14	26.92	0.91	4.59	1.72	5.98	0.488	0.133
Blend 9	48.06	27.17	0.90	4.51	1.70	5.97	0.515	0.130
Blend 10	50.76	30.06	0.96	2.08	1.03	6.31	0.505	0.113
Blend 11	49.98	29.07	0.99	2.72	1.08	7.34	0.398	0.118
Blend 12	46.18	30.29	0.91	3.42	1.49	6.32	0.644	0.088
Blend 13	48.14	27.39	0.88	4.44	1.66	5.90	0.571	0.129

Each of the coals that produce the blends for injection, share common phases. All contain phases of kaolinite, illite, quartz, muscovite, pyrite and siderite as found previously in the work of Yang *et al.*[115,116]. Siderite appears only in coals D and E according to Figure 121. According to Table 28, these two coals are similar which explains why these coals would share phases. Coals D and E also display more intense peaks for quartz, this reinforces the SiO_2 analysis from Table 29, as these particular coals contain more SiO_2 as analysed using the XRF. The changing morphology of the amorphous carbon peak was investigated later in this thesis, but each of the shapes indicates different degrees of aromaticity and the difference between the peaks was clear in Figure 121.

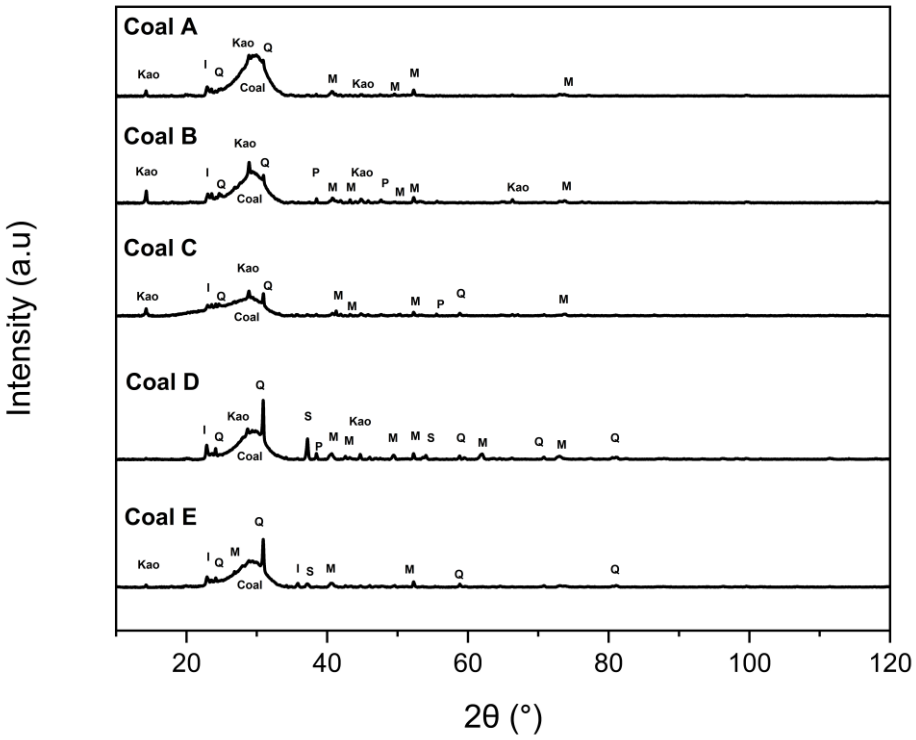

Figure 121 Powder XRD patterns for coal samples. KaO = Kaolinite ($Al_2Si_2O_5(OH)_4$ – COD# 9014999), I = Illite ($Al_2H_2KO_{12}Si_4$ -COD# 9013719), Q = Quartz (SiO_2 – COD# 1536389), P = Pyrite (FeS_2 – COD# 9000594), M = Muscovite ($Al_3H_2KO_{12}Si_3$ – COD# 1101029), S = Siderite ($CFeO_3$ – COD# 9015534), Coal = Amorphous Region

The reduction in ash chemistry between Coal E and Coal D observed in Table 29, was also observed in the spectra for blends 4 and 5 in Figure 122, distinctly lacking in kaolinite and muscovite peaks in comparison to the other blends that contain more coal E. Blend 7 also displays a similar pattern, but there was an increase in Coal B in this blend, to offset the use of Coal A here, differentiating blend 7 from blends 1, 2 and 3. The larger amorphous region in blend 5 confirms the higher volatile content of Coal C as observed in Table 28, which was unique to this blend. According to Table 28 and Table 29 Coal C has a higher iron content, but this was not seen in the spectra observed in blend 5, at 17%, the concentration of Coal C was relatively small compared to the other coals, which explains why some of the features may not be present in the spectra in Figure 122.

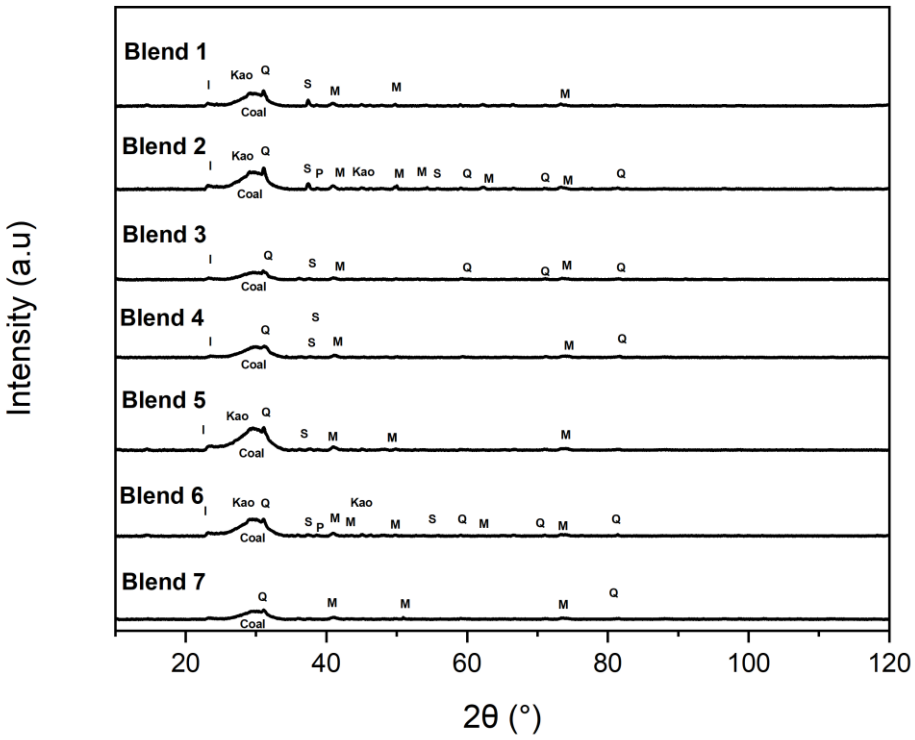

Figure 122 Powder XRD patterns for coal blend samples 1-7. KaO = Kaolinite ($Al_2Si_2O_5(OH)_4$– COD# 9014999), I = Illite ($Al_2H_2KO_{12}Si_4$ -COD# 9013719), Q = Quartz (SiO_2 – COD# 1536389), P = Pyrite (FeS_2 – COD# 9000594), M = Muscovite ($Al_3H_2KO_{12}Si_3$ – COD# 1101029), S = Siderite ($CFeO_3$ – COD# 9015534), Coal = Amorphous Region

Blends 8 and 13 contain Coal A at relatively low concentrations, 12.5% and 7% respectively, Coal A was low volatile and high carbon according to Table 28, but this was not clear in the spectra of Figure 123, because the concentration within the blend was low. Blend 10 was 99% Coal E, and the spectra are similar but not identical to the Coal E spectra in Figure 121, due to the addition of Coal B. The quartz peaks are less intense due to the difference in the shape of the amorphous coal peak[117]. This changing shape indicates a change in lattice layering and aromaticity of the carbon within the coal. The difference between blends 9 and 12 was clear in Figure 123, the change of Coal D to Coal E appears to influence the presence of kaolinite in the blended properties.

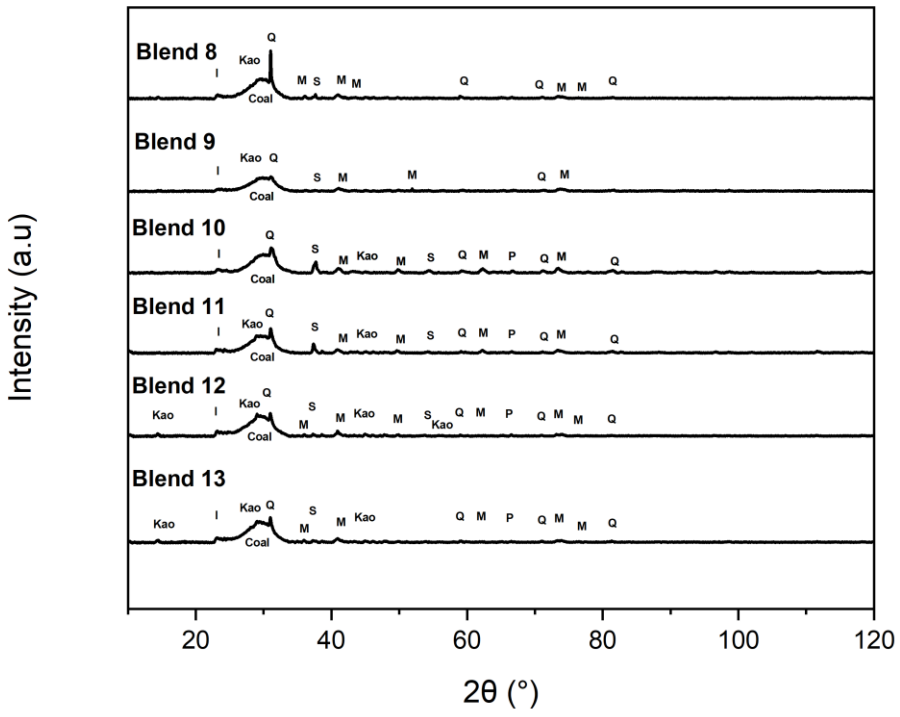

Figure 123 Powder XRD patterns for coal blend samples 8-13. KaO = Kaolinite ($Al_2Si_2O_5(OH)_4$ – COD# 9014999), I = Illite ($Al_2H_2KO_{12}Si_4$ -COD# 9013719), Q = Quartz (SiO_2 – COD# 1536389), P = Pyrite (FeS_2 – COD# 9000594), M = Muscovite ($Al_3H_2KO_{12}Si_3$ – COD# 1101029), S = Siderite ($CFeO_3$ – COD# 9015534), Coal = Amorphous Region

It was clear from the XRD spectra and the characterisation of the coal types and subsequent blends, that the aim of coal blending for blast furnace ironmaking was consistency. Although changes in the XRD spectra have been discussed, the degree of difference was relatively small. Similarly, the chemistries of the blends remain consistent throughout the different blends with little variation. It was important to consider the natural variation within coal seams, influencing the individual coals. Coal A for example will change in chemistry depending on the exact seam and location of the material. This explains any differences observed between the expected blend chemistries and raw coals. When blending coals, parameters such as volatile matter should be predictable based on linear weighting of each component. However, this is often influenced by the natural variation in the coal across the bulk of the material. According to the work by Steer *et al.* and Hong *et al.* phases can influence the combustion of coal and subsequent char, the presence of illite has been known to promote combustion in the raceway as discussed in the literature review in section

2.8.3[54]. The mechanism for this though is hotly debated in the literature. Works by Hong *et al.* suggest that increased mineral matter has a clogging effect on the pore structure of char, but Mendez *et al.* suggest that minerals facilitate the formation of wide channel pores[118,119]. The increased porosity of coal and the subsequent char will determine whether it burns out in the raceway and hence exits the furnace in the form of dust.

4.3.3 Combustibility of Coals

The recognised technique for determining coal burnout was discussed in section 2.8.3, the use of a DTF helps recreate the conditions of a raceway which are high temperatures and very short residence times. Using CO_2 as a reaction gas will determine the degree of coal gasification and using O_2 or air as a reaction gas will determine oxidation and burnout. TGA can be used for determining coal reactivity. The experimental techniques including heating profiles for the coal analysis were following the procedure outlined in section 3.5.1. Each of the coals selected were blended according to section 3.2.11 and were subjected to the same temperature and gas conditions. In Figure 124, the key stages for combustion as discussed in section 2.7 of the literature review, can be observed in the TGA data. According to Niroj *et al.*, the stages begin with a mass loss at 100^{o}C which indicates the evaporation of moisture, followed by a mass increase for oxygen adsorption starting at 270^{o}C. The large decrease in mass starting around 500^{o}C was related to coal combustion, followed by a flattening of the curve which was the slow burnout of the remaining char in simple terms[136,157]. The effects of coal blending have been discussed by Shan Wen Du *et al.* outlined in section 2.8.1, of the literature review. Blending can improve burnout and reduce the costs associated with coal injection. The differences between the blends and coals can be seen in Figure 124, coals with higher moisture contents have a larger initial mass loss. More reactive coals such as Coal C, begin to lose mass before the rest of the coals. The difference in gradient between blends 11, 12 and 13 when compared to 8, 9 and 10 was clear in this example in Figure 124. This determines the speed at which coal will combust, the steeper gradient starting at 500^{o}C means coals will burnout faster. Hence blends 11, 12 and 13 should burnout faster in the blast furnace than the other blends in similar conditions. The balance between carbon and burnout here is important to note, despite blend 11 combusting well, it has a lower carbon concentration, providing less carbon for the Boudouard reactions which will be an

important coal selection consideration. The final mass remaining after the heating profile was indicative of the ash residue remaining after combustion. After reaction in all cases, according to Figure 124, all the final residues are within a confined area of the graph which was reflective of the ash chemistries in Table 29 as these have a fine spread. The lower ash residue and faster burnout coals such as blends 11, 12 and 13 would allow for an increased injection rate, offsetting more coke as a fuel than blends 7 and 9. There is another balance between burnout and replacement ratio when selecting coals for injection because the amount of hydrogen required for the correct reduction conditions for iron production is important to be maintained as well as carbon[99].

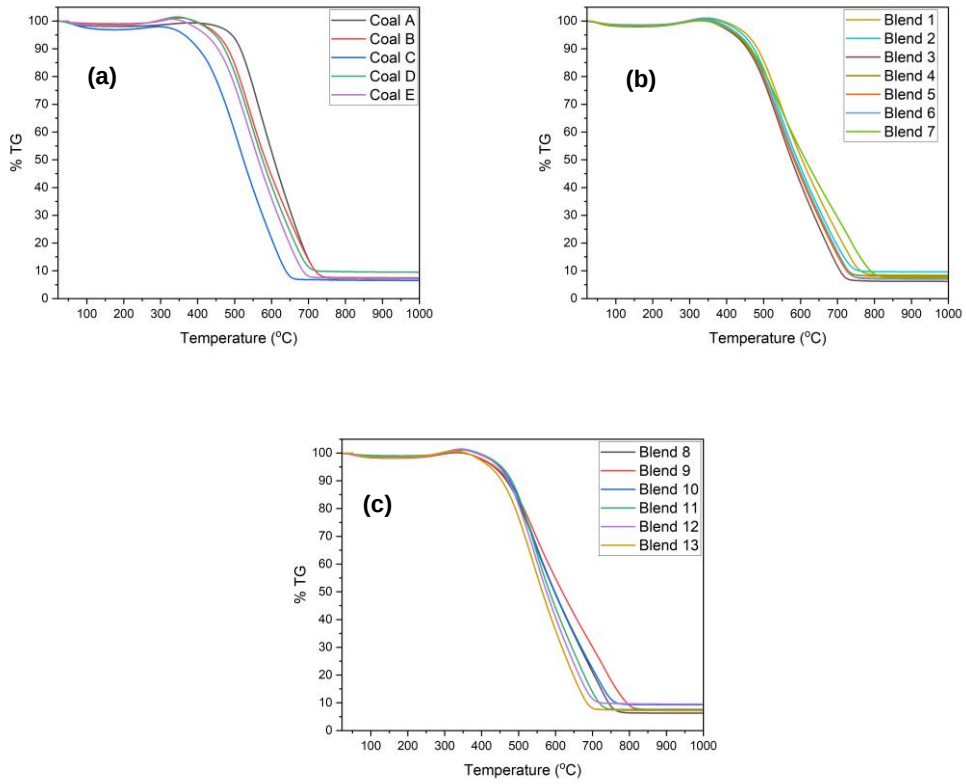

Figure 124 TG Graphs for coals and blends a) individual coals b) blends 1-7 c) blends 8-13

Figure 125 shows the DTG plots for each of the coals and the respective blends. The small peak around 100°C in each of the plots indicates the presence of moisture in the samples. The onset line determines when the combustion stage starts and ends, this was set at 0.1 %/min. The height of the DTG curve indicates the rate of reaction, higher rates have higher peaks. The breadth of the peak was indicative of reaction time, narrow bands indicate short reaction times[158]. The interesting observations in the blends here are 7 and 9, the double peak in the DTG indicates the 2 stages of

combustion, normally the first with reference to a smouldering reaction followed shortly by ignition which was the highest peak[136]. A wide peak with multiple stages was indicative of multiple phases in the material, blends 7 and 9 appear to combust less readily than the other blends, similar to the observations in Figure 124. Blend 5 was the only blend containing Coal C which has the lowest ignition temperature, despite low concentrations in the blend, the effect on the height of the DTG in blend 5 can be seen, this blend has a high reaction rate change. Blend 1 also has a wide reaction range in the DTG and would not be as reactive as blends 11, 12 and 13. This would mean it was less likely to be chosen as an injection blend. Hence it was only used on one occasion as can be observed further into the chapter.

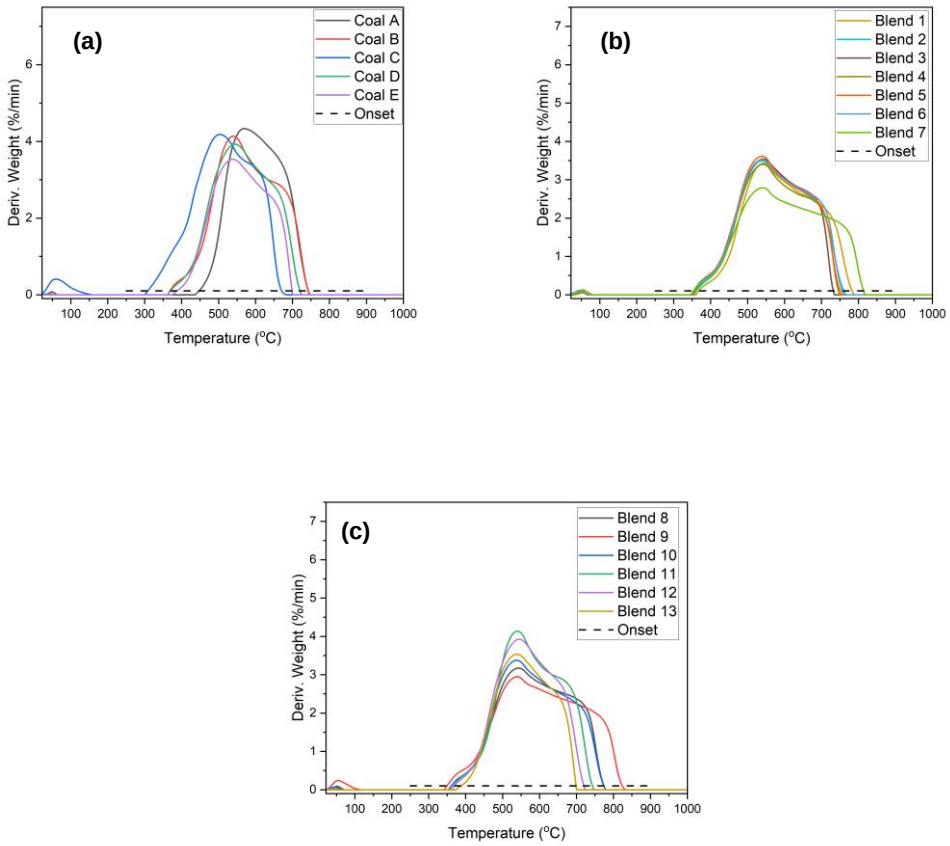

Figure 125 DTG graphs for coals and blends a) the individual coals b) blends 1-7 c) blends 8-13

The TG parameters of the coal blends as outlined in section 3.5.1, were analysed from the TG and DTG plots in Figure 124 and Figure 125 respectively and can be observed in Table 30. The ignition temperature was relatively consistent throughout the coals and because the range of chemistries throughout the blends was

small, this was expected. Blends 7 and 9 have high values for T0.5, indicating that for half of the coal to oxidise, the temperature was required to be higher. This means that blends 7 and 9 should take longer to react than the others, this was reflected in the burnout temperature Tb, this temperature was also high for blends 7 and 9. The combustibility index indicates that blends 5, 6 and 11 should combust more readily than the other blends. The T_{max} of each of the blends was consistent with the combustibility index, the T_{max} of blend 11 was low, hence the reaction occurs at lower temperatures. Blend 11 appears to perform the best in terms of combustibility, as opposed to blends 7 and 9 which are worse performing, according to the data in the DTG and TG parameters.

Table 30 TG parameters of coals and subsequent blends

	Ti	Tmax	T0.5	Tb	Combustibility Index ($x10^9$)
Coal A	446.33	569.68	614.85	742.76	20.52556
Coal B	367.85	539.89	592.24	743.41	30.6448
Coal C	307.7	503.92	531.83	671.45	51.46512
Coal D	368.43	544.69	587.91	720.44	27.81352
Coal E	385.78	538.43	573.10	699.09	20.08478
Blend 1	367.35	543.45	618.09	783.25	23.45931
Blend 2	360.77	538.51	609.96	760.84	25.25389
Blend 3	355.24	542.00	584.38	732.22	27.00592
Blend 4	357.42	541.68	596.47	746.18	24.62409
Blend 5	355.07	538.83	592.67	750.94	27.8206
Blend 6	353.05	539.40	596.88	757.22	27.59501
Blend 7	352.97	540.95	628.83	814.35	19.42474
Blend 8	360.43	543.14	607.30	774.58	22.40669
Blend 9	348.67	538.67	633.08	824.5	22.63575
Blend 10	361.43	538.51	613.53	774.25	24.02364
Blend 11	360.02	525.07	588.43	755.2	31.49283
Blend 12	378.93	531.75	559.04	726.92	26.05912
Blend 13	387.65	528.41	549.14	690.61	20.13573

As previously stated, blend 11 had the best TGA combustion characteristics as opposed to blends 7 and 9. Hence the thought was, that dust samples analysed on days where coal blends injected had high combustibility parameters, should contain less LOC. The values for each TG parameter were compared to its equivalent LOC value for each sample according to Figure 126. Each coal was used on multiple occasions throughout the sampling campaign and on the days where LOC was measured the results were graphed. The degree of stratification in the data was clear, this was due to the lack of diversity in the changing blends, in comparison to the variation in the dust itself. There are no standout relationships between LOC and TG parameters, but it was observed in the Ti versus LOC in dust relationship, that with increasing Ti of the coal blend in use, the LOC in the dust increased, which would support this theory, but the correlation is more likely to be coincidental as there is no clear relationship. The other relationships are minimal or non-existent and the stratification is clear as per Figure 126.

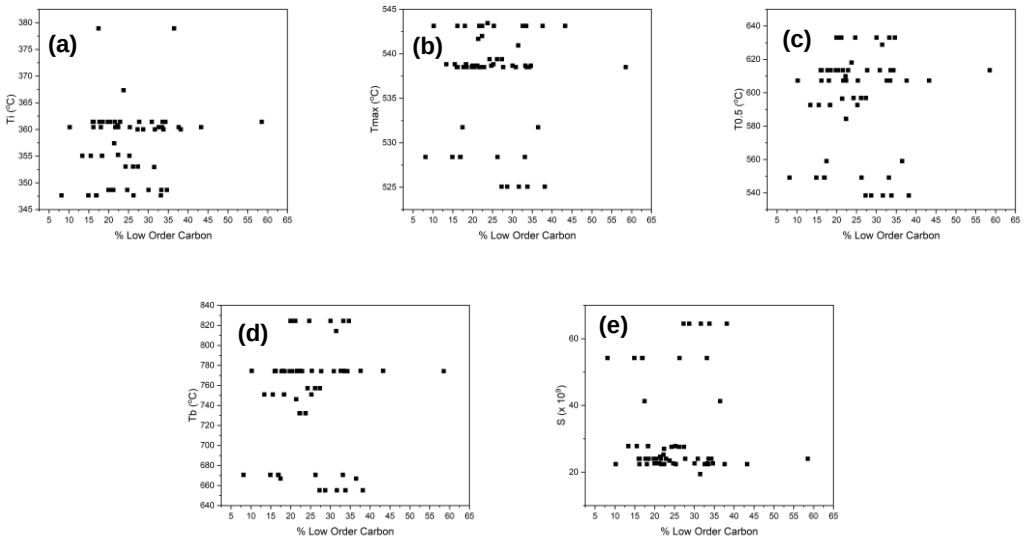

Figure 126 Scatter graphs showing TGA parameters versus LOC carbon in the dust. a) Ti b) Tmax c) T0.5 d) Tb e) combustibility index

Table 31 outlines the relationships between the TGA parameters, the LOC and the LO:HO ratio relationship in the dust samples from each of the abatements of the blast furnace. All of the correlations are weak, including the strongest between Ti and Dust LO:HO ratio at 0.187. The R^2 at 0.035, shows there was a high degree of uncertainty in the relationship. This would indicate that there was no relationship in any of the parameters at all. The limitation here was the lack of variation in the data, due to the consistency in coal types and chemistries used. The inverse relationship with

Tmax appears to indicate that with decreasing reactivity temperature there was more LOC in the dust, which would contradict the theory. But the relationship was not strong enough to understand the relationship fully here and it was more likely that the data was random as opposed to ordered.

Table 31 Pearson's correlation and R^2 values for relationships between low-order carbon and the TGA parameters of the coal blends

	Dust LOC		Dust LO:HO		Slurry LOC		Slurry LO:HO	
	Pearson's Correlation	R^2	Pearson's Correlation	R^2	Pearson's Correlation	R^2	Pearson's Correlation	R^2
Ti	0.1481	0.0219	0.187	0.035	0.0895	0.008	-0.0186	0.0003
Tmax	-0.0443	0.002	-0.0928	0.0086	0.0436	0.0019	-0.1076	0.0116
T0.5	0.0215	0.0005	-0.0888	0.0079	0.0942	0.0089	-0.0462	0.0021
Tb	0.0227	0.0005	-0.1077	0.0116	0.0973	0.0095	-0.0439	0.0019
S x10^9	0.0405	0.0016	0.081	0.0066	-0.04	0.0016	0.083	0.0069

The relationship between each TG parameter, exclusive of the LOC in the dust was used to identify the possibility of combined influences on the dust generation as per Table 32. There are strong relationships between Ti and Tmax, T0.5 and Tb, which would be anticipated, with an inverse relationship between T0.5 and the combustibility index.

Table 32 Pearson's correlation between each TG parameter

	Ti	***TMax***	***T0.5***	***Tb***	***Combustibility Index (S x10^9)***
Ti	1.00				
TMax	0.83	1.00			
T0.5	0.31	0.70	1.00		
Tb	0.04	0.50	0.96	1.00	
Combustibility Index (S x10^9)	-0.38	-0.71	-0.87	-0.79	1.00

It was clear with the variation in the LOC levels in the dust, that more parameters will influence this value as opposed to coal type alone. The coal in simple terms doesn't vary significantly, but the LOC in the dust does. The effects of process conditions are analysed later in this thesis, but not just the coal properties have an effect. The coal blend needs to be combustible and meet the desired characteristics outlined in section 2.8.1, the variation between the blends was minimal to maintain stable operations, which justifies the investigation of process parameters on the LOC.

4.3.4 The Effect of Coal Chemistry on Top Gas Carbon

As observed previously, the influence of coal parameters on the LOC in the dust was limited by the variation in the coal type. This effect can be seen in the stratification of the scatter in Figure 127. Work by Thong *et al.* in section 2.8.3 of the literature review made predictions for coal burnout based on blast furnace parameters, but this work aimed to improve upon this and identify relationships with live data from the furnace. There was no obvious correlation between the coal blend type and the LOC in the dust. The box plot in Figure 127 shows that the average LOC content per blend would be more or less representative, due to the size variation in the data set. Blends 1, 8, 9, 10 and 11 have only 1 observation, it was therefore not proficient to compare the average dust output for these blends against blend 7 for example which has a much wider range of analysis available. This indicates that there's a requirement for more data to draw more confident conclusions. Blend 11 was the most likely blend to burn out as described in section 4.3.3. However as can be seen in Figure 127, the LOC presence within the dust was equal to blends 7 and 9.

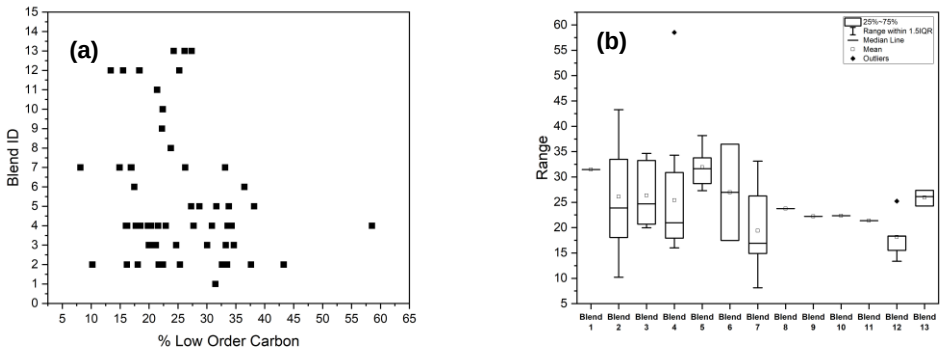

Figure 127 Coal blend ID's versus low-order carbon output a) Scatter left b) box plots

Table 33 summarises the 2-dimensional relationships between each process parameter and the LOC and LO:HO ratio in slurries and dust samples. It was observed that the relationships with LOC and slurry parameters are similar to those with the dust parameters and LOC. The LO:HO ratio appears to correlate more strongly than the LOC in some parameters such as proximate analysis and ultimate analysis but less in the process parameters, but these correlations are too weak to consider them significant. The scatter graphs in appendices 19-21 in section 7.3.1 clearly show that any of the values of correlation in Table 33 are completely circumstantial. There are no clearly identifiable trends in the data which clearly shows a lack of resolution in the

sampling. This indicates that the coal blending is so consistent that it creates a lack of variation in the coal chemistry, this was a limiting factor for evaluating the effects of coal parameters on LOC in the dust. The limitations of obtaining a representative sample of the process dust should be considered when analysing the data, the best available sample was taken.

Table 33 Pearson's correlation and R^2 values for coal chemistry versus LOC and LO:HO ratio in the dust samples and slurry samples

	Dust LOC		Dust LO:HO Ratio			Slurry LOC		Slurry LO:HO Ratio	
	Pearson's Correlation	R^2	Pearson's Correlation	R^2		Pearson's Correlation	R^2	Pearson's Correlation	R^2
Blend ID	-0.15	0.02	0.06	0.00	**Blend ID**	0.01	0.00	0.03	0.00
Coal H_2O	0.16	0.03	0.28	0.08	**Coal H_2O**	0.20	0.04	0.13	0.02
Coal Ash	-0.06	0.00	-0.23	0.05	**Coal Ash**	-0.09	0.01	-0.05	0.00
Coal Volatile Matter	0.16	0.02	0.24	0.06	**Coal Volatile Matter**	0.11	0.01	0.16	0.03
Coal S	0.10	0.01	0.29	0.08	**Coal S**	0.08	0.01	0.12	0.01
Coal P	-0.22	0.05	-0.25	0.06	**Coal P**	-0.26	0.07	-0.16	0.02
Coal Ash Fe	0.23	0.05	0.26	0.07	**Coal Ash Fe**	0.19	0.04	0.16	0.02
Coal Ash Mn	-0.05	0.00	-0.25	0.06	**Coal Ash Mn**	0.01	0.00	-0.05	0.00
Coal Ash P	-0.25	0.06	-0.10	0.01	**Coal Ash P**	-0.29	0.09	-0.12	0.02
Coal Ash SiO_2	0.07	0.00	0.18	0.03	**Coal Ash SiO_2**	0.17	0.03	0.15	0.02
Coal Ash Al_2O_3	0.05	0.00	0.26	0.07	**Coal Ash Al_2O_3**	0.06	0.00	0.10	0.01
Coal Ash TiO_2	0.22	0.05	0.27	0.07	**Coal Ash TiO_2**	0.24	0.06	0.15	0.02
Coal Ash CaO	-0.08	0.01	-0.26	0.07	**Coal Ash CaO**	-0.12	0.01	-0.13	0.02
Coal Ash MgO	-0.10	0.01	-0.27	0.07	**Coal Ash MgO**	-0.14	0.02	-0.15	0.02
Coal Ash Na_2O	-0.15	0.02	-0.25	0.06	**Coal Ash Na_2O**	-0.20	0.04	-0.17	0.03
Coal Ash K_2O	0.05	0.00	0.26	0.07	**Coal Ash K_2O**	0.04	0.00	0.08	0.01
Coal Ash Zn	-0.07	0.01	0.18	0.03	**Coal Ash Zn**	-0.04	0.00	0.05	0.00
Coal C	-0.16	0.03	-0.14	0.02	**Coal C**	-0.15	0.02	-0.16	0.03
Coal H	0.13	0.02	0.29	0.08	**Coal H**	0.14	0.02	0.16	0.02
Coal N	-0.08	0.01	-0.27	0.07	**Coal N**	-0.08	0.01	-0.11	0.01
Coal O	0.22	0.05	0.18	0.03	**Coal O**	0.21	0.04	0.16	0.03

Coal Process Parameters

Incremental changes are made to the coal blend to ensure consistency of blast furnace performance. The process parameters though, change more regularly based on the conditions within the furnace. As an example, when the coke availability and quality are good, more coal can be used, reducing the running cost of the blast furnace. Coal per unit oxygen appears to have the largest influence on the LOC in the dust according to Table 34, however, all of the correlations are too small to be considered definitive relationships. The scatter graphs in appendices 22-23 in section 7.3.2 show that the data is more randomly scattered as opposed to ordered. The coal per unit oxygen which

correlated the strongest albeit with a very weak correlation was used to inform the work of chapter 4.4, this was a parameter to monitor with increased data. To improve upon the work thus far, continuous sampling of the dust should be completed over the campaign of the blast furnace to capture many more coal blend iterations and improve the data set size. This will give a more detailed insight into the effect of coal type on dust LOC.

Table 34 Pearson's correlation and R^2 values for each coal parameter versus LOC and LO:HO ratio in the dust samples and slurry samples

	Dust LOC		Dust LO:HO Ratio			Slurry LOC		Slurry LO:HO Ratio	
	Pearson's Correlation	R^2	Pearson's Correlation	R^2		Pearson's Correlation	R^2	Pearson's Correlation	R^2
Coal Rate	0.37	0.13	0.20	0.04	**Coal Rate**	0.26	0.07	0.17	0.03
Coal per Unit Oxygen Molecular	0.42	0.18	0.21	0.05	**Coal per Unit Oxygen Molecular**	0.30	0.09	0.19	0.03
Coal per Unit Oxygen Mass	0.43	0.18	0.21	0.05	**Coal per Unit Oxygen Mass**	0.30	0.09	0.19	0.03
Coal Flow	0.24	0.06	0.01	0.00	**Coal Flow**	0.13	0.02	0.03	0.00
Replacement Ratio	-0.16	0.03	-0.07	0.01	**Replacement Ratio**	-0.14	0.02	-0.13	0.02
Gas Composition $Co_{(a)}$	0.23	0.05	-0.08	0.01	**Gas Composition $Co_{(a)}$**	0.14	0.02	-0.07	0.01
Gas Composition $CO_{2\,(a)}$	0.36	0.13	0.16	0.03	**Gas Composition $CO_{2\,(a)}$**	0.34	0.12	0.22	0.05
Gas Composition $H_{2\,(a)}$	0.39	0.15	0.21	0.04	**Gas Composition $H_{2\,(a)}$**	0.30	0.09	0.20	0.04
Gas Composition $Co_{(b)}$	0.22	0.05	-0.18	0.03	**Gas Composition $Co_{(b)}$**	0.15	0.02	-0.09	0.01
Gas Composition $Co_{2\,(b)}$	0.40	0.16	0.17	0.03	**Gas Composition $Co_{2\,(b)}$**	0.37	0.14	0.24	0.06
Gas Composition $H_{2\,(b)}$	0.38	0.15	0.20	0.04	**Gas Composition $H_{2\,(b)}$**	0.29	0.08	0.20	0.04
Gas Efficiency	0.15	0.02	0.29	0.08	**Gas Efficiency**	0.22	0.05	0.31	0.09

4.3.5 The Effect of Process Parameters on Top Gas Carbon

It was also important to consider non-coal-related operating parameters and observe the effects on the LOC in the dust. The theoretical relationship with O_2 and LOC in the dust was inverse because O_2 promotes coal combustion and therefore, with increased O_2 less unburnt char should be present in the dust based on the work of Tiwari *et al.* and Thong *et al.* outlined in the literature review section 2.8.3, where the authors outline the importance of increased oxygen to promote burnout. However, the

observed relationship was positively correlated albeit a weak relationship that appears to be circumstantial according to Table 35 and the scatters in appendices 24-27 in section 7.3.3. The weak positive correlations, although they appear to be randomly scattered, were used to inform the work of chapter 4.4 with increase data resolution this information could be used to confirm any potential relationship. The 12-hour averages in the data can hide a multitude of changes throughout the period, specifically in the blast volume parameter. Parameters such as blast volume are more susceptible to change during the 12 hour period, than coke rate or steam and therefore justify the weak relationships identified in Table 35. The variability of the blast volume parameter can be seen in Figure 128, the degree of variation would be masked by the 12 hour average and helped inform the work in chapter 4.4 as a need for increased sampling resolution is clear.

Table 35 Pearson's correlation and R^2 values for each process parameter versus LOC and LO:HO ratio in the dust samples and slurry samples

	Dust LOC		Dust LO:HO Ratio			Slurry LOC		Slurry LO:HO Ratio	
	Pearson's Correlation	R^2	Pearson's Correlation	R^2		Pearson's Correlation	R^2	Pearson's Correlation	R^2
O_2 Setpoint	0.26	0.07	0.19	0.04	**O_2 Setpoint**	0.25	0.06	0.23	0.05
O_2 Volume	0.18	0.03	0.01	0.00	**O_2 Volume**	0.12	0.01	0.07	0.00
Total Oxygen	-0.04	0.00	-0.14	0.02	**Total Oxygen**	-0.08	0.01	-0.10	0.01
Oxygen Flow	-0.04	0.00	-0.14	0.02	**Oxygen Flow**	-0.08	0.01	-0.10	0.01
Steam	-0.20	0.04	0.01	0.00	**Steam**	-0.18	0.03	0.07	0.01
Flame Temperature	0.31	0.10	0.03	0.00	**Flame Temperature**	0.25	0.06	0.02	0.00
Blast Volume	-0.20	0.04	-0.22	0.05	**Blast Volume**	-0.22	0.05	-0.20	0.04
Blast Pressure	0.05	0.00	-0.05	0.00	**Blast Pressure**	0.00	0.00	-0.10	0.01
Blast Temperature	0.30	0.09	0.30	0.09	**Blast Temperature**	0.20	0.04	0.19	0.04
Delta P	0.33	0.11	0.24	0.06	**Delta P**	0.30	0.09	0.20	0.04
Production Rate	0.07	0.01	-0.12	0.01	**Production Rate**	0.01	0.00	-0.07	0.01
Hot Metal Si	-0.14	0.02	0.11	0.01	**Hot Metal Si**	-0.13	0.02	0.00	0.00
Coke Rate	-0.36	0.13	-0.13	0.02	**Coke Rate**	-0.29	0.08	-0.14	0.02
Max Differential Pressure	0.32	0.10	0.24	0.06	**Max Differential Pressure**	0.21	0.04	0.25	0.06
High Top Pressure	0.00	0.00	-0.09	0.01	**High Top Pressure**	-0.10	0.01	-0.08	0.01
Top Temperature	0.15	0.02	0.14	0.02	**Top Temperature**	0.15	0.02	0.05	0.00
Permeability	-0.09	0.01	-0.07	0.01	**Permeability**	-0.12	0.01	0.01	0.00

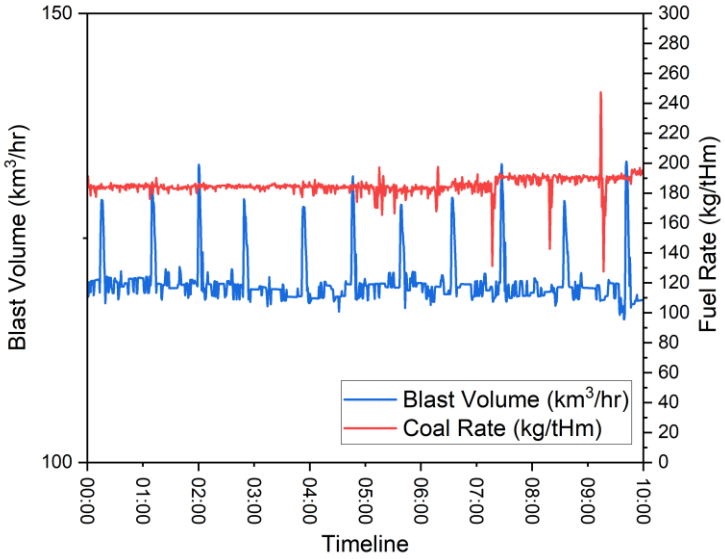

Figure 128 12-hour process trace showing blast volume degree of variation

4.3.6 Summary

It has been determined that relationships between coal types, coal blends, operating parameters and LOC in the dust, cannot be identified using the CET with the proposed resolution of sampling. Despite the capabilities of the analysis technique as demonstrated in section 4.2.3, it is clear that the variation in the processes are not captured in the samples. Dust samples from both the wet and dry abatements were analysed for LOC and LO:HO ratio and plotted against coal chemistries and an average of the process conditions, from a 12-hour period before the material was sampled.

The limitations of the resolution of sampling were made clear in this chapter. Process conditions such as blast volume and coal rate vary to a greater degree than the coal types used which influenced the relationships in the data. This causes uncertainty when analysing the outputs and determining a model of which parameters have the largest influence on the LOC in the dust.

Coals were analysed and blended in line with the blends used in production at the time of dust sampling. The importance of minimising elements such as phosphorous and sulphur was stated, as was the importance of stability in the blends for consistency in production. The ash chemistry has been discussed to influence the permeability of the descending burden and it has been discussed that the basicity of slag formation is important to protect the refractory lining of the furnace. Basicity also influences the LOC in the dust. The coal selection process was clearly geared towards

maintaining stable operations, a high replacement ratio and maintaining the integrity of the furnace refractories with tight control on basicity. This means that variation in the coal chemistry data was limited and it was difficult to draw reliable conclusions, based on coal chemistry and properties alone.

The difference in combustibility of the coal blends was analysed using the TGA and TG parameters were calculated on the resultant mass loss profiles. The variation between each of the curves was minimal as expected because coal blends are selected to ensure consistency in operation. Blends 11, 12 and 13 were more readily combustible as opposed to 7 and 9 which were less combustible. Blend 7, with reference to the XRD, did not contain illite, which could explain why it didn't burnout as well as the others. The combustibility of coal blends was compared to the LOC in the dust, and despite the stratification and weak correlation, it could be observed that ignition temperature was related to increased LOC in the dust.

Relationships between coal blend chemistry and LOC concentration in the dust were difficult to ascertain, due to the stratification in the data caused by the lack of variation in the coal type.

The introduction of coal-related process data removed the stratification in the scattered data sets. Although there was more variation in the process data, this was still too limited to draw any reliable conclusions as to which parameter has any influence on the LOC in the dust

The lack of relationship in all of the parameters identified the limitations of the 12-hour averaging. The fast-changing parameters were not truly represented by the averaged data and hence relationships were not observable. In this case, it has been recognised that a campaign-long analysis of coal types and LOC in the dust was required to provide enough data, to reduce the effects of stratification and provide more information on potential impacts on LOC in the dust.

The process data, especially blast volume highlighted the further limitation for the 12-hour data average, observations made were that increased blast volume led to decreased dust output. The weak correlation and the fast-changing blast volume mean that the data was not a true reflection of the process and LOC in the dust.

The lack of relationships identified in the process data in this chapter was the inspiration for the work in chapter 4.4 to increase the sampling resolution. The limited observations with the coal, however, are more difficult to overcome and it has been

recommended that an increased sampling and testing regime was required in future work to overcome the stratification in the data. This will allow a deeper understanding of the coal-type influence along with the process parameters. This work was aimed at testing the hypothesis ‘Coal combustion in the raceway can be impacted by process parameters and the evidence can be found in the fingerprint of blast furnace dust.’ The limited data acquired from the analysis within this chapter meant that further work was required to answer this hypothesis. To help test the hypothesis further, the increased resolution of sampling was addressed with the introduction of a dust probe to continually monitor the dust output in chapter 4.4.

4.4 Integrating Technology onto the Plant

4.4.1 Introduction

It is possible for steel plants to experience large, semi-isolated dust release incidents, where volumes of material can saturate the wet cleaning system. These incidents present the extremes of dust output and process conditions need to be further understood so that these events can be mitigated[120]. Integrating the technologies developed during this thesis will allow for continuous monitoring of the dust output to pinpoint the exact time of dust release, it would also provide the platform to look back at live data and optimise conditions for minimising dust levels.

To build upon the work from chapter 4.3 of this thesis and provide a continuous monitor for dust output, a move towards live monitoring of the dust conditions of the furnace was proposed. Many techniques to monitor the dust output were explored, including microwave technology for inside the downcomer for continuous emissions monitoring (CEM), optical imagery of the dust cloud in the downcomer and infrared technologies. The access to the downcomer was rejected due to safety concerns and the high concentrations of CO in the area, restricting access for installation and maintenance. The cost of microwave technologies exceeded £150,000 and was therefore deemed beyond the scope of this work. As an alternative, a suspended solids probe was procured, to monitor the dust output after the first gas cleaning system. This method was cost effective and safe to implement. Here, the dust catcher has stripped around 50% of the dust, and the remaining gas and dust travel through a water cleaning system, where around 750m^3/hr of flowing water, washes the remaining dust out of the gas[68,121].

There are many benefits to optimising the dust output and the degree of coal gasification of the ironmaking process. Experimental injectants and reductants can be used on the furnace and the output can be monitored to highlight any detrimental effect with ease, also experimenting with lower-cost blends of fuels can offset the cost of iron manufacture significantly. Coke is replaced when injecting coal into a blast furnace, around 200 kg/tHM of coal is the limit of injection currently, but with a greater understanding of coal and dust generation, this value can be maximised. Dust reduction was another key benefit. Approximately 80 tonnes of dust per day is generated in each blast furnace, but it can be anticipated that this figure could be reduced by up to 15%,

with a deeper understanding of how the blast furnace process parameters influence dust generation and ensuring the maximum gasification of coal is realised in the furnace.

The present work aims to compare the dust output of the furnace with process parameters and conditions, to identify which parameters have the largest influence on dust generation. Using a high-frequency sampling device, the output of the furnace can be measured and compared against the process parameters at that given time. Once the relationship is understood, the conditions can be modified to minimise the dust output. Another key target of the work was to identify a relationship between dust output and the carbon types within the dust itself. It was hypothesised that increasing dust output was related to increasing LOC, should this be true, the high frequency sampling device can be used to measure the degree of coal gasification of the process.

4.4.2 Event Analysis

Blast furnace iron manufacturing is a continuous process, only stopping for routine or unplanned maintenance. Process conditions and operating parameters change regularly to maintain a stable operation and production of high-quality material. After a period of instability lasting approximately 15 hours, the operators reported a volume of black dust material floating on top of the clarifying pond. The discovery was very similar to the incident that occurred at Redcar steel works as depicted in Figure 129. The first observation was that the material was very fine compared to typical BF dust and the material was oily. The oil prevented the particle size distribution characterisation technique from being carried out. Another observation was the sheer quantity of material when compared to the normal conditions in Figure 130, the mass of material was more indicative of an accumulation of events as opposed to a singular event such as a blow-through, which was an area of increased porosity in the descending burden, allowing a direct channel for dust through the burden into the gas stream. The final observation was that the material was in fact floating. Typical BF dust sinks to the bottom of the pond, hence the weir system design where dust sinks to the bottom and clean water flows over the sides. The floating material indicates hygroscopic properties. Charcoal and low-ordered carbon types are hygroscopic according to the work of Wang *et al.*[122]. This observation infers that the material was likely to be coal char.

Figure 129 Blast furnace of Teesside char float, image obtained from meeting with blast furnace expert Peter Warren[120]

Figure 130 a) BF5 weir pond with no float material b) normal degree of float material expected

4.4.3 Material Analysis – Event Analysis

To determine the source of the dust, the morphology of the float material identified in section 3.2.7 and 4.4.2, the sample was compared to a typical BF dust in Figure 131. To understand the results from the analysis of the float material, sample 1 from the

catalogue of samples discussed in section 3.2.7 was analysed to draw direct comparisons. The similarities and differences were used to identify the material and sources of material constituents. The size distribution was much finer than BF dust, and the morphology was more regular in the float dust, indicating the heat processing of the material. The presence of cenospheres was not clear in the bottom images of Figure 131, which would indicate the presence of coal char, but the very fine dark particles indicate the presence of carbon dust according to the work by Nedeljković *et al.*[168]. The particle circled in Figure 131, indicates the presence of either potassium or sodium chloride, similar particles have been found in the work by Stamboroski *et al.*[169]. The increase in chloride for the float material according to the EDS in Table 36 was noted, along with potassium and sodium which supports the findings in the image. The increase in alkali metals, including zinc, was indicative of coal or coke carbon presence in the dust as previously discussed in section 4.1.2 of this thesis. The decrease in oxygen indicates a decrease in oxides present and infers the alkali metals are in the form of chlorides as opposed to oxides. The presence of chlorides indicates the presence of coal char in the dust[170]. Chlorides present in BF dust exist when chlorine was released during coal combustion, as indicated by the work of Sun *et al.* and Nomura *et al.*[171–173]. The increase in sulphur supports the presence of coke and coal in the dust as discussed in section 4.1.2.

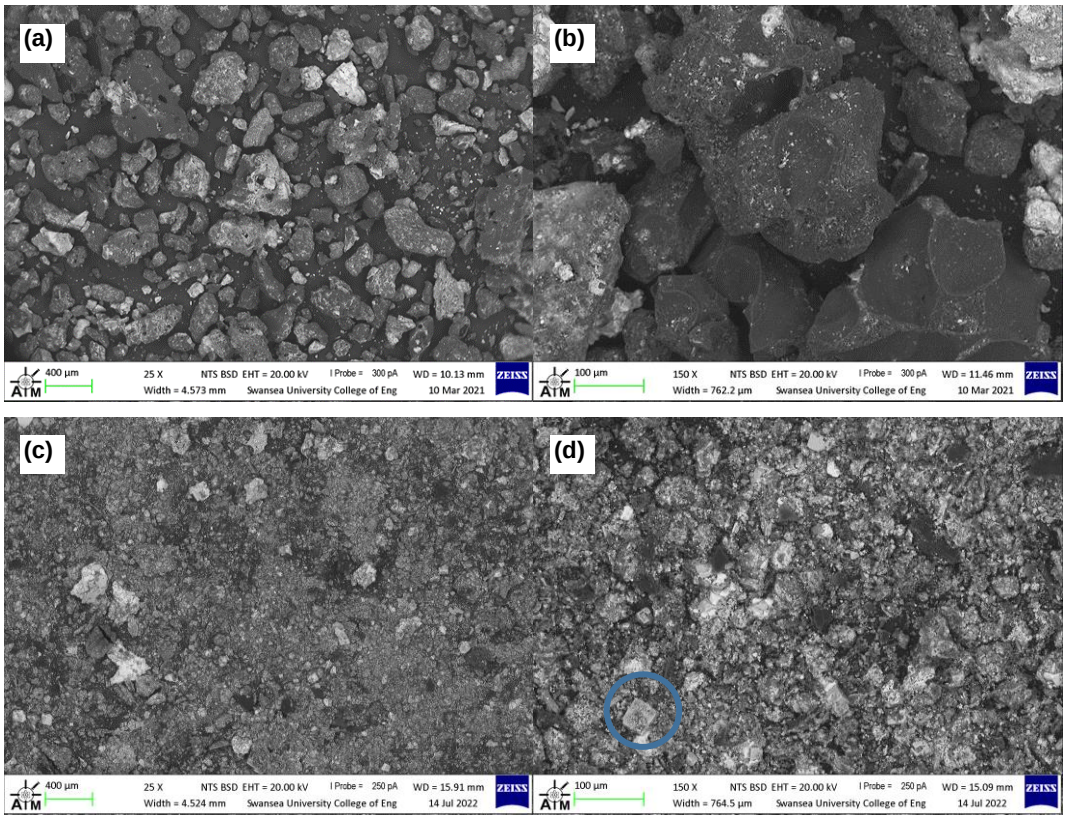

Figure 131 SEM Micrographs of blast furnace and float dust a) 25x magnification blast furnace dust b) 150x magnification blast furnace dust c) 25x magnification float dust d) 150x magnification float dust

Table 36 EDS analysis of BF dust and float dust

SEM	Cl %	O %	Fe %	K %	Na %	Zn %	Ca %	Mg %	S %	Si %	Al %
BF dust	0.9	62.2	12.3	1.3	0.0	2.4	1.5	0.4	0.9	1.6	0.0
Float Dust	27.3	18.9	12.5	10.3	10.0	8.0	3.9	3	2.9	1.8	1.5

The increase in sodium, zinc and potassium are also noted in the ICP-OES analysis in Table 37. The iron content was the same in both the furnace dust and the float dust. Indicating the changing material type was caused by the carbonaceous raw materials as opposed to the ferrous-based materials.

Table 37 ICP - OES analysis of BF dust and float dust

ICP-OES	Fe %	Zn %	Cr %	K %	Pb %	Ni %	Cu %	Ba %	V %	Na %
BF dust	20.61	0.09	0.00	0.09	0.00	0.01	0.00	0.09	0.03	0.01
Float Material	20.31	0.18	0.00	0.33	0.00	0.00	0.00	0.00	0.00	0.03

The CET reveals that 62% of the material was LOC and 2.7% was HOC, the DTG in Figure 132, shows the DTG for the float dust resembles that of coal char. A very large LOC peak compared to the HOC peak indicates the material was predominately coal char. The lack of coal hump at 270ºC was clear in the TG for float material, indicating the coal has been heat-treated, and was present in the form of char as opposed to raw coal.

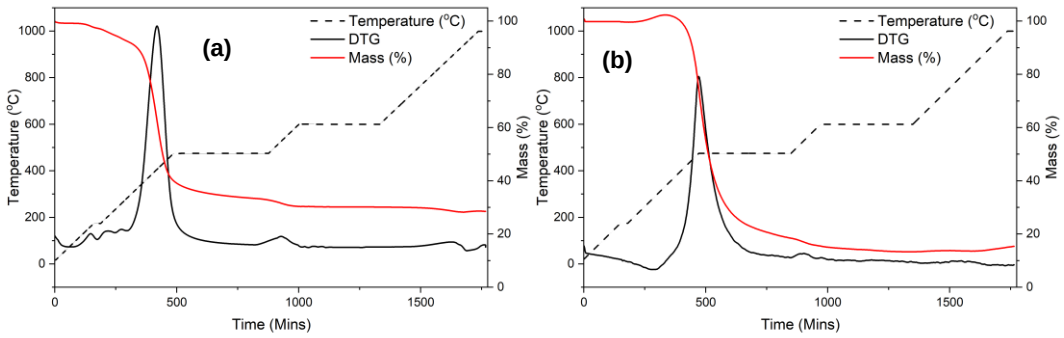

Figure 132 DTG and TG analysis a) float dust left b) coal char

The XRD spectra in Figure 133, shows the key differences in the phases for float dust versus typical BF dust. The amorphous carbon region between 28 and 33º was far smaller in the float dust because there was less influence from graphitised carbon or HOC. The peak shows more aromaticity in the carbon type. The increase in quartz was notable and it was likely this supports the analysis that it was coal char or coke material predominately. The CaO_4S peak indicated the presence of flux in the dust. The increased intensity in Metallic Fe indicates the reduction of iron ore at higher levels within the furnace, possibly due to unstable temperature conditions or increased CO, from the oxidation of increased carbon levels further up the furnace. The increased presence of AlO in the dust, according to the work of Zhongmin *et al.* indicates the presence was due to slag formation, however, the work of Czarna-Juszkiewicz *et al.* indicates the presence was due to coal ash, which supports the Thermogravimetric analysis[174,175].

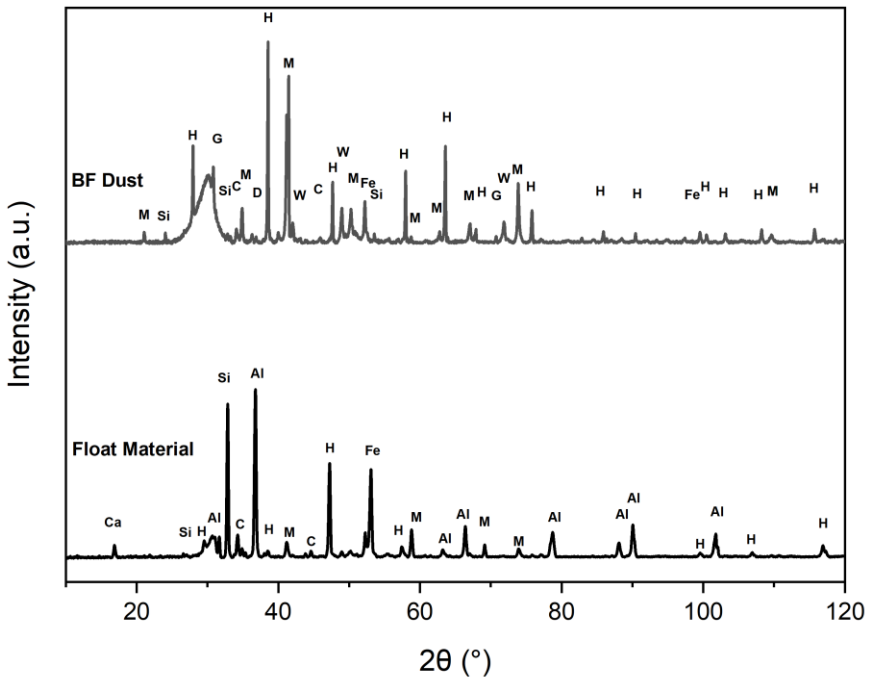

Figure 133 Powder X-Ray diffraction of BF Dust and float materials. H = Hematite (Fe_2O_3 – COD# 9000139), M = Magnetite (Fe_3O_4 -COD# 1011084), W = Wustite (FeO – COD# 9008636), C = Calcite ($CCaO_3$ – COD# 9016200), Si = Quartz High (O_2Si – COD# 1011200), G = Graphite (C – COD#9011577), D = Dolomite ($CaMg(CO_3)_2$ – COD# 9000885), Fe = Iron (Fe – COD# 4113941), Al = Aluminium Oxide (Al_2O_3 – COD# 4124784), Ca = Calcium Sulphate (CaO_4S – COD# 1537315)

Process Conditions

The analysis indicates that the material floating on the clarifying pond was likely coal char. For such a vast quantity of coal char, this presented a unique opportunity to identify the root cause in terms of process parameters. Figure 134, shows that 37 hours before the discovery, the coke rate was increased by 160kg/tHM. This action is normally taken to improve stability, by removing coal injection when an issue arises. As can be seen in Figure 134, the coal rate remained high for 7 hours after the coke rate was stepped up. The fuel rate in the furnace for 7 hours was imbalanced, potentially leading to a build-up in coal char, although it was not uncommon to overlap the fuelling to allow for the coke to descend the furnace to replace the coal as a reductant. The increase in blast volume at the time of the coal rate stop was to improve the combustion environment of the raceway in the absence of an injectant.

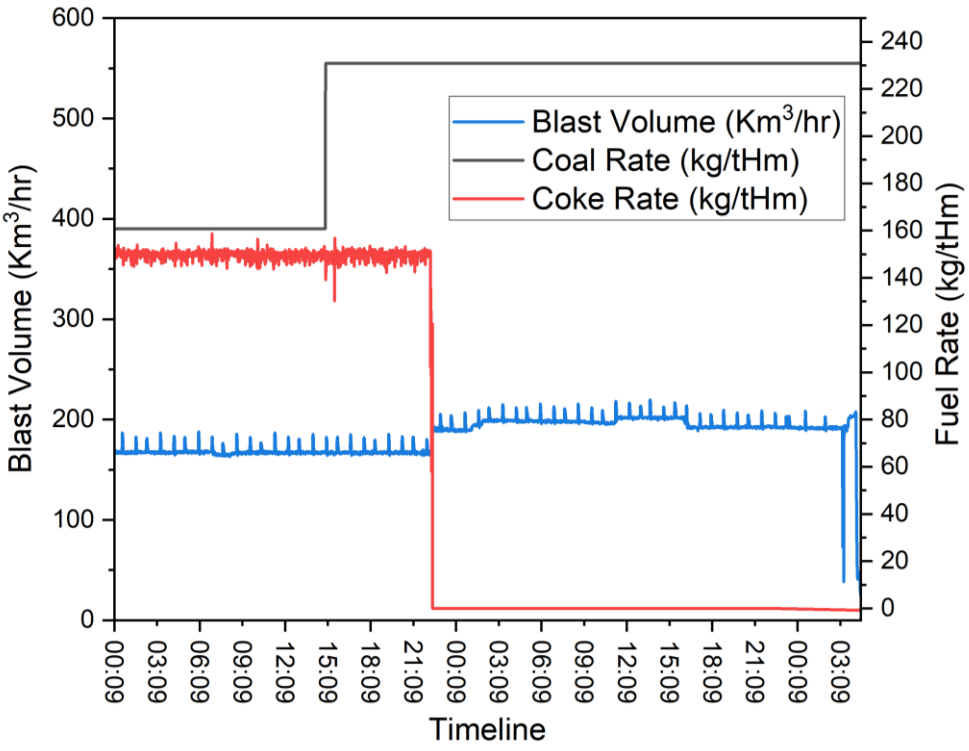

Figure 134 Line graph to show blast volume, coal rate and coke rate, for 52 hours before the sampling event.

Figure 135 shows that at the same time the coal was taken away from the furnace, the oxygen setpoint was reduced to 0% also. Any remaining carbon in the raceway at that time would be subject to a depleted oxygen condition and combustion would not be favourable. At this time, the coke rate was high in the furnace and fuelling from Figure 134 had been imbalanced for 7 hours potentially leading to an accumulation of non-combusted carbon in the furnace. This information proposes that although the root cause was a singular event of fuel imbalance and lacking oxygen conditions, the accumulation of 7 hours of overlap contributed to the volume of coal char floating on the surface of the clarifying pond.

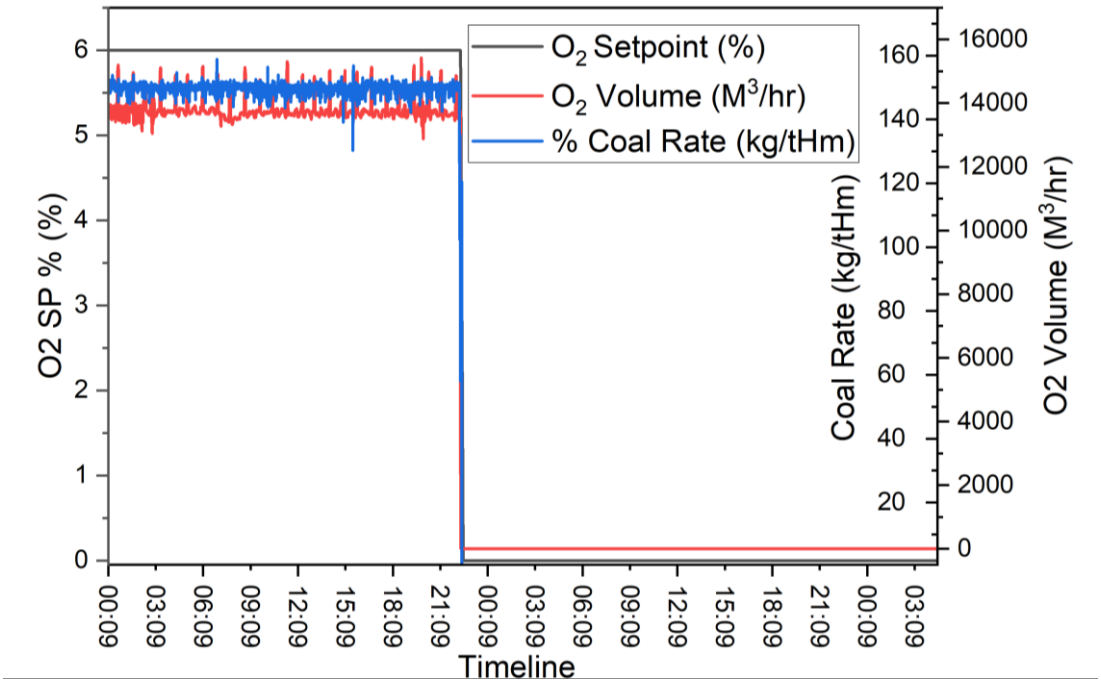

Figure 135 Line graph to show O_2 setpoint, O_2 volume and coal rate, for 52 hours before the sampling event.

The gas conditions in Figure 136 show a large drop off in gas efficiency at the end of the event, meaning the CO increased in comparison to a decrease in CO_2, indicating the incomplete combustion of coal. The changes in blast volume after the coal was removed are reflected in the instability in gas efficiency. In the right-hand graph, after the coal was removed there was a drop-off in H_2 generation. H_2 as discussed previously was beneficial to iron reduction but was present due to the combustion of coal. The decrease in H_2 shows that less combustion of the coal was occurring hence less H_2 is liberated.

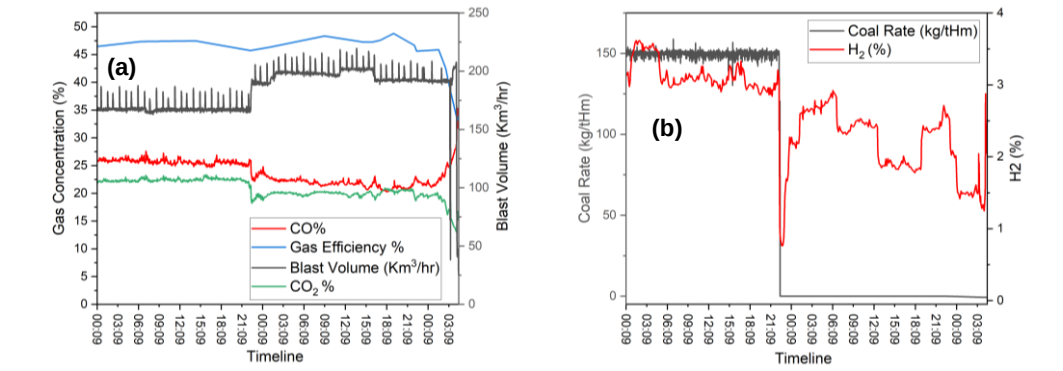

Figure 136 Line graphs of process traces over time for 52 hours before the sampling event a) CO%, CO_2%, gas efficiency and blast volume b) coal rate and H_2

The pressure data in Figure 137, shows a steady decline in blast pressure and delta pressure. There was a drop-off of maximum differential pressure around 22 hours before the discovery of the dust. This indicates that the permeability of the furnace was higher at this point, and the difference between the high top pressure and blast pressure was less at this point. The increased permeability would lead to unburnt particles reaching the gas stream, being a more likely occurrence than with periods of decreased permeability, with fewer channels for the gas and the dust to pass through in low permeability, high max differential pressure scenarios. The operators here reduced the max differential pressure due to the instability within the furnace to control burden descent conditions[99].

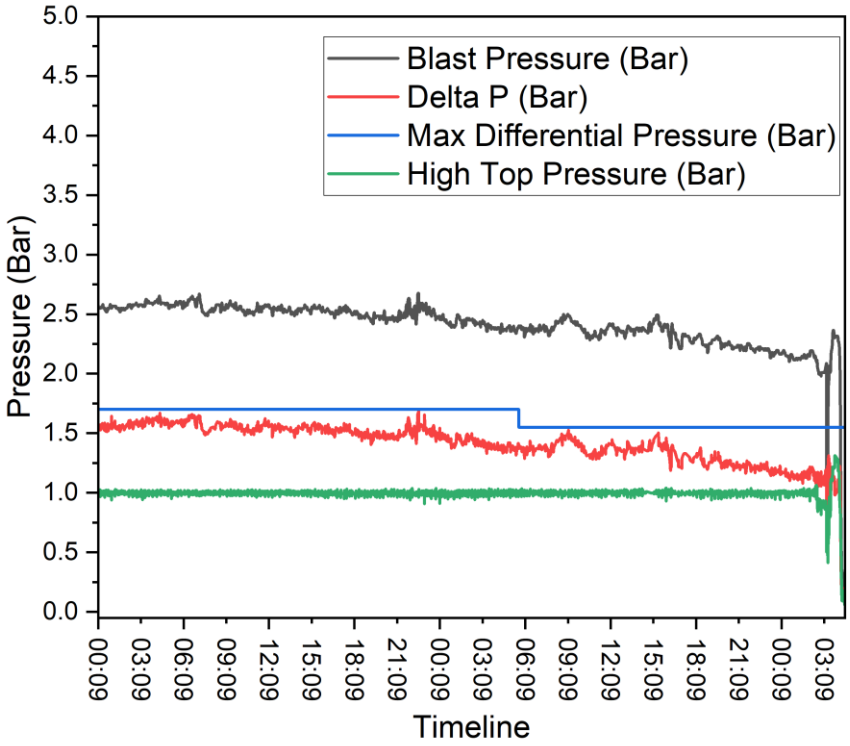

Figure 137 Line graph to show blast pressure, Delta P, max differential pressure and high top pressure, for 52 hours before the sampling event.

The temperature conditions were monitored in Figure 138, where the temperature can be seen to reduce around 7 hours after the coke increase, in line with when the coal injection stops. The work by Shan Wen Du outlined in section 2.8.3 of the literature review says that blast temperature promotes burnout of coal. The blast temperature was lowered to control the flame temperature of the raceway, with an all-coke fuelling, the furnace runs hotter than with coal. The flame temperature was indicative of no coal combustion, but the decrease in blast temperature at the time when coal injection was shut off would have led to decreased combustion of any coal present in the furnace at the time. The top temperature loses stability with increased coke rate and the variation indicates issues with burden permeability, hence the switch in max differential pressure in Figure 137.

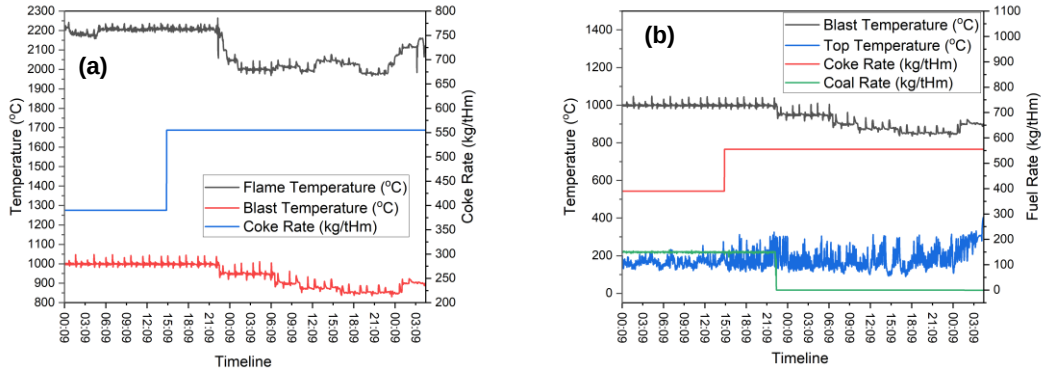

Figure 138 Line graphs of process traces over time for 52 hours before the sampling event a) flame temperature, blast temperature and coke rate b) blast temperature, top temperature, coke rate and coal rate

From the process information the largest influence and leading cause of coal char in the dust, was the fuelling rate imbalance for the 7 hours before coal was shut down. The decrease in blast temperature shortly after certainly influenced the combustion of any coal remaining, as did the decrease in oxygen rate at the time. The operators were trying to balance burden descent and retain stability by switching fuels and changing the max differential pressure, but the build-up appeared to have begun before it could be remedied. In the event of instability and a requirement to switch to all coke use on the blast furnace. It is therefore advisable to ensure any coal flowing into the furnace is accounted for in terms of combustion environment, to prevent coal char flooding the gas stream and the change to all coke is gradual as opposed to instant. Such a large change to the furnace would allow a slug of material to exit the furnace which appears to have occurred on this occasion.

4.4.4 Dust Monitoring and Validation

To quantify the dust coming out of the furnace at any given time, the probe was used to measure the dust concentration of the water from the wet abatement of the blast furnace as per Figure 139. This was a step towards a live data output of the furnace dust and visualisation of process conditions that influence the dust output. Justification for this probe also stems from the event discussed in section 4.4.2. If this probe was in place, the dust flowing into the pond could have been pinpointed within 30 seconds of release and the exact conditions analysed, to troubleshoot the issue better.

Figure 139 a) The location for sampling b) the reading in g/l for the dust monitor c) the probe submerged

Relating dust output to combustion conditions

The previous work of chapter 4.3.5 highlighted limitations in terms of using 12-hour composite samples to analyse the carbon type within the dust, for diagnosing issues with the coal injection or process parameters. Samples were taken in parallel to measurements for dust output using the probe and analysed for LOC to HOC ratio (LO:HO) ratio. Figure 140 shows the trend for the LO:HO, for the dust within the water and the mass flow of solids out of the furnace. The LO:HO decreasing demonstrates an increase in LOC or coal-originating carbon type per HOC or coke-originating carbon type. There was a weak negative correlation between the LO:HO ratio and the dust output with a Pearson's coefficient of correlation of -0.23, in essence as the LOC concentration within carbon increases, there was an increase in dust output also. The presence of this relationship was more significant than the strength of it. Typically, the CET takes >1600 minutes for one sample, on the contrary, this probe technique allows for continuous measurements of the dust output, with a resolution of 30 seconds. The enormous increase in data would provide a better representation of blast furnace processes. The relationship means that total dust output from the blast

furnace can be used to identify the conditions to minimise the dust output, and it was likely that the degree of gasification of coal was improved as a result. Occurrences where dust generation was low and LOC content was low would indicate a strong combustion environment within the furnace and a desirable operating condition.

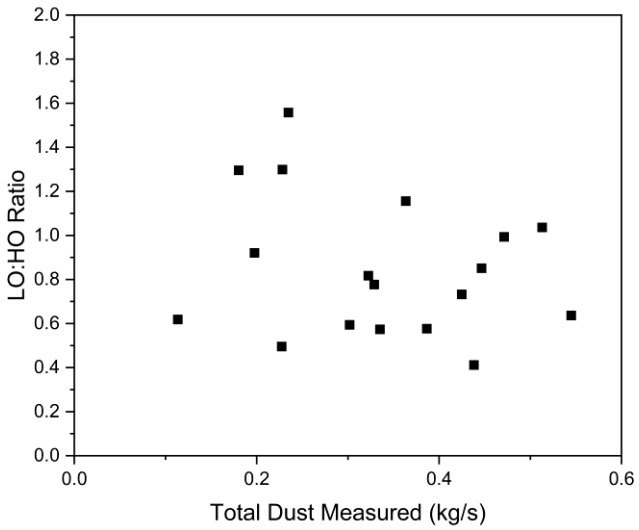

.

Figure 140 Total dust output versus LO:HO ratio to demonstrate the relationship

Oxygen Trial

According to Zhou *et al.* oxygen is often utilized to promote combustion in the raceway. Increasing oxygen leads to increased carbon conversion to CO_2 and improved combustion conditions within the raceway[176]. A trial was undertaken where the oxygen set point of the furnace was adjusted and the dust output measured whilst maintaining all other conditions and stable operations. The output of the trial can be seen in Figure 141. There was no clear change in the dust output observable, which was related to manipulating the oxygen set point. A second trial was conducted (Trial 2) where there appears to be a decrease in the dust output when the setpoint was decreased, which would contradict the literature, but this being the only observation, it was not clear enough to say the decrease in oxygen was the cause of the change in the dust. A notable difference between the trials includes steam use, steam was used during Trial 1 and not in Trial 2. This appears to have reduced the variability of the dust output, due to improved raceway temperature stability. The oxygen setpoint on average was higher in Trial 2. This would also lead to increased variability of dust

output due to the instability of the raceway condition. The *Charfoco* report and Wing *et al.* according to section 2.9 in the literature review, show that oxygen enrichment showed no significant effect on the conversion degree of coal and it was determined that the complete conversion of coal could not be reached under high injection rates. Wing *et al.* did mention that high oxygen enrichment led to increased char consumption in the raceway.

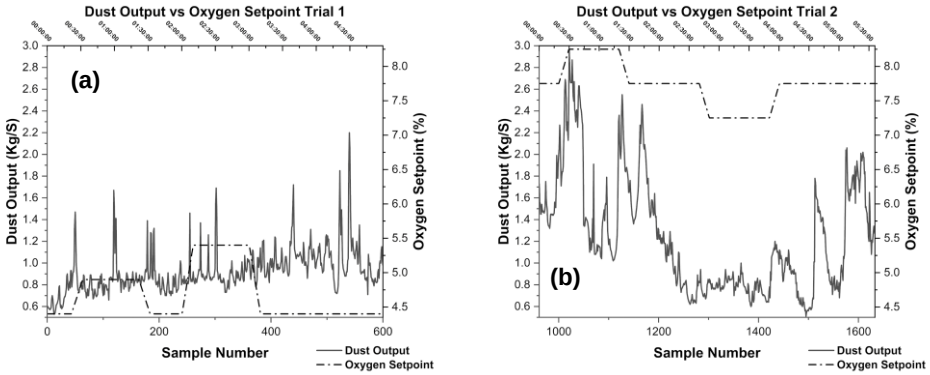

Figure 141 Graphs to show dust output versus oxygen conditions of the blast furnace a) trial 1 b) trial 2

With increased oxygen there is generally increased fuelling demand, this phenomenon was examined in Figure 142. Figure 142 shows 3 graphs of the measured dust output versus a coal per unit oxygen ratio (CPO ratio), this ratio calculates the moles of carbon per moles of oxygen present in the furnace at any given time. This was an improved measure for considering dust output, essentially higher values for CPO infer an abundance of carbon per oxygen in the furnace at any given time. These conditions are unfavourable in terms of combustion in the raceway, therefore it was observed that with increasing CPO there was increasing dust output in graph (a) of Figure 142. In graph (b) it can be observed that high values for CPO cause instability and spikes in the dust output. In graph (c) the observation was made that the dust output was not sensitive to big deviations in CPO, but after the burden check event, the dust output remained low, despite the CPO returning to stable levels. A burden check is where the blast is reduced temporarily allowing for a pressure drop in the furnace, to move a stuck burden to allow it to descend again. Graphs (d) and (e) show that despite the CPO returning to normal levels, there was a large decrease in coal flowing into the furnace as indicated in the drop in the production rate of graph (e). A clear relationship exists between oxygen and coal, although these parameters do not influence the dust

in isolation. The coal flowing into the furnace appears to have a larger influence than the oxygen conditions alone.

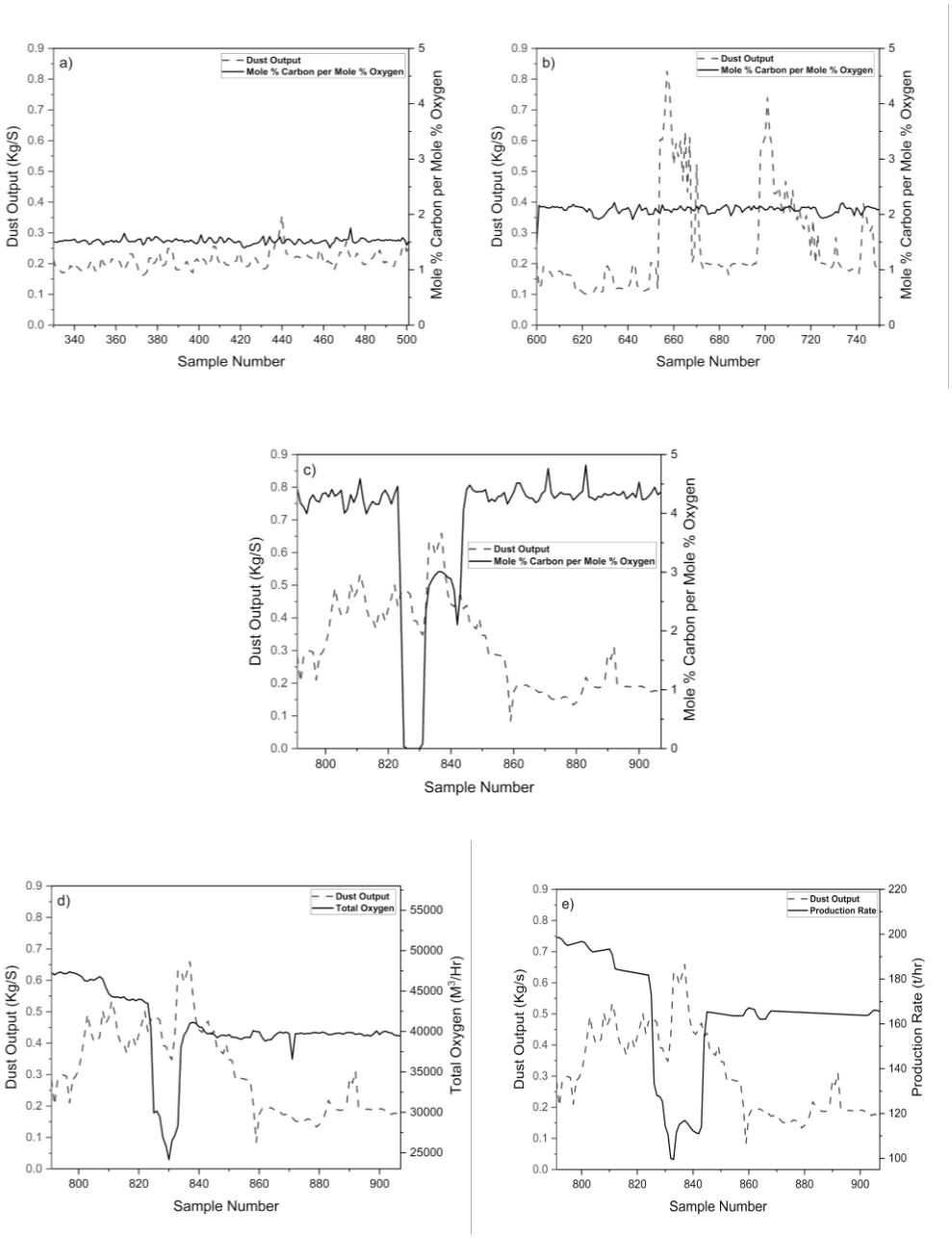

Figure 142 Graph a) dust output versus CPO observation 1, graph b) dust output versus CPO observation 2, graph c) dust output versus CPO observation 3, graph d) dust output versus total oxygen observation 3, graph e) dust output versus production rate observation 3

Blast Volume

Blast volume is the volume of hot air that is blasted into the bottom of the furnace, providing the heat and oxygen required for the necessary Boudouard reactions to occur, for the reduction of iron ore. Gas residence time is related to blast volume, with

increasing volume leading to decreasing residence times according to Yu *et al.*[166]. This means with lower residence time, the coal is not subjected to the higher temperatures and oxygen conditions of the raceway long enough for it to fully undergo the five key stages of combustion discussed in section 2.7. The observations of blast volume versus dust output are seen in Figure 143. In graph (a), spikes in the blast volume were followed closely by a spike in the dust output. In graph (b), low blast volume conditions led to an unstable dust output. In graph (c), there was a step down in the blast volume followed by a decrease in the dust output. The data for dust output was clearly sensitive to the changes in blast volume and therefore it must be a significant influencing factor in the reduction of dust output.

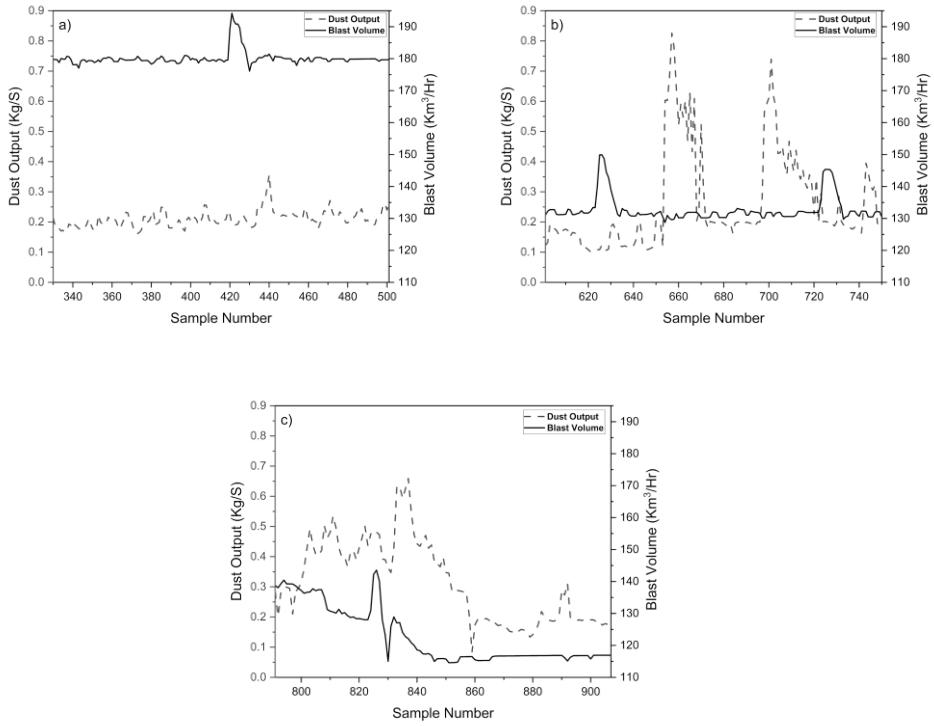

Figure 143 Graph a) dust output versus blast volume observation 1, graph b) dust output versus blast volume observation 2, graph c) dust output versus blast volume observation 3

Blast Pressure

Blast pressure is similar to blast volume, in that increased pressure leads to reduced residence times of the gas and coal in the raceway[99,177]. This translates to increasing the blast pressure, which should increase the dust output of the furnace. However, the key difference between pressure and volume is that blast pressure is a variable that operators adjust to maintain an overall differential pressure in the blast furnace. This was a reaction to changes in the permeability of the burden present in the

furnace, with decreased permeability there was a decrease in the differential pressure. The observations can be seen in Figure 144. Graph (a) shows a contradiction to the expectations from the work of Azadi *et al.*, with increasing blast pressure, there was a decrease in the dust output. In Figure 144 graph (b) there was another contradiction to the literature, where the dips in the blast pressure, are shortly followed by spikes in the dust output. Figure 144 graph (c) supports the literature, a step down in blast pressure led to a decrease in dust output average, and the same effect was observed in Figure 144 graph (d). To discuss the contradictions in the data from graph (a), the high blast volume at the time of these measurements was notable from Figure 143 graph (a) at this given time. The high blast volume appears to have a larger influence on the dust output than the blast pressure. For the disagreement of the state of knowledge, observed in graph (b), the low blast volume observed in Figure 143 graph (b) at this given time and the high coal rate in Figure 144 graph (e) appears to have a larger influence than blast pressure alone. This shows that the coal rate appears to have a large influence despite the low residence time, contributing to the instability within the data. The influence of blast pressure and the contradictions help support the theory that furnace parameters are not influencing the dust output in isolation. Parameters should be considered in pairs or triples to identify the conditions to maintain or produce low dust outputs.

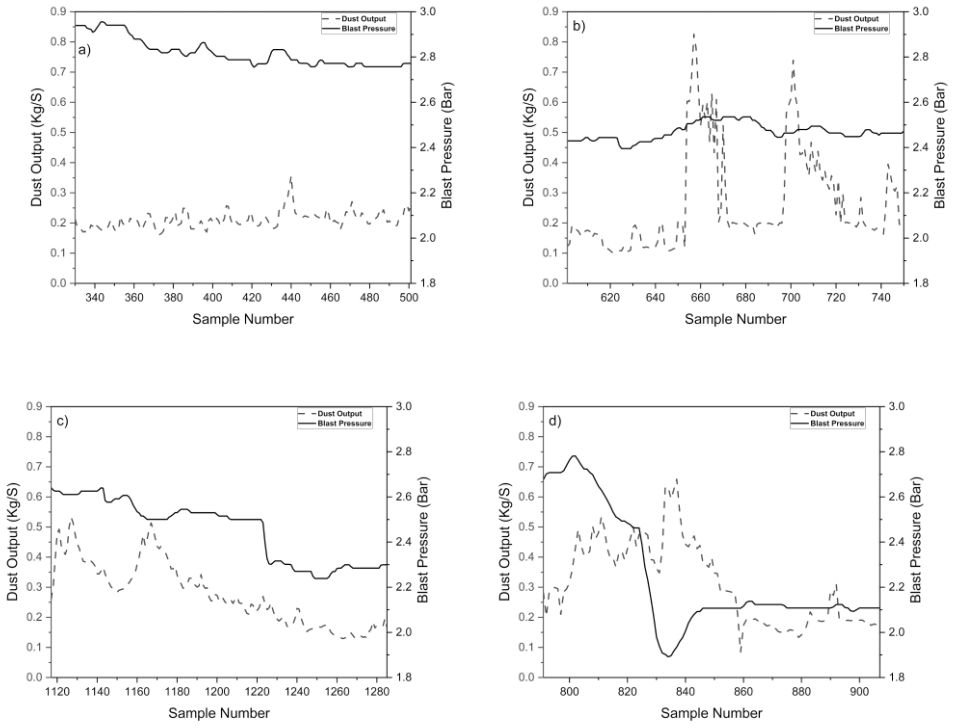

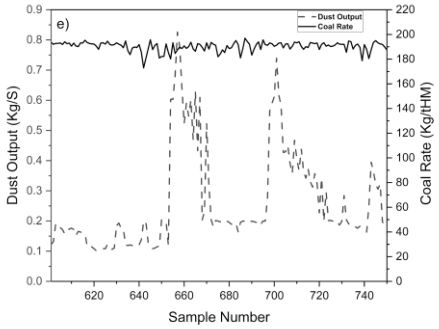

Figure 144 Graph a) dust output versus blast pressure observation 1, graph b) dust output versus blast pressure observation 2, graph c) dust output versus blast pressure observation 3, graph d) dust output versus blast pressure observation 4, graph e) dust output versus coal rate observation 2

4.4.5 Node Mapping and Future Work

To improve the understanding of the impact of all process parameters on the dust output, a Ball Mapper algorithm has been applied to the data presented in this paper[123]. The aim of this map is to highlight areas of interest within a large dataset. The aim is to select nodes where dust output is low and investigate the conditions of the blast furnace at that given time, this information will inform the model of an ideal set of conditions for low dust output in the furnace. This algorithm aims to group the high-dimensional data into nodes to create a representation of the data as presented in Figure 145. Each node corresponds to a ball of a fixed radius in the space of parameters. This means that all the observations in the same node have similar values for the parameter values. Since the object of the study was to investigate dust output, this was not used as a parameter in constructing the map. Where observations were shared between different nodes when the parameter values are close to observations in both nodes, a connection was drawn between the two nodes. The size of a node indicates the number of observations contained therein. The x and y axis and location of the nodes has no bearing on the output of the map, nodes are grouped together with other nodes that contain similar variables.

To enable further analysis, each node in Figure 145, was labelled with a number. The nodes were coloured according to the mean dust output for the observations in that node. Note that this information was not used when constructing the Ball Mapper graph. White nodes indicate low output, and purple nodes have high

output. The darker the colour the higher the dust output produced by the conditions described in each node was.

Nodes 4, 5 and 6 together contain only 8 observations and were of little interest. Nodes 7 through 12 contained 129 observations around a burden check event on the blast furnace and therefore are not useful in this analysis. A burden check is where the blast furnace temporarily stops to allow a stuck burden to descend. This node mapping exercise suggests that the key areas of interest were node 1, with 600 observations, the entire first sample run, which includes a set of conditions that were responsible for generating a low dust output condition, and nodes 2, 3, 13 and 14, which had moderate dust output and form part of a cluster of 1,440 observations, which also includes higher dust output nodes. This observation indicates the existence of multiple distinct combinations of parameters resulting in low-dust performance. The existence of combinations enables different ways of minimising the dust outcome depending on the initial condition of the furnace.

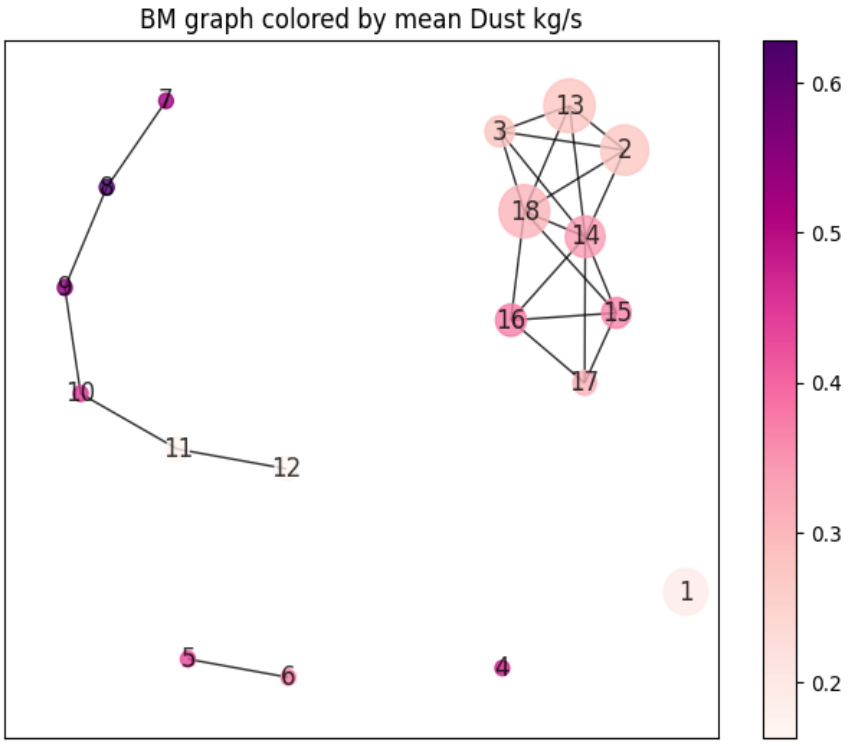

Figure 145 Node map grouping nodes of similar datasets. Blast furnace parameters versus dust output

The ball mapper algorithm was applied to the data collected using the probe as described previously. In Table 38, the values in node 1 are compared with the values

in the larger cluster. The mean value for the region was compared to the global mean. Almost all variables are different from 0 at the 95% significance level. The separation of these two groups indicates that the variables differed before considering the dust output. Table 38, therefore, shows the difference between node 1, which was precisely the set of observations from Trial 1, and the other observations. It was not possible to conclude which variables are responsible for the lower dust levels in Node 1. This trial featured high blast volume, blast temperature and blast pressure, and steam was applied throughout, making it particularly unusual.

In Table 39 the larger cluster was considered in more detail. Within this cluster, dust output was positively correlated with variables relating to the intensity of the process, such as blast volume, production rate and coal flow rate. Variables relating to temperatures, such as flame temperature and blast temperature, are associated with lower dust output. This supports the theory that coal combustion was relative to dust output. Higher temperatures lead to an improved combustion environment and therefore lower dust output. The effect of increasing blast volume, coal flow rate and blast volume are all detrimental to the combustion environment and reduce residence time for the coal within the environment, hence higher dust outputs were anticipated and found in these regions of the cluster.

The power of the Ball Mapper technique was clear. It allows the user to cluster the observations to study the differences between clusters and the relationships within clusters. Since the data was collected at high frequency, many of the data points were similar to the previous and subsequent data points, hence giving a false sense of data size. Around 2000 data points were considered in the model, most data points fall into the same set of nodes as the immediately preceding point. Only 123 observations generated a movement within the map. To improve the model, more data points must be obtained. A fixed probe will be installed in the launder in place of the probe used for these trials. The ability to measure continuously at 30-second increments will provide the data required to improve the model enough, to allow it to produce a set of ideal conditions for generating low dust output of the blast furnace.

Table 38 Comparison of parameter values in the largest cluster of nodes with Trial 1. Note that the two values are highly negatively correlated since the remaining data points do not contain many observations.

	Main cluster	Trial 1	Difference		Main cluster	Trial 1	Difference
	Standard Deviations Away from Mean				Standard Deviations Away from Mean		
Max Diff Pressure Bar	0.61	-1.57	2.18	**CO B %**	0.04	-0.26	0.30
O2 Set Point %	0.53	-1.50	2.03	**Production Rate t/hr**	0.13	0.06	0.07
CO2 B %	0.56	-1.37	1.93	**Top Temperature ºC**	-0.02	0.17	-0.19
Coal Rate kg/tHM	0.54	-1.35	1.88	**Delta P Bar**	-0.05	0.53	-0.58
H2 B %	0.57	-1.25	1.82	**Hot Metal Si %**	-0.15	0.48	-0.63
Coal per Oxygen Kg/Hr	0.52	-1.29	1.81	**Coke Rate kg/tHM**	-0.50	0.45	-0.95
O2 Volume m3/hr	0.52	-1.12	1.64	**Blast Pressure Bar**	-0.18	0.86	-1.04
Flame Temperature ºC	0.37	-1.19	1.57	**High Top Pressure Bar**	-0.22	0.89	-1.12
Coal Flow Rate Kg/Hr	0.47	-0.91	1.38	**Blast Volume Km3/hr**	-0.22	0.90	-1.12
Gas Efficiency % Co2/(Co+Co2)	0.37	-0.56	0.94	**Blast Temperature ºC**	-0.41	0.80	-1.21
Dust kg/s	0.30	-0.63	0.93	**Steam t/hr**	-0.39	1.12	-1.52

Table 39 Considering each node within the main cluster as a single observation, the correlations between dust output and other parameters

	Correlation		Correlation
Dust kg/s	1.00	**Delta P Bar**	0.49
Blast Volume Km3/hr	0.91	**Steam t/hr**	0.33
High Top Pressure Bar	0.83	**H2 B %**	0.05
Blast Pressure Bar	0.83	**H2 %**	0.01
Production Rate t/hr	0.81	**Coke Rate kg/tHM**	-0.25
Coal Flow Rate Kg/Hr	0.75	**CO %**	-0.49
Max Diff Pressure Bar	0.74	**CO B %**	-0.57
Hot Metal Si %	0.69	**Flame Temperature ºC**	-0.64
O2 Volume m3/hr	0.68	**O2 Set Point %**	-0.69
Gas Efficiency % Co2/(Co+Co2)	0.66	**Coal Rate kg/tHM**	-0.75
CO2 B %	0.66	**Blast Temperature ºC**	-0.81
CO2 %	0.65	**Coal per Oxygen Kg/Hr**	-0.83
Top Temperature Bar	0.59		

Figure 146 illustrates how the low dust output region of the largest cluster was also the area with the highest variability of dust output. The darker the purple colour the higher the standard deviation for the series of data. Node 1, the observations from the first trial have low standard deviation compared to the remainder of the dataset. To improve on this, in future work it has been recommended to install a fixed probe to gather vast sets of data over a variety of operating conditions.

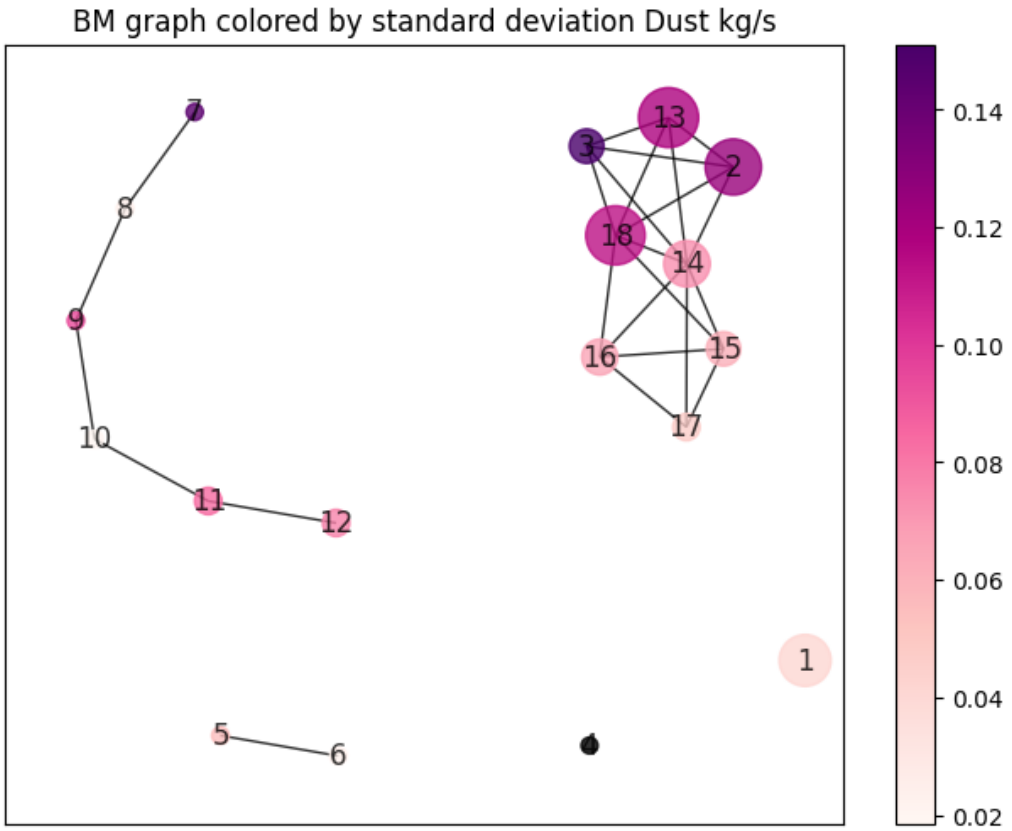

Figure 146 Node mapping coloured according to standard deviation of dust output.

4.4.6 Summary

The event of coal char floating on top of the clarifying pond, was analysed and it was found that 62% of the material consisted of LOC, likely in the form of coal char, this was supported by the SEM-EDS and XRD techniques. The process conditions showed that an imbalance in the fuelling of the furnace for a 7-hour period during the fuel switchover, led to an accumulation of non-combusted coal in the form of char in the dust. This fuelling imbalance combined with changes in max differential pressure with decreases in oxygen and temperature conditions, also contributed to the lack of coal combustion. Operators made changes in process parameters, unaware of the implications it would have on dust generation. This section also highlights the techniques that can be applied to all blast furnace wet cleaning systems in the event of dust on the clarifying pond.

A novel application for a suspended solids probe has been used to increase the frequency of sampling for the dust output of the blast furnace. The justification for this technique stemmed from the coal char incident on the clarifying pond and the limitations of the sampling of BF dust for the CET. There was a relationship between

dust output and LOC. With increasing LOC per HOC concentration within the carbon of the dust itself, there appears to be increased dust output. The suspended solids in water converted into dust mass flow measurements, were successful in determining some key operating parameters that can influence the dust output.

Blast volume, coal parameters, oxygen parameters and pressure all appear to influence the dust output to different extents, with some observations in pressure contradicting the literature. The weighting of such parameters carries the most influence and explains the contradictions in pressure. This work addressed the hypothesis after the limitations of data found in chapter 4.3, 'Coal combustion in the raceway can be impacted by process parameters and the evidence can be found in the fingerprint of blast furnace dust'

Combinations of multiple parameters appear to influence the dust output, as highlighted by the Ball Mapper graph. The conditions for low dust outputs can be identified using weighted correlations, however, the data set was relatively small in this case. According to the Ball Mapper, there are multiple regions of different operating parameters that have a low dust output, to explore these effectively, the high-frequency sampling process of the fixed probe will provide the data necessary to find these sets of operating parameters. Many of the 2000 data points the model consists of are too similar, to significantly validate the model. With increased data, an ideal set of conditions can be derived for the low production of dust, based on the observations from normal routine operations.

The increased data will stem from the installation of the fixed monitor, to be installed during a blast furnace stop, where the flow of water will be reduced. It has been recommended in future work that the output from the probe be analysed using the Ball Mapper technique to determine a model for a set of conditions, designed for low dust output and stable conditions in blast furnace ironmaking.

5 Conclusions

The aim of this research was to understand what raw materials from the blast furnace ironmaking process were present within the blast furnace dust. The focus was on the LOC or coal char type carbon present within the dust as this presents limitations in terms of coal combustion in the raceway. The scope for the research included the development of novel techniques for carbon type differentiation, right through to the application of techniques to identify the impact of process parameters on dust generation. The following hypotheses were answered throughout the thesis:

1. 'The raw materials that feed the blast furnace are expelled into the gas stream and all influence the blast furnace dust'

2. 'Thermal techniques can be used to differentiate carbon sources in dust generated in blast furnaces that use granulated coal injection'.

3. 'Coal combustion in the raceway can be impacted by process parameters and the evidence can be found in the fingerprint of blast furnace dust'

The most impactful conclusions of the work presented were as follows:

- The Winkler method[78] proved most successful when the acid stage was optimised to an acid blend of Aqua Regia named Acid 1. This was deemed a suitable replacement technique for the CET because of the ability to run samples in batches and reduce the testing time.
- The separation of the dust outlined in section 4.1.3 supports the modelling work of Winfield *et al.* but with the use of live data[68]. The dry abatement of the gas cleaning system was the most representative place to capture the dust containing the carbon-based materials and the slurry appeared to show the presence of ferrous-based material carryover.
- The CET can be modified by increasing the ramp rate to 20^{o}C / min and return results within a reasonable degree of uncertainty (0.98) for LOC
- There is a relationship between dust output volumes of the blast furnace and the LOC concentration within the carbon of the dust, the increasing dust output leads to increases in LOC concentration within the dust.
- A novel technique for monitoring the dust output of the blast furnace for continuous monitoring has been used to demonstrate that blast volume, coal parameters, oxygen parameters and pressure all appear to influence the dust

output to different extents the weighting of each has been proposed to be investigated.

- 62% of the material found floating on top of the clarifying pond was LOC likely to be char. An imbalance in the fuelling of the furnace for a 7-hour period during the fuel switchover, led to an accumulation of non-combusted coal in the form of char in the dust. Max differential pressure, Oxygen and temperature conditions, also contributed to the lack of coal combustion.
- The novel dust output monitoring technique has the potential to unlock cost savings of offsetting coke as fuel by 20kg/tHM by optimising the process conditions, to improve the combustion of coal without the detriment to the formation of dust. The opportunity for the use of novel reductants is now less of a risk to business continuity as the effects on the dust output can be monitored using the dust probe.
- Blast furnace dust contains particulates from each of the raw materials that are used in blast furnace ironmaking. The presence of coal char indicates that coal gasification is not always successful in processes that rely on granulated coal injection.
- It was determined by TG parameters that blends 11, 12 and 13, which were the blends used within this work, with lower ash contents and higher volatile matters, should combust more readily when compared to the other blends, due to ignition temperature.
- Evidence of raw coal and not just coal char was identified in the dust as determined by TGA, SEM and XRD. Further work has been proposed to investigate the likelihood of coal to burnout in blast furnace gas conditions at lower temperatures.
- The novel application for dust generation using the suspended solids probe was validated using a recognised laboratory technique and it is deemed suitable for monitoring the dust output of the blast furnace.

Overall, this thesis has addressed the hypotheses and thesis aims raised following the comprehensive literature review. Opportunities to expand the body of knowledge even further have been identified and outlined. The impact of this work on industry and academia was apparent with the development of new tests right through to the application of known techniques to processes not previously examined.

6 Recommendations for Future Work

Opportunities to further expand the body of knowledge in this field of study have been identified through the research and have been identified in the thesis. These include works where either time was a limiting factor, or equipment availability was problematic. The opportunities have been summarised as follows:

From the experimental and methods chapter

- Samples from the cast house and the gas analysers should be considered in future comparisons with dust samples from the wet and dry abatements. This would give a more complete picture of dust generation and carbon distribution. Currently, carbon in the dust can be tracked from wet and dry abatements and hot metal, but some carbon will be present in the cast house dust and this is an opportunity for exploration.

From the carbon type differentiation chapter

- The identified digestion and combustion technique should be further refined, and an investigation into further shortening the combustion and digestion times should be carried out to optimise the conditions. Shorter turnaround times would lead to increased analysis potential.
- The effect of pre-treatment using the acids identified in the digestion and combustion technique of the samples for CET should be investigated. Removing residual elements whilst minimising the impact on the carbon type should be considered. This removes any residual chemistry effect on the DTG profile of the CET and gives a better carbon differentiation.
- The use of smart thresholding tools such as Intellisis should be explored as the potential of using the techniques on 3d imagery from the MicroCT. This has the power to unlock the potential for char counting in the dust and removes the human error aspect and the time constraints of the technique.
- Raman mapping of samples should be considered. The power of Raman in differentiating carbon types is huge but limited with point analysis. This would remove that limitation.

From the influence of process parameters chapter

- Extend the research on coal chemistry and coal type impact on dust generation to the length of the campaign of a blast furnace. This would remove the

stratification of the data with an increase in data size. This could take 8 years to obtain but with the lack of variation in coal data, there was a clear limitation to short-term studies.

- Burnout in the upper levels of the furnace should be considered to determine which coal blends if the coal gets through the raceway unreacted, would contribute less to the dust generation. This could be identified using gas burnout in the TGA, or burnout with gas conditions as follows. To determine whether raw coal that leaves the raceway would combust in the upper levels of the furnace, 1g ± 0.1g of the sample should be weighed into an incinerating square and heated to 600^{o}C and 800^{o}C in a 45-litre tube furnace under an inert 500ml/min N_2 atmosphere. Once at temperature, the reaction gas should be switched and the sample reacted for 30 minutes, before cooling back to room temperature under N_2 to prevent any further combustion. The samples should be weighed before and after to determine the burnout characteristics of the material in the upper levels of the furnace. The gases and temperatures recommended are outlined in Table 40.

Table 40 Parameters for upper-level furnace combustion trials

Trial ID	Temperature (ºC)	Gas Composition (%)				
		Air	N_2	CO	CO_2	H_2
1	600	100				
2	800	100				
3	600		100			
4	800		100			
5	600		55.2	20.8	21.3	2.7
6	800		55.2	20.8	21.3	2.7
7	600		46.0	25.8	23.9	4.3
8	800		46.0	25.8	23.9	4.3

From the integrating technology onto the plant chapter

- Microwave technology or alternatives should be investigated for suitability in the downcomer. The work in Chapter 4.1 of this thesis outlines the difference between material reaching the wet abatement and dry abatement. A sampling

probe at the source of the dust would provide better insight and provide stronger relationships with process conditions.

- To remedy the limitations of the manual probe, an automated probe was purchased and was due to be installed in position. The resolution of measurements could be set to any time, however, a sampling increment of 30 seconds was determined to suffice based on the frequency of changing conditions in the blast furnace. The probe was to be calibrated against a standard reference material, 4000 Formazin Nephelometric Unit FNU for ViSolid¨700 IQ and manual samples should be tested in the laboratory to validate the technique. Figure 147a shows the probe, the desired position of the probe in Figure 149b and the control unit Figure 149c. The probe will be installed during the next blast furnace stop. The flow of water should be stopped for correct installation and reinstated after calibration. It was recommended for future work, that process data and dust data from the automated probe should be analysed using the Ball mapper technique outlined in section 4.4.5. This increased data will provide a model on which the operating parameters of the blast furnace can be set for low dust output, without impacting the stability of production.

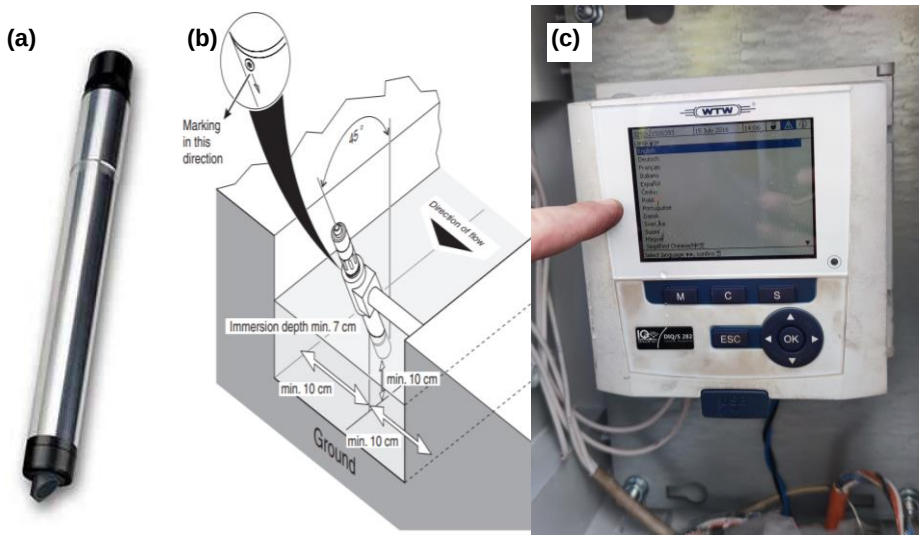

Figure 147 a) Fixed probe b) installation positioning c) control unit, images adapted from Xylem Analytics website with permission[178]

- With the fixed probe in place alternative reductants should be explored to evaluate their effect on dust generation. If biomass can be used in place of injection coal, without an impact on the dust generation then this should be

considered. Coal is a non-renewable carbon intense energy source for the blast furnace. To replace this with a renewable source of carbon such as biomass would be a move towards lessening the environmental impact of the blast furnace.

7 Appendix

7.1 Scatter Graphs from Chapter 4.1

7.1.1 Relationships Between Dust and Carbon

Appendix 1 Scatter graphs of each of the XRF analytes versus carbon in dust samples a) SiO_2 b) Al_2O_3 c) TiO_2 d) CaO e) MgO f) Fe g) Fe_2O_3 h) FeO i) P j) Mn

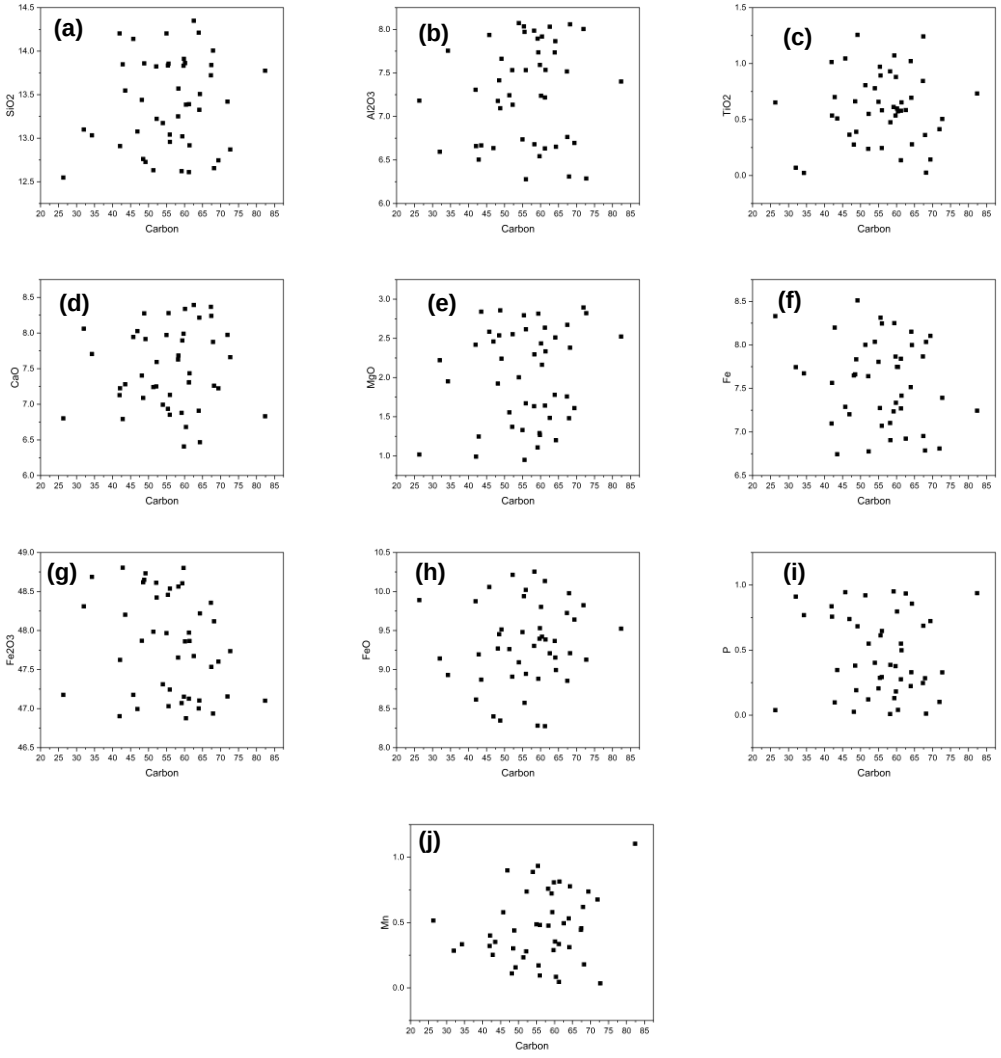

Appendix 2 Scatter graphs of each of the ICP analytes versus carbon in dust samples a) Na_2O b) K_2O c) Fe d) Zn e) Cr f) K g) Pb h) Ni i) Cu j) Ba k) V l) Na

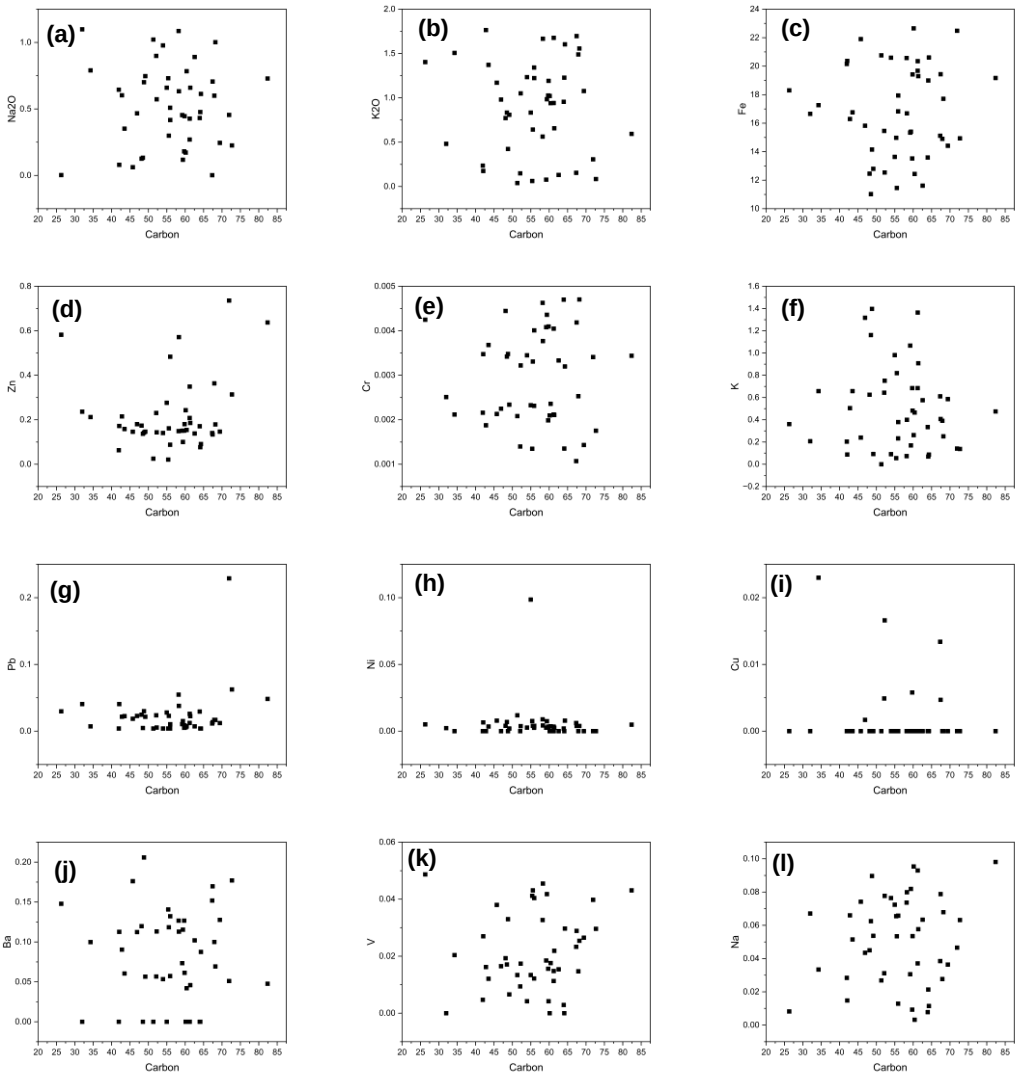

Appendix 3 Scatter graphs of each of the combustion-based analytes versus carbon in dust samples a) LOI b) S c) volatile matter d) ash

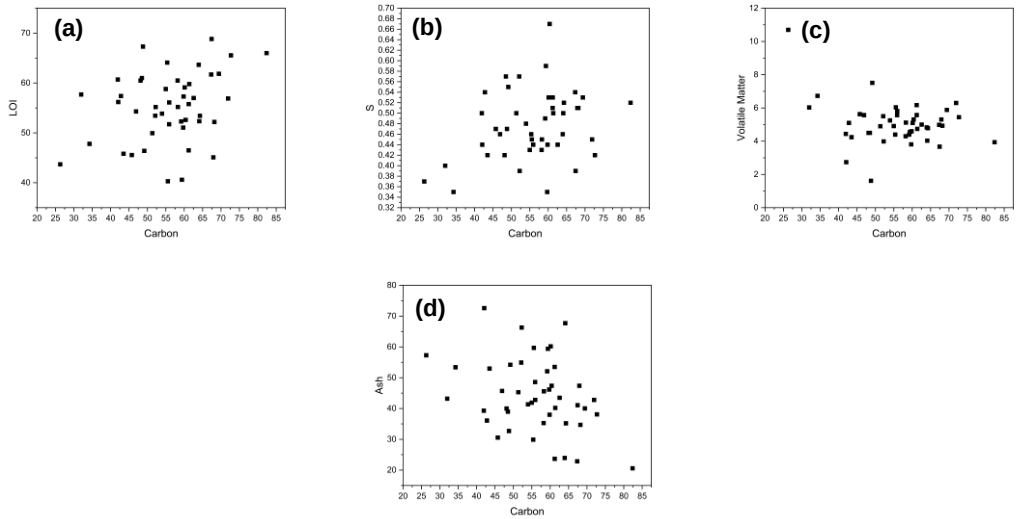

Appendix 4 Scatter graphs of each of the physical material properties versus carbon in dust samples a) Dx10 b) Dx50 c) Dx90 d) Dx99 e) Dx100 f) Bulk Density

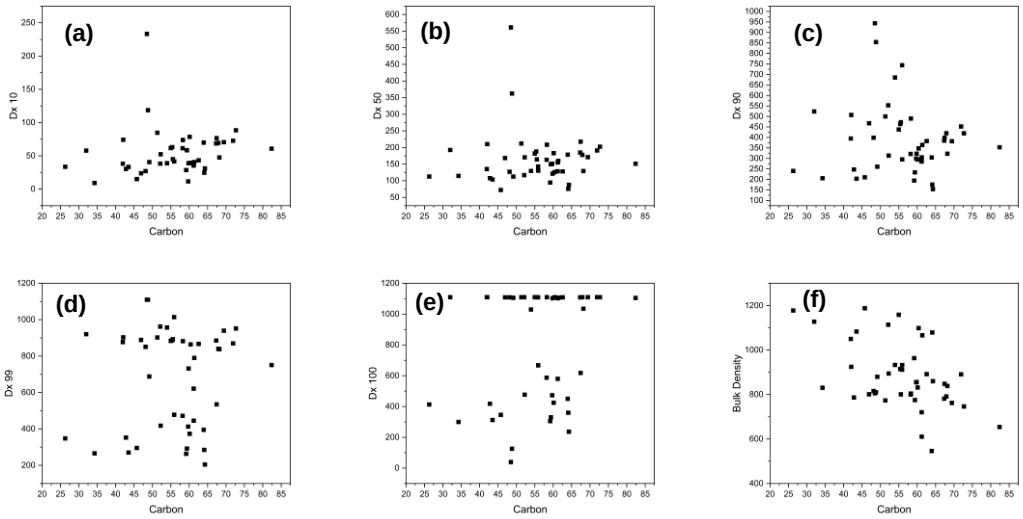

7.1.2 Relationships Between Slurry and Carbon

Appendix 5 Scatter graphs of each of the XRF analytes versus carbon in slurry samples a) SiO_2 b) Al_2O_3 c) TiO_2 d) CaO e) MgO f) Fe g) Fe_2O_3 h) FeO i) P j) Mn

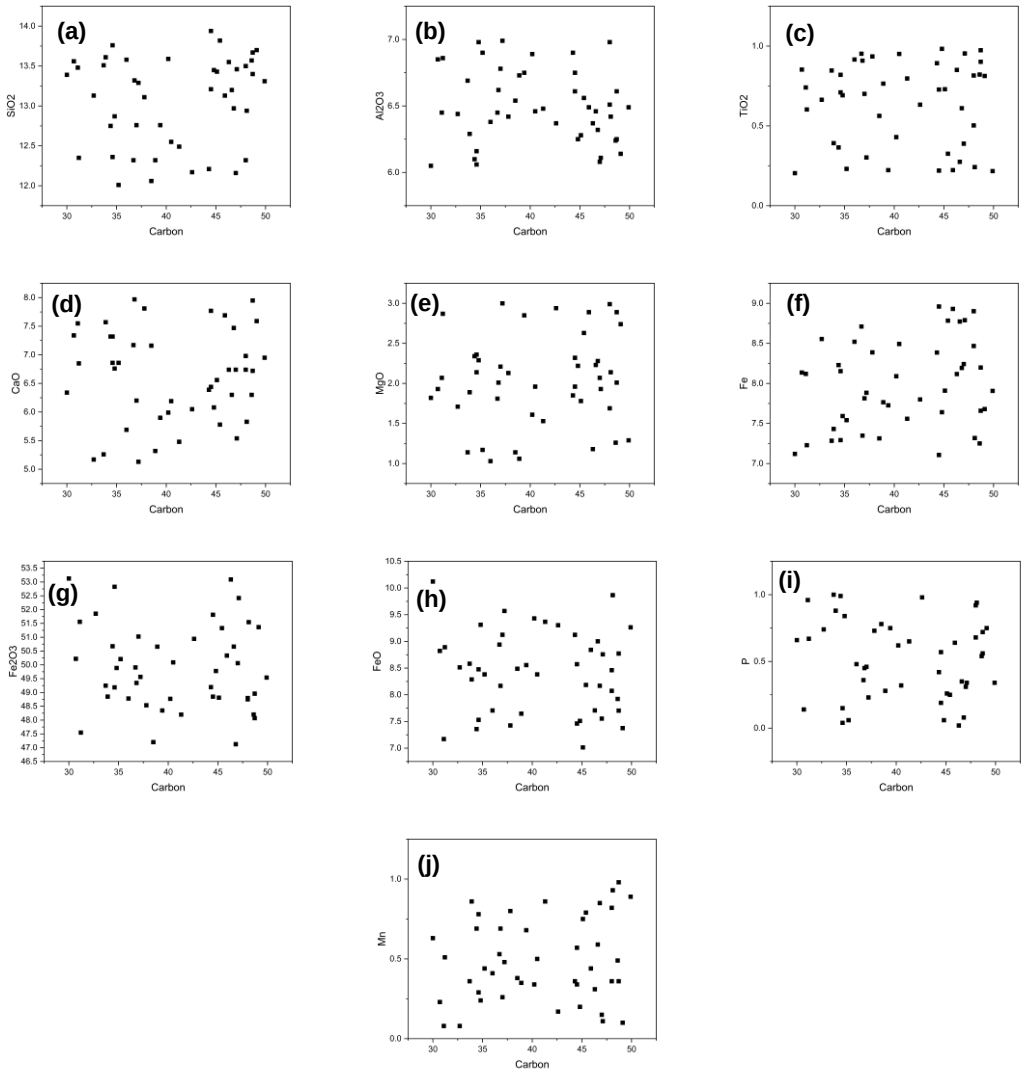

Appendix 6 Scatter graphs of each of the ICP analytes versus carbon in slurry samples a) Na_2O b) K_2O c) Fe d) Zn e) Cr f) K g) Pb h) Ni i) Cu j) Ba k) V l) Na

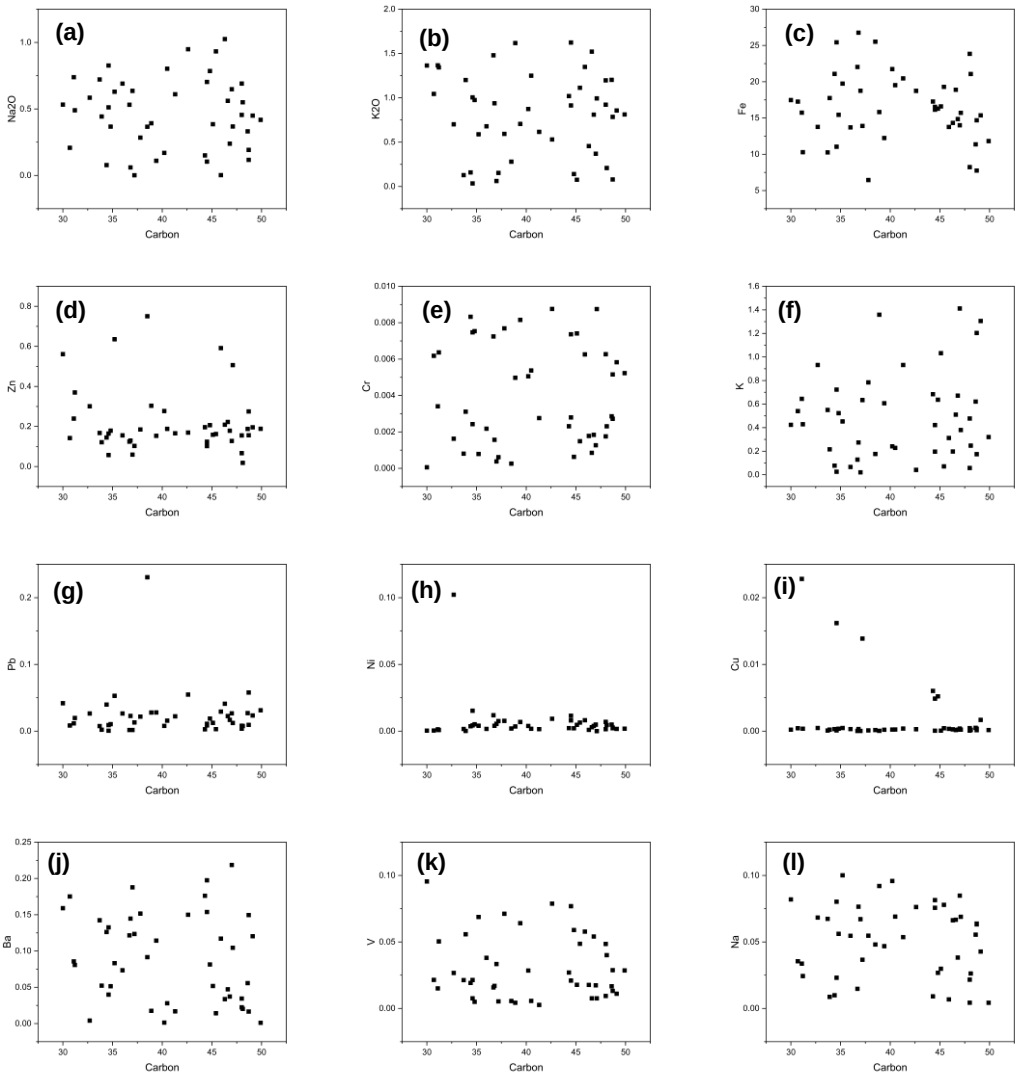

Appendix 7 Scatter graphs of each of the combustion-based analytes versus carbon in slurry samples a) LOI b) S c) volatile matter d) ash

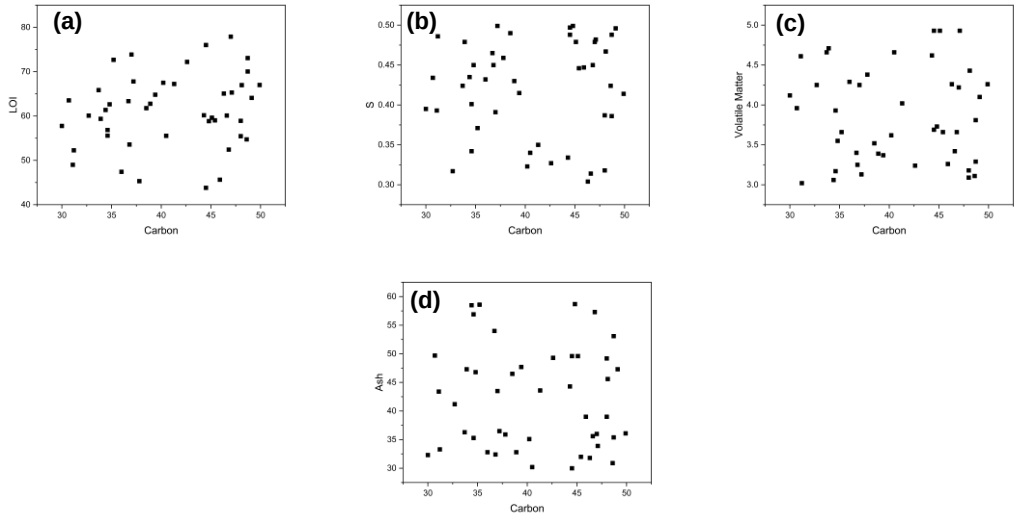

Appendix 8 Scatter graphs of each of the physical properties of the slurry versus the carbon a) Dx10 b) Dx50 c) Dx90 d) Dx99 e) Dx100 f) Bulk Density

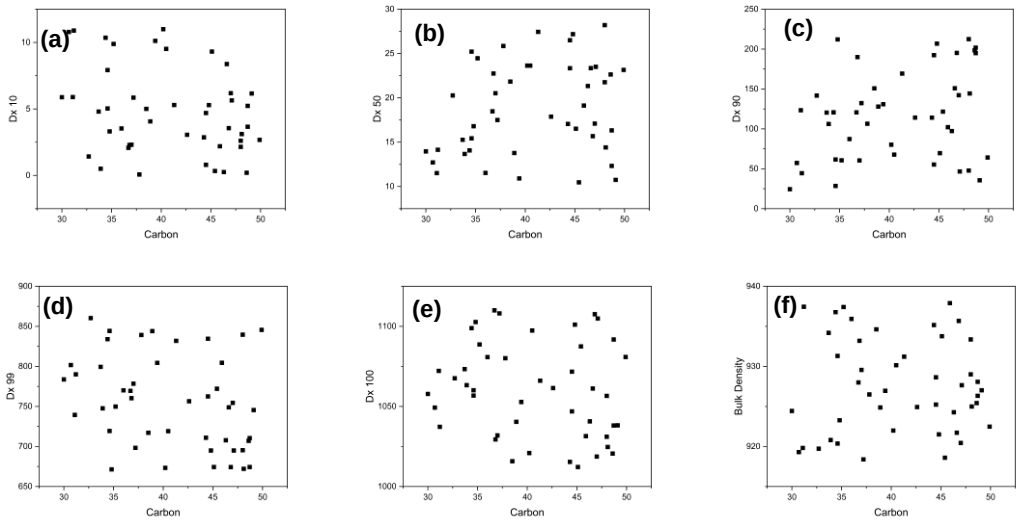

7.2 Statistical Data from Chapter 4.2

Appendix 9 Pearson's correlation and R^2 values for XRD parameters of the amorphous region of coal and dust samples

	Pearson's Correlation	R^2
FA	0.00	0.00
Rank	-0.18	0.03
La(nm)	-0.38	0.14
Lc (nm)	0.11	0.01
d002 (A)	0.06	0.00

Appendix 10 Statistical data for comparing the original CET with the modified TGA technique

	LOC	HOC	Soot	Ash	Moisture
Pearson's Correlation	0.97	0.92	0.82	0.88	0.77
R^2	0.94	0.84	0.66	0.76	0.57
Mean Error (%)	2.14	1.57	0.77	1.56	0.15
Mean Squared Error	6.88	5.03	1.21	15.11	0.03
Max Error (%)	6.43	6.54	2.78	14.08	0.29
Root Mean Squared Error	2.62	2.22	1.10	3.89	0.17

Appendix 11 Regression graphs for the CET versus the XRD parameters a) aromaticity b) rank c) La d) Lc

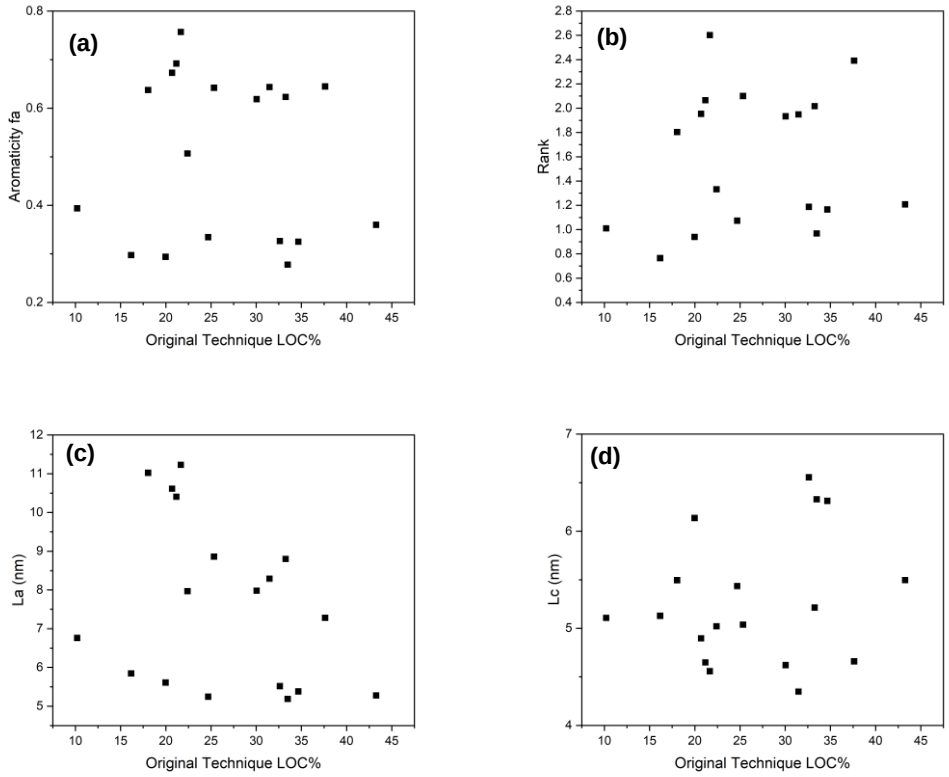

Appendix 12 Pearson's correlation, coefficient of determination and errors for results from XRD parameters versus CET

	Pearson's Correlation	R^2	Mean Error (%)	Mean Squared Error	Max Error (%)	Root Mean Squared Error
Aromaticity	<0.10	<0.10	25.98	743.94	42.90	27.28
Rank	0.13	<0.10	24.91	687.95	42.06	26.23
La (nm)	<0.10	<0.10	18.86	440.89	37.99	21.00
Lc (nm)	0.21	<0.10	21.21	516.55	37.77	22.73
Interlayer Spacing	0.69	0.44	23.07	600.38	39.83	24.50

Appendix 13 Pearson's correlation for the LOC result from each of the improved acids outlined in Table 24 versus LOC from the CET

	Pearson's Correlation	R^2	Mean Error (%)	Mean Squared Error	Max Error (%)	Root Mean Squared Error
Acid 1	0.88	0.77	3.17	15.06	8.26	3.88
Acid 2	0.83	0.69	3.50	18.88	9.29	4.35
Acid 3	0.65	0.42	5.03	37.11	12.60	6.09
Acid 4	0.59	0.35	5.12	41.36	14.12	6.43
Acid 5	0.50	0.25	5.84	49.44	15.15	7.03
Acid 6	0.28	0.08	4.57	28.58	10.82	5.35

Appendix 14 Pearson's correlation and coefficient of determination for results from Eltra C/S500 versus CET

	Pearson's Correlation	R^2	Mean Error (%)	Mean Squared Error	Max Error (%)	Root Mean Squared Error
Carbon	0.786326	0.618308	33.568	1154.958	47.91695	33.98467
Sulphur	0.136699	0.018687	26.01195	745.0265	42.84443	27.29517

Appendix 15 Graphs of D90 versus LOC using the CET a) line graph b) scatter graph

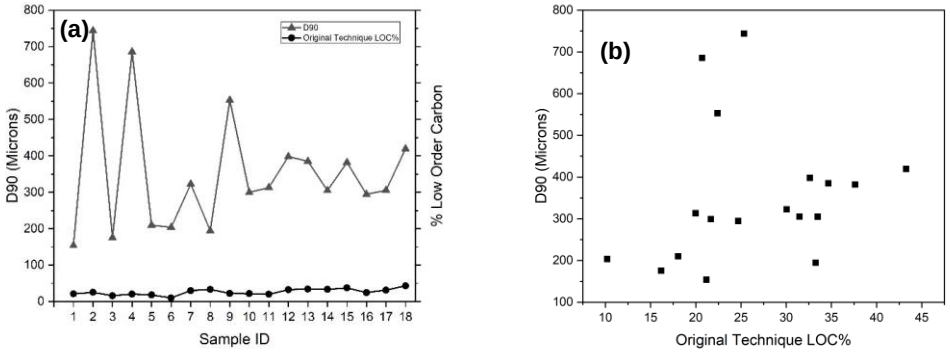

Appendix 16 Pearson's correlation and coefficient of determination for results from particle size distribution versus CET

	Pearson's Correlation	R^2	Mean Error (%)	Mean Squared Error	Max Error (%)	Root Mean Squared Error
D10	0.679979	0.462371	22.77189	750.063	53.9224	27.38728
D50	0.65202	0.42513	116.1623	14931.05	184.8815	122.1927
D90	0.174857	0.030575	326.1013	131730.7	718.5619	362.9473
D99	0.450241	0.202717	553.9358	391448.3	989.0619	625.6583

Appendix 17 Pearson's correlation and coefficient of determination for results from bulk density versus CET

	Pearson's Correlation	R^2	Mean Error (%)	Mean Squared Error	Max Error (%)	Root Mean Squared Error
Bulk Density	-0.69778	0.486899	853.9617	757474.4	1169.908	870.3301

Appendix 18 Pearson's correlation and coefficient of determination for results from BET surface area versus CET

	Pearson's Correlation	R^2	Mean Error (%)	Mean Squared Error	Max Error (%)	Root Mean Squared Error
BET	0.69	0.48	7.787784	92.65273	23.72991	9.625629

Appendix 19 Pearson's correlation and coefficient of determination for results from ImageJ particle identification versus CET

	Pearson's Correlation	R^2	Mean Error (%)	Mean Squared Error	Max Error (%)	Root Mean Squared Error
ImageJ	-0.57914	0.335405	38.51859	1653.879	62.38361	40.66791

Appendix 20 Pearson's correlation and coefficient of determination for results from Friedman model free kinetics Ea versus CET

	Pearson's Correlation	R^2	Mean Error (%)	Mean Squared Error	Max Error (%)	Root Mean Squared Error
Kinetics (Ea)	0.71886	0.51676	50.51244	2604.513	65.01054	51.03443

7.3 Scatter Graphs from Chapter 4.3

7.3.1 The Effect of Coal Chemistry on Top Gas Carbon

Appendix 21 Scatter graphs showing proximate analysis of the coal blends versus LOC in the dust a) H_2O b) ash c) volatile matter d) sulphur e) phosphorous

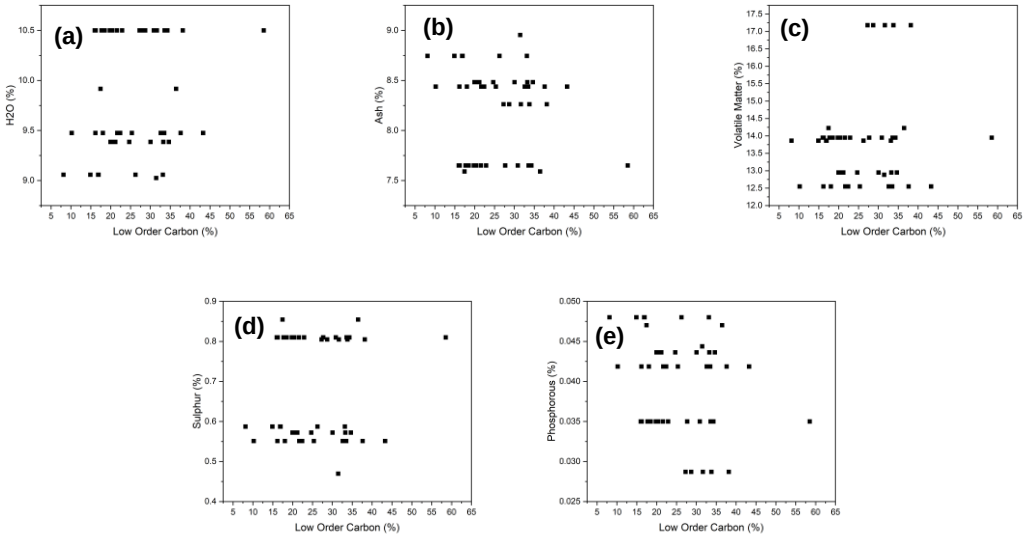

Appendix 22 Scatter graphs showing ash chemistry analysis of the coal blends versus low-order carbon in the dust a) Fe b) Mn c) P d) SiO_2 e) Al_2O_3 f) TiO_2 g) CaO h) MgO

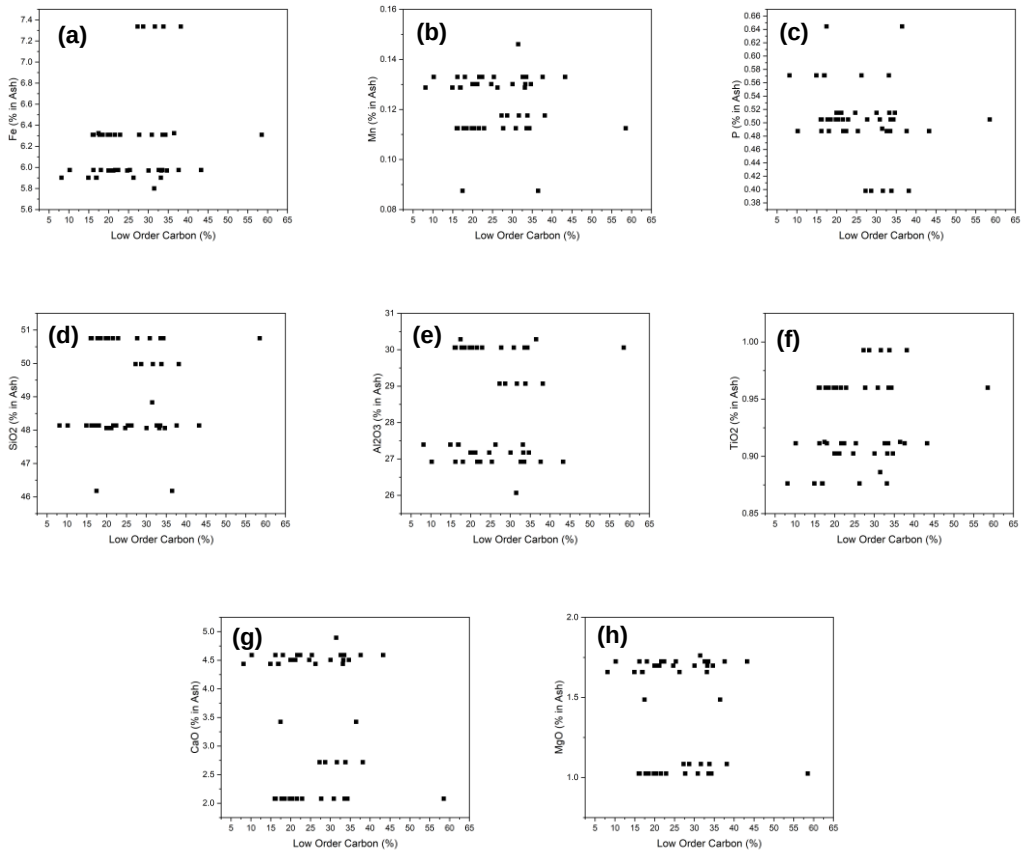

Appendix 23 Scatter graphs showing the ultimate analysis of the coal blends versus low-order carbon in the dust a) C b) H c) N d) O

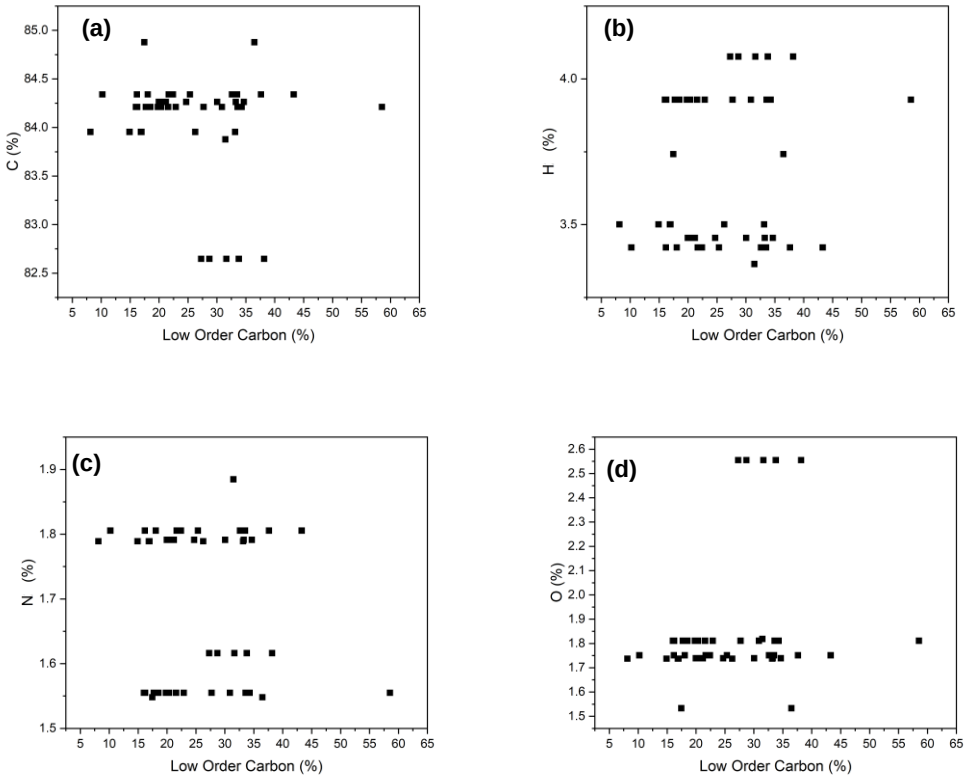

7.3.2 The Effect of Coal Process Parameters on Top Gas Carbon

Appendix 24 Scatter graphs showing coal process parameters versus low-order carbon in the dust. a) coal rate b) coal per unit oxygen c) coal per unit oxygen mass d) coal flow e) replacement ratio

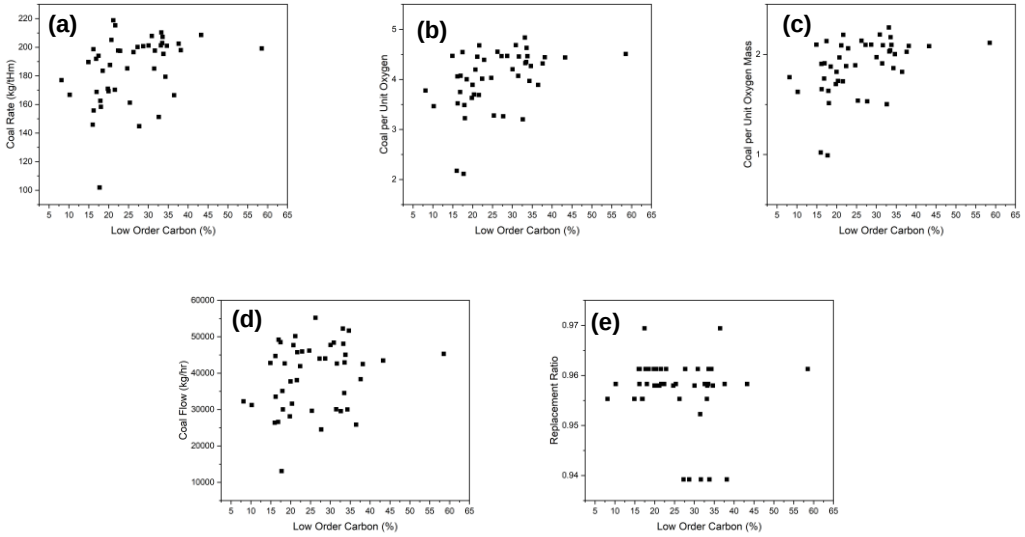

Appendix 25 Scatter graphs showing top gas concentrations versus low-order carbon in the dust a) CO A b) CO_2 A c) H_2 A d) CO B e) CO_2 B f) H_2 B g) gas efficiency

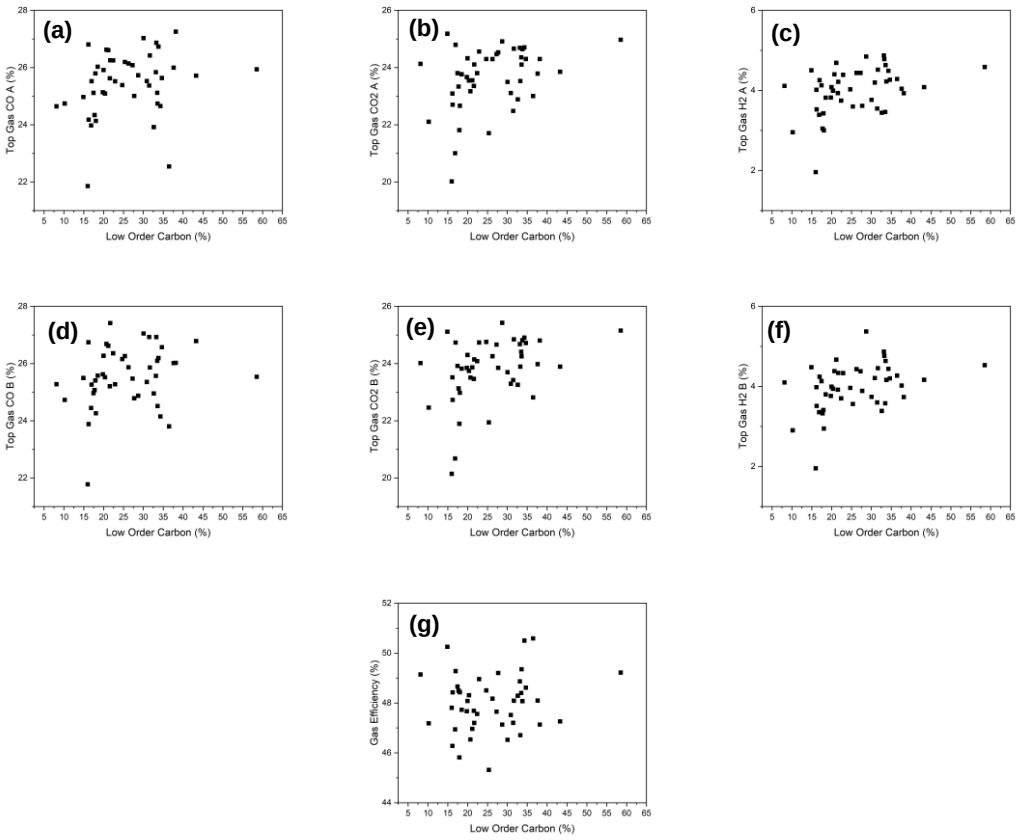

7.3.3 The Effect of Process Parameters on Top Gas Carbon

Appendix 26 Scatter graphs showing oxygen-based parameters versus low-order carbon in the dust a) O_2 setpoint b) O_2 volume c) total O_2 volume d) O_2 mass flow e) steam

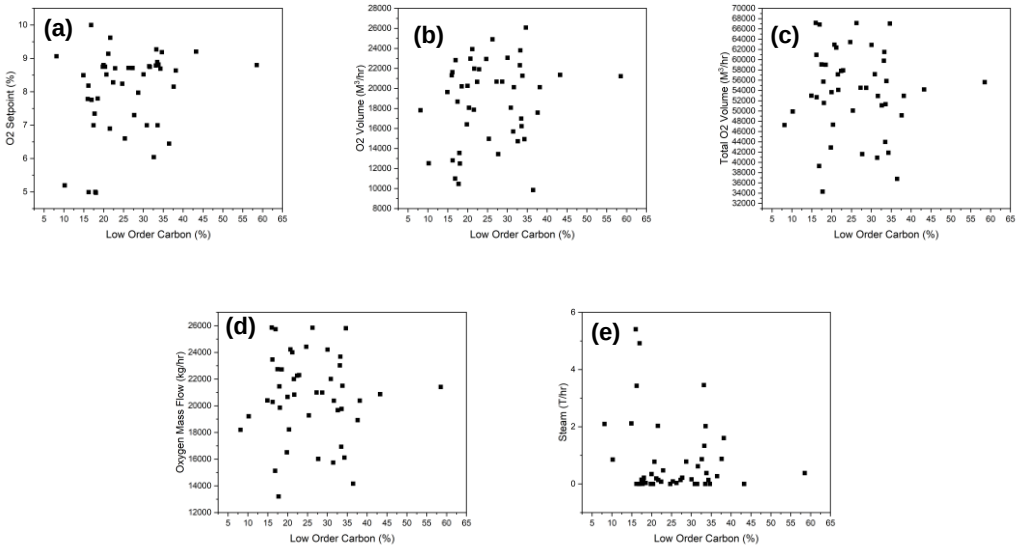

Appendix 27 Scatter graphs showing production-based parameters versus low-order carbon in the dust a) blast volume b) production rate c) hot metal SiO_2 d) coke rate

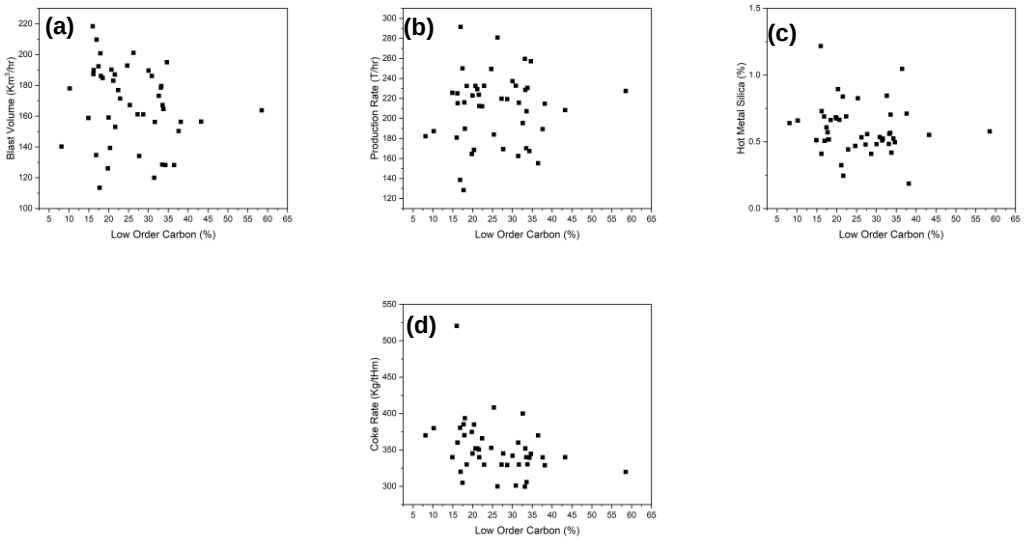

Appendix 28 Scatter graphs showing temperature parameters versus low-order carbon in the dust a) blast temperature b) RAFT c) top temperature

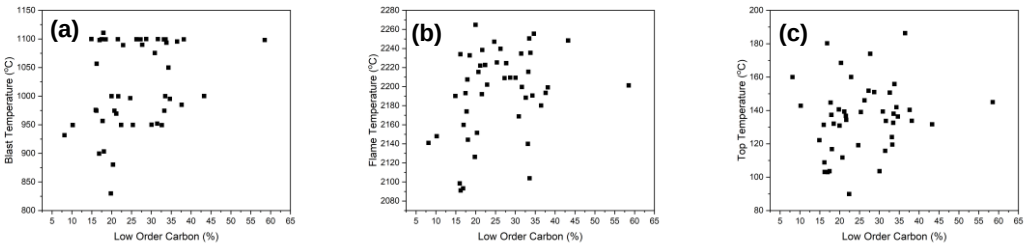

Appendix 29 Scatter graphs showing pressure parameters versus low-order carbon in the dust a) blast pressure b) Delta P c) max differential d) high top pressure e) permeability

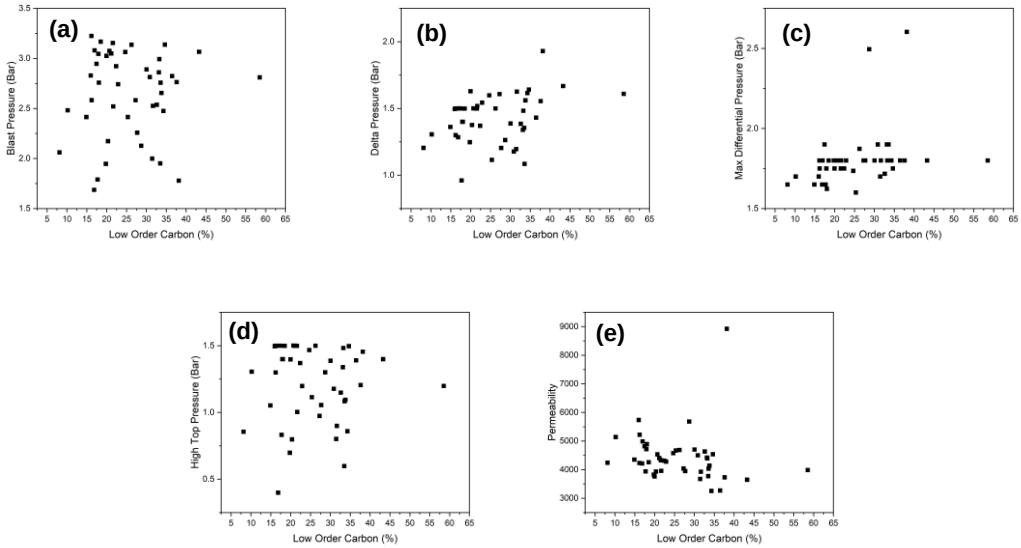

8 References

[1] World Steel Association. About Steel. World Steel Association 2019:1–4. https://www.worldsteel.org/about-steel.html (accessed May 7, 2020).

[2] Jiang HB, Zhang JL, Fu JX, Chang J, Li J. Properties and Structural Optimization of Pulverized Coal for Blast Furnace Injection. Journal of Iron and Steel Research International 2011;18:6–12. https://doi.org/doi.org/10.1016/S1006-706X(11)60029-0.

[3] Du SW, Yeh CP, Chen WH, Tsai CH, Lucas JA. Burning characteristics of pulverized coal within blast furnace raceway at various injection operations and ways of oxygen enrichment. Fuel 2015;143:98–106. https://doi.org/doi.org/10.1016/j.fuel.2014.11.038.

[4] Gupta S, Sahajwalla V, Burgo J, Chaubal P, Youmans T. Carbon structure of coke at high temperatures and its influence on coke fines in blast furnace dust. Metallurgical and Materials Transactions B: Process Metallurgy and Materials Processing Science 2005;36:385–94. https://doi.org/10.1007/s11663-005-0067-3.

[5] Net Zero Steel - A Vision for the Future of UK Steel Production | Make UK n.d. https://www.makeuk.org/about/uk-steel/net-zero-steel---a-vision-for-the-future-of-uk-steel-production (accessed April 1, 2023).

[6] UK steel industry sets out vision for Net Zero transition, securing green jobs and investment | Tata Steel in Europe n.d. https://www.tatasteeleurope.com/corporate/news/uk-steel-industry-sets-out-vision-for-net-zero-transition-securing-green-jobs-and-investment (accessed April 1, 2023).

[7] Tata Steel | Climate Action n.d. https://www.tatasteel.com/sustainability-6-2/our-approach/climate-action/ (accessed April 1, 2023).

[8] Tata Steel Nederland Together we make the difference 2021.

[9] Royal Society of Chemistry n.d. https://www.rsc.org/404notfound.aspx?aspxerrorpath=%2Fnews%2Devents%2Farticles%2F2020%2Fmar%2Fcoronavirus%2Dcovid%2D19%2Dguidance%2Dfor%2Dscientists%2F&e=1 (accessed April 3, 2023).

[10] Meehan MT, Rojas DP, Adekunle AI, Adegboye OA, Caldwell JM, Turek E, et al. Modelling insights into the COVID-19 pandemic. Paediatr Respir Rev 2020;35:64. https://doi.org/10.1016/J.PRRV.2020.06.014.

[11] Smil V. Still the Iron Age: Iron and Steel in the Modern World. 2016.

[12] Nyanin K. Combustion of Granulated Coal in Blast Furnace. Swansea University, 2013.

[13] Umadevi T, Brahmacharyulu A, Karthik P, Mahapatra PC, Prabhu M, Ranjan M. Recycling of steel plant mill scale via iron ore sintering plant. Http://DxDoiOrg/101179/1743281211Y0000000063 2013;39:222–7. https://doi.org/10.1179/1743281211Y.0000000063.

[14] Cavaliere P. Ironmaking and steelmaking processes: Greenhouse emissions, control, and reduction. 2016.

[15] TATA Steel. Knowledge document Processes Heavy End at IJmuiden. 2016.

[16] Fojtik D, Tuma J, Faruzel P. Computer modelling of burden distribution in the blast furnace equipped by a bell-less top charging system. Https://DoiOrg/101080/0301923320211952829 2021;48:1226–38. https://doi.org/10.1080/03019233.2021.1952829.

[17] Lu Y, Wu S, Du B, Zhou H. Increasing the Softening as well as Melting Behaviors for Iron Ore Materials within the Blast Furnace Cohesive Zone through the High-temperature Interactivity. ISIJ International 2020;60:1461–8. https://doi.org/10.2355/ISIJINTERNATIONAL.ISIJINT-2019-713.

[18] Zi-Zhao D, Zhang S, Qiang L, Ming-Hui D, Rui G, Jie-Ping W, et al. Boudouard reaction accompanied by graphitization of wrinkled carbon layers in coke gasification: A theoretical insight into the classical understanding. Fuel 2021;297:120747. https://doi.org/10.1016/J.FUEL.2021.120747.

[19] Geerdes M, Toxopeus H, van der Vliet C. Modern blast furnace ironmaking. An introduction. 2009.

[20] Su X, Zhang S, Yin Y, Xiao W. Prediction model of permeability index for blast furnace based on the improved multi-layer extreme learning machine and wavelet transform. J Franklin Inst 2018;355:1663–91. https://doi.org/10.1016/J.JFRANKLIN.2017.05.001.

[21] Shi L, Li Z ling, Yu T, Li J peng. Model of Hot Metal Silicon Content in Blast Furnace Based on Principal Component Analysis Application and Partial Least

Square. Journal of Iron and Steel Research, International 2011;18:13–6. https://doi.org/10.1016/S1006-706X(12)60015-6.

[22] Fang H ming, Han J, Zhang H jie, Zhao B, Qin L bo. Effect of coal moisture content on coke's quality and yields of products during coal carbonization. Journal of Central South University 2019 26:12 2020;26:3225–37. https://doi.org/10.1007/S11771-019-4248-7.

[23] Ghosh B, Sahoo BK, Chakraborty B, Manjhi KK, Das SK, Sahu JN, et al. Influence of coke structure on coke quality using image analysis method. Int J Coal Sci Technol 2018;5:473–85. https://doi.org/10.1007/S40789-018-0227-0/FIGURES/10.

[24] Ivanov VP. Assessing the Coking Properties and Value of Coal for Blast-Furnace Coke Production. Coke and Chemistry 2018 61:2 2018;61:29–37. https://doi.org/10.3103/S1068364X18020023.

[25] Xing X, Rogers H, Zhang G, Hockings K, Zulli P, Ostrovski O. Coke Degradation under Simulated Blast Furnace Conditions. ISIJ International 2016;56:786–93. https://doi.org/10.2355/ISIJINTERNATIONAL.ISIJINT-2015-704.

[26] Yu X, Shen Y. Model Study of Blast Furnace Operation with Central Coke Charging. Metallurgical and Materials Transactions B: Process Metallurgy and Materials Processing Science 2019;50:2238–50. https://doi.org/10.1007/S11663-019-01657-2/FIGURES/13.

[27] Zhao H bo, Bai Y qiang, Cheng S sen. Effect of Coke Reaction Index on Reduction and Permeability of Ore Layer in Blast Furnace Lumpy Zone Under Non-Isothermal Condition. Journal of Iron and Steel Research, International 2013;20:6–10. https://doi.org/10.1016/S1006-706X(13)60074-6.

[28] Gavel DJ. A review on nut coke utilisation in the ironmaking blast furnaces. Https://DoiOrg/101080/0267083620161183073 2016;33:381–7. https://doi.org/10.1080/02670836.2016.1183073.

[29] Kumar D, Saxena VK, Tiwari HP, Nandi BK, Verma A, Tiwary VK. Variability in Metallurgical Coke Reactivity Index (CRI) and Coke Strength after Reaction (CSR): An Experimental Study. ACS Omega 2022;7:1703. https://doi.org/10.1021/ACSOMEGA.1C04270.

[30] Lv QQ, Tian YS, Du P, Zhou JL, Wang GH. A study on the characteristics of coke in the hearth of a superlarge blast furnace. PLoS One 2021;16. https://doi.org/10.1371/JOURNAL.PONE.0247051.

[31] Coke Price Chart,China Coke Price Today-Shanghai Metals Market n.d. https://price.metal.com/Coke (accessed October 30, 2022).

[32] Guo Z, Jiao K, Zhang J, Ma H, Meng S, Wang Z, et al. Graphitization and Performance of Deadman Coke in a Large Dissected Blast Furnace. ACS Omega 2021;6:25430–9. https://doi.org/10.1021/ACSOMEGA.1C03398/ASSET/IMAGES/LARGE/AO1C03398_0012.JPEG.

[33] Fragoso HP, Pohlmann JG, MacHado JGMDS, Vilela ACF, Osorio E. Combustion behavior of granulated and pulverized coal in a PCI rig: combustibility and pressure variation analysis. Journal of Materials Research and Technology 2019;8:5847–52. https://doi.org/10.1016/J.JMRT.2019.09.055.

[34] Sahu SG, Mukherjee A, Kumar M, Adak AK, Sarkar P, Biswas S, et al. Evaluation of combustion behaviour of coal blends for use in pulverized coal injection (PCI). Appl Therm Eng 2014;73:1014–21. https://doi.org/10.1016/j.applthermaleng.2014.08.071.

[35] de Castro JA, Araújo GDM, da Mota IDO, Sasaki Y, Yagi JI. Analysis of the combined injection of pulverized coal and charcoal into large blast furnaces. Journal of Materials Research and Technology 2013;2:308–14. https://doi.org/10.1016/J.JMRT.2013.06.003.

[36] Sexton DC, Steer JM, Marsh R, Greenslade M. Investigating char agglomeration in blast furnace coal injection. Fuel Processing Technology 2018;178:24–34. https://doi.org/10.1016/j.fuproc.2018.05.013.

[37] Osório E, de Lourdes Ilha Gomes M, Vilela ACF, Kalkreuth W, de Almeida MAA, Borrego AG, et al. Evaluation of petrology and reactivity of coal blends for use in pulverized coal injection (PCI). Int J Coal Geol 2006;68:14–29. https://doi.org/10.1016/j.coal.2005.11.007Get.

[38] Lu L, Kong C, Sahajwalla V, Harris D. Char structural ordering during pyrolysis and combustion and its influence on char reactivity. Fuel 2002;81:1215–25. https://doi.org/10.1016/S0016-2361(02)00035-2.

[39] Niksa S, Liu G, Hurt RH, Liu G-S. Coal conversion submodels for design applications at elevated pressures. Part I. Devolatilization and char oxidation Biomass Co-Firing with Coal View project Process Chemistry of Coal Utilization: Chemistry Toolkit for Furnaces and Gasifiers View project Coal conversion submodels for design applications at elevated pressures. Part I. devolatilization and char oxidation 2003. https://doi.org/10.1016/S0360-1285(03)00033-9.

[40] Driessen RT, Kersten SRA, Brilman DWF. A Thiele Modulus Approach for Nonequilibrium Adsorption Processes and Its Application to CO2 Capture. Ind Eng Chem Res 2020;59:6874–85. https://doi.org/10.1021/ACS.IECR.9B05503/ASSET/IMAGES/LARGE/IE9B05503_0013.JPEG.

[41] Ishii K. Advanced Pulverized Coal Injection Technology And Blast Furnace Operation. 2000.

[42] Asadi Zeydabadi B, Mowla D, Shariat MH, Fathi Kalajahi J. Zinc recovery from blast furnace flue dust. Hydrometallurgy 1997;47:113–25. https://doi.org/10.1016/S0304-386X(97)00039-X.

[43] Wang C, Larsson M, Lövgren J, Nilsson L, Mellin P, Yang W, et al. Injection of Solid Biomass Products into the Blast Furnace and its Potential Effects on an Integrated Steel Plant. Energy Procedia 2014;61:2184–7. https://doi.org/10.1016/J.EGYPRO.2014.12.105.

[44] Moon J, Sahajwalla V. Investigation into the role of the boudouard reaction in self-reducing iron oxide and carbon briquettes. Metallurgical and Materials Transactions B 2006 37:2 2006;37:215–21. https://doi.org/10.1007/BF02693151.

[45] Coal Rank, Kentucky Geological Survey, University of Kentucky n.d. https://www.uky.edu/KGS/coal/coal-rank.php (accessed October 30, 2022).

[46] Born S, Babich A, van der Stel J, Ho HT, Sert D, Ansseau O, et al. Char Formation by Coal Injection and Its Behavior in the Blast Furnace. Steel Res Int 2020;91:2000038. https://doi.org/10.1002/SRIN.202000038.

[47] Gupta GS, Rudolph V. Comparison of blast furnace raceway size with theory. ISIJ International 2006;46:195–201. https://doi.org/10.2355/ISIJINTERNATIONAL.46.195.

[48] Lu H, Guo X, Jin Y, Gong X. Effect of moisture on flowability of pulverized coal. Chemical Engineering Research and Design 2018;133:326–34. https://doi.org/10.1016/J.CHERD.2018.03.023.

[49] Born S, Pridhivi V, Van der Stel J, Babich A, Ho HT, Gupta P, et al. Char formation , transportation and consumption in the blast furnace and its impact on coke rate. Luxembourg: n.d. https://doi.org/10.2777/046097.

[50] Du SW, Chen WH, Lucas JA. Pulverized coal burnout in blast furnace simulated by a drop tube furnace. Energy 2010;35:576–81. https://doi.org/10.1016/j.energy.2009.10.028.

[51] Tiwari HP, Das A, Singh U. Novel technique for assessing the burnout potential of pulverized coals/coal blends for blast furnace injection. Appl Therm Eng 2018;130:1279–89. https://doi.org/10.1016/j.applthermaleng.2017.11.115.

[52] Ho HT et al. Towards Prediction of Coal Conversion Behaviour in the Blast Furnace. In: 7th European Coke and Ironmaking Congress, editor., Austria: 2017, p. 163–72.

[53] BSI Standards publication. BSI Standards Publication Coal — Proximate analysis. 2010.

[54] Steer JM, Marsh R, Morgan D, Greenslade M. The effects of particle grinding on the burnout and surface chemistry of coals in a drop tube furnace. Fuel 2015;160:413–23. https://doi.org/10.1016/j.fuel.2015.07.094.

[55] Ray S, Giroux L, Macphee T, Ng KW, Todoschuk T. Evaluation of PCI Coals in New Injection Facility at CanmetENERGY-OTTAWA. AISTech - Iron and Steel Technology Conference Proceedings, 2015, p. 926–37.

[56] Zyrkowski M, Neto RC, Santos LF, Witkowski K. Characterization of fly-ash cenospheres from coal-fired power plant unit. Fuel 2016;174:49–53. https://doi.org/10.1016/J.FUEL.2016.01.061.

[57] Pohlmann JG, Osorio E, Vilela ACF, Borrego AG. Reactivity to CO2 of chars prepared in O2/N2 and O2/CO2 mixtures for pulverized coal injection (PCI) in blast furnace in relation to char petrographic characteristics. Int J Coal Geol 2010;84:293–300. https://doi.org/10.1016/j.coal.2010.10.008.

[58] Sima-Ella E, Yuan G, Mays T. A simple kinetic analysis to determine the intrinsic reactivity of coal chars. Fuel 2005;84:1920–5. https://doi.org/10.1016/j.fuel.2005.03.022.

[59] Ng KW, Giroux L, MacPhee T, Todoschuk T, Taggart L, Scott G. Carbon type differentiation technique for diagnosing pulverised coal injection efficiency. Ironmaking and Steelmaking 2016;43:214–9. https://doi.org/10.1179/1743281215Y.0000000034.

[60] Xiao X, Zhang S, Sher F, Chen J, Xin Y, You Z, et al. A Review on Recycling and Reutilization of Blast Furnace Dust as a Secondary Resource. Journal of Sustainable Metallurgy 2021;7:340–57. https://doi.org/10.1007/S40831-021-00377-9.

[61] Ng KW, Giroux L, MacPhee T, Todoschuk T, Taggart L, Scott G. Carbon type differentiation technique for diagnosing pulverised coal injection efficiency. Ironmaking and Steelmaking 2016;43:214–9. https://doi.org/10.1179/1743281215Y.0000000034.

[62] Ng KW. Development of TGA technique for carbon-type characterisation in blast furnace dust n.d. https://www.researchgate.net/publication/287428158_Development_of_TGA_technique_for_carbon-type_characterisation_in_blast_furnace_dust (accessed April 4, 2023).

[63] Schwalbe R, Peters M, Schmöle P, Mittelstädt H. Carbonaceous Forms in Blast Furnace Dust at High Coal Injection Rates. 2011.

[64] Zhao D, Zhang J, Wang G, Conejo AN, Xu R, Wang H, et al. Structure characteristics and combustibility of carbonaceous materials from blast furnace flue dust. Appl Therm Eng 2016;108:1168–77. https://doi.org/10.1016/j.applthermaleng.2016.08.020.

[65] Steer J, Greenslade M, Marsh R. A Comparison of Laboratory Coal Testing with the Blast Furnace Process and Coal Injection 2021. https://doi.org/10.3390/met11091476.

[66] Gao Q, Xiao X, Suo Z, Long F, Shen F. Thermal reactivity and flowability of pulverized coal blending with iron-bearing dust injection in blast furnace process. Case Studies in Thermal Engineering 2023;41:102598. https://doi.org/10.1016/J.CSITE.2022.102598.

[67] Cecala AB et al. Dust Control Handbook for Industrial Minerals Mining and Processing. 2012.

[68] Winfield D, Paddison D, Cross M, Croft N, Craig I. Performance comparison of a blast furnace gravity dust-catcher vs. tangential triple inlet gas separation cyclone using computational fluid dynamics. Sep Purif Technol 2013;115:205–15. https://doi.org/10.1016/j.seppur.2013.04.035.

[69] ISO 11272:2017 - Soil quality — Determination of dry bulk density n.d. https://www.iso.org/standard/68255.html (accessed April 5, 2023).

[70] British Standards Institution. Tests for general properties of aggregates 1997.

[71] Steer J. Meeting with Dr Julian Steer of Cardiff University, Samples of Char Obtained. Cardiff: 2019.

[72] Wang Y, Zou C, Zhao J, Wang F. Combustion Characteristics of Coal for Pulverized Coal Injection (PCI) Blending with Steel Plant Flying Dust and Waste Oil Sludge. ACS Omega 2021;6:28548–60. https://doi.org/10.1021/ACSOMEGA.1C02554/ASSET/IMAGES/LARGE/AO1C02554_0014.JPEG.

[73] Grammelis P, Margaritis N, Karampinis E. Solid fuel types for energy generation: Coal and fossil carbon-derivative solid fuels. Fuel Flexible Energy Generation: Solid, Liquid and Gaseous Fuels 2016:29–58. https://doi.org/10.1016/B978-1-78242-378-2.00002-X.

[74] Dauter Z. Collection of X-ray diffraction data from macromolecular crystals. Methods Mol Biol 2017;1607:165. https://doi.org/10.1007/978-1-4939-7000-1_7.

[75] Stewart DJC. VALUE GENERATION BY RECOVERING BY-PRODUCTS FROM STEELMAKING PROCESSES: DEZINCIFICATION OF BASIC OXYGEN STEELMAKING DUST. Swansea University, 2022.

[76] Hseu ZY. Evaluating heavy metal contents in nine composts using four digestion methods. Bioresour Technol 2004;95:53–9. https://doi.org/10.1016/J.BIORTECH.2004.02.008.

[77] Sexton D. Coal Agglomeration in Blast Furnace Injection Coals. Cardiff Univesity, 2019.

[78] Winkler MG. Charcoal analysis for paleoenvironmental interpretation: A chemical assay. Quat Res 1985;23:313–26. https://doi.org/10.1016/0033-5894(85)90038-9.

[79] Soil Health | Natural Resources Conservation Service n.d. https://www.nrcs.usda.gov/conservation-basics/natural-resource-concerns/soils/soil-health (accessed April 8, 2023).

[80] Duan D. Efficient and comprehensive utilization of blast furnace dust in metalized pelletizing process | Request PDF n.d. https://www.researchgate.net/publication/279710525_Efficient_and_comprehensive_utilization_of_blast_furnace_dust_in_metalized_pelletizing_process (accessed April 8, 2023).

[81] Glossary of Steel Industry Terms - American Iron and Steel Institute n.d. https://www.steel.org/steel-technology/steel-production/glossary/ (accessed April 8, 2023).

[82] da S. Machado A, Mexias AS, Vilela ACF, Osorio E. Study of coal, char and coke fines structures and their proportions in the off-gas blast furnace samples by X-ray diffraction. Fuel 2013;114:224–8. https://doi.org/10.1016/J.FUEL.2012.07.064.

[83] Cullity BD. Elements of X-ray diffraction. Addison-Wesley; 1978.

[84] Bragg's Law n.d. http://hyperphysics.phy-astr.gsu.edu/hbase/quantum/bragg.html (accessed September 11, 2022).

[85] Yan J, Yang Q, Zhang L, Lei Z, Li Z, Wang Z, et al. Investigation of kinetic and thermodynamic parameters of coal pyrolysis with model-free fitting methods. Carbon Resources Conversion 2020;3:173–81. https://doi.org/10.1016/J.CRCON.2020.11.002.

[86] Tang H, Meng F, Zhao Z, Zhang L. Modeling Coal/coke Combustion Behavior in Tuyere-raceway-dripping Zone in Blast Furnace. Procedia Eng 2015;102:1583–92. https://doi.org/10.1016/j.proeng.2015.01.294.

[87] Jayaraman K, Kök MV, Gökalp I. Combustion mechanism and model free kinetics of different origin coal samples: Thermal analysis approach. Energy 2020;204:117905. https://doi.org/10.1016/J.ENERGY.2020.117905.

[88] Fidalgo B, Chilmeran M, Somorin T, Sowale A, Kolios A, Parker A, et al. Non-isothermal thermogravimetric kinetic analysis of the thermochemical conversion of human faeces. Renew Energy 2019;132:1177–84. https://doi.org/10.1016/J.RENENE.2018.08.090.

[89] Naderi M. Surface Area: Brunauer–Emmett–Teller (BET). Progress in Filtration and Separation 2015:585–608. https://doi.org/10.1016/B978-0-12-384746-1.00014-8.

[90] Zhang TY, Suen CY. A fast parallel algorithm for thinning digital patterns. Commun ACM 1984;27:236–9. https://doi.org/10.1145/357994.358023.

[91] Ashrit SS, Chatti R v., Sarkar S. Identification of the carbon source in blast furnace flue dust through characterisation and statistical analysis. Int J Environ Anal Chem 2019;101:1378–92. https://doi.org/10.1080/03067319.2019.1682142.

[92] Yu J, Sun L, Xiang J, Hu S, Su S, Wang Y. New Method of Quantitative Determination of the Carbon Source in Blast Furnace Flue Dust. Energy and Fuels 2014;28:7235–42. https://doi.org/10.1021/EF501863R.

[93] Zhong Y, Qiu X, Gao J, Guo Z. Structural Characterization of Carbon in Blast Furnace Flue Dust and Its Reactivity in Combustion. Energy and Fuels 2017;31:8415–22. https://doi.org/10.1021/ACS.ENERGYFUELS.7B01146/SUPPL_FILE/EF7B01146_SI_001.PDF.

[94] Dunlop T. Work completed in collaboration with Dr Thomas Dunlop Swansea University. Swansea: 2020.

[95] Lester E, Goonetilleke-Rezel T. Collaborative petrographic analysis. Nottingham: 2019.

[96] Xing X. Petrographic Analysis of Cokes Reacted under Simulated Blast Furnace Conditions. Energy & Fuels 2019;33:4146–57. https://doi.org/10.1021/ACS.ENERGYFUELS.9B00417.

[97] Wang CA, Liu Y, Zhang X, Che D. A Study on Coal Properties and Combustion Characteristics of Blended Coals in Northwestern China. Energy and Fuels 2011;25:3634–45. https://doi.org/10.1021/EF200686D.

[98] Kou M, Zhou H, Wang LP, Hong Z, Yao S, Xu H, et al. Numerical simulation of effects of different operational parameters on the carbon solution loss ratio of coke inside blast furnace. Processes 2019;7:1–14. https://doi.org/10.3390/PR7080528.

[99] Maarten Geerdes, Rénard Chaigneau, Ivan Kurunov, Oscar Lingiardi JR. Modern Blast Furnace Ironmaking. 2015. https://doi.org/10.3233/978-1-61499-499-2-i.

[100] Kiga T, Takano S, Kimura N, Omata K, Okawa M, Mori T, et al. Characteristics of pulverized-coal combustion in the system of oxygen/recycled flue gas combustion. Energy Convers Manag 1997;38:S129–34. https://doi.org/10.1016/S0196-8904(96)00258-0.

[101] Lanzerstorfer C. Mechanical properties of dusts collected from blast furnace dust catchers and cast house dedusting filters. Particulate Science and Technology 2016;34:366–72. https://doi.org/10.1080/02726351.2015.1089347.

[102] Water in FTIR n.d. https://webbook.nist.gov/cgi/cbook.cgi?ID=C7732185&Type=IR-SPEC&Index=0 (accessed November 3, 2022).

[103] della Ventura G, Radica F, Bellatreccia F, Cavallo A, Cinque G, Tortora L, et al. FTIR imaging in diffusion studies: CO2 and H2O in a synthetic sector-zoned beryl. Front Earth Sci (Lausanne) 2015;3:33. https://doi.org/10.3389/FEART.2015.00033/BIBTEX.

[104] Nesseu K, Telephone B, Hill M. THE CHARACTERIZATION OF BERYL AI{D EMERALD BY VISIBLE AND INFRARED ABSORPTION SPECTROSCOPY 2007. https://doi.org/Not available.

[105] What could be the reason for the appearance of an inverted doublet at 2360 cm-1? | ResearchGate n.d. https://www.researchgate.net/post/What-could-be-the-reason-for-the-appearance-of-an-inverted-doublet-at-2360-cm-1 (accessed November 3, 2022).

[106] Measuring Turbidity, TSS, and Water Clarity - Environmental Measurement Systems n.d. https://www.fondriest.com/environmental-measurements/measurements/measuring-water-quality/turbidity-sensors-meters-and-methods/ (accessed September 22, 2022).

[107] Doxaran D, Lamquin N, Park Y-J, Ryu J-H, Wang M, Poteau A. Retrieval of the seawater reflectance for suspended solids monitoring in the East China Sea using MODIS, MERIS and GOCI satellite data. Remote Sens Environ 2014;146:36–48. https://doi.org/10.1016/j.rse.2013.06.020.

[108] Standard Operating Procedure for: Total Suspended Solids n.d.

[109] Branigan J. Development of a Field Test for Total Suspended Solids Analysis n.d.

[110] Heikkilä A, Iljana M, Heikkinen EP, Koskela A, Fabritius T. Effect of Coal and Coke Ash on Blast Furnace Slag Properties: A Comparison Between Pulverized Coal, Charcoal, Fossil-Based Coke, and Biocoke. Steel Res Int 2022;93:2100188. https://doi.org/10.1002/SRIN.202100188.

[111] Tsuge H, Yoshida T, Aoki H, Miura T. The effect of pulverized coal injection and volatile matter content of coal on combustion characteristics around the raceway zone in the blast furnace. Symposium (International) on Combustion 1994;25:493–501. https://doi.org/10.1016/S0082-0784(06)80678-8.

[112] Nicolaas F, Schrama H, Beunder EM, van den Berg B, Yang Y, Boom R. Ironmaking & Steelmaking Processes, Products and Applications Sulphur removal in ironmaking and oxygen steelmaking Sulphur removal in ironmaking and oxygen steelmaking 2017. https://doi.org/10.1080/03019233.2017.1303914.

[113] Bytnar K, Burmistrz P. Alkalis in coal and coal cleaning products. Archives of Mining Sciences 2013;58:913–24. https://doi.org/10.2478/AMSC-2013-0064.

[114] Gupta RC. Energy Resources, Its Role and Use in Metallurgical Industries. Treatise on Process Metallurgy 2014;3:1425–58. https://doi.org/10.1016/B978-0-08-096988-6.00034-1.

[115] Takagi H, Maruyama K, Yoshizawa N, Yamada Y, Sato Y. XRD analysis of carbon stacking structure in coal during heat treatment. Fuel 2004;83:2427–33. https://doi.org/10.1016/J.FUEL.2004.06.019.

[116] Yang N, Tang S, Zhang S, Chen Y. Mineralogical and geochemical compositions of the No. 5 coal in chuancaogedan mine, Junger Coalfield, China. Minerals 2015;5:788–800. https://doi.org/10.3390/MIN5040525.

[117] Li S, Zhu Y, Wang Y, Liu J. The Chemical and Alignment Structural Properties of Coal: Insights from Raman, Solid-State 13C NMR, XRD, and HRTEM Techniques. ACS Omega 2021;6:11266–79. https://doi.org/10.1021/ACSOMEGA.1C00111/ASSET/IMAGES/LARGE/AO1C00111_0014.JPEG.

[118] Menéndez R, Alvarez D, Fuertes AB, Hamburg G, Vleeskens J. Effects of Clay Minerals on Char Texture and Combustion. Energy and Fuels 1994;8:1007–15. https://doi.org/10.1021/EF00047A001/ASSET/EF00047A001.FP.PNG_V03.

[119] Zhang H, Pu WX, Ha S, Li Y, Sun M. The influence of included minerals on the intrinsic reactivity of chars prepared at 900 °C in a drop tube furnace and a muffle furnace. Fuel 2009;88:2303–10. https://doi.org/10.1016/J.FUEL.2009.05.014.

[120] Warren P. Peter Warren - Blast Furnace Discussion. Middlesbrough: 2019.

[121] Afanga K, Mirgaux O, Patisson F. Assessment of Top Gas Recycling Blast Furnace: A Technology To Reduce CO2 Emissions in the Steelmaking Industry. Carbon Management Technology Conference 2012 2012:675–85. https://doi.org/10.7122/151137-MS.

[122] Wang M, Chen Y, Fu H, Qu X, Li B, Tao S, et al. An investigation on hygroscopic properties of 15 black carbon 1 (BC)-containing particles from different carbon sources: Roles 2 of organic and inorganic components 3 4 n.d. https://doi.org/10.5194/acp-20-7941-2020.

[123] Dłotko P. Ball mapper: a shape summary for topological data analysis 2019. https://doi.org/10.48550/arxiv.1901.07410.

[124] Wen Y, Sánchez-Román M, Li Y, Wang C, Han Z, Zhang L, et al. Nucleation and stabilization of Eocene dolomite in evaporative lacustrine deposits from central Tibetan plateau. Sedimentology 2020;67:3333–54. https://doi.org/10.1111/SED.12744.

[125] Tonžetić IŽ. Quantitative analysis of iron ore using SEM-based technologies. Iron Ore: Mineralogy, Processing and Environmental Sustainability 2022:179–208. https://doi.org/10.1016/B978-0-12-820226-5.00018-5.

[126] Li T, Sun C, Liu X, Song S, Wang Q. The effects of MgO and Al2O3 behaviours on softening–melting properties of high basicity sinter. Ironmaking and Steelmaking 2018;45:755–63. https://doi.org/10.1080/03019233.2017.1337263.

[127] (PDF) The Use of Metallurgical Coke as Carburizing Material in the Foundry n.d. https://www.researchgate.net/publication/277821595_The_Use_of_Metallurgi

cal_Coke_as_Carburizing_Material_in_the_Foundry (accessed October 13, 2022).

[128] Singh PK, Avala Lava K, Katiyar PK, Maurya R. Agglomeration behaviour of steel plants solid waste and its effect on sintering performance. Journal of Materials Research and Technology 2017;6:289–96. https://doi.org/10.1016/J.JMRT.2016.11.005.

[129] YANG X, CHU M, SHEN F, ZHANG Z. Mechanism of zinc damaging to blast furnace tuyere refractory. Acta Metallurgica Sinica (English Letters) 2009;22:454–60. https://doi.org/10.1016/S1006-7191(08)60123-4.

[130] Ma A, Zheng X, Li S, Wang Y, Zhu S. Zinc recovery from metallurgical slag and dust by coordination leaching in NH3–CH3COONH4–H2O system. R Soc Open Sci 2018;5. https://doi.org/10.1098/RSOS.180660.

[131] Manoj B, Kunjomana AG. Study of Stacking Structure of Amorphous Carbon by X-Ray Diffraction Technique. Int J Electrochem Sci 2012;7:3127–34. https://doi.org/No DOI Available.

[132] Li S, Zhu Y, Wang Y, Liu J. The Chemical and Alignment Structural Properties of Coal: Insights from Raman, Solid-State 13C NMR, XRD, and HRTEM Techniques. ACS Omega 2021;6:11266–79. https://doi.org/10.1021/ACSOMEGA.1C00111/ASSET/IMAGES/LARGE/AO1C00111_0014.JPEG.

[133] Johra FT, Lee JW, Jung WG. Facile and safe graphene preparation on solution based platform. Journal of Industrial and Engineering Chemistry 2014;20:2883–7. https://doi.org/10.1016/J.JIEC.2013.11.022.

[134] Ghetti P, de Robertis U, D'Antone S, Villani M, Chiellini E. Coal combustion: Correlation between surface area and thermogravimetric analysis data. Fuel 1985;64:950–5. https://doi.org/10.1016/0016-2361(85)90150-4.

[135] Toniţă VV, Cârâc G, Teodor VG. Characterization of blast furnace dust for reintroduction into the agglomeration process. E3S Web of Conferences 2022;336:00079. https://doi.org/10.1051/E3SCONF/202233600079.

[136] Kumar Mohalik N, Mandal S, Kumar Ray S, Mobin Khan A, Mishra D, Krishna Pandey J. TGA/DSC study to characterise and classify coal seams conforming to susceptibility towards spontaneous combustion. Int J Min Sci Technol 2022;32:75–88. https://doi.org/10.1016/J.IJMST.2021.12.002.

[137] Avila C, Wu T, Lester E. Estimating the Spontaneous Combustion Potential of Coals Using Thermogravimetric Analysis 2014. https://doi.org/10.1021/ef402119f.

[138] Wang K, Deng J, Zhang Y-N, Wang • Cai-Ping. Kinetics and mechanisms of coal oxidation mass gain phenomenon by TG-FTIR and in situ IR analysis n.d. https://doi.org/10.1007/s10973-017-6916-x.

[139] SEM working principle: the detection of backscattered electrons - UK n.d.

[140] Asif M, Paul N, Panigrahi DC, Ojha K. Pore characterization of coal of Jharia coalfield for coalbed methane using Pore Image Analysis. 79th EAGE Conference and Exhibition 2017 2017. https://doi.org/10.3997/2214-4609.201701548.

[141] Liu L, Cao Y, Liu Q, Yang J. Experimental and kinetic studies of coal–CO2 gasification in isothermal and pressurized conditions. RSC Adv 2017;7:2193–201. https://doi.org/10.1039/C6RA25994D.

[142] Hou SS, Chen CH, Chang CY, Wu CW, Ou JJ, Lin TH. Firing blast furnace gas without support fuel in steel mill boilers. Undefined 2011;52:2758–67. https://doi.org/10.1016/J.ENCONMAN.2011.02.009.

[143] Grammelis P, Margaritis N, Karampinis E. Solid fuel types for energy generation: Coal and fossil carbon-derivative solid fuels. Fuel Flexible Energy Generation: Solid, Liquid and Gaseous Fuels 2016:29–58. https://doi.org/10.1016/B978-1-78242-378-2.00002-X.

[144] Trinkel V, Mallow O, Aschenbrenner P, Rechberger H, Fellner J. Characterization of Blast Furnace Sludge with Respect to Heavy Metal Distribution 2016. https://doi.org/10.1021/acs.iecr.6b00617.

[145] VOGEL Industrial Coatings. Technical Brief #11 Particle Size Distribution n.d. https://www.diamondvogel.com/documents/sites/documents.vogelpaint.com/files/documents/TechBrief_11_Particle_Size_Distribution.pdf (accessed September 10, 2022).

[146] Bulk Density - Measurement | Fact Sheets | soilquality.org.au n.d. https://soilquality.org.au/factsheets/bulk-density-measurement (accessed September 10, 2022).

[147] Chen W, Shi S, Nguyen T, Chen M, Zhou X. Effect of temperature on the evolution of physical structure and chemical properties of bio-char derived from

co-pyrolysis of lignin with high-density polyethylene. Bioresources 2016;11:3923–36. https://doi.org/10.15376/BIORES.11.2.3923-3936.

[148] Yang X, Tong C, Chen G, Zhang Y, Jin B. An investigation of pore structure of blended coal coke produced by pyrolysis of three kinds of coal. Https://DoiOrg/101080/1939269920222089126 2022. https://doi.org/10.1080/19392699.2022.2089126.

[149] Al-Qayim K, Nimmo W, Hughes K, Pourkashanian M. Kinetic parameters of the intrinsic reactivity of woody biomass and coal chars via thermogravimetric analysis n.d.

[150] Dadyburjor DB. Constant-coke arrhenius plots: A diagnostic tool. J Catal 1983;79:222–6. https://doi.org/10.1016/0021-9517(83)90308-1.

[151] Du RL, Wu K, Xu DA, Chao CY, Zhang L, Du XD. A modified Arrhenius equation to predict the reaction rate constant of Anyuan pulverized-coal pyrolysis at different heating rates. Fuel Processing Technology 2016;148:295–301. https://doi.org/10.1016/J.FUPROC.2016.03.011.

[152] Cheng N, Pan J, Shi M, Hou Q, Han Y. Using Raman spectroscopy to evaluate coal maturity: The problem. Fuel 2022;312:122811. https://doi.org/10.1016/J.FUEL.2021.122811.

[153] Raman images explained n.d. https://www.renishaw.com/en/raman-images-explained--25810 (accessed November 4, 2022).

[154] Recording Raman spectral images and profiles - HORIBA n.d. https://www.horiba.com/int/scientific/technologies/raman-imaging-and-spectroscopy/recording-spectral-images-and-profiles/ (accessed November 4, 2022).

[155] Stevie FA, Garcia R, Shallenberger J, Newman JG, Donley CL. Sample handling, preparation and mounting for XPS and other surface analytical techniques. Journal of Vacuum Science & Technology A: Vacuum, Surfaces, and Films 2020;38:063202. https://doi.org/10.1116/6.0000421.

[156] Chaves D, Trujillo M, Garcia E, Barraza J, Lester E, Barajas M, et al. Automated inspection of char morphologies in Colombian coals using image analysis. Intelligent Automation and Soft Computing 2020;26:397–405. https://doi.org/10.32604/IASC.2020.013916.

[157] Marinov VN. Self-ignition and mechanisms of interaction of coal with oxygen at low temperatures. 1. Changes in the composition of coal heated at constant rate to 250 °C in air. Fuel 1977;56:153–7. https://doi.org/10.1016/0016-2361(77)90136-3.

[158] Chen MM. Thermal Analysis. Materials Science and Engineering of Carbon: Characterization 2016:249–72. https://doi.org/10.1016/B978-0-12-805256-3.00012-X.

[159] Cheng J, Wang X, Si T, Zhou F, Wang Z, Zhou J, et al. Maximum burning rate and fixed carbon burnout efficiency of power coal blends predicted with back-propagation neural network models. Fuel 2016;172:170–7. https://doi.org/10.1016/J.FUEL.2016.01.035.

[160] Cheng J, Zhou F, Xuan X, Liu J, Zhou J, Cen K. Comparison of the catalytic effects of eight industrial wastes rich in Na, Fe, Ca and Al on anthracite coal combustion. Fuel 2017;187:398–402. https://doi.org/10.1016/J.FUEL.2016.09.083.

[161] Lee YS, Min DJ, Jung SM, Yi SH. Influence of basicity and FeO content on viscosity of blast furnace type slags containing FeO. ISIJ International 2004;44:1283–90. https://doi.org/10.2355/ISIJINTERNATIONAL.44.1283.

[162] Backreedy RI, Jones JM, Pourkashanian M, Williams A. Burn-out of pulverised coal and biomass chars☆. Fuel 2003;82:2097–105. https://doi.org/10.1016/S0016-2361(03)00174-1.

[163] Costa M, Silva P, Azevedo JLT. Measurements of gas species, temperature, and char burnout in a low-NOx pulverized-coal-fired utility boiler. Combustion Science and Technology 2003. https://doi.org/10.1080/00102200390123764.

[164] Murphy JJ, Shaddix CR. Combustion kinetics of coal chars in oxygen-enriched environments. Combust Flame 2006;144:710–29. https://doi.org/10.1016/j.combustflame.2005.08.039.

[165] Harvey WR, Hutton P. Carbon monoxide: chemistry, role, toxicity and treatment. Curr Anaesth Crit Care 1999;10:158–63. https://doi.org/10.1016/S0953-7112(99)80008-8.

[166] Yu X, Shen Y. Model analysis of gas residence time in an ironmaking blast furnace. Chem Eng Sci 2019;199:50–63. https://doi.org/10.1016/J.CES.2018.12.062.

[167] Aich S, Behera D, Nandi BK, Bhattacharya S. Relationship between proximate analysis parameters and combustion behaviour of high ash Indian coal. Int J Coal Sci Technol 2020;7:766–77. https://doi.org/10.1007/S40789-020-00312-5.

[168] Nedeljković M, Ghiassi B, Ye G. Role of Curing Conditions and Precursor on the Microstructure and Phase Chemistry of Alkali-Activated Fly Ash and Slag Pastes. Materials 2021, Vol 14, Page 1918 2021;14:1918. https://doi.org/10.3390/MA14081918.

[169] Stamboroski S, Boateng K, Leite Cavalcanti W, Noeske M, Beber VC, Thiel K, et al. Effect of interface-active proteins on the salt crystal size in waterborne hybrid materials. Applied Adhesion Science 2021;9:1–22. https://doi.org/10.1186/S40563-021-00137-8/FIGURES/15.

[170] Murav'eva I v., Bebeshko GI. Determining the chlorine content in the blast-furnace system. Steel in Translation 2017;47:287–90. https://doi.org/10.3103/S0967091217050084.

[171] Zhou C, Xi W, Yang L, Li B. Chlorine emission characteristics and control status of coal-fired units. Energy Reports 2022;8:51–8. https://doi.org/10.1016/J.EGYR.2021.11.129.

[172] Sun Q, Fang T, Chen J, Da C. Characteristics of Chlorine Releasing from Coal-Fired Power Plant. Atmosphere 2021, Vol 12, Page 1550 2021;12:1550. https://doi.org/10.3390/ATMOS12121550.

[173] Nomura S. Behavior of coal chlorine in cokemaking process. Int J Coal Geol 2010;83:423–9. https://doi.org/10.1016/J.COAL.2010.06.003.

[174] Czarna-Juszkiewicz D, Cader J, Wdowin M. From coal ashes to solid sorbents for hydrogen storage. J Clean Prod 2020;270:122355. https://doi.org/10.1016/J.JCLEPRO.2020.122355.

[175] Li Z, Li J, Sun Y, Seetharaman S, Liu L, Wang X, et al. Effect of Al2O3 Addition on the Precipitated Phase Transformation in Ti-Bearing Blast Furnace Slags. Metallurgical and Materials Transactions B: Process Metallurgy and Materials Processing Science 2016;47:1390–9. https://doi.org/10.1007/S11663-015-0576-7.

[176] Zhou Z, Wang R, Yi Q, Wang G, Ma C. Combustion Enhancement of Pulverized Coal with Targeted Oxygen-Enrichment in an Ironmaking Blast

Furnace. Processes 2021, Vol 9, Page 440 2021;9:440. https://doi.org/10.3390/PR9030440.

[177] Azadi P, Minaabad SA, Bartusch H, Klock R, Engell S. Nonlinear Prediction Model of Blast Furnace Operation Status. Computer Aided Chemical Engineering 2020;48:217–22. https://doi.org/10.1016/B978-0-12-823377-1.50037-9.

[178] WTW IQ SensorNet 281 n.d. https://www.xylemanalytics.co.uk/wtw-iq-sensornet-281/ (accessed November 5, 2022).